Effects of Deregulation of Ribonucleotide Reductase in Mice

A Dissertation Presented to the Faculty of the Graduate School of Cornell University in Partial Fulfillment of the Requirements for the Degree of Doctor of Philosophy

by

Jennifer L. Page

May 2011

Effects of deregulating ribonucleotide reductase in mice

Jennifer L. Page, Ph. D.

Cornell University 2011

Nucleotide levels play a critical role in genome stability, and proper regulation of these pools is crucial for survival. Ribonucleotide reductase (RNR) catalyzes the rate- limiting step in *de novo* dNTP biosynthesis. The enzyme is composed of two non-identical homodimeric subunits, a large subunit encoded by a single gene Rrm1, and a small subunit encoded by either Rrm2 or a DNA-damage-inducible gene p53R2. In mammals, RNR activity is thought to be controlled by two main mechanisms: limitation of small subunit protein levels and allosteric feedback control. Studies in yeast and cultured mammalian cells have shown that disabling RNR regulation results in increased mutation rates. The objective of the studies described here was to develop mouse models to elucidate the physiological consequences of disrupting RNR regulatory mechanisms *in vivo*, either individually or in combination. We first overrode the control of RNR protein levels by generating multiple mouse strains that featured overexpression of individual RNR subunits. Mice that overexpressed either small RNR subunit developed lung cancer at a high frequency, while mice that overexpressed both Rrm1 and either small RNR subunit developed age-dependent mitochondrial DNA depletion in addition to lung cancer. These findings highlight the impact of RNR deregulation on the stability of both the nuclear and mitochondrial DNA genomes. In order to disrupt RNR allosteric

control, we also generated transgenic mice that overexpress a feedback-resistant form of Rrm1, Rrm1-D57N, as well as knock-in mice in which the D57N mutation was introduced directly into the Rrm1 genomic locus. These mouse strains were used individually or in various combinations to assess the effects of loss of RNR regulation on genome maintenance, tumorigenesis, and survival. Although mice that overexpress Rrm1-D57N were grossly normal, mice that overexpress Rrm1-D57N in combination with either small RNR subunit were inviable, indicating that simultaneous loss of both main RNR regulatory mechanisms is incompatible with survival. Preliminary work suggested large dNTP pool alterations in the skeletal muscle of bitransgenic neonates, resulting in pathological changes in multiple organ systems and premature lethality. It was also found that mice homozygous for the Rrm1-D57N knock-in mutation are inviable, further indicating that proper allosteric feedback control of RNR is critical for survival. All together, these results indicate that RNR plays a central role in genome maintenance, and that alterations in RNR activity are detrimental for survival.

BIOGRAPHICAL SKETCH

Jennifer Leigh Page (Jenn) received her B.S. in Biological Sciences from Clemson University in 2004. At Clemson, she was a member of the Calhoun Honors College and graduated Magna Cum Laude and with Departmental Honors. Her first research experience was in the lab of Dr. Julia Frugoli, where she studied signaling through the plant hormone auxin during the process of nodulation in the model legume *Medicago truncatula*. The project involved using *A. rhizogenes* to transfer the GUS reporter gene (the plant version of β-galactosidase) into the roots of the plant, but this technique was inefficient and led to chimeric roots which would interfere with the ability to track auxin. Later parts of the project involved attempting to make transgenic plants so that GUS would be expressed equally throughout all parts of the plant. While this failed, Jenn discovered a love for generating new strains of model organisms that would come in handy later.

At Cornell, Jenn rotated in the labs of Dr. Robert Weiss, Dr. Mariana Wolfner, and Dr. Kelly Liu. Seeing the limited lab experience Jenn had, Dr. Weiss patiently taught her the techniques needed for a successful rotation, most importantly how to figure out new experiments. The Wolfner lab further taught self-reliance, as the rotation began with a brief introduction to *D. melanogaster* and was followed by weeks of collecting virgins without guidance from the grad student she was working with (in his defense, he was still on vacation). In the Liu lab, Jenn finally learned to stop and think carefully when trouble-

shooting experiments, which never really sank in until maybe 5 years later. In the end, Jenn earned authorship on two publications during her rotations, and it was the invitation to make a new mouse for the Weiss lab that led her to join the lab.

ACKNOWLEDGEMENTS

I would like to thank the members of my committee, Dr. Robert Weiss, Dr. Jun Kelly Liu, Dr. John Schimenti, and Dr. Patrick Stover for invaluable advice and guidance. I'd next like to thank the members of the Weiss lab for suggestions and help. I'd especially like to thank Dr. Xia Xu, Minxing Li, Joshua Levy, Joshua Darfler, Lee Gerwitz, Sarah Lagedrost, J. R. Cho, and Young Lu, who all worked on RNR and provided ideas, support, and materials, or who worked with me during my time on this project.

I'd also like to thank Emil Ylikallio, Henna Tynnismaa, Anu Suomalainen for their hard work towards the final project and for a rewarding collaboration. In addition, Dr. Vera Bianchi and her lab provided guidance in measuring dNTP pools, allowing us to obtain accurate dNTP measurements quickly.

I'd also like to thank Dr. Vimal Selvaraj for help in constructing the Rrm1D57B knock-in strain of mice, and Drs. Rachel Peters and Teresa Southard for help in analyzing the phenotype of all RNR mouse strains used in this study.

I'd like to thank the Stover lab for allowing me to use their HPLC and for training me with this technique. Christina Cota provided advice and suggestions to improve success with timed matings and embryo phenotyping, while Suzanne Hartford provided suggestions for cell culture and embryo analysis.

I'd also like to thank Kevin Yager, Dale Walters, and all of the members of the mouse room staff and CARE who helped maintain the mice and provide veterinary services.

I'd also like to acknowledge the Pages, who supported me financially through my undergrad and provided moral support and an ear to complain to when things were rough. Most especially I'd like to thank my mom for keeping me calm across the miles before my A-exam, probably the real reason I didn't fail.

I'd lastly like to thank my husband Zane Bergman (a soon-to-be Ph.D.) for many, many things throughout my time here at Cornell. Including technical advice, reagents, ideas and suggestions, support, distraction, rides, and company in lab, Zane has always been there when I needed him and was there from the beginning.

TABLE OF CONTENTS

LIST OF FIGURES

LIST OF TABLES

Chapter 1: Role of ribonucleotide reductase in regulating dNTP metabolism and maintenance of genomes

1.1 Overview of nucleotide metabolism

1.1A Biological significance of nucleotides

Proper maintenance and transmission of genetic information is key to the survival of all species. In order to preserve genetic information, DNA needs to be maintained and replicated exactly throughout the life of the organism. DNA is also under constant stress from both exogenous and endogenous processes, and so the ability to repair or replace damaged DNA bases is necessary for survival. Nucleotides, specifically deoxynucleoside triphosphates (dNTPs), are the building blocks of DNA, and it is crucial to maintain an adequate supply of dNTPs so that DNA replication and repair can occur accurately. Organisms have evolved many mechanisms to ensure the proper supply and balance of dNTPs, and regulate both the production and the degradation of dNTPs to keep nucleotides at an optimal level.

1.1B Summary of nucleotide synthesis

Nucleotides are generated via *de novo* and salvage pathways. Salvage pathways convert bases back into ribonucleosides by conjugating a ribose moiety to the base. *De novo* purine and pyrimidine biosynthetic pathways follow separate patterns. Pyrimidine bases are synthesized first and then attached to a ribose sugar, while purines are assembled piece by piece onto a ribose. Biosynthesis of both purines and pyrimidines utilize 5-phosphoribosyl

1-pyrophosphate (PRPP) to link a 5-phosphoribosyl moiety onto the nitrogen atom of an aglycone(6). The enzyme responsible for generation of PRPP, ribosepyrophosphorylase, was isolated by Kornberg, Lieberman, and Simms and demonstrated to couple a pyrophosphate to ribose-1-phosphate on carbon 1(7).

1.1C *De novo* synthesis of pyrimidine nucleotides

Pyrimidine biosynthesis (summarized in Figure 1.1) starts from bicarbonate, Mg^{2+}ATP, and glutamine(8). Glutamine supplies the ammonia, which is combined with bicarbonate in a multi-step reaction catalyzed by carbamoyl phosphate synthetase (CPS) to produce carbamoyl phosphate(8). Two isoforms of CPS exist; CPS I is localized to the mitochondrion, where it participates in arginine biosynthesis and the urea cycle, and CPS II is cytosolic and is involved in the *de novo* production of pyrimidine nucleotides(8). The enzyme aspartate transcarbamoylase couples an aspartate to carbamoyl phosphate to produce carbamoylaspartate, which is cyclized by dihydroorotate synthetase to produce dihydroorotate(9). These first 3 enzymes responsible for the initial steps in *de novo* pyrimidine biosynthesis were demonstrated to be a trifunctional enzyme polypeptide, termed CAD, an acronym based on the enzyme names(10).

The product of these enzymes, dihydroorotate, diffuses into the mitochondria to be converted into orotate by dihydroorotate dehydrogenase (DHOdeHase).

Figure 1.1 Overview of *de novo* pyrimidine biosynthesis. *A*. Synthesis of uridine. *B*. Interconversion of uridine, cytosine, and thymidine. Enzymes: (1) Carbamoyl phosphate synthetase; (2) aspartate transcarbamoylase; (3) dihydroorotate synthetase; (4) pyrimidine phosphoribosyltransferase; (5) cytidine synthetase; (6) cytidine deaminase; (7) ribonucleotide reductase; (8) thymidine synthetase. Modified from Berg *et al.* Biochemistry 5th ed.

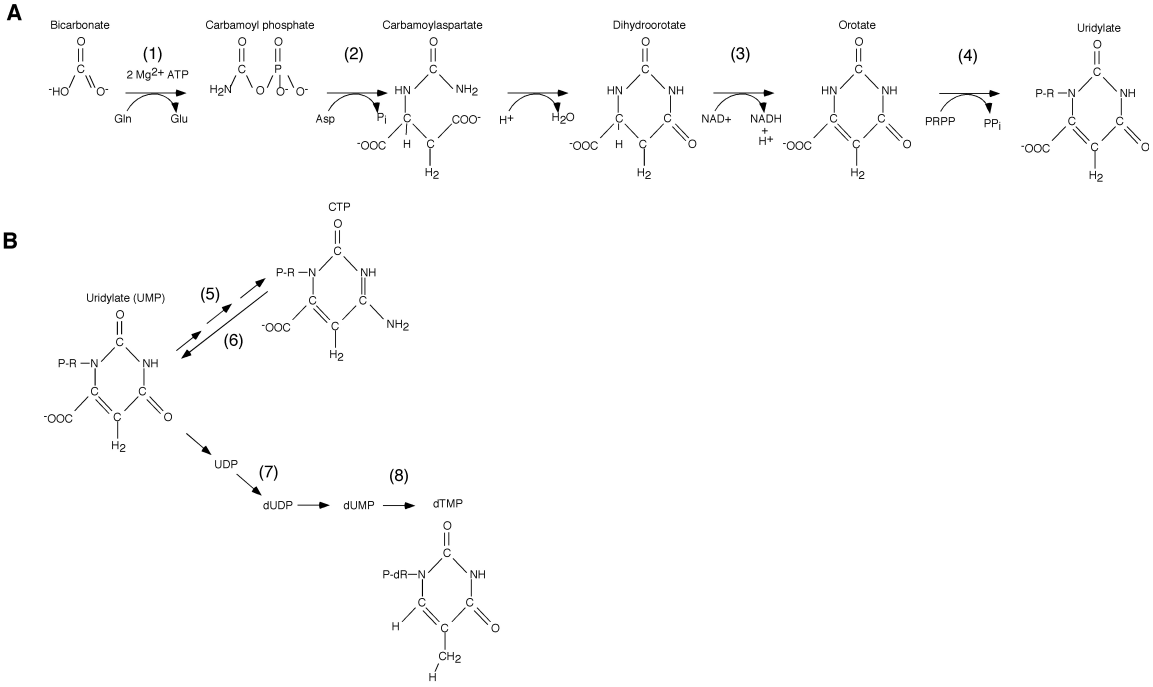
A
Bicarbonate
(1)
2 Mg2+ ATP
Gln
Glu
Carbamoyl phosphate
(2)
Asp
Pi
Carbamoylaspartate
H+
H2O
Dihydroorotate
(3)
NAD+
NADH
+
H+
Orotate
(4)
PRPP
PPi
Uridylate
B
CTP
Uridylate (UMP)
(5)
(6)
UDP
(7)
dUDP
(8)
dUMP
dTMP

The unique situation of DHOdeHase within the inner mitochondrial membrane allows it to participate in both the synthesis of pyrimidines and in the respiratory chain(9). DHOdeHase uses an NAD+ to oxidize dihydroorotate to orotate, which diffuses back into the cytosol for the final steps. A final bifunctional enzyme, UMP synthetase, contains the enzymes orotate phosphoribosyltransferase and orotidine 5'-monophosphate decarboxylase. Orotate phosphoribosyltransferase couples orotate to an activated ribose from PRPP(6, 11). Orotidylate decarboxylase removes the carboxyl from orotidylate to produce uridine -5'-monophosphate (UMP)(11). UMP is the precursor for all other pyrimidine nucleotides.

UMP is first phosphorylated by UMP/CMP kinase to produce uridine-5'-diphosphate (UDP)(9). From here, UDP can be converted into 3 different nucleotides or be used in the production of UDP sugars(9). UDP is phosphorylated by nucleoside diphosphate kinase to produce uridine-5'-triphosphate (UTP), which is used in RNA synthesis, or can be aminated to produce cytidine-5'-triphosphate (CTP) by CTP synthetase(9). To be used for DNA synthesis, CTP must be dephosphorylated into CDP in order to be a substrate for ribonucleotide reductase (RNR), which removes the 2'-OH to produce dCDP(12). One nucleoside diphosphate kinase acts to phophorylate all NDPs and dNDPs to produce NTPs and dNTPs(13). CMP can be converted back into UMP by CMP deaminase, an important enzyme for controlling nucleotide pool ratios(14).

UDP can also be a substrate for RNR to produce dUDP(15). dUDP is not itself a substrate for DNA synthesis, but is instead dephosphorylated to produce dUMP. dUMP is methylated to form dTMP by thymidylate synthetase (Figure 1.3). 5, 10-methylene-5,6,7,8- tetrahydrofolate serves as a cofactor and donates a methyl group to dUMP to produce dTMP and 7,8-dihydrofolate(16). dTMP is phosphorylated into dTTP through the actions of dTMP kinase(13).

1.1D *De novo* synthesis of purine nucleotides

Purine biosynthesis begins with PRPP(6) (illustrated in Figure 1.2). The 1-pyrophosphate within PRPP is displaced by ammonia to form 5-phosphoribosyl-1-amine (PRA). The enzyme glutamine phosphoribosyl amidotransferase catalyzes this reaction, using an ammonia from glutamine(17). The reaction proceeds as two half-reactions, channeling an unstable ammonia intermediate between separate active sites to catalyze each step of the process(18). The first half-reaction is the hydrolysis of glutamine to form glutamate and ammonia, and the second is the replacement of the pyrophosphate from PRPP with ammonia, forming phosphoribosylamine (PRA)(18). From here, 9 enzymatic steps assemble the two-ring structures of guanine and adenine. First a glycine is added to the amino group of PRA to form glycinamide ribonucleotide, in a reaction catalyzed by glutamine PRPP amidotransferase(19). The enzyme glycinamide ribonucleotide transformylase uses N^{10}-formyl tetrahydrofolate to transfer a formyl group to the amino group

on the glycine residue to form formylglycinamide ribonucleotide. Step 3 involves phosphorylation of the carboxy oxygen on the glycine residue and replacement of the phosphate with ammonia from glutamine, forming formylglycinamidine ribonucleotide. Hydrolysis of an ATP stimulates an intramolecular coupling reaction to produce 5-aminoimidazole ribonucleotide. Bicarbonate is first added to an amino group within the ring to be the first exocyclic group and then transfers to the adjacent carbon atom, producing carboxyaminoimidazole ribonucleotide. ATP hydrolysis couples an aspartate residue to the bicarbonate, forming 5-aminoimidazole-4-(N-succinylcarboxamide) ribonucleotide. A fumarate molecule is released, forming 5-aminoimidazole-4-carboxamide ribonucleotide. N^{10}-formyltetrahydrofolate supplies another formyl residue to produce 5-formylaminoimidazole-4-carboxamide ribonucleotide, which cyclizes, releasing a water molecule and forming inosine-5'-monophosphate (IMP)(20).

IMP is the precursor purine from which AMP and GMP are formed. The enzyme adenylosuccinate synthetase uses aspartate to donate an ammonia to IMP, eventually releasing fumarate and adenosine-5'-monophosphate(19). To produce GMP, additional steps are required. A water is added to IMP by inosine-5'-monophosphate dehydrogenase and is then dehydrogenated by NAD^+ to add a second carbonyl moiety to the molecule, producing xanthine -5'-monophosphate(20). An ammonia derived from glutamine replaces the carbonyl, yielding the final GMP nucleotide.

Figure 1.2. *De novo* synthesis of purines. *A*. Generation of IMP. *B*. Interconversion of IMP, AMP, and GMP. Enzymes: (1) Glutamine phosphoribosyl transferase; (2) adenyl-succinate synthetase; (3) GMP synthetase. Modified from Berg *et al.* Biochemistry 5th ed.

A

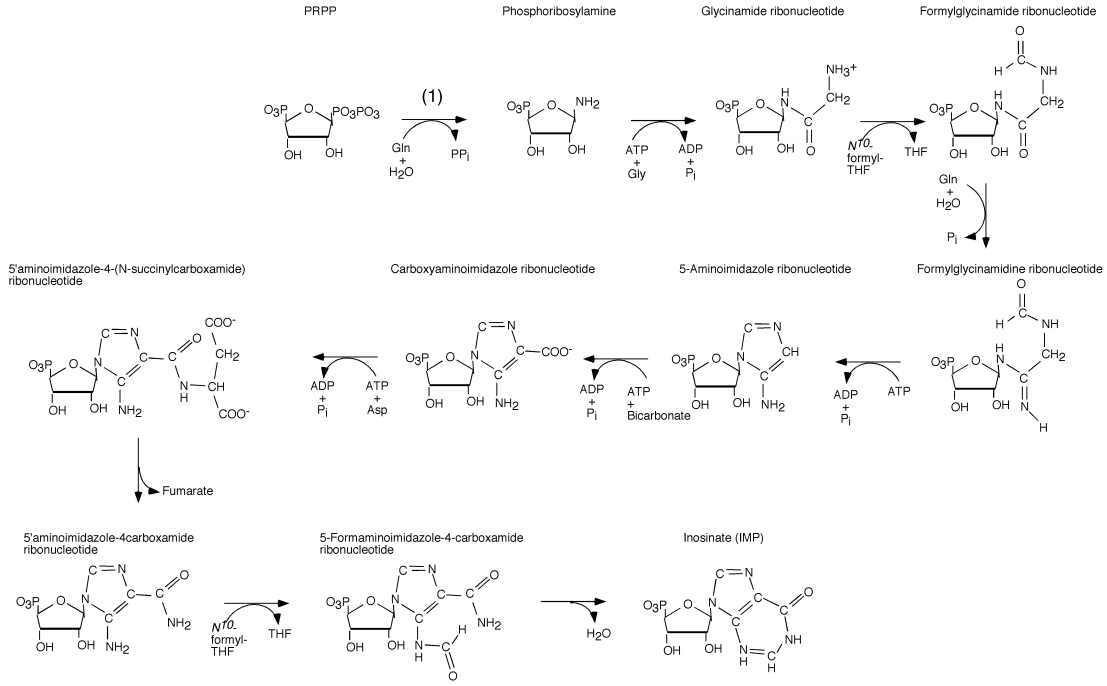
PRPP
Phosphoribosylamine
Glycinamide ribonucleotide
Formylglycinamide ribonucleotide
(1)
Gln + H2O
PPi
ATP + Gly
ADP + Pi
N10-formyl-THF
THF
Gln + H2O
Pi
5'aminoimidazole-4-(N-succinylcarboxamide) ribonucleotide
Carboxyaminoimidazole ribonucleotide
5-Aminoimidazole ribonucleotide
Formylglycinamidine ribonucleotide
ADP + Pi
ATP + Asp
ATP + Bicarbonate
Fumarate
5'aminoimidazole-4carboxamide ribonucleotide
5-Formaminoimidazole-4-carboxamide ribonucleotide
Inosinate (IMP)
H2O

B

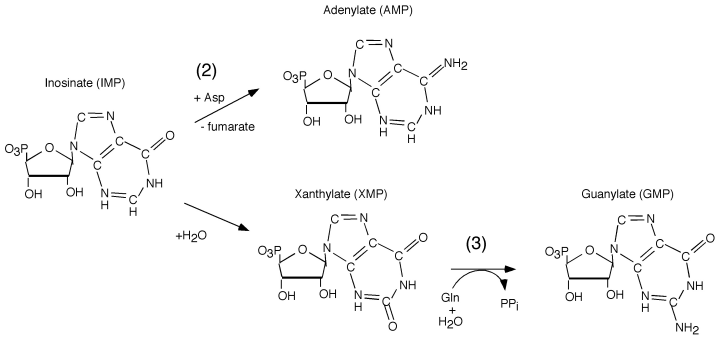
Adenylate (AMP)
Inosinate (IMP)
(2)
+ Asp
- fumarate
+H2O
Xanthylate (XMP)
Guanylate (GMP)
(3)
Gln + H2O
PPi

The enzyme which catalyzes this process is GMP synthetase(19). AMP and GMP are phosphorylated to ADP and GDP, respectively by their own unique kinases. Similar to UDP and CDP, ADP and GDP are also substrates for ribonucleotide reductase, forming dADP and dGDP, which are phosphorylated to dATP and dGTP by the same nucleotide diphosphate kinase as the pyrimidines(20).

1.1E Overview of nucleotide salvage pathways

Nucleotide salvage pathways serve to recycle dNTPs from the diet or from damaged DNA and prepare them for new DNA synthesis. Nucleosides (without phosphates) from the diet are carried into cells through broad-spectrum nucleoside transporters(13). The liver has been suggested to be a major site of dNTP salvage from dietary sources, having high levels of activity of PRPP amidotransferase(21). Like *de novo* nucleotide synthesis, the salvage pathways also utilize PRPP(21). The purine salvage enzyme hypoxanthine/guanosine ribosyltransferase (HPRT) combines hypoxanthine to PRPP to form IMP(21), which can be converted into AMP or GMP as discussed previously.

Cells can utilize salvaged thymidine nucleoside by thymidine kinase 1-dependent phosphorylation(22). Mitochondrial DNA replication is independent of cell cycle stage, but draws from the same nucleotide pool as the nuclear genome. Mitochondrial membranes harbor specific nucleotide transporters, which traffic dNDPs and dNTPs between the mitochondria and cytosol in both

directions(4). Mitochondria contain salvage enzymes distinct from those of the rest of the cell. Especially in quiescent tissues lacking RNR activity, mitochondria can utilize thymidine kinase 2 (TK2) and deoxyguanosine kinase (dGK) to produce dNTPs to replicate their DNA(22). TK2 is specific for phosphorylating pyrimidine nucleotides, while dG and dA are phosphorylated by dGK(23). The dNMPs are further phosphorylated by mitochondrial nucleotide monophosphate kinases, and the dNDPs are phosphorylated by mitochondrial nucleotide diphosphate kinases, a multifunctional enzyme(23).

One mechanism in place for limiting dNTP production to S-phase is degradation of TMP kinase and TK1 by the anaphase-promoting complex (APC). Both the APC^{Cdc20} and APC^{Cdh1} complexes degrade TMPK(24). Knockdown of the APC leads to dramatic dNTP pool imbalances, characterized most by a huge increase in dTTP levels(24). Additionally, reduction of NDPs into dNDPs by ribonucleotide reductase is largely limited to S-phase of the cell cycle(25), and will be discussed in detail later (Chapter 1.3).

1.1F Overview of nucleotide catabolism

In addition to feedback control mechanisms that limit the production of dNTPs, cells do harbor mechanisms conferring the ability to degrade excessive nucleotides. The major step in nucleotide catabolism is the removal of the 5'phosphates by 5'nucleotidases, yielding nucleosides(26).

Figure 1.3. Summary of nucleotide substrate cycles and cross-talk between cytosolic and mitochondrial nucleotide pools. *A*. Regulation of thymidine pools between the cytosol and mitochondria (modified from Ferraro *et al.*(2)) *B*. Regulation of guanine nucleotide pools between the cytosol and mitochondria (Modified from Leanza *et al.*(4)). *C*. Regulation of cytidine pools.

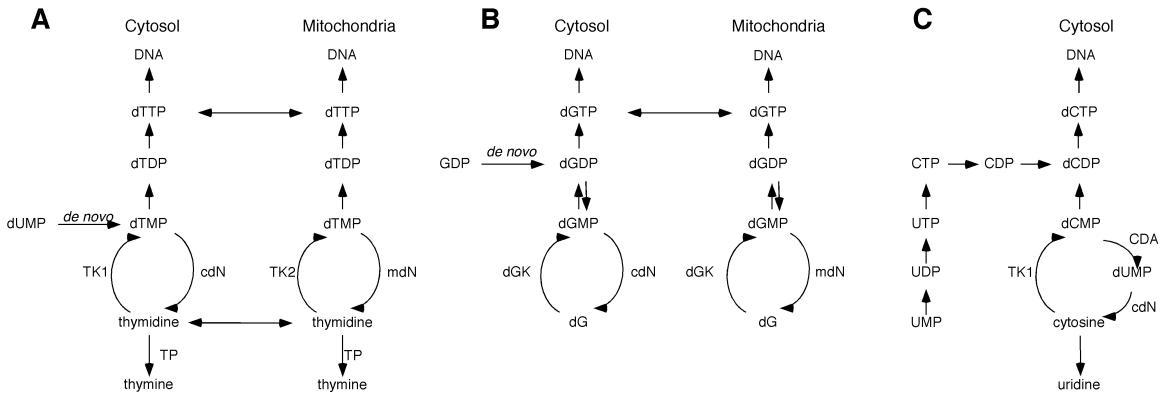
A
Cytosol
Mitochondria
DNA
DNA
dTTP
dTTP
dTDP
dTDP
dUMP
de novo
dTMP
dTMP
TK1
cdN
TK2
mdN
thymidine
thymidine
TP
TP
thymine
thymine
B
Cytosol
Mitochondria
DNA
DNA
dGTP
dGTP
GDP
de novo
dGDP
dGDP
dGMP
dGMP
dGK
cdN
dGK
mdN
dG
dG
C
Cytosol
DNA
dCTP
CTP
CDP
dCDP
UTP
dCMP
CDA
UDP
TK1
dUMP
cdN
UMP
cytosine
uridine

Nucleotidase activity is constant in cells undergoing *de novo* dNTP synthesis, sometimes balancing out the effect of nucleoside kinases, leading to a substrate cycle(27). Experiments in cultured cells have shown a tight balance between nucleoside phosphorylation and nucleotide dephosphorylation(28, 29). Inhibition of DNA synthesis in the continued presence of *de novo* dNTP biosynthesis leads to enhanced nucleoside excretion from the cell and no net increase in dNTP pools, while inhibition of *de novo* synthesis with hydroxyurea stimulated nucleoside uptake and phosphorylation(28). Mammalian cells contain several 5'-nucleotidases, the cytosolic high K_m 5'-nucleotidase (hkm-NT)(26), a cytosolic 5'-deoxynucleotidase (dNT-1)(26) a mitochondrial 5'-deoxynucleotidase (dNT-2)(26, 30), and a cell membrane-bound ectonucleotidease(26). Through substrate-flow experiments, it was shown that hkm-NT degrades ribonucleotides GMP and IMP, while dNT-1 degraded pyrimidine deoxynucleotides dCMP and dUMP(26), but was later found to also degrade purine deoxynucleotides(30). dNT-2 was shown to have specificity towards dTTP and deoxyuridine, suggesting a possible mechanism for protection of mitochondrial dNTP pools from cytosolic imbalances(30).

Another important step in nucleotide catabolism is cleavage of the C-N glycosidic bond to release the ribose sugar from the free base(31). This process is carried out by nucleotide phosphorylases, of which there are two main families. Members of the phosphorylase-I family harbor a single domain

fold and can work on a range of purine and pyrimidine substrates(31). The phosphorylase-II family harbors a dimeric structure and cleaves exclusively pyrimidine nucleotides(31). Rather than using hydrolysis to cleave the glycosidic bond, it has been shown that the process is carried out through phosphorolysis, yielding the nucleotide base as well as ribose-1-phosphate(31). Loss of function of the purine nucleoside phosphorylase (PNP) leads to accumulation of dGTP in lymphoid tissues(27). Loss of function of thymidine phosphorylase (TP) leads to accumulation of both dTTP and dGTP in the mitochondria(32). Both dC and dA (by adenosine deaminase (ADA)(27)) must be deaminated prior to this step, yielding dU and dI, respectively(13). Accumulation of adenosine and 2'-deoxyadenosine in ADA-null mice results in a wide spectrum of phenotypes, from pulmonary insufficiency to renal abnormalities(33, 34).

Hyperactive nucleotide degradation results in elevated levels of xanthine, hypoxanthine, and uric acid in the blood. The cause/effect relationship is unclear, however elevated uric acid is associated with hypertension in rats(35). Additionally, elevated purine degradation products are found in the bloodstream of hypertensive and exercise-intolerant patients(36, 37). Elevated uric acid levels are also linked to essential hypertension in humans, which can lead to stroke, congestive heart failure, renal disease, and myocardial infarction(38). Elevated uric acid in humans can also cause gouty arthritis and renal stones(39).

1.2 Nucleotides and mutagenesis

The cellular processes outlined above all participate towards a common goal: to keep nucleotide levels balanced and in adequate, but not excessive, supply. Accurate replication of DNA and transmission of genetic information depends on the fidelity of the replicative DNA polymerases, which are all impacted by perturbations in nucleotide pools. This chapter will discuss first the fidelity of the individual DNA polymerases as well as evidence for enhanced mutagenesis by each in conditions of elevated or unbalanced dNTPs. Next we will focus on effects of inadequate nucleotide supplies on genome maintenance.

1.2A Fidelity of replicative DNA polymerases

It is proposed that the bulk of correct base-base pairing during DNA replication occurs at the initial step of incorporating a new base into the strand, as polymerases that lack proofreading domains still show low substitution rates(40). Such high specificity was proposed to occur through a combination of entropy/enthalpy balance in Watson-Crick base pairing of the correct bases(41), and through tight arrangement of residues within the active site of the polymerase, so that correct base-base pairs fit snugly but incorrect pairs encounter steric clashes(41, 42). Indeed, experiments show that mutating key residues within the active site which allow the replicative polymerase to detect the correct base is mutagenic in yeast and homozygous lethal in

mammals(42). Heterozygous mutant animals show a decreased lifespan, increased genomic instability and increased cancer formation(42).

The next step in accurate DNA synthesis is proper function of 3'-5' exonuclease domains, which proofreads the polymerase's work. The mechanism proposed to be at work here is an inefficiency of extending past a mismatched base(42). A loss of speed in elongating from the primer terminus allows the mismatch time to detach from its pairing partner and move towards the exonuclease domain for cleavage(42).

Eukaryotic systems utilize three main nuclear DNA polymerases, DNA polymerase α (Pol α), polymerase δ (Pol δ), and DNA polymerase ε (Pol ε), which catalyze the bulk of DNA replication. Pol α lacks a 3'-5' exonuclease domain, making it a low-fidelity enzyme, while δ(43) and ε both harbor a proofreading domain. Pol α forms a complex with DNA primase to synthesize RNA/DNA primers on both the leading strand and the lagging strand to initiate replication. DNA pol α has a low fidelity(40), and recent work suggests it does not have a role in primer extension; instead a polymerase-switch occurs on each strand(44-46). This switch on the lagging strand allows Pol δ to replace any errors made by Pol α(45). It is hypothesized that Pol δ and Pol ε replicate the leading and lagging strands, and data suggests that Pol δ replicates the bulk of the lagging strand(44, 45) and is responsible for Okazaki fragment maturation(44). Further data indicates that Pol ε replicates the leading strand(46).

Pol δ and Pol ε have base substitution rates around 10^{-8} to 10^{-6}, due in large part to high selectivity for the correct base and an exonuclease domain that removes the wrong base. Exonuclease-deficient Pol δ and Pol ε have fidelity rates of 10^{-6} to 10^{-4} [41]. *In vitro* work with Pol ε and Pol δ purified from calf thymus have shown a mutation frequency of around 7×10^{-4} and 19×10^{-4}, respectively at optimal dNTP concentrations. Both Pol δ and Pol ε were shown to have fairly high fidelity for single base changes (transitions and transversions) and small frameshift errors(40).

Mitochondrial DNA is replicated by DNA polymerase γ (Pol γ), a nuclear-encoded enzyme localized exclusively to the mitochondria(42). Pol γ belongs to the B-family of replicative polymerases, harboring a proofreading domain(41, 42, 47). Disabling the proofreading domain of Pol γ in mice increased the misincorporation rate to as high as 5-fold that of wild type(48). Studies of Pol γ from porcine liver showed a high fidelity both in the presence of balanced but excessive dNTPs and in the presence of dGMP, which inhibits the proofreading domain(47). Further experiments seeking to explain the high prevalence of mtDNA mutations in certain mutational hotspots of the mitochondrial genome found again very high fidelity, similar to the previously-reported most faithful enzyme(49). Extensive work from the Bianchi lab indicates that dNTP pools in the cytosol and mitochondria are tightly linked and mitochondrial dNTP pools reflect cytosolic dNTP pools(50). Therefore, under normal situations, mtDNA synthesis by Pol γ should be quite faithful.

Experiments with minorly unbalanced dNTP pools and Pol γ showed extremely high fidelity again, even in the presence of high concentrations of dGMP(47).

1.2B Effects of elevated, unbalanced, or depleted nucleotide pools on DNA replication fidelity

Elevated dNTP pools can be beneficial in many ways. In yeast, elevated dNTP pools were able to promote lesion bypass by the replicative polymerase, at the expense of a higher mutation rate(51, 52). Damage-induced dNTP synthesis provides dNTPs for other essential processes, from homologous recombination repair of a DNA double-strand break, to replacement of excised bases. Consistent with this is the fact that treatment of specific mutagens such as UV light, X-rays, ethylmethane sulfonate (EMS), or MNNG(53) induces increases in dNTP pools. In mammals, dNTPs are rapidly produced following DNA damage, and are used for repair at an equal rate, leading to stable dNTP pools(54).

Elevated or unbalanced dNTP pools are mutagenic. Elevated nucleotide pools cause base-base mismatches during DNA replication through direct substitution of the correct base by an incorrect base, and can also cause increased mismatches through a “next-nucleotide effect”, where an overrepresented base at the correct position influences the misincorporation rate of the base before it(13). More specifically, the availability of the “next nucleotide” a DNA polymerase will incorporate causes reduced proofreading of the base it is in the process of incorporating, making a mistake more likely.

This is likely to be the mechanism by which excessive but balanced nucleotide pools are mutagenic. However, not all mismatches induced by mutagenic dNTP pools can be explained this way. Increases in a particular dNTP can directly inhibit the proofreading domain of some DNA polymerases, such as Pol III from *E. coli*(53). Moreover, DNA polymerase proofreading domains may be less efficient at correcting some mismatches than others, allowing some mistakes to persist(53). DNA polymerase susceptibility to these mutagenic pools is variable. When dNTP pools were increased as much as 50-fold for Pol ε, mutation rates increased 3-fold, while a 5-fold increase in dNTP concentration doubled the mutation frequency by Pol δ(40).

Further unbalanced dNTP pools can cause more dramatic genome instability, especially in the mitochondrial genome. A recent study(55) found grossly unbalanced dNTP pools in wild type rat mitochondria, and *in vitro* assays of Pol γ fidelity using these pools showed drastically increased mutation rates. While the measurements of dNTP pools in this study were flawed, and a later study indicated balanced nucleotide pools within the mitochondria(56), the Song *et al.* study again underscores the effect unbalanced nucleotide pools can have on DNA replication fidelity. Studies culturing HeLa cells in artificially unbalanced dNTP pools stimulated long deletions in mitochondrial DNA(32). Mutation(57) or loss of TK2 both cause dNTP pool imbalances(58, 59) which lead to mitochondrial DNA depletion and disease phenotypes. Individuals harboring dGK mutations show liver failure

and neurological abnormalities resulting from depletion of mtDNA(60), from dNTP pool imbalances caused by reduction of dGTP and dATP within the mitochondria(61). Cultured myotubes from patients with dGK deficiency showed the same mitochondrial DNA depletion, which could be partially rescued by supplementation with exogenous dGMP and dAMP(62). Loss of thymidine phosphorylase in the TTP substrate cycle also leads to dNTP pool imbalances and causes destabilization of the mitochondrial genome(63).

Eukaryotic systems also utilize polymerases that can bypass damaged DNA bases. These translesion synthesis (TLS) polymerases show a very low fidelity, sometimes misincorporating an incorrect base with higher efficiency than the correct base(41).

1.3 Ribonucleotide reductase (RNR)

1.3A Introduction to RNR

De novo dNTP biosynthesis takes place in the cytosol(64) and is catalyzed by the conserved enzyme ribonucleotide reductase. RNR is a cytosolic enzyme(65, 66), and dNTPs are shuttled into the nucleus or the mitochondria in order to take part in DNA synthesis and repair. All organisms found have an RNR that belongs to one of 3 classes(67). The differences between the 3 classes is found in which metal cofactor is used for catalysis; Class I has two subclasses, differing in homology of polypeptide sequences and allosteric control patterns. Class I reductases utilize an iron cofactor and are oxygen-dependent(68). *E. coli*, *S. cerevisiae*, and mammals have Class Ia

enzymes(67). Class II enzymes utilize a cobaltous cofactor, while Class III enzymes utilize an iron-sulfur cluster(67).

1.3B RNR structure

The enzyme is composed of two subunits, each proposed to comprise a dimer (Figure 1.4). In yeast, the large or R1 subunit is a homodimer of Rnr1p, while the small (R2) subunit is a heterodimer of Rnr2p and Rnr4p(69, 70). In mammals, RNR is traditionally described as being composed of two homodimers. The large subunit (Figure 1.5) is encoded by a single gene, *Rrm1*, while the small subunit is encoded by either the *Rrm2* or *Rrm2*b (a.k.a. *p53R2*) gene(71) (Figure 1.6). Recent reports have challenged the notion that the bulk of active RNR is an a_2b_2 tetramer, instead suggesting that it is an $\alpha_6\beta_6$ dodecamer(72) or an $\alpha_6\beta_2$ octamer(73). Yeast, but not mammals, also contains a fourth RNR gene, a DNA damage-inducible large subunit Rnr3p(74), which can form a heterodimer with Rnr1p. A homodimer of Rnr3p has low catalytic activity(74).

The large subunit of RNR harbors the catalytic site as well as binding sites for allosteric effectors(67). The small subunit (Figure 1.6) generates a tyrosyl radical which is transferred to the large subunit for catalysis(15, 67, 69, 70, 75). The radical is generated when dioxygen is split to generate 2 water molecules(67). The protons necessary for this come from each iron within the

diiron center and another comes from the tyrosine (Y177 in mammals), generating the radical. The fourth hydrogen is currently of unknown origin, but is speculated to come from an external source(67). Due to the extremely reactive nature of radicals, the radical is generated in a location that is buried about 10 Å inside the protein and is not transferred to the large subunit until substrate is bound(76). However buried the radical may be, it is located at the edge of a channel through the small subunit that is large enough for hydroxyurea to fit in and strip away the radical, thus inhibiting RNR activity(77). Mutation of residues within this channel to bulkier residues blocks access by HU and protects the radical(77). The radical transfer takes place through a proton-coupled electron transfer mechanism and covers a long range and involves many residues(78). Mutation of residues within the path, such as Y370 or Arg 265, decrease or abolish RNR activity by preventing the radical from reaching the catalytic site(78).

The large subunit (Figure 1.5) is composed of three large domains. The largest domain forms an a/b barrel in 2 antiparallel halves. The other 2 domains are a smaller N-terminal domain and excursions of the α/β barrel(79). Protected within the barrel domain is a β-hairpin structure, containing at its tip one of the most important conserved residues, Cys 439(79). Two other conserved redox-active cysteines within the catalytic site serve to abstract the 2'-OH from the substrate(67). The three cysteines are located far apart in the primary structure but are brought into close proximity in the barrel domain,

however not so close that they can form interfering disulfide bonds. They are positioned so as to be able to interact with the 2'- and 3'-OH, while the third cysteine is able to remove the 3'-H during the reaction(79).

(12)

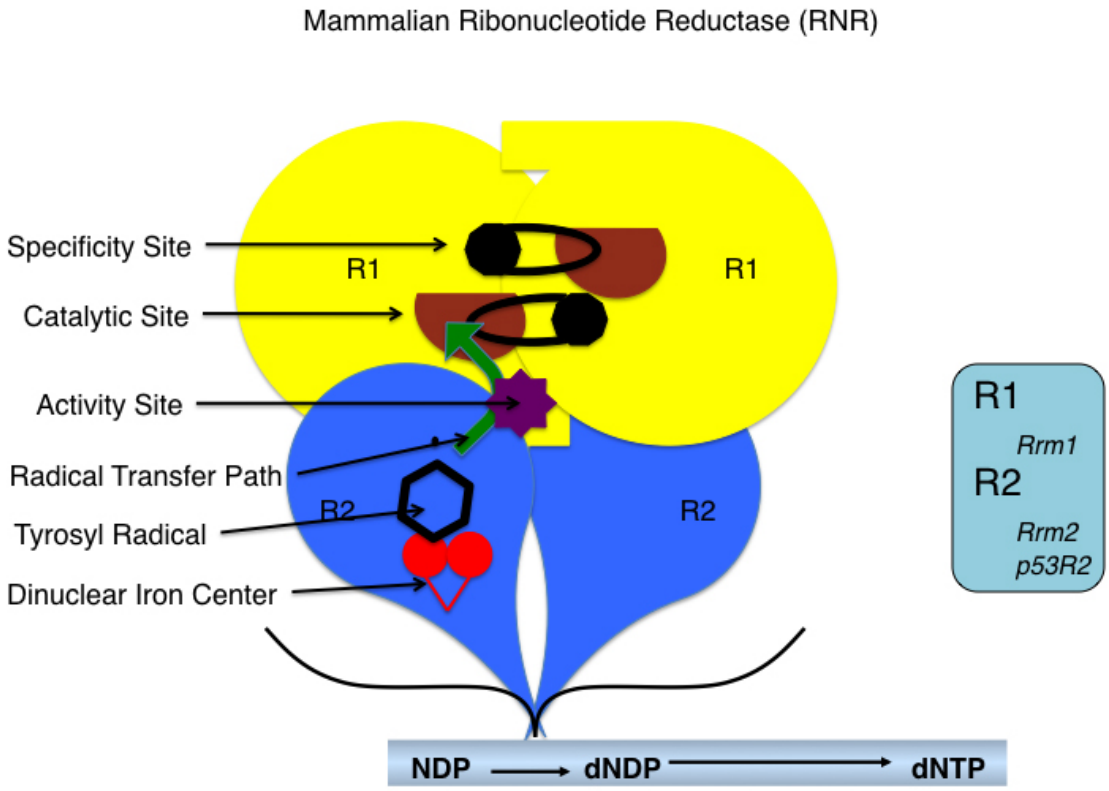

Figure 1.4. Schematic depicting RNR structure. Key enzyme sites are highlighted. General structure is simplified from Eriksson *et al.*(3), Smith *et al.*(1), and Uppsten, *et al.*(5).

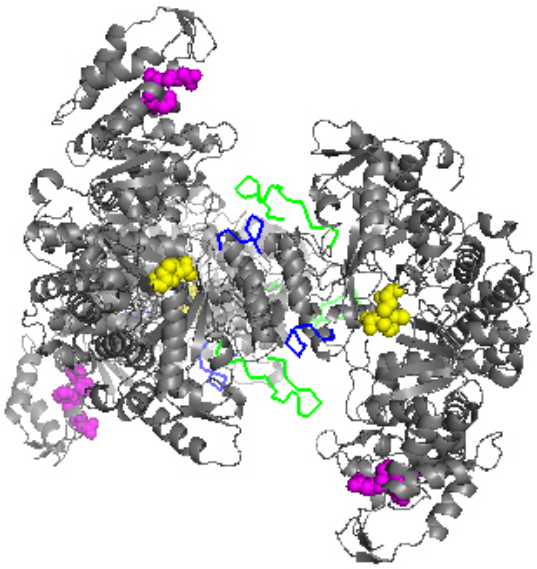

Figure 1.5. Crystal structure of R1 dimer from *E. coli.* Critical sites are highlighted. Yellow, redox-reactive cysteines; magenta, allosteric activity site; blue, specificity site Loop 1; green, specificity site Loop 2. Loop 3 is not visible in this structure. A third R1 monomer is visible in the background but does not interact with either monomer within the dimer, Structure solved by Eriksson *et al.*(3)

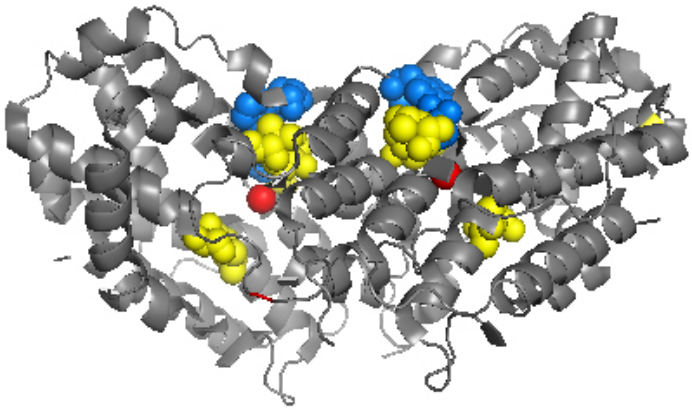

Figure 1.6. Crystal structure of human *p53R2* protein. Critical residues are highlighted. Red, iron cofactor; yellow, iron-coordinating residues; blue, radical transfer pathway. Structure was solved by Smith *et al.*(1).

1.3C Regulation of RNR in yeast

Yeast RNR is a tetramer encoded by four separate genes. *RNR1* encodes the large subunit and is expressed in a cell-cycle dependent manner(80). *rnr1D* is lethal to yeast. *RNR2* and *RNR4* together encode the small subunits(81), which in the active complex form a heterodimer(70). Rnr2p generates a tyrosine radical that is necessary for catalysis, while Rnr4p does not contain an iron center and cannot generate a radical(70, 81). The fourth RNR gene is encoded by *RNR3*, which is a DNA damage-inducible large subunit(74).

In yeast, RNR activity is controlled by four known mechanisms with possibly more yet to be discovered. Three of the four mechanisms seem to be of equal importance, as disabling each of these independently shows the same phenotype. Primarily, RNR activity is limited to S-phase in the cell cycle by limiting the availability of the large subunit protein(80), and overall activity is limited by allosteric feedback control through an activity site within the large subunit(82). Substrate choice is controlled by a second allosteric regulatory site, the specificity site(80). An equally important mechanism is direct inhibition by the small protein *SML1* in *S. cerevisiae*(83). A similar protein in the fission yeast *Schizosaccharomyces pombe*, Spd1, performs the same function(84). To date, no similar small protein has been found in mammals. The fourth RNR regulatory mechanism in yeast is differential subcellular localization, in which in the absence of DNA damage, Wtm1 anchors both Rnr2p and Rnr4p in the

nucleus while Rnr1p is cytoplasmic(85, 86). Following DNA damage, Rnr2p and Rnr4p translocate to the cytoplasm to form a complex with Rnr1p to produce dNTPs. During S-phase, Rnr2p and Rnr4p are found in both the nucleus and the cytoplasm, while Rnr1p remains cytoplasmic(85).

Mutation of *SML1* was originally noted to be able to suppress the lethality caused by loss of the essential checkpoint kinase *MEC1*(87). During DNA replication, encounters with DNA damage causes activation of a stress response and a signaling cascade, which ultimately results in the repair of DNA damage. In the absence of *MEC1*, the cells cannot recover from the replication stress and accumulate ssDNA which is prone to breakage, ultimately killing the cell(88). *sml1*D functions to increase the dNTP pool. This allows for increased survival by promoting lesion bypass(51) so that during replication, DNA damage is not a complete block to synthesis, and ssDNA does not accumulate, allowing cells to survive(87).

1.3D Allosteric regulation of RNR in mammals

Two sites within the large subunit bind allosteric effectors to influence RNR activity (Figure 1.5). Binding of allosteric effectors not only influences which substrate is bound for reduction, but also stimulates dimerization of the subunits, a step that is necessary for activity. In the specificity site, dATP (or ATP), dGTP, and dTTP bind in order to determine substrate choice, promoting reduction of CDP/UDP, ADP, or GDP, respectively(67). A somewhat-disordered loop (Loop 2) within R1 forms part of this specificity site; mutation

of residues within loop 2 inhibits proper specificity site function and leads to imbalances and mutagenic dNTP pools(89). There is a cross-talk between the specificity and catalytic sites between two large subunit monomers; binding of an effector in the specificity site of one monomer will affect the conformation of Loop 2 and its interaction with the catalytic site of the other monomer, influencing substrate choice (refer back to Figure 1.4) (89, 90). In crystal structures with an effector bound at the specificity site, Loop 2 takes on a conformation that participates in shaping the active site uniquely to fit the proper substrate(91). Further crystal structures of *Rrm1* show that this site, formed from the 100 N-terminal amino acids, is close to where the R2 subunit is proposed to bind and could affect subunit interactions(3). Studies show that in the absence of allosteric effectors, R1 exists as monomers while R2 exists in a dimeric form already. Binding of effectors to the large subunit stimulates formation of the R1 homodimer, which then forms strong associations with the R2 dimer, leading to the active tetramer(92).

A second allosteric site binds ATP and dATP and determines whether RNR activity will continue or not. This is a simple feedback system, such that binding of ATP stimulates activity, while binding dATP signals to the protein that there are enough dNTPs and activity stops(93). It is proposed that the mechanism of dATP inhibition of RNR activity is not through dATP-promoted

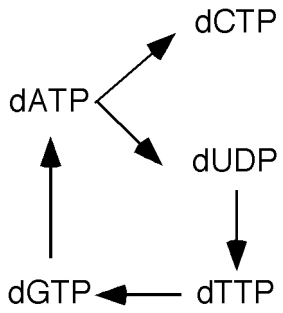

Figure 1.7. Summary of RNR specificity site effects. Binding of dATP within the specificity site promotes reduction of CDP and UDP. dTTP binding promotes reduction of GDP, and dGTP binding promotes reduction of ADP.

subunit dissociation, but through interference of the radical transfer pathway, blocking access by the radical to the catalytic site(92). Interestingly, dATP binding can have both a stimulatory and an inhibitory effect. The affinity for dATP is higher at the specificity site, so the inhibitory effect is only seen at high dNTP concentrations(67). This site will be discussed in detail further.

A third allosteric site was proposed recently, in which ATP binding stimulates hexamerization of the subunits (to an $\alpha_6\beta_6$ structure)(72). The presence of a third allosteric regulatory site would provide a model for the enzyme transitioning from an inactive state to a highly active state in S-phase, to a state (in the tetrameric situation) of lower activity to provide low amounts of dNTPs outside S-phase.

1.3E Regulation of RNR activity in mammals through small subunit availability

In addition to allosteric regulation, RNR activity is controlled by other mechanisms. Mammals limit *Rrm2* protein levels outside of S-phase so that an *Rrm1-Rrm2* complex cannot be formed, and dNTPs are not produced(67, 94). During S-phase, *Rrm2* is transcribed to a maximal level that is unchanged even when DNA damaging agents are introduced, and *Rrm2* protein is stabilized such that levels are constant throughout S-phase, even if damaging agents artificially prolong S-phase(95). It is proposed that in S-phase, the R2 protein is induced to such a high extent that it becomes the excessive subunit and the R1 subunit is therefore limiting(96). *Rrm1* also shows S-phase-specific

transcription(97), but due to a long protein half-life, *Rrm1* protein levels are relatively constant throughout the cell cycle(98). When no longer needed to produce dNTPs for DNA synthesis, *Rrm2* is specifically degraded in M-phase(95), by the APC^{Cdh1} complex(94). Cells that overproduce *Rrm2* by roughly 14-fold were shown to also elevate enzymatic activity 6-fold, further confirming that RNR activity is partially limited by controlling availability of the R2 subunit(99).

p53R2 follows a distinct pattern of regulation from *Rrm2*. Expressed at only low levels throughout the cell cycle(54), *p53R2* is induced by p53 following DNA damage(71, 100). *Rrm2*, but not *p53R2*, contains a KEN box, targeting *Rrm2* for proteolytic degradation by the APC^{Cdh1} complex at M-phase. *p53R2* harbors a dinuclear iron radical-producing center similar to *Rrm2*, and can form an active complex with *Rrm1*(101), although *in vitro* studies on recombinant proteins have indicated lower activity in an *Rrm1-p53R2* complex than in an *Rrm1-Rrm2* complex(102). In quiescent cells, *Rrm2* protein is undetectable, yet dNTP production persists and can be inhibited by treatment with hydroxyurea, indicating that a complex of *Rrm1* and *p53R2* is active(103). A study showed that while purified *Rrm2* was able to oxidize a reporter molecule H_2-DCFDA, purified *p53R2* did not, and in fact was able to scavenge radicals *in vitro*(104).

1.4 RNR plays a role in maintaining genome stability

1.4A Protective functions of RNR

RNR is part of a regulatory pathway in yeast that begins with the Mec1 kinase, the yeast homologue of Atm/Atr. The role of Atr and Mec1 is to survey the genome during S-phase and respond to replication stress, signaling downstream effectors that include RNR(105). Loss of Mec1 is lethal except in the presence of an unlinked suppressor known as *sml1-1*(87). It was found that *sml1-1* is able to suppress *mec1Δ* lethality by allowing for increased activity of RNR, increasing dNTP pools and enabling cells to survive DNA damage(87). Following DNA damage in wild type cells, Sml1p is rapidly degraded, allowing for greater activity and elevating dNTP pools(106).

1.4B RNR and the DNA-damage response

p53R2 is transcriptionally regulated by p53, and contains a p53-binding motif in the first intron(71, 107). Following several types of DNA-damaging events, *p53R2* is induced, producing dNTPs which are then incorporated into DNA as the damage is repaired(107). In human oropharyngeal cancer (KB) cells, UV irradiation induced expression not only of *p53R2* but also of *Rrm2*, while in a p53-null cancer cell line, UV irradiation only induced expression of *Rrm2*(108). A separate study reports that *Rrm1* is also induced following UV irradiation, forming the holoenzyme with *p53R2* in order to generate dNTPs for repair(101). This same study failed to detect *Rrm2* induction following UV treatment, in opposition to the previous study(101). Furthermore, ectopic

expression of high-risk human papilloma virus oncoproteins suppressed *p53R2* induction following oxidative stress, and cells derived from HPV-positive cervical carcinoma cells were completely unable to elevate *p53R2* following H_2O_2 treatment, suggesting that carcinogenesis is inhibited by *p53R2* expression(109).

In yeast, DNA damage induces expression of each RNR gene(74, 81, 82). RNR is also released from its regulatory constraints; Sml1p is degraded(83) and Wtm1p allows Rnr2p and Rnr4p to translocate to the cytosol(86), permitting ribonucleotide reduction and elevating dNTP pools for DNA repair(82). Following DNA damage in mammals, *p53R2* is induced, presumably in order to provide dNTPs for DNA repair(71). However, unlike in yeast, an increase in dNTP pools was not observed after DNA damage in mammalian cells (54). It was found that while *p53R2* was induced and complexed with *Rrm1*, the dNTPs produced were used directly for DNA repair. Treatment of cells following DNA damage with hydroxyurea caused a decrease in dNTP pools, indicating that *p53R2* was actively producing dNTPs(54).

1.4C Mutagenic effects of RNR deregulation

Overexpression of Rnr1p or expression of a feedback-resistant mutant of Rnr1p, *rnr1-D57N*, in yeast results in increased dNTPs levels(52, 82, 110, 111) and an increased mutation rate, as would be expected from previous discussions of the fidelity of each replicative DNA polymerase. Somewhat

paradoxically, these increases are associated with improved survival following DNA damage. This is hypothesized to be due to an ability of cells to bypass DNA lesions or promote restart of stalled replication forks when enough (i.e. excessive) dNTPs are available, resulting in increased point mutations but decreased chromosomal rearrangements, such as sister-chromatid exchanges(52, 82).

The previous manipulations had the effect of generating elevated dNTP pools within yeast. However, unbalanced dNTP pools can also be extremely mutagenic. Unbalanced dNTP pools were generated in yeast by mutating various residues within Loop 2, thereby disrupting the specificity site function. These mutations all generated a mutator phenotype(89). Furthermore, mutations which generated pools in which at least one dNTP was depleted activated the intra-S-phase checkpoint(89).

1.4D RNR and carcinogenesis

RNR also has several links to cancer. In a colorectal adenocarcinoma-derived cell line (HCT116), *p53R2* contains a point mutation which decreases enzyme activity by the *Rrm1-p53R2* complex(107). Overexpression of *Rrm2* in KB cells also led to hydroxyurea resistance and increased invasive potential(99).

In mice, overexpression of either *Rrm2* or *p53R2* elevated lung cancer incidence in FVB mice, a background strain that is particularly susceptible to lung tumorigenesis(112). Overexpression of *Rrm1* did not lead to lung

tumorigenesis, and another study reports that ***Rrm1*** overexpression is protective in an induced lung cancer model(113), and suppresses metastasis and invasion in cancer cells through PTEN induction(114). Both *Rrm2* and *p53R2* overexpression were able to synergize with deletion of *Msh6* in mice to reduce lifespan, while again, *Rrm1* overexpression was not(112), indicating that *Rrm2* and *p53R2* overexpression is mutagenic. The lack of mutagenesis in *Rrm1*-overexpressing mice can have several possible explanations. Firstly, the *Rrm1* transgene showed limited overexpression in mouse tissues, while both *Rrm2* and *p53R2* were highly overexpressed in a broad range of tissues, most notably the lungs. Cell-cycle regulation of RNR is also a factor, as the *Rrm1* protein is expressed at relatively constant levels throughout the cell cycle and is normally in excess, so that additional overexpression has limited effects. Meanwhile, *Rrm2* and *p53R2* are either tightly limited to S-phase or expressed at low levels, so that constantly high-level overexpression represents a complete loss of a regulatory mechanism. Lastly, both *Rrm2* and *p53R2* participate to form a free radical for catalysis, so elevated oxidative stress within the lungs (already a high-oxygen environment) overwhelms the DNA damage-repair machinery and leads to transformation and tumorigenesis. These possibilities are not mutually exclusive, however, and further work is underway to dissect the molecular mechanisms of RNR-induced lung tumorigenesis.

1.4E RNR and mitochondrial genome maintenance

Consistent with a role for *p53R2* in maintaining genomic stability, it was found that *p53R2*-knockout mice are inviable(115). These mice die at around 3 months of age from severe renal failure, and have depletion of mitochondrial DNA. The link between *p53R2* and mitochondrial DNA maintenance is further supported by the discovery of *p53R2* truncating mutations(116) and a homozygous missense mutation (G229V)(117) in humans with severe mtDNA depletion. Two other missense mutations were also reported that are proposed to interfere with the *Rrm1*/*p53R2* docking interface and reduce enzyme activity, again causing mitochondrial DNA depletion and mitochondrial neurogastrointestinal encephalopathy (MNGIE)(118).

In yeast, overexpression of the large (limiting) subunit of RNR, RNR1p, causes an expansion of mtDNA and can rescue mtDNA depletion. Similarly, mtDNA levels are elevated when a hyperactive mutant of RNR1p is expressed at physiological levels(82). Both treatments have previously been shown to elevate dNTP pools, indicating that nucleotide levels are an important determinant of mtDNA copy number. Interestingly, it was found that dNTPs are not limiting for mtDNA synthesis, as these changes lengthen the cell cycle, allowing more time for mtDNA synthesis at a normal rate. Deletion of *RAD53* also lengthens the cell cycle, and allows for mtDNA accumulation independently of dNTP levels(119).

1.5 *Rrm1*^{D57N}, a feedback-resistant large RNR subunit

The existence of separate regulatory sites within the enzyme was demonstrated by studies in murine lymphoma cell lines(93, 111, 120). Two separate cell lines exhibiting altered nucleotide pools were selected, and each had a mutator phenotype(93). Cells were selected to survive in an excess of dGTP, which normally stimulates the production of dATP, and inhibits CDP reduction(93). These cells were still sensitive to dATP inhibition, indicating that there are 2 sites that bind allosteric effectors, and only one was mutated(93, 120). Cells were also selected that were resistant to dATP inhibition. RNR from these cells was stimulated by dATP binding when it should be inhibited(93). The mutation responsible for the dATP insensitivity was mapped to the third exon of *Rrm1*, and is a G-to-A transition at codon 57 (D57N)(111). The question was posed as to whether the activity site of RNR is unresponsive to dATP due to a lowered affinity of binding dATP, or if affinity is unchanged but the ability to distinguish ATP from dATP is lost. Studies on the corresponding residue (His 59) in the *E. coli* R1 homologue (*NrdA*) show that mutant proteins are 1) able to bind dATP with the same affinity as wild type; and 2) dATP binding in both the wild type and mutant proteins increases the association between the R1 and R2 subunits(121). These studies support the model proposed by Ingemarson and Uhlin(92), that dATP inhibition does not involve dissociation of the subunits, and further indicates that dATP insensitivity is through the inability to distinguish ATP from dATP in the activity

site. In transfected mammalian cells, the *Rrm1*^{D57N} mutation caused elevated and dATP-resistant RNR activity, which conferred a mutator phenotype(111).

In yeast, mutation of Rnr1p to *rnr1-D57N* results in 2-fold elevated (but balanced) dNTP pools, which lead to a 3-fold increase in mutation rate, as measured by canavanine resistance(82). The mutator phenotype was confirmed in a second study that found a synergistic increase in canavanine resistance when *rnr1-D57N* was combined with deletion of MutSa components Msh2 or Msh6(112). Also in yeast, constitutive overexpression of *rnr1-D57N* had a more dramatic phenotype, increasing pools of dNTPs while also decreasing pools of NTPs(110). This had the effect of slowing the cell cycle and preventing entry into S-phase, but did not trigger activation of the S-phase checkpoint(110). The DNA-damage checkpoint was actually inhibited in these cells, possibly because dNTP pools were already elevated.

1.6 Summary and remaining questions

This chapter discussed how nucleotides are generated and maintained, how they affect DNA replication and impact genome stability, and how RNR specifically is regulated and how it controls nucleotide pools and genome stability. The details of RNR regulation in mammals are still something of an unknown, however. Previous work has revealed that the basic regulatory mechanisms discovered in other organisms such as allosteric feedback control and transcriptional control, are present in mammals(25, 95, 120). It is still unknown how these mechanisms interact, and what is the impact of disabling

regulatory control of RNR. In yeast, RNR can be manipulated through overexpression or by loss of allosteric site function to elevate RNR activity, but whether these same manipulations alter RNR activity in mammals is untested. The main questions we want to answer are: how do the two main RNR regulatory mechanisms interact in mammals? What physiological function does RNR play in genome maintenance? Can RNR activity by manipulated through overexpression or hyperactivity, and can this have a therapeutic value for treatment of MDS?

We have demonstrated the consequences of overexpressing either small subunit of RNR in mice. However, aside from generating lung tumors in mice, the full effects of *Rrm2* and *p53R2* overexpression are still unknown, in terms of RNR activity and dNTP pool effects. Moreover, we expect that lung tumorigenesis is caused by nuclear genome instability, but the impact on mitochondrial genome stability cannot be ascertained from those experiments. Previous work in mice and yeast has shown that dysfunction of RNR causes mitochondrial genome instability and that unbalanced nucleotide pools can cause mtDNA depletion. In yeast, overexpression of Rnr1p causes elevated mtDNA levels. It still remains to be seen whether similar RNR manipulation in mammals can cause increases in mtDNA content.

RNR can be further deregulated in mammals. For example, simultaneous overexpression of *Rrm1* and *Rrm2* or *p53R2* might be expected to further deregulate the enzyme and create a more hyperactive RNR.

Alternative methods to deregulate RNR in mammals may also be employed. The effect of the feedback-insensitive mutant *Rrm1*^{D57N} is known in cultured mammalian cells and yeast, but the effect of expressing that mutant in a multicellular organism is unknown. Lastly, overexpressing the feedback-insensitive mutant *Rrm1*D57N simultaneously disabled both main regulatory mechanisms in yeast. In mice, this could be accomplished by overexpressing either small RNR subunit in the presence of the *Rrm1*^{D57N} mutant. If simultaneous disruption of both RNR regulatory mechanisms has the same effect in mammals as it has in yeast, we would expect that the slow cell proliferation would cause lethality during embryonic time points. Together, these experiments will allow us to more fully understand the importance of RNR regulation in mammals.

In Chapter 2, I generated mice that overexpress multiple RNR subunits. With collaborators, I found that *Rrm1*^{Tg} + *Rrm2*^{Tg} and *Rrm1*^{Tg} + *p53R2*^{Tg} bitransgenic mice displayed altered RNR activity, which generated unbalanced dNTP pools and caused late-onset mitochondrial DNA depletion. In Chapter 3, we deregulated RNR by disabling the other main regulatory mechanism, allosteric feedback control. I found that mice with one regulatory mechanism of RNR disabled were grossly normal, but mice in which both main regulatory mechanisms were disabled are not viable. In Chapter 4, I generated mice in which the *Rrm1-D57N* allele was knocked in to the endogenous locus. I found

that mice homozygous for the mutant allele are not viable, and die during embryonic time points.

References

1. Smith P, Zhou B, Ho N, Yuan YC, Su L, Tsai SC, et al. 2.6 A X-ray crystal structure of human p53R2, a p53-inducible ribonucleotide reductase. Biochemistry. 2009;48(46):11134-41. PMCID: 2844085.

2. Ferraro P, Pontarin G, Crocco L, Fabris S, Reichard P, Bianchi V. Mitochondrial deoxynucleotide pools in quiescent fibroblasts: a possible model for mitochondrial neurogastrointestinal encephalomyopathy (MNGIE). J Biol Chem. 2005;280(26):24472-80.

3. Eriksson M, Uhlin U, Ramaswamy S, Ekberg M, Regnstrˆm K, Sjˆberg B, et al. Binding of allosteric effectors to ribonucleotide reductase protein R1: reduction of active-site cysteines promotes substrate binding. Structure. 1997;5(8):1077-92.

4. Leanza L, Ferraro P, Reichard P, Bianchi V. Metabolic interrelations within guanine deoxynucleotide pools for mitochondrial and nuclear DNA maintenance. Journal of Biological Chemistry. 2008;283(24):16437.

5. Uppsten M, Farnegardh M, Domkin V, Uhlin U. The first holocomplex structure of ribonucleotide reductase gives new insight into its mechanism of action. Journal of molecular biology. 2006;359(2):365-77.

6. Carter CE. Metabolism of purines and pyrimidines. Annu Rev Biochem. 1956;25:123-46.

7. Kornberg A, Lieberman I, Simms ES. Enzymatic synthesis and properties of 5-phosphoribosylpyrophosphate. J Biol Chem. 1955;215(1):389-402.

8. Holden H, Thoden J, Raushel F. Carbamoyl phosphate synthetase: an amazing biochemical odyssey from substrate to product. Cellular and Molecular Life Sciences. 1999;56(5):507-22.

9. Huang M, Graves L. De novo synthesis of pyrimidine nucleotides; emerging interfaces with signal transduction pathways. Cellular and Molecular Life Sciences. 2003;60(2):321-36.

10. Jones M. Pyrimidine nucleotide biosynthesis in animals: genes, enzymes, and regulation of UMP biosynthesis. Annual review of biochemistry. 1980;49(1):253-79.

11. Lieberman I, Kornberg A. Enzymatic synthesis and breakdown of a pyrimidine, orotic acid. I. Dihydroortic acid, ureidosuccinic acid, and 5-carboxymethylhydantoin. J Biol Chem. 1954;207(2):911-24.

12. Nordlund P, Reichard P. Ribonucleotide reductases. Annu Rev Biochem. 2006;75:681-706.

13. Reichard P. Interactions between deoxyribonucleotide and DNA synthesis. Annual review of biochemistry. 1988;57(1):349-74.

14. Bianchi V, Pontis E, Reichard P. Interrelations between substrate cycles and de novo synthesis of pyrimidine deoxyribonucleoside triphosphates in 3T6 cells. Proceedings of the National Academy of Sciences of the United States of America. 1986;83(4):986.

15. Nordlund P, Reichard P. Ribonucleotide reductases. 2006.

16. Carreras C, Santi D. The catalytic mechanism and structure of thymidylate synthase. Annual review of biochemistry. 1995;64(1):721-62.

17. Hartman S. Phosphoribosyl pyrophosphate amidotransferase. Journal of Biological Chemistry. 1963;238(9):3024.

18. Smith J. Glutamine PRPP amidotransferase: snapshots of an enzyme in action. Current opinion in structural biology. 1998;8(6):686-94.

19. Smith J. Enzymes of nucleotide synthesis. Current opinion in structural biology. 1995;5(6):752-7.

20. Hartman S, Buchanan J. Nucleic acids, purines, pyrimidines (nucleotide synthesis). Annual review of biochemistry. 1959;28(1):365-410.

21. Murray A. The biological significance of purine salvage. Annual review of biochemistry. 1971;40(1):811-26.

22. Frangini M, Rampazzo C, Franzolin E, Lara MC, Vila MR, Marti R, et al. Unchanged thymidine triphosphate pools and thymidine metabolism in two lines of thymidine kinase 2-mutated fibroblasts. FEBS J. 2009;276(4):1104-13.

23. Saada A. Deoxyribonucleotides and disorders of mitochondrial DNA integrity. DNA Cell Biol. 2004;23(12):797-806.

24. Ke PY, Kuo YY, Hu CM, Chang ZF. Control of dTTP pool size by anaphase promoting complex/cyclosome is essential for the maintenance of genetic stability. Genes Dev. 2005;19(16):1920-33. PMCID: 1186191.

25. Chabes AL, Bjorklund S, Thelander L. S Phase-specific transcription of the mouse ribonucleotide reductase R2 gene requires both a proximal repressive E2F-binding site and an upstream promoter activating region. J Biol Chem. 2004;279(11):10796-807.

26. Gazziola C, Ferraro P, Moras M, Reichard P, Bianchi V. Cytosolic high K M 5 -nucleotidase and 5 (3)-deoxyribonucleotidase in substrate cycles involved in nucleotide metabolism. Journal of Biological Chemistry. 2001;276(9):6185.

27. Hˆglund L, Reichard P. Cytoplasmic 5'(3')-nucleotidase from human placenta. Journal of Biological Chemistry. 1990;265(12):6589.

28. Bianchi V. Regulation of deoxynucleotide pools by substrate cycles. Adv Exp Med Biol. 1998;431:501-6.

29. Hˆglund L, Pontis E, Reichard P. Effects of deoxycytidine and thymidine kinase deficiency on substrate cycles between deoxyribonucleosides and their 5 -phosphates. Cancer research. 1988;48(13):3681.

30. Gallinaro L, Crovatto K, Rampazzo C, Pontarin G, Ferraro P, Milanesi E, et al. Human Mitochondrial 5 -Deoxyribonucleotidase. Journal of Biological Chemistry. 2002;277(38):35080.

31. Pugmire M, Ealick S. Structural analyses reveal two distinct families of nucleoside phosphorylases. Biochemical Journal. 2002;361(Pt 1):1.

32. Song S, Wheeler LJ, Mathews CK. Deoxyribonucleotide pool imbalance stimulates deletions in HeLa cell mitochondrial DNA. J Biol Chem. 2003;278(45):43893-6.

33. Blackburn MR, Aldrich M, Volmer JB, Chen W, Zhong H, Kelly S, et al. The use of enzyme therapy to regulate the metabolic and phenotypic consequences of adenosine deaminase deficiency in mice. Differential impact on pulmonary and immunologic abnormalities. J Biol Chem. 2000;275(41):32114-21.

34. Blackburn MR, Kellems RE. Adenosine deaminase deficiency: metabolic basis of immune deficiency and pulmonary inflammation. Adv Immunol. 2005;86:1-41.

35. Mazzali M, Hughes J, Kim YG, Jefferson JA, Kang DH, Gordon KL, et al. Elevated uric acid increases blood pressure in the rat by a novel crystal-independent mechanism. Hypertension. 2001;38(5):1101-6.

36. Guyenet P. The sympathetic control of blood pressure. Nature Reviews Neuroscience. 2006;7(5):335-46.

37. Zandi-Nejad K, Luyckx V, Brenner B. Adult hypertension and kidney disease: the role of fetal programming. Hypertension. 2006;47(3):502.

38. Feig DI, Nakagawa T, Karumanchi SA, Oliver WJ, Kang DH, Finch J, et al. Hypothesis: Uric acid, nephron number, and the pathogenesis of essential hypertension. Kidney Int. 2004;66(1):281-7.

39. Wu X, Wakamiya M, Vaishnav S, Geske R, Montgomery C, Jr., Jones P, et al. Hyperuricemia and urate nephropathy in urate oxidase-deficient mice. Proc Natl Acad Sci U S A. 1994;91(2):742-6. PMCID: 43025.

40. Thomas D, Roberts J, Sabatino R, Myers T, Tan C, Downey K, et al. Fidelity of mammalian DNA replication and replicative DNA polymerases. Biochemistry. 1991;30(51):11751-9.

41. Kunkel T. DNA replication fidelity. Journal of Biological Chemistry. 2004;279(17):16895.

42. McCulloch S, Kunkel T. The fidelity of DNA synthesis by eukaryotic replicative and translesion synthesis polymerases. Cell research. 2008;18(1):148-61.

43. Byrnes JJ, Downey KM, Black VL, So AG. A new mammalian DNA polymerase with 3' to 5' exonuclease activity: DNA polymerase delta. Biochemistry. 1976;15(13):2817-23.

44. Nick McElhinny SA, Gordenin DA, Stith CM, Burgers PM, Kunkel TA. Division of labor at the eukaryotic replication fork. Mol Cell. 2008;30(2):137-44. PMCID: 2654179.

45. Pavlov Y, Frahm C, McElhinny S, Niimi A, Suzuki M, Kunkel T. Evidence that Errors Made by DNA Polymerase [alpha] are Corrected by DNA Polymerase [delta]. Current Biology. 2006;16(2):202-7.

46. Pursell ZF, Isoz I, Lundstrom EB, Johansson E, Kunkel TA. Yeast DNA polymerase epsilon participates in leading-strand DNA replication. Science. 2007;317(5834):127-30. PMCID: 2233713.

47. Kunkel T, Mosbaugh D. Exonucleolytic proofreading by a mammalian DNA polymerase. gamma. Biochemistry. 1989;28(3):988-95.

48. Trifunovic A, Wredenberg A, Falkenberg M, Spelbrink J, Rovio A, Bruder C, et al. Premature ageing in mice expressing defective mitochondrial DNA polymerase. Nature. 2004;429(6990):417-23.

49. Zheng W, Khrapko K, Coller H, Thilly W, Copeland W. Origins of human mitochondrial point mutations as DNA polymerase [gamma]-mediated errors. Mutation Research/Fundamental and Molecular Mechanisms of Mutagenesis. 2006;599(1-2):11-20.

50. Rampazzo C, Ferraro P, Pontarin G, Fabris S, Reichard P, Bianchi V. Mitochondrial deoxyribonucleotides, pool sizes, synthesis, and regulation. J Biol Chem. 2004;279(17):17019-26.

51. Sabouri N, Viberg J, Goyal DK, Johansson E, Chabes A. Evidence for lesion bypass by yeast replicative DNA polymerases during DNA damage. Nucleic Acids Res. 2008;36(17):5660-7. PMCID: 2553575.

52. Fasullo M, Tsaponina O, Sun M, Chabes A. Elevated dNTP levels suppress hyper-recombination in Saccharomyces cerevisiae S-phase checkpoint mutants. Nucleic Acids Res. 2010;38(4):1195-203. PMCID: 2831302.

53. Kunz B, Kohalmi S. Modulation of mutagenesis by deoxyribonucleotide levels. Annual review of genetics. 1991;25(1):339-59.

54. Hakansson P, Hofer A, Thelander L. Regulation of mammalian ribonucleotide reduction and dNTP pools after DNA damage and in resting cells. J Biol Chem. 2006;281(12):7834-41.

55. Song S, Pursell Z, Copeland W, Longley M, Kunkel T, Mathews C. DNA precursor asymmetries in mammalian tissue mitochondria and possible contribution to mutagenesis through reduced replication fidelity. Proceedings of the National Academy of Sciences of the United States of America. 2005;102(14):4990.

56. Ferraro P, Nicolosi L, Bernardi P, Reichard P, Bianchi V. Mitochondrial deoxynucleotide pool sizes in mouse liver and evidence for a transport mechanism for thymidine monophosphate. Proc Natl Acad Sci U S A. 2006;103(49):18586-91. PMCID: 1693706.

57. Akman HO, Dorado B, Lopez LC, Garcia-Cazorla A, Vila MR, Tanabe LM, et al. Thymidine kinase 2 (H126N) knockin mice show the essential role of

balanced deoxynucleotide pools for mitochondrial DNA maintenance. Hum Mol Genet. 2008;17(16):2433-40.

58. Zhou X, Solaroli N, Bjerke M, Stewart JB, Rozell B, Johansson M, et al. Progressive loss of mitochondrial DNA in thymidine kinase 2-deficient mice. Hum Mol Genet. 2008;17(15):2329-35.

59. Ashley N, Adams S, Slama A, Zeviani M, Suomalainen A, Andreu AL, et al. Defects in maintenance of mitochondrial DNA are associated with intramitochondrial nucleotide imbalances. Hum Mol Genet. 2007;16(12):1400-11.

60. Mandel H, Szargel R, Labay V, Elpeleg O, Saada A, Shalata A, et al. The deoxyguanosine kinase gene is mutated in individuals with depleted hepatocerebral mitochondrial DNA. Nat Genet. 2001;29(3):337-41.

61. Saada A. Mitochondrial deoxyribonucleotide pools in deoxyguanosine kinase deficiency. Mol Genet Metab. 2008;95(3):169-73.

62. Bulst S, Abicht A, Holinski-Feder E, Muller-Ziermann S, Koehler U, Thirion C, et al. In vitro supplementation with dAMP/dGMP leads to partial restoration of mtDNA levels in mitochondrial depletion syndromes. Hum Mol Genet. 2009;18(9):1590-9.

63. Nishino I, Spinazzola A, Hirano M. Thymidine phosphorylase gene mutations in MNGIE, a human mitochondrial disorder. Science. 1999;283(5402):689-92.

64. Pontarin G, Fijolek A, Pizzo P, Ferraro P, Rampazzo C, Pozzan T, et al. Ribonucleotide reduction is a cytosolic process in mammalian cells independently of DNA damage. Proc Natl Acad Sci U S A. 2008;105(46):17801-6. PMCID: 2584719.

65. Engstrom Y, Rozell B, Hansson HA, Stemme S, Thelander L. Localization of ribonucleotide reductase in mammalian cells. EMBO J. 1984;3(4):863-7. PMCID: 557439.

66. Engstrom Y, Rozell B. Immunocytochemical evidence for the cytoplasmic localization and differential expression during the cell cycle of the M1 and M2 subunits of mammalian ribonucleotide reductase. EMBO J. 1988;7(6):1615-20. PMCID: 457144.

67. Kolberg M, Strand KR, Graff P, Andersson KK. Structure, function, and mechanism of ribonucleotide reductases. Biochim Biophys Acta. 2004;1699(1-2):1-34.

68. Gon S, Beckwith J. Ribonucleotide reductases: influence of environment on synthesis and activity. Antioxid Redox Signal. 2006;8(5-6):773-80.

69. Ortigosa AD, Hristova D, Perlstein DL, Zhang Z, Huang M, Stubbe J. Determination of the in vivo stoichiometry of tyrosyl radical per betabeta' in Saccharomyces cerevisiae ribonucleotide reductase. Biochemistry. 2006;45(40):12282-94.

70. Chabes A, Domkin V, Larsson G, Liu A, Graslund A, Wijmenga S, et al. Yeast ribonucleotide reductase has a heterodimeric iron-radical-containing subunit. Proc Natl Acad Sci U S A. 2000;97(6):2474-9. PMCID: 15953.

71. Tanaka H, Arakawa H, Yamaguchi T, Shiraishi K, Fukuda S, Matsui K, et al. A ribonucleotide reductase gene involved in a p53-dependent cell-cycle checkpoint for DNA damage. Nature. 2000;404(6773):42-9.

72. Kashlan O, Scott C, Lear J, Cooperman B. A Comprehensive Model for the Allosteric Regulation of Mammalian Ribonucleotide Reductase. Functional Consequences of ATP-and dATP-Induced Oligomerization of the Large SubunitÜ. Biochemistry. 2002;41(2):462-74.

73. Rofougaran R, Vodnala M, Hofer A. Enzymatically active mammalian ribonucleotide reductase exists primarily as an 6 2 octamer. Journal of Biological Chemistry. 2006;281(38):27705.

74. Domkin V, Thelander L, Chabes A. Yeast DNA damage-inducible Rnr3 has a very low catalytic activity strongly stimulated after the formation of a cross-talking Rnr1/Rnr3 complex. J Biol Chem. 2002;277(21):18574-8.

75. Tong W, Burdi D, Riggs-Gelasco P, Chen S, Edmondson D, Huynh BH, et al. Characterization of Y122F R2 of Escherichia coli ribonucleotide reductase by time-resolved physical biochemical methods and X-ray crystallography. Biochemistry. 1998;37(17):5840-8.

76. Uhlin U, Eklund H. Structure of ribonucleotide reductase protein R1. Nature. 1994;370(6490):533-9.

77. Sneeden JL, Loeb LA. Mutations in the R2 subunit of ribonucleotide reductase that confer resistance to hydroxyurea. J Biol Chem. 2004;279(39):40723-8.

78. Narvaez AJ, Voevodskaya N, Thelander L, Graslund A. The involvement of Arg265 of mouse ribonucleotide reductase R2 protein in proton transfer and catalysis. J Biol Chem. 2006;281(36):26022-8.

79. Uhlin U, Eklund H. The Ten-stranded [beta]/[alpha] Barrel in Ribonucleotide Reductase Protein R1. Journal of molecular biology. 1996;262(3):358-69.

80. Elledge SJ, Zhou Z, Allen JB. Ribonucleotide reductase: regulation, regulation, regulation. Trends Biochem Sci. 1992;17(3):119-23.

81. Wang PJ, Chabes A, Casagrande R, Tian XC, Thelander L, Huffaker TC. Rnr4p, a novel ribonucleotide reductase small-subunit protein. Mol Cell Biol. 1997;17(10):6114-21. PMCID: 232461.

82. Chabes A, Georgieva B, Domkin V, Zhao X, Rothstein R, Thelander L. Survival of DNA damage in yeast directly depends on increased dNTP levels allowed by relaxed feedback inhibition of ribonucleotide reductase. Cell. 2003;112(3):391-401.

83. Chabes A, Domkin V, Thelander L. Yeast Sml1, a protein inhibitor of ribonucleotide reductase. Journal of Biological Chemistry. 1999;274(51):36679.

84. Hakansson P, Dahl L, Chilkova O, Domkin V, Thelander L. The Schizosaccharomyces pombe replication inhibitor Spd1 regulates ribonucleotide reductase activity and dNTPs by binding to the large Cdc22 subunit. J Biol Chem. 2006;281(3):1778-83.

85. Yao R, Zhang Z, An X, Bucci B, Perlstein D, Stubbe J, et al. Subcellular localization of yeast ribonucleotide reductase regulated by the DNA replication and damage checkpoint pathways. Proceedings of the National Academy of Sciences. 2003;100(11):6628.

86. Lee YD, Elledge SJ. Control of ribonucleotide reductase localization through an anchoring mechanism involving Wtm1. Genes Dev. 2006;20(3):334-44. PMCID: 1361704.

87. Zhao X, Muller EG, Rothstein R. A suppressor of two essential checkpoint genes identifies a novel protein that negatively affects dNTP pools. Mol Cell. 1998;2(3):329-40.

88. Feng W, Collingwood D, Boeck M, Fox L, Alvino G, Fangman W, et al. Genomic mapping of single-stranded DNA in hydroxyurea-challenged yeasts identifies origins of replication. Nature cell biology. 2006;8(2):148-55.

89. Kumar D, Viberg J, Nilsson AK, Chabes A. Highly mutagenic and severely imbalanced dNTP pools can escape detection by the S-phase checkpoint. Nucleic Acids Res. 2010.

90. Reichard P, Eliasson R, Ingemarson R, Thelander L. Cross-talk between the allosteric effector-binding sites in mouse ribonucleotide reductase. J Biol Chem. 2000;275(42):33021-6.

91. Larsson KM, Jordan A, Eliasson R, Reichard P, Logan DT, Nordlund P. Structural mechanism of allosteric substrate specificity regulation in a ribonucleotide reductase. Nat Struct Mol Biol. 2004;11(11):1142-9.

92. Ingemarson R, Thelander L. A Kinetic Study on the Influence of Nucleoside Triphosphate Effectors on Subunit Interaction in Mouse Ribonucleotide ReductaseÜ. Biochemistry. 1996;35(26):8603-9.

93. Eriksson S, Gudas LJ, Clift SM, Caras IW, Ullman B, Martin DW, Jr. Evidence for genetically independent allosteric regulatory domains of the protein M1 subunit of mouse ribonucleotide reductase. J Biol Chem. 1981;256(19):10193-7.

94. Chabes AL, Pfleger CM, Kirschner MW, Thelander L. Mouse ribonucleotide reductase R2 protein: a new target for anaphase-promoting complex-Cdh1-mediated proteolysis. Proc Natl Acad Sci U S A. 2003;100(7):3925-9. PMCID: 153024.

95. Chabes A, Thelander L. Controlled protein degradation regulates ribonucleotide reductase activity in proliferating mammalian cells during the normal cell cycle and in response to DNA damage and replication blocks. J Biol Chem. 2000;275(23):17747-53.

96. Lin ZP, Belcourt MF, Carbone R, Eaton JS, Penketh PG, Shadel GS, et al. Excess ribonucleotide reductase R2 subunits coordinate the S phase checkpoint to facilitate DNA damage repair and recovery from replication stress. Biochem Pharmacol. 2007;73(6):760-72.

97. Bjorklund S, Skog S, Tribukait B, Thelander L. S-phase-specific expression of mammalian ribonucleotide reductase R1 and R2 subunit mRNAs. Biochemistry. 1990;29(23):5452-8.

98. Engstrom Y, Eriksson S, Jildevik I, Skog S, Thelander L, Tribukait B. Cell cycle-dependent expression of mammalian ribonucleotide reductase. Differential regulation of the two subunits. J Biol Chem. 1985;260(16):9114-6.

99. Zhou B, Tsai P, Ker R, Tsai J, Ho R, Yu J, et al. Overexpression of transfected human ribonucleotide reductase M2 subunit in human cancer cells enhances their invasive potential. Clinical and Experimental Metastasis. 1998;16(1):43-9.

100. Yamaguchi T, Matsuda K, Sagiya Y, Iwadate M, Fujino MA, Nakamura Y, et al. p53R2-dependent pathway for DNA synthesis in a p53-regulated cell cycle checkpoint. Cancer Res. 2001;61(22):8256-62.

101. Guittet O, Hakansson P, Voevodskaya N, Fridd S, Graslund A, Arakawa H, et al. Mammalian p53R2 protein forms an active ribonucleotide reductase in vitro with the R1 protein, which is expressed both in resting cells in response to DNA damage and in proliferating cells. J Biol Chem. 2001;276(44):40647-51.

102. Yen Y, Chu B, Yen C, Shih J, Zhou B. Enzymatic property analysis of p53R2 subunit of human ribonucleotide reductase. Adv Enzyme Regul. 2006;46:235-47.

103. Pontarin G, Ferraro P, Hakansson P, Thelander L, Reichard P, Bianchi V. p53R2-dependent ribonucleotide reduction provides deoxyribonucleotides in quiescent human fibroblasts in the absence of induced DNA damage. J Biol Chem. 2007;282(23):16820-8.

104. Xue L, Zhou B, Liu X, Wang T, Shih J, Qi C, et al. Structurally dependent redox property of ribonucleotide reductase subunit p53R2. Cancer research. 2006;66(4):1900.

105. Elledge SJ, Davis RW. Two genes differentially regulated in the cell cycle and by DNA-damaging agents encode alternative regulatory subunits of ribonucleotide reductase. Genes Dev. 1990;4(5):740-51.

106. Zhao X, Chabes A, Domkin V, Thelander L, Rothstein R. The ribonucleotide reductase inhibitor Sml1 is a new target of the Mec1/Rad53 kinase cascade during growth and in response to DNA damage. EMBO J. 2001;20(13):3544-53. PMCID: 125510.

107. Yamaguchi T, Matsuda K, Sagiya Y, Iwadate M, Fujino M, Nakamura Y, et al. p53R2-dependent pathway for DNA synthesis in a p53-regulated cell cycle checkpoint. Cancer research. 2001;61(22):8256.

108. Zhou B, Liu X, Mo X, Xue L, Darwish D, Qiu W, et al. The human ribonucleotide reductase subunit hRRM2 complements p53R2 in response to UV-induced DNA repair in cells with mutant p53. Cancer research. 2003;63(20):6583.

109. Lembo D, Donalisio M, Cornaglia M, Azzimonti B, Demurtas A, Landolfo S. Effect of high-risk human papillomavirus oncoproteins on p53R2 gene expression after DNA damage. Virus Res. 2006;122(1-2):189-93.

110. Chabes A, Stillman B. Constitutively high dNTP concentration inhibits cell cycle progression and the DNA damage checkpoint in yeast Saccharomyces cerevisiae. Proc Natl Acad Sci U S A. 2007;104(4):1183-8. PMCID: 1783093.

111. Caras IW, Martin DW, Jr. Molecular cloning of the cDNA for a mutant mouse ribonucleotide reductase M1 that produces a dominant mutator phenotype in mammalian cells. Mol Cell Biol. 1988;8(7):2698-704. PMCID: 363480.

112. Xu X, Page JL, Surtees JA, Liu H, Lagedrost S, Lu Y, et al. Broad overexpression of ribonucleotide reductase genes in mice specifically induces lung neoplasms. Cancer Res. 2008;68(8):2652-60. PMCID: 2459241.

113. Gautam A, Bepler G. Suppression of lung tumor formation by the regulatory subunit of ribonucleotide reductase. Cancer Res. 2006;66(13):6497-502.

114. Gautam A, Li Z, Bepler G. RRM1-induced metastasis suppression through PTEN-regulated pathways. Oncogene. 2003;22(14):2135-42.

115. Kimura T, Takeda S, Sagiya Y, Gotoh M, Nakamura Y, Arakawa H. Impaired function of p53R2 in Rrm2b-null mice causes severe renal failure through attenuation of dNTP pools. Nat Genet. 2003;34(4):440-5.

116. Bourdon A, Minai L, Serre V, Jais JP, Sarzi E, Aubert S, et al. Mutation of RRM2B, encoding p53-controlled ribonucleotide reductase (p53R2), causes severe mitochondrial DNA depletion. Nat Genet. 2007;39(6):776-80.

117. Kollberg G, Darin N, Benan K, Moslemi AR, Lindal S, Tulinius M, et al. A novel homozygous RRM2B missense mutation in association with severe mtDNA depletion. Neuromuscul Disord. 2009;19(2):147-50.

118. Shaibani A, Shchelochkov OA, Zhang S, Katsonis P, Lichtarge O, Wong LJ, et al. Mitochondrial neurogastrointestinal encephalopathy due to mutations in RRM2B. Arch Neurol. 2009;66(8):1028-32. PMCID: 2747647.

119. Lebedeva MA, Shadel GS. Cell cycle- and ribonucleotide reductase-driven changes in mtDNA copy number influence mtDNA Inheritance without compromising mitochondrial gene expression. Cell Cycle. 2007;6(16):2048-57. PMCID: 2606055.

120. Weinberg G, Ullman B, Martin DW, Jr. Mutator phenotypes in mammalian cell mutants with distinct biochemical defects and abnormal deoxyribonucleoside triphosphate pools. Proc Natl Acad Sci U S A. 1981;78(4):2447-51. PMCID: 319363.

121. Birgander P, Kasrayan A, Sjˆberg B. Mutant R1 proteins from Escherichia coli class Ia ribonucleotide reductase with altered responses to dATP inhibition. Journal of Biological Chemistry. 2004;279(15):14496.

Chapter 2: Ribonucleotide reductase is not limiting for mitochondrial DNA copy number in mice[1]

ABSTRACT

Ribonucleotide reductase (RNR) is the rate-limiting enzyme in deoxyribonucleoside triphosphate (dNTP) biosynthesis, with important roles in nuclear genome maintenance. RNR is also essential for maintenance of mitochondrial DNA (mtDNA) in mammals. The mechanisms regulating mtDNA copy number in mammals are only being discovered. In budding yeast, RNR overexpression resulted in increased mtDNA levels, and rescued the disease phenotypes caused by a mutant mtDNA polymerase. This raised the question

---

[1]

Emil Ylikallio[1], Jennifer L. Page[2], Xia Xu[2], Milla Lampinen[1], Gerold Bepler[3], Tomomi Ide[4], Henna Tyynismaa[1], Robert S. Weiss[2*] and Anu Suomalainen[1]

Note: This article has been published by Oxford University Press[,5*].

"Ribonucleotide reductase is not limiting for mitochondrial DNA copy number in mice." *Nucleic Acids Res*. 2010 Dec 1;38(22)8208-18.

The authors wish it to be known that, in their opinion, the first two authors should be regarded as joint First Authors.

Author contributions are indicated by author initials within figure legends.

of whether mtDNA copy number increase by RNR induction could be a strategy for treating diseases with mtDNA mutations. We show here that high-level overexpression of RNR subunits (Rrm1, Rrm2 and p53R2; separately or in different combinations) in mice does not result in mtDNA copy number elevation. Instead, simultaneous expression of two RNR subunits leads to imbalanced dNTP pools and progressive mtDNA depletion in the skeletal muscle, without mtDNA mutagenesis. We also show that endogenous RNR transcripts are downregulated in response to large increases of mtDNA in mice, which is indicative of nuclear-mitochondrial crosstalk with regard to mtDNA copy number. Our results establish that RNR is not limiting for mtDNA copy number in mice, and provide new evidence for the importance of balanced dNTP pools in mtDNA maintenance in postmitotic tissues.

INTRODUCTION

Ribonucleotide reductase (RNR) catalyzes the rate-limiting step in *de novo* synthesis of deoxyribonucleoside triphosphates (dNTPs) [reviewed in (1)]. The enzyme is known to contribute to malignant transformation (2, 3). During S-phase, RNR is abundant as a tetramer composed of homodimers of the large Rrm1 and small Rrm2 subunits. In non-cycling cells, Rrm2 is replaced by the alternative small subunit p53R2 (4). The latter is induced by

the tumour suppressor p53 and was initially considered to contribute to nuclear DNA damage responses (5, 6).

Mutation of p53R2 has recently been found to be an important cause of human inherited diseases. Inactivating mutations of *RRM2B*, the gene encoding p53R2, were not associated with neoplasms, but caused early-onset fatal depletion of mitochondrial DNA (mtDNA) (MIM #612075) (7). Similarly, knock-out mice lacking p53R2 exhibited near-total loss of mtDNA and died shortly after weaning (7, 8). We recently reported that a dominant *RRM2B* mutation led to truncated p53R2 and caused adult-onset progressive external ophthalmoplegia (PEO) with multiple mtDNA deletions (9). Certain compound heterozygote *RRM2B* mutations have also been shown to result in mitochondrial neurogastrointestinal encephalopathy (MNGIE; MIM #603041) (10). Defects in p53R2 can therefore cause diseases of differing severity, ranging from fatal multisystem disorders with mtDNA depletion in children, to an adult-onset muscle disorder with multiple mtDNA deletions. These results highlight the essential role of RNR in mtDNA maintenance in postmitotic cells. Increasing mtDNA copy number has emerged as an attractive target of intervention for mtDNA diseases. Even a minimal amount of wild-type mtDNA can compensate a functionally recessive mutant (11). In the budding yeast *Saccharomyces cerevisiae*, RNR overexpression led to elevation of mtDNA copy number (12) and to the rescue of the *petite* phenotype of mtDNA polymerase mutants that carried mutations equivalent to those in autosomal

dominant PEO (13). This suggested that RNR levels, by affecting dNTP pools, might be rate-limiting for mtDNA synthesis, and that increasing the availability of the enzyme might be a tool for increasing mtDNA abundance. Whether RNR induction could increase mtDNA in mammals, as it does in yeast, has so far not been investigated.

In mice, considerable increase of mtDNA copy number has only been achieved in two mouse models, overexpressing the mitochondrial transcription factor A (TFAM) or the mitochondrial DNA helicase Twinkle (14, 15). TFAM is required for mtDNA transcription, but it also binds DNA with low specificity and packages mtDNA in a histone-like manner (16-18). Its levels closely follow mtDNA levels. Twinkle helicase is known to increase mtDNA copy number by affecting the replication initiation rate (19). In this study, we set out to determine whether overexpression of RNR subunits, alone or in combination with each other, influence mtDNA copy number in mammalian tissues.

MATERIALS AND METHODS

Generation of transgenic mice

The $Rrm1^{Tg}$, $Rrm2^{Tg}$, and $p53R2^{Tg}$ mice have been previously described (3). Briefly, the mice were maintained on a pure *FVB/N* strain background and expressed their transgene under the control of chicken beta-actin promoter and cytomegalovirus enhancer regulatory sequences. The transgenic mice seemed grossly normal and were fertile. The presence of the transgene was

verified by PCR analysis as described previously (3). Rrm1^{Tg} mice showed restricted overexpression of Rrm1 protein primarily in the skeletal muscle by immunoblotting whereas Rrm2^{Tg} and p53R2^{Tg} mice had widespread, high-level overexpression of the transgene in all tested tissues. For this study, we created mice overexpressing Rrm1 together with either Rrm2 or p53R2 by cross-breeding mice that were hemizygous for each transgene. Because the PCR assay used to detect Rrm1^{Tg} and p53R2^{Tg} is not transgene-specific (3), the presence of Rrm1^{Tg} or p53R2^{Tg} in offspring from these crosses was determined by Southern blotting. Briefly, tail DNA obtained from offspring was digested overnight with BamHI (Rrm1^{Tg}) or EcoRV (p53R2^{Tg}). After DNA was immobilized on a nylon membrane (GeneScreen Plus, Perkin Elmer), transgene bands were detected by hybridization with radiolabeled probes derived from previously described pCaggs RNR expression constructs (3). Pathological examination of lung neoplasms was performed as before (3). The Twinkle^{Tg} (15) and TFAM^{Tg} mice (20) used here were also previously described. Both were in *C57BL/6* background, and expressed the transgene under a ubiquitous beta-actin promoter. The Twinkle-mice were backcrossed to *C57BL/6* from *FVB/N* for more than twelve generations, and the congeneity was confirmed with the Mouse Medium Density SNP Panel (Illumina).

Quantification of RNR transgene overexpression

Western blotting for RNR subunits was performed as previously described (3). Chemiluminescent signal was detected on a VersaDoc Imaging system and quantified using Quantity One software (Bio-Rad Laboratories). Band intensity was determined for each dilution series sample and plotted following subtraction of background signal. The measured intensity for each undiluted wild-type band was fitted to the generated line for the corresponding RNR^{Tg} dilution series. Fold overexpression values were corrected for loading by standardization based on α-tubulin signal.

Southern blotting for mtDNA copy number determination

Total DNA was isolated from tissues by proteinase K digestion and standard phenol-chloroform extraction. Southern blotting was performed essentially as described (21). Briefly, three micrograms total DNA was digested with SacI overnight at 37°C, samples were then separated by electrophoresis in an agarose gel and blotted by alkaline transfer onto a Hybond N+ membrane (Amersham Biosciences). The membrane was hybridized overnight at 68°C in a roller hybridizer using 5 μCi/ml ^{32}P-dCTP labeled (PCR-generated) mouse mtDNA probe, and 18S rDNA probe in pBR322 plasmid. Phosphoimager analysis was done with Typhoon 9400 (Amersham Biosciences) and mtDNA was quantified against the 18S rDNA signal using ImageQuant v5.0 software (Amersham Biosciences).

Real time PCR

For mtDNA quantification, the quantitative real-time (Q)PCR reactions were done with 25 ng total DNA used as template and normalizing the *mt-Cytb* gene amplification level (primer sequences: 5'-GCTTTCCACTTCATCTTACCATTTA-3' and 5'-TGTTGGGTTGTTTGATCCTG-3') against the nuclear beta actin gene (primer sequences: 5'-GGAAAAGAGCCTCAGGGCAT-3' and 5'-GAAGAGCTATGAGCTGCCTGA-3'). Samples were run on an Abi Prism SDS 7000 machine (Applied Biosystem). Amplification conditions were: 95°C for 7 minutes followed by 35 cycles of 95°C for 10 seconds and 60°C for 30 seconds. Dissociation curves were checked to ensure the existence of a single PCR product. Each sample was run in duplicate, and samples with significant variation between duplicates were excluded. QPCR data were analyzed using 7000 System Sequence Detection Software version 1.2.3 (Applied Biosystems).

For gene expression analysis, 1000 ng total RNA was DNase digested using the Amplification Grade DNase I kit (Invitrogen) according to the manufacturer's instructions. Reverse transcription was done using M-MLV reverse transcriptase (Promega). Taqman gene expression assay for *Rrm2b* (assay ID Mm01165706_m1) and the *Gapdh* endogenous control were purchased from Applied Biosystems. The PCR reactions for *Rrm2b* and

Gapdh were done using TaqMan Universal PCR Master Mix (Applied Biosystems), and run on an Abi Prism SDS 7000 machine (Applied Biosystem) according to the manufacturer's protocol. The PCR for *Rrm1* was done using the DyNAmo™ Flash SYBR® Green QPCR Kit (Finnzymes) as above (primer sequences 5'-TGGACTCAACATGGACTTTG-3' and 5'-GGCCTTGGATTACTTTCATG-3'). QPCR data were analyzed using 7000 System Sequence Detection Software version 1.2.3 (Applied Biosystems). The amplification level of *Rrm2b* or *Rrm1* was normalized by dividing by the *Gapdh* amplification level.

MtDNA point mutation analysis

For mtDNA point mutation analysis we used primers that specifically amplified the *mt-Cytb* gene (nucleotide pair 14,073–14,906) and non-coding control region (15,357–138) of mouse mtDNA. In the PCR, we utilized the high fidelity Phusion polymerase (Finnzymes) according to the manufacturer's instructions, with 25 ng total DNA from quadriceps femoris muscle as template. The PCR program was 98°C for 30 seconds followed by 30 cycles of 98°C for 10 seconds, 61°C for 10 seconds and 72°C for 30 seconds. PCR products were cloned into pCR®2.1 plasmid using the TA cloning kit (Invitrogen) according to the manufacturer's instructions. Multiple PCR clones were sequenced to generate approximately 30,000 bp of sequence for each region.

Long PCR

Long PCR to amplify the entire mitochondrial genome or selectively deleted mtDNA molecules was done using the Expand Long Template PCR System (Roche). 50 ng total DNA was used as template. Cycling conditions were: 92°C for 2 minutes followed by 30 cycles of 92°C for 10 seconds and 68°C for 12 minutes. PCR products were separated by electrophoresis on 1% agarose gels and visualized with a Typhoon 9400 scanner (Amersham Biosciences). Primers hybridized to the control region of mtDNA located at nucleotide positions 1953-1924 and 2473-2505.

Measurement of nucleotide pools in skeletal muscle

Nucleotides were extracted from skeletal muscle of aged mice using previously described methods with modifications (22, 23). Briefly, skeletal muscle was excised following euthanasia by CO_2 asphyxiation and snap-frozen in liquid nitrogen. When sufficient tissue was available, samples were divided into two equal portions, processed separately, and compared to assess measurement consistency. Tissues were weighed and immersed in approximately 5μL/mg 10% trichloroacetic acid, 10mM $MgCl_2$. Tissues were homogenized in a Qiagen Tissue Lyser by six cycles of 30 seconds at 30 Hz followed by 30 seconds on ice. Tissue homogenates were incubated on ice for 20 minutes, then spun at 13,000g for 1 minute. The supernatant was taken to a fresh tube and re-spun. An approximately equal volume of 0.5N trioctylamine

in fluorotrichloromethane was added to the supernatant. The samples were vortexed briefly and spun for 2 minutes at 16,000g. The volume of the upper phase was estimated by pipetting and aliquots were snap-frozen in liquid nitrogen and stored at -80C until nucleotide measurements were performed. dNTPs were measured using an indirect enzymatic assay as reported by Ferraro *et al*. (24). Standard curves were prepared from concentrated stocks of pure individual dNTPs (Fermentas). Reactions in 50 μL total volume were incubated for 1 hour and then 30mL was spotted to Whatman DE81paper discs and dried. Discs were washed three times in 5%Na_2HPO_4, and once each in dH_2O and 95% EtOH. Discs were dried and counted on a Beckman Coulter LS6500 scintillation counter. Measurement of ribonucleosides was performed as in N. Kochanowski *et al*. (25) with modifications. Analyses were carried out on a Shimadzu UHPLC system. Samples were separated on a Supelco LC-18T column in 30mM KH_2PO_4 and 10mM tetrabutylammonium hydrogen sulfate, pH 6.5 : methanol (A=91.7:8.3, B=71.6:28.4) over a 40-minute time period. The program ran 0%-100%B from 0-24 minutes, 1 minute at 100% B, and 100%-0% B from 25-30 minutes at a flow rate of 1 mL/minute. Identities of analytes were confirmed both by comparison of elution time to known standards and by wavelength of maximum absorbance (λ_{max}). Sample extracts in which ATP comprised less than 65% of the total adenine nucleotides were excluded from further analysis.

RESULTS

Generation of RNR transgenic mice

Transgenic mice that express recombinant *Rrm1*, *Rrm2*, or *p53R2* (referred to as "*Rrm1*^{Tg}", "*Rrm2*^{Tg}", and "*p53R2*^{Tg}" mice hereafter) were generated previously and showed broad, high-level RNR overexpression (3). Since active RNR requires the presence of the large and the small subunit, simultaneous overexpression of both subunits could cause a greater increase in RNR activity. We therefore interbred *Rrm1*^{Tg} mice with *Rrm2*^{Tg} or *p53R2*^{Tg} mice to generate bitransgenic mice. The *Rrm1*^{Tg}+*Rrm2*^{Tg} and *Rrm1*^{Tg}+*p53R2*^{Tg} mice were born at expected frequencies and showed no gross abnormalities (Table 2.1). The endogenous RNR subunits were barely or not at all detectable by Western blotting of 25 μg protein for each muscle tissue extract, whereas significant overexpression was observed in RNR^{Tg} samples. We therefore made serial dilutions from each RNR^{Tg} sample, and plotted the band intensities against the dilution level. Fitting the corresponding wild-type samples onto this plot allowed us to estimate the fold overexpression for each transgene-encoded protein (Figure 2.1). The calculated threshold dilutions for bitransgenic mice are shown in Table 2.2. The level of transgene overexpression was comparable between single RNR transgenic and bitransgenic mice (Figure 2.2).

Rrm2^{Tg} and *p53R2*^{Tg} mice were previously found to have increased lung tumour prevalence at ~17 months of age (3), *Rrm2* being a more potent

tumour inducer than *p53R2*. In bitransgenic mice, the lung tumour formation occurred with similar frequency as in mice overexpressing either of the small RNR subunits alone (Table 2.3). The bitransgenic mice were followed up to ~17 months age and, excluding lung tumour formation, they appeared grossly normal during this time.

RNR overexpression does not elevate mtDNA copy number in mouse tissues

We used Southern blotting to investigate the effect of RNR expression on mtDNA copy number in the skeletal muscle (Figure 2.3A), heart (Figure 2.3B), liver and kidney (Figure 2.4) of the various RNR^{Tg} mice. No significant increases in mtDNA copy number were observed in any of the tissues from 9-12 weeks old mice. In the skeletal muscle of the bitransgenic mice, there was actually a modest reduction in mtDNA abundance: $Rrm1^{Tg}$+$Rrm2^{Tg}$ mice had on average 71% (p=0.026) and $Rrm1^{Tg}$+$p53R2^{Tg}$ mice 62% (p=0.0075)

Table 2.1. Genotypes of offspring from crosses between *Rrm1*^{Tg} mice and *Rrm2*^{Tg} or *p53R2*^{Tg} mice.

cross	genotype	#observed (#expected)
Rrm1^{Tg} x Rrm2^{Tg}	Wild-type	57 (48.75)
	Rrm1^{Tg}	54 (48.75)
	Rrm2^{Tg}	38 (48.75)
	Rrm1^{Tg} + Rrm2^{Tg}	46 (48.75)
Rrm1^{Tg} x p53R2^{Tg}	Wild-type	29 (37.25)
	Rrm1^{Tg}	52 (37.25)
	p53R2^{Tg}	35 (37.25)
	Rrm1^{Tg} + p53R2^{Tg}	33 (37.25)

Note: *Rrm1*^{Tg} mice were bred to mice carrying either the *Rrm2* or *p53R2* transgene. Progeny were genotyped at weaning by Southern blot. (J.P.)

Figure 2.1. RNR overexpression in skeletal muscle and cardiac muscle from *Rrm1*^{Tg} + *Rrm2*^{Tg} and *Rrm1*^{Tg} + *p53R2*^{Tg} bitransgenic mice. Western-blot analysis of RNR protein expression was performed on total protein extracts prepared from skeletal muscle (*A* and *C*) or cardiac muscle (*B* and *D*) from wild-type (WT) as well as *Rrm1*^{Tg} + *Rrm2*^{Tg} or *Rrm1*^{Tg} + *p53R2*^{Tg} bitransgenic mice. Extracts were left undiluted (1×) or diluted as indicated and then subjected to immunoblotting with antibodies specific to Rrm1, Rrm2 or p53R2. The asterisk indicates a non-specific band in the anti-Rrm2 immunoblot. α-Tubulin signal in undiluted skeletal (*C*) and cardiac (*D*) muscle samples was used to normalize for protein loading. The analysis was performed on three mice of each genotype, and representative bands are shown for clarity of comparison. The calculated fold overexpression values are shown in Table 1. (J.P.)

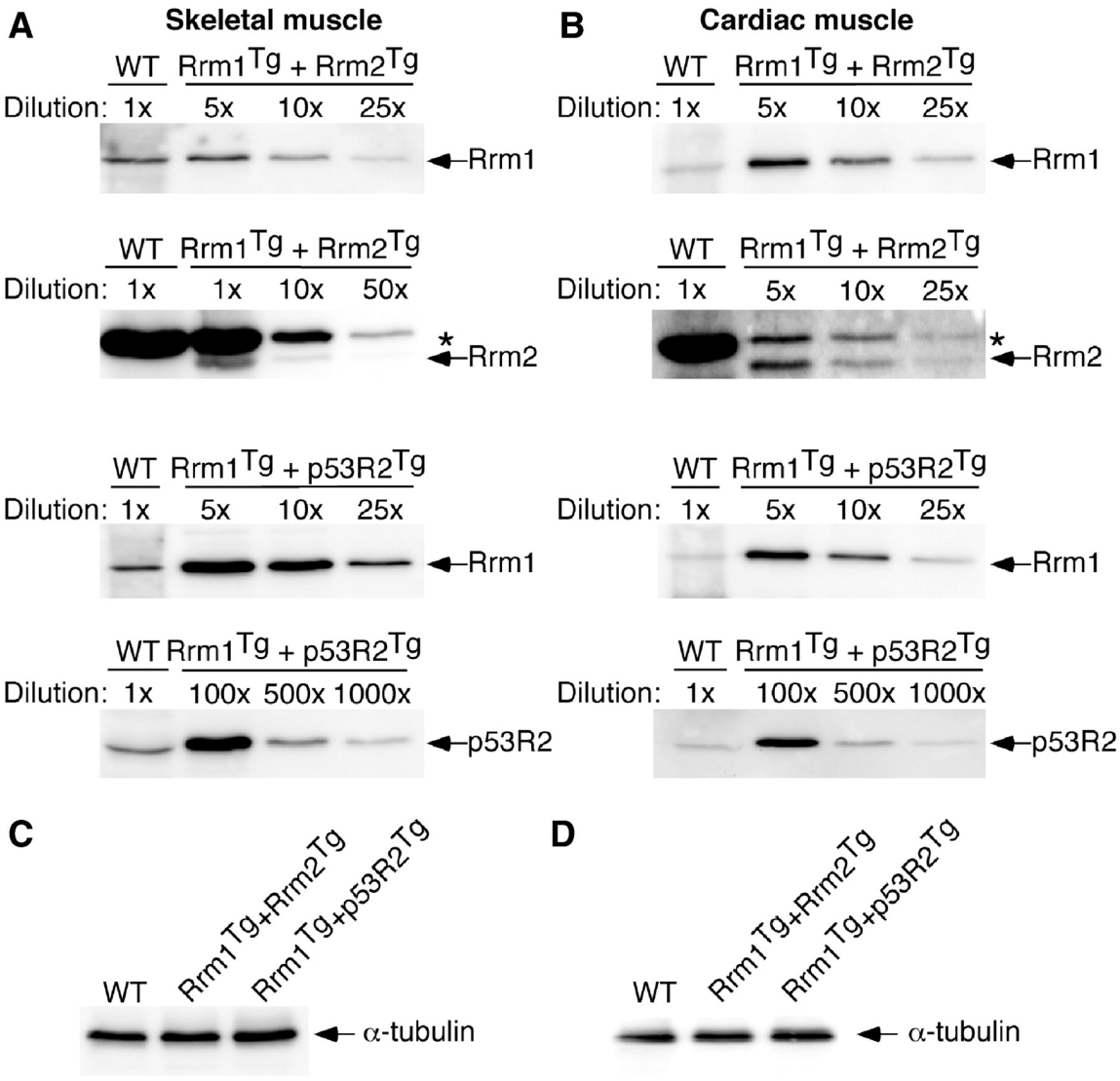
A
Skeletal muscle
WT
Rrm1Tg + Rrm2Tg
Dilution: 1x 5x 10x 25x
←Rrm1
WT
Rrm1Tg + Rrm2Tg
Dilution: 1x 1x 10x 50x
*
←Rrm2
WT
Rrm1Tg + p53R2Tg
Dilution: 1x 5x 10x 25x
←Rrm1
WT
Rrm1Tg + p53R2Tg
Dilution: 1x 100x 500x 1000x
←p53R2
B
Cardiac muscle
WT
Rrm1Tg + Rrm2Tg
Dilution: 1x 5x 10x 25x
←Rrm1
WT
Rrm1Tg + Rrm2Tg
Dilution: 1x 5x 10x 25x
*
←Rrm2
WT
Rrm1Tg + p53R2Tg
Dilution: 1x 5x 10x 25x
←Rrm1
WT
Rrm1Tg + p53R2Tg
Dilution: 1x 100x 500x 1000x
←p53R2
C
WT
Rrm1Tg+Rrm2Tg
Rrm1Tg+p53R2Tg
←α-tubulin
D
WT
Rrm1Tg+Rrm2Tg
Rrm1Tg+p53R2Tg
←α-tubulin

Figure 2.2. RNR overexpression in skeletal muscle from *Rrm1*^{Tg}, *Rrm2*^{Tg}, and *p53R2*^{Tg} transgenic mice. *A*. Western-blot analysis of RNR protein expression was performed on total protein extracts prepared from skeletal muscle from wild-type (WT) as well as *Rrm1*^{Tg}, *Rrm2*^{Tg}, or *p53R2*^{Tg} transgenic mice. Extracts were left undiluted (1×) or diluted as indicated and then subjected to immunoblotting with antibodies specific to Rrm1, Rrm2 or p53R2. The asterisk indicates a non-specific band in the anti-Rrm2 immunoblot. α-Tubulin signal in undiluted skeletal muscle samples (*B*) was used to normalize for protein loading. (J.P.)

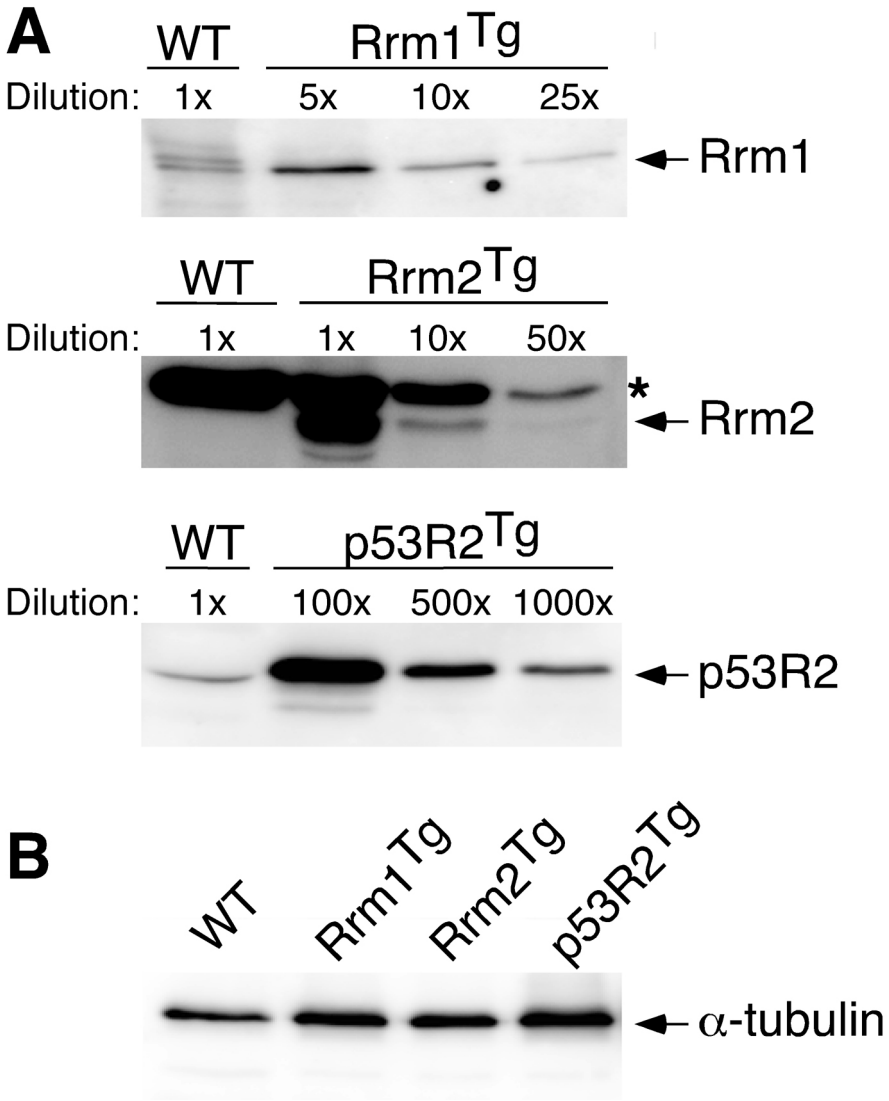
A
WT
Rrm1Tg
Dilution:
1x
5x
10x
25x
Rrm1
WT
Rrm2Tg
Dilution:
1x
1x
10x
50x
*
Rrm2
WT
p53R2Tg
Dilution:
1x
100x
500x
1000x
p53R2
B
WT
Rrm1Tg
Rrm2Tg
p53R2Tg
α-tubulin

Table 2.2 Transgene-encoded protein levels.

Genotype	Protein	Skeletal muscle	Cardiac muscle
Rrm1^{Tg} + *Rrm2*^{Tg}	Rrm1	3.3 (± 2.1)	33.7 (± 7.6)
	Rrm2	>35.7 (± 11.1)	>23.7 (± 3.4)
Rrm1^{Tg} + *p53R2*^{Tg}	Rrm1	11.7 (± 6.7)	34.7 (± 24.5)
	p53R2	355.3 (± 25)	975.3 (± 726.3)

Table 2.3. Lung neoplasm characteristics in RNR bitransgenic mice

Mouse genotype	# of animals	Age (days)	% of mice with lung neoplasms	Average lung neoplasm size (mm)±SD	% of mice with multiple lung neoplasms	% of mice with lung adenocarcinoma	% of mice with other neoplasms[§]
WT FVB[†]	9	508	22%	8.0 ± 8.5	0%	11%	11%
Rrm1^{Tg}	13	466	8%	6.00 ± 0	0%	8%	0%
Rrm2^{Tg}	4	489	100%*	5.3 ± 3.3	100%*	50%*	25%
p53R2^{Tg}	6	516	67%*	1.6 ± 1.1	50%*	0%	0%
Rrm1^{Tg} *Rrm2*^{Tg}	14	427	93%*	6.4 ± 2.9	100%*	57%*	21%
Rrm1^{Tg} *p53R2*^{Tg}	9	461	56%*	4.7 ± 2.9	40%*	30%	33%

NOTE: Mice were aged until moribund for up to approximately 500 days, euthanized by asphyxiation using carbon dioxide, and subjected to pathological examination as described in Materials and Methods. (X.X.)

[†] *WT FVB* refers to transgene-negative control mice.

*Statistically significant difference ($p<0.05$) relative to *WT FVB* mice. Incidences were compared by Chi-square analysis. Neoplasm sizes were compared by t-test analysis.

[§] Other neoplasms included lymphoma, ovary tumor, urinary bladder tumor.

residual mtDNA amounts compared to their wild-type littermates (Figure 2.3A). The mtDNA depletion in skeletal muscle was progressive; at 11-15 months of age, the residual mtDNA copy number was 42% in *Rrm1*^{Tg}+*Rrm2*^{Tg} mice (p=0.030) and 34% in *Rrm1*^{Tg}+*p53R2*^{Tg} mice (p=0.0011) (Figure 2.3B). The mtDNA levels in the other examined tissues remained unchanged also at the older age. Therefore, overexpression of RNR did not elevate mtDNA copy number in differentiated mouse tissues and was associated with progressive mtDNA depletion in bitransgenic animals.

RNR overexpression does not affect mtDNA integrity or mutagenesis

Overexpression of RNR causes nuclear genome mutagenesis and promotes cancer (3). We therefore asked whether RNR overexpression leads to mtDNA instability as well. We examined the presence of mtDNA point mutations in the skeletal muscle of a 16- month-old *Rrm1*^{Tg}+*Rrm2*^{Tg} mouse by amplifying and cloning mtDNA regions from the control region (1080 bp) and *mt-Cytb* gene (833 bp), which encodes cytochrome b, followed by sequencing of ~30 kb of DNA from each region. We previously reported the point mutation rate in wild-type *FVB/N* mice to be ~0.5 mutations per 10 kb in the control region and ~0.25 mutations per 10 kb in the *mt-Cytb* gene (15). The 16-month-old *Rrm1*^{Tg}+*Rrm2*^{Tg} showed similar or lower point mutation loads compared to a wild-type control (Table 2.4).

Figure 2.3 mtDNA quantification in young (9–12 weeks) and aged (11–15 months) mice. Southern blots of digested total DNA from skeletal (*A*) and cardiac and (*B*) muscle were probed for full-length mtDNA and the nuclear 18S rDNA gene to control for loading. (*A*) mtDNA to nuclear DNA ratios were determined by densitometric quantification of Southern blots and by qPCR, both methods yielding similar results. mtDNA depletion was found in young and aged bitransgenic mice. (*B*) No change in mtDNA copy number was observed in the cardiac muscle of RNR^{Tg} mice. Error bars indicate SEM. $^{*}P<0.05$, $^{**}P<0.01$, Student's *t*-test compared to wild-type where $N \geq 3$ individual animals. (E. Y.)

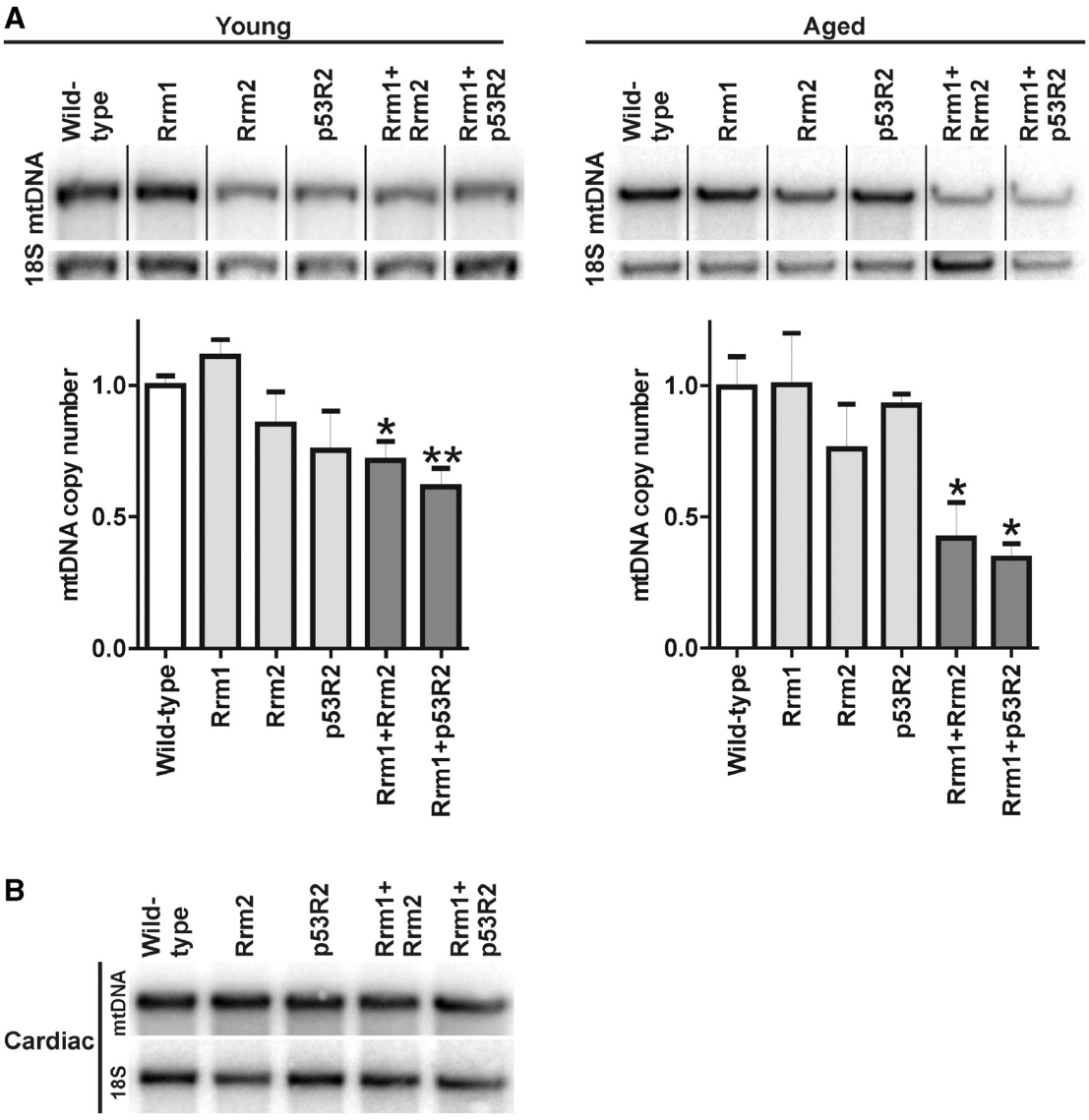
A
Young
Aged
Wild-type
Rrm1
Rrm2
p53R2
Rrm1+ Rrm2
Rrm1+ p53R2
mtDNA
18S
mtDNA copy number
1.0
0.5
0.0
*
**
Wild-type
Rrm1
Rrm2
p53R2
Rrm1+Rrm2
Rrm1+p53R2
B
Cardiac

Figure 2.4. mtDNA copy number determination. Southern blots of digested total DNA extracted from liver and kidney of 9-12 week-old mice of the indicated gentoypes were probed for full-length mtDNA and nuclear 18S rDNA. No significant change in mtDNA abundance was observed in the RNR^{Tg} mice. (E. Y.)

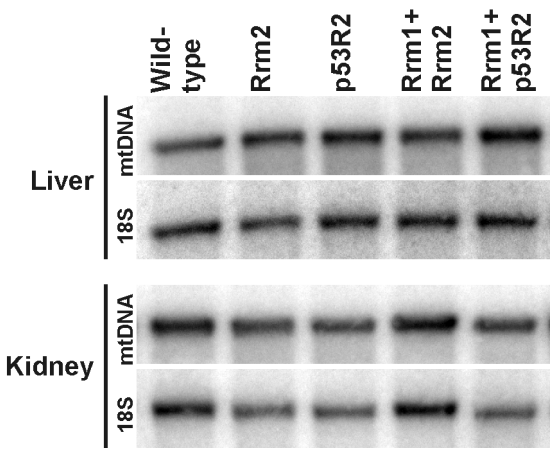
Wild-type
Rrm2
p53R2
Rrm1+ Rrm2
Rrm1+ p53R2
Liver
mtDNA
18S
Kidney
mtDNA
18S

Table 2.4 Effect of RNR overexpression upon mtDNA point mutagenesis. (E.Y.)

	mt-Cytb gene		Control Region	
Mouse genotype	Sequenced basepairs	Mutation rate per 10 kb	Sequenced basepairs	Mutation rate per 10 kb
Wild-type	30,844	0.648	27,332	0.366
Rrm1^{Tg} + *Rrm2*^{Tg}	39,438	0.000	28,034	0.356

In a long-range PCR assay, full length mtDNA was readily amplified in the skeletal muscle of aged bitransgenic mice, with no additional small amplifying products. This ruled out the presence of large mtDNA deletions (Figure 2.5). These analyses showed that bitransgenic RNR overexpression did not increase deletion formation or point mutagenesis of mtDNA, but only caused mtDNA depletion.

RNR overexpression leads to dNTP pool imbalance in skeletal muscle

In many human diseases and mouse models, mtDNA depletion and instability have been suggested to occur as the result of perturbed dNTP pools (26-28). To understand the mechanism of mtDNA depletion in RNR overexpressors, we measured the relative levels of dNTP pools in muscle extracts. Nucleotides are known to easily undergo quick dephosphorylation during the extraction procedure (29-31). Under conditions when dNTPs are dephosphorylated during sample preparation, ATP is similarly degraded to ADP and AMP. Therefore, the level of ATP in the extract closely mirrors that of the dNTPs, and can be used as an internal marker of unwanted dNTP destruction (30). We measured dNTP levels in skeletal muscle extracts from 12- month-old mice by a primer extension assay, using 2-3 mice of each genotype. The levels of ATP, ADP and AMP were measured from the same extracts by HPLC.

Figure 2.5. Analysis of mtDNA integrity in RNR^{Tg} mice by mtDNA deletion assay. To look for mtDNA deletions, a long-PCR assay was used to amplify the entire mtDNA genome from the skeletal muscle of 12-month old wild-type, $Rrm1^{Tg} + Rrm2^{Tg}$ and $Rrm1^{Tg} + p53R2^{Tg}$ mice. The full-length mtDNA (16 kb) was readily amplified from all samples. A Deletor mouse sample was included as a positive control; this sample shows multiple mtDNA fragments of smaller size. The DNA ladder λ Hind was used as a size marker. (E. Y.)

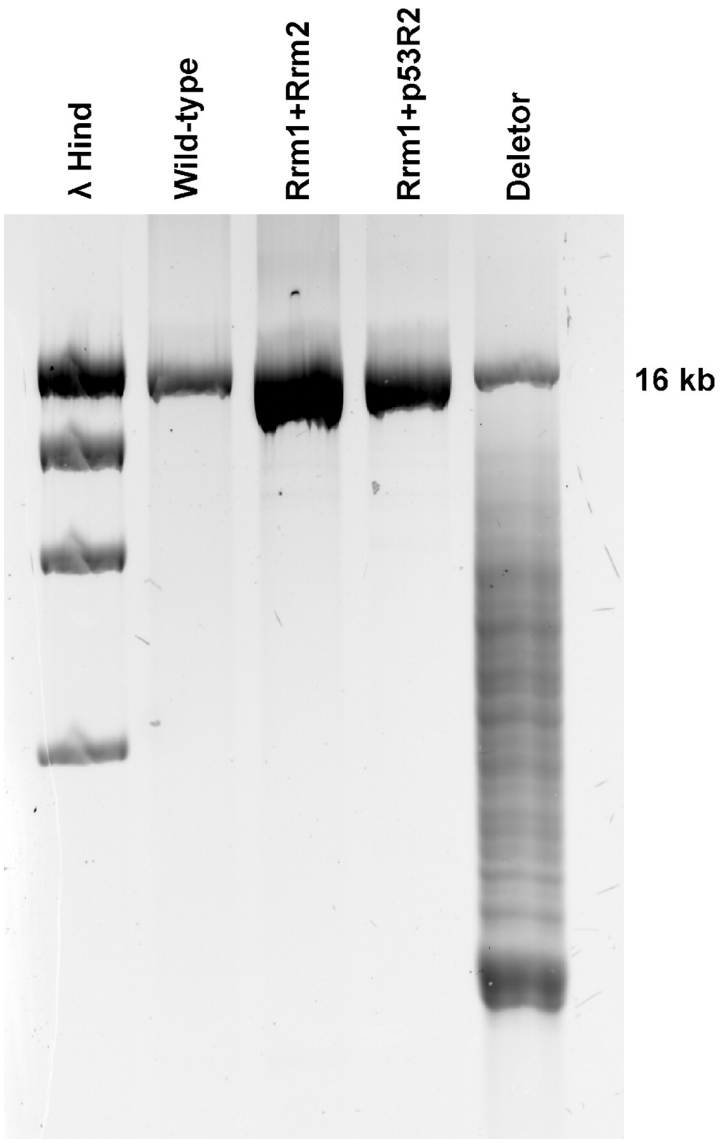
λ Hind
Wild-type
Rrm1+Rrm2
Rrm1+p53R2
Deletor
16 kb

The average ATP levels were similar across the genotypes, the levels of ADP were >10-fold lower than that of ATP, and AMP mounted to <1% of the total adenine nucleotide pools (Figure 2.6). These ATP/ADP ratios corresponded well with previously reported numbers from mouse liver (30), and suggested that general dNTP dephosphorylation did not have a major effect on the dNTP level determination. The only exceptions were the *Rrm1*^{Tg}+*Rrm2*^{Tg} mice, which did exhibit a somewhat lower average ATP/ADP ratio than the other genotypes (Figure 2.6), suggesting that dNTP measurements may have been underestimated in those mice. To ensure that the high level of RNR overexpression did not lead to substrate depletion, we also measured the levels of CDP, UDP and GDP, and found no significant differences in their levels between the genotypes (Figure 2.7).

The amounts of the individual dNTPs are shown in Figure 2.8. Data are presented according to the respective crosses, with the *Rrm1*^{Tg} X *p53R2*^{Tg} crosses in panels A-D and the *Rrm1*^{Tg} X *Rrm2*^{Tg} crosses in panels E-H. We observed increases in the levels of dATP and dCTP in all of the transgenic lines, as compared to wild-type control samples. The mice expressing either small subunit showed greater relative increases in dATP and dCTP than the *Rrm1*^{Tg} mice.

Figure 2.6. Measurement of AMP, ADP, and ATP levels in skeletal muscle extracts from RNR^{Tg} mice. The pools of ATP, ADP and AMP were measured from skeletal muscle extracts by an HPLC assay and quantified relative to standard curves. Results are presented as the means of results from two (for wild-type) or three (for all other genotypes) mice. The average levels of the adenine nucleotides were plotted on linear (*A*) and logarithmic (*B*) scales, and found to be similar across genotypes, which suggested comparable extraction efficiencies. The only exception was with the $Rrm1^{Tg} + Rrm2^{Tg}$ mice, which had lower average ATP levels and ATP/ADP ratios compared to the other genotypes. This may cause dNTP pool levels in these mice to be underestimated. Error bars indicate SEM. (J.P)

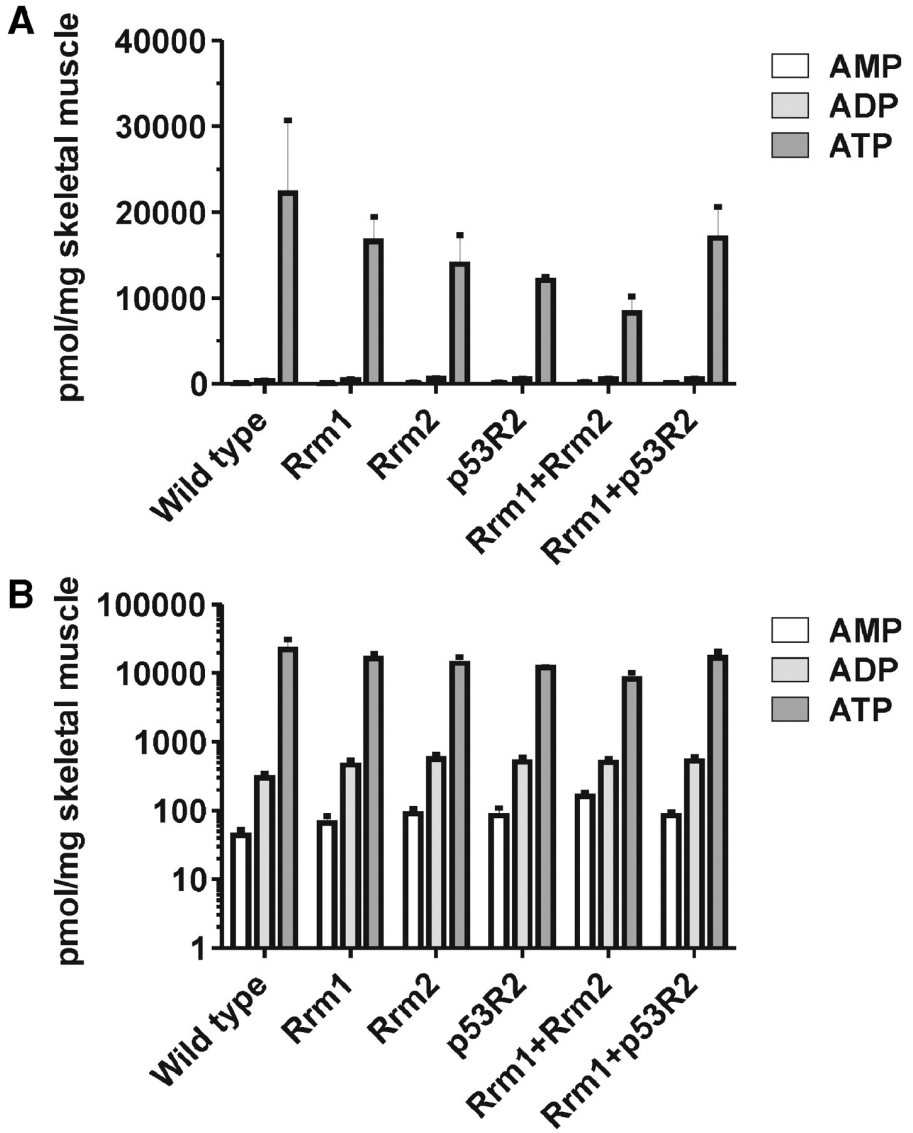
A
pmol/mg skeletal muscle
40000
30000
20000
10000
0
AMP
ADP
ATP
Wild type
Rrm1
Rrm2
p53R2
Rrm1+Rrm2
Rrm1+p53R2
B
pmol/mg skeletal muscle
100000
10000
1000
100
10
1
AMP
ADP
ATP
Wild type
Rrm1
Rrm2
p53R2
Rrm1+Rrm2
Rrm1+p53R2

Figure 2.8. Overexpression of RNR does not lead to substrate depletion. HPLC was used to measure the levels of CDP, UDP and GDP, which are substrates of RNR, in skeletal muscle from 12-month-old mice of the indicated genotypes. There were no significant differences between the genotypes. Data are averages from 2 or 3 mice of each genotype. Error bars indicate SEM. (J.P.)

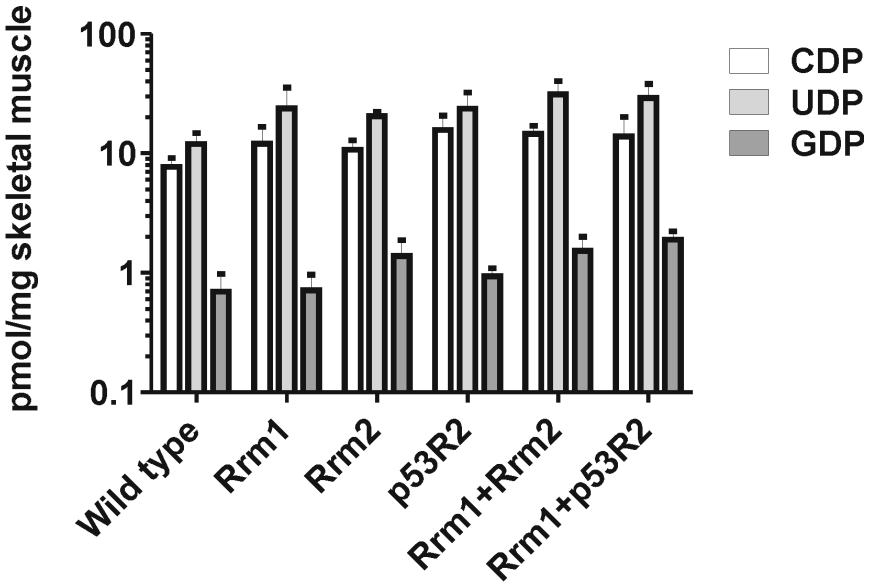
pmol/mg skeletal muscle
100
10
1
0.1
CDP
UDP
GDP
Wild type
Rrm1
Rrm2
p53R2
Rrm1+Rrm2
Rrm1+p53R2

There was also a clear tendency towards higher dATP and dCTP values in the bitransgenic *Rrm1*^{Tg}+*p53R2*^{Tg} and *Rrm1*^{Tg}+*Rrm2*^{Tg} mice as compared to the *p53R2*^{Tg} (Figure 2.8 A and D) and *Rrm2*^{Tg}(Figure 2.8 E and H) single transgenic mice, respectively. In contrast to the elevated levels of dATP and dCTP, the levels of dGTP were unchanged in all of the transgenic mice (Figure 2.8 B and F), and the levels of dTTP were actually decreased significantly in the *p53R2*^{Tg} and *Rrm1*^{Tg}+*p53R2*^{Tg} mice (Figure 2.8C), and, to a lesser degree, in the *Rrm1*^{Tg}, *Rrm2*^{Tg}, and *Rrm1*^{Tg}+*Rrm2*^{Tg} mice (Figure 2.8G). Taken together, these data suggested that RNR overexpression led to significant changes in dNTP pools and considerable imbalances between the different dNTPs, with the most pronounced changes in bitransgenic RNR^{Tg} mice. Similar changes in dNTP pools were observed in young bitransgenic mice. (Figure 2.9).

Increased mtDNA copy number is associated with decreased RNR expression

RNR is involved in a signalling pathway that regulates mtDNA copy number in yeast (12), and regulation of RNR expression could be part of a homeostatic mechanism to control mtDNA copy number in mammals. We therefore utilized mouse models that express recombinant wild-type mouse Twinkle (15) or human TFAM (20), with ~2-fold and ~3-fold respective increases of mtDNA copy numbers in their skeletal muscle at the age of ten weeks

Figure 2.8. RNR overexpression alters dNTP pools in skeletal muscle. The levels of the four dNTPs were measured by polymerase assay and expressed per unit weight of skeletal muscle. Pool sizes for the indicated dNTPs were compared between wild-type control mice and mice from $Rrm1^{Tg} \times p53R2^{Tg}$ (*A*–*D*) or $Rrm1Tg \times Rrm2^{Tg}$ (*E*–*H*) breedings. Results are presented as the means of results from two (for wild-type) or three (for all other genotypes) mice. Results for the same wild-type and $Rrm1^{Tg}$ mice are presented in (*A*–*D*) and (*E*–*H*) for comparative purposes. The levels of dATP (*A* and *E*) were significantly increased in $p53R2^{Tg}$ and $Rrm1^{Tg} + p53R2^{Tg}$ mice as well as in $Rrm2^{Tg}$ and $Rrm1^{Tg} + Rrm2^{Tg}$ mice. The dGTP levels (*B* and *F*) were unchanged in all mice. dTTP (*C* and *G*) was decreased in $p53R2^{Tg}$ and $Rrm1^{Tg} + p53R2^{Tg}$ mice and to a lesser degree also in $Rrm1^{Tg}$, $Rrm2^{Tg}$, and $Rrm1^{Tg} + Rrm2^{Tg}$ mice. dCTP (*D* and *H*) showed a similar pattern as dATP, with increases in $p53R2^{Tg}$ and $Rrm1^{Tg} + p53R2^{Tg}$ mice as well as in $Rrm2^{Tg}$ and $Rrm1^{Tg} + Rrm2^{Tg}$ mice. In each case, the $Rrm1^{Tg}$ mice showed similar but less pronounced dNTP changes as the mice overexpressing the small subunits. Error bars indicate SEM, $^{*}P < 0.05$, Student's *t*-test as compared to wild-type. (J.P.)

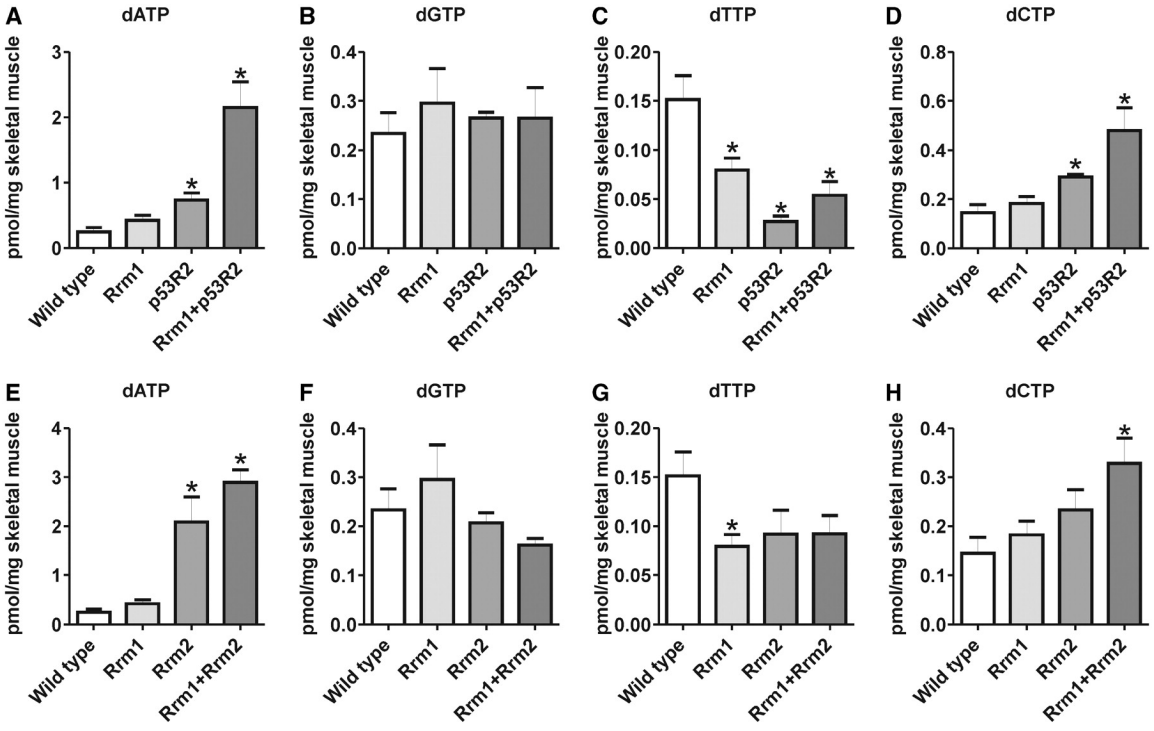
A
dATP
pmol/mg skeletal muscle
Wild type
Rrm1
p53R2
Rrm1+p53R2
B
dGTP
C
dTTP
D
dCTP
E
dATP
Rrm2
F
dGTP
G
dTTP
H
dCTP

Figure 2.9. Nucleotide pool levels in young RNR^{Tg} mice. Nucleotide levels were measured in skeletal muscle from 9-12 week-old mice of the indicated genotypes, using 1 or 2 mice for each genotype. First, to control for nucleotide extraction efficiency, the levels of ATP and ADP in each extract were measured by HPLC, and results are presented both on linear (*A*) and logarithmic (*B*) scales. The dNTP levels in the same extracts were then measured by polymerase assay using the assay originally described (*Anal. Biochem* 1989 Aug 1;**180** (2):222-6) and are presented separately for the *Rrm1*^{Tg} X *p53R2*^{Tg} (*C-F*) and *Rrm1*^{Tg} X *Rrm2*^{Tg} crosses (*G-J*). Data are averages. The same wild type and *Rrm1*^{Tg} values are shown with each cross. Error bars indicate standard deviations. (J.P.)

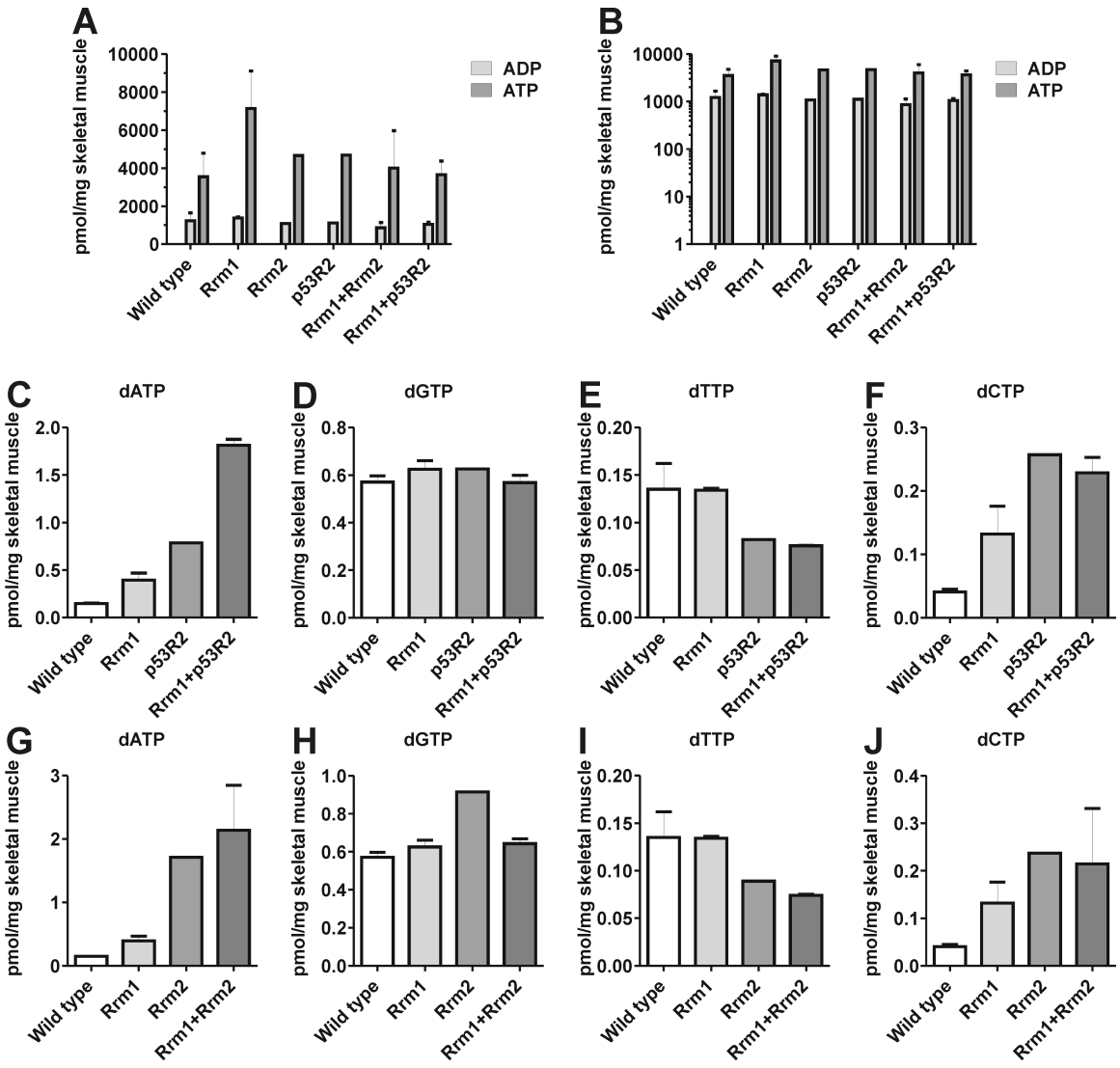
A
pmol/mg skeletal muscle
10000
8000
6000
4000
2000
0
ADP
ATP
Wild type
Rrm1
Rrm2
p53R2
Rrm1+Rrm2
Rrm1+p53R2
B
pmol/mg skeletal muscle
10000
1000
100
10
1
ADP
ATP
Wild type
Rrm1
Rrm2
p53R2
Rrm1+Rrm2
Rrm1+p53R2
C
dATP
pmol/mg skeletal muscle
2.0
1.5
1.0
0.5
0.0
Wild type
Rrm1
p53R2
Rrm1+p53R2
D
dGTP
pmol/mg skeletal muscle
0.8
0.6
0.4
0.2
0.0
Wild type
Rrm1
p53R2
Rrm1+p53R2
E
dTTP
pmol/mg skeletal muscle
0.20
0.15
0.10
0.05
0.00
Wild type
Rrm1
p53R2
Rrm1+p53R2
F
dCTP
pmol/mg skeletal muscle
0.3
0.2
0.1
0.0
Wild type
Rrm1
p53R2
Rrm1+p53R2
G
dATP
pmol/mg skeletal muscle
3
2
1
0
Wild type
Rrm1
Rrm2
Rrm1+Rrm2
H
dGTP
pmol/mg skeletal muscle
1.0
0.8
0.6
0.4
0.2
0.0
Wild type
Rrm1
Rrm2
Rrm1+Rrm2
I
dTTP
pmol/mg skeletal muscle
0.20
0.15
0.10
0.05
0.00
Wild type
Rrm1
Rrm2
Rrm1+Rrm2
J
dCTP
pmol/mg skeletal muscle
0.4
0.3
0.2
0.1
0.0
Wild type
Rrm1
Rrm2
Rrm1+Rrm2

. We measured the expression levels of *Rrm1* and *Rrm2b*, the genes encoding Rrm1 and p53R2 respectively, in skeletal muscle of Twinkle^{Tg} and TFAM^{Tg} mice. *Rrm1* mRNA was decreased to 76% (p=0.011) and 70% (p=0.010) in the Twinkle^{Tg} and TFAM^{Tg} mice, respectively (Figure 2.10A). *Rrm2b* mRNA was similarly decreased to 78% (p=0.045) and 77% (p=0.0093) of normal in the Twinkle^{Tg} and TFAM^{Tg} mice, respectively (Figure 2.10B). Thus the expression of RNR genes was found to correlate inversely with mtDNA copy number in two mouse models.

DISCUSSION

RNR is essential for both nuclear and mitochondrial DNA replication. The enzyme is limiting for mtDNA copy number in yeast, but whether the same is true in mammals has not been studied previously. dNTP pool regulation has emerged as a potential tool to increase mtDNA levels, and thereby to slow down progression of mtDNA disease. *In vitro* supplementation with two deoxyribonucleoside monophosphates (dNMPs) rescued mtDNA depletion in cultured patient myotubes with mutations in the mitochondrial deoxyribonucleoside salvage pathway enzyme deoxyguanosine kinase (dGK) (32). However, mtDNA depletion due to patient mutations in the mtDNA polymerase gamma (Pol γ) was not restored through nucleotide

Figure 2.10. RNR expression levels in mice with high mtDNA copy number. A QPCR assay was used to measure the expression levels of *Rrm1* and *Rrm2b*, the genes encoding Rrm1 and p53R2, respectively, in the skeletal muscle of mice overexpressing Twinkle or TFAM. These mice have increased mtDNA copy number. (*A*) *Rrm1* expression was downregulated in the Twinkle-mice and TFAM-mice compared to controls. (*B*) *Rrm2b* was similarly downregulated. Error bars indicate SEM, $*P<0.05$, $**P<0.01$, Student's *t*-test compared to wild-type where $N \geq 3$ individual animals. (E.Y.)

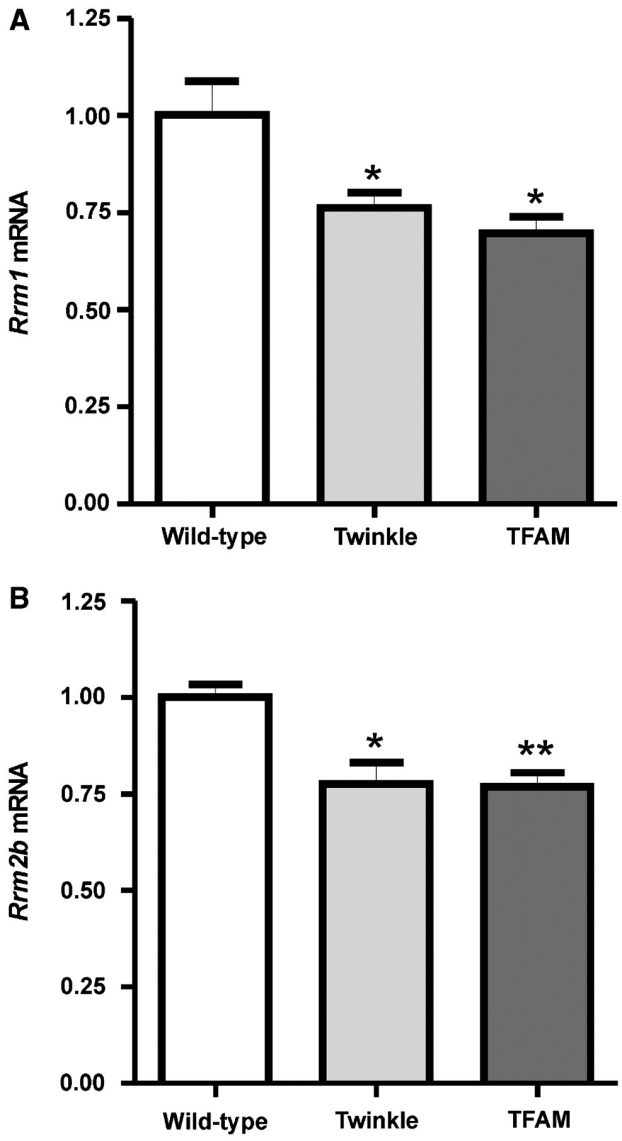
A
1.25
1.00
0.75
0.50
0.25
0.00
Rrm1 mRNA
*
*
Wild-type
Twinkle
TFAM
B
1.25
1.00
0.75
0.50
0.25
0.00
Rrm2b mRNA
*
**
Wild-type
Twinkle
TFAM

supplementation in the same study. Likewise, nucleotide supplementation to healthy myotubes did not increase mtDNA levels significantly above normal (32). These results suggested that although dNTP pool expansion may be beneficial in cases of dNTP deficiency, other factors than the size of the mitochondrial dNTP pool are limiting for mtDNA copy number in normal cells or in mtDNA replication defects.

RNR overexpression in yeast resulted in elevated mtDNA levels (12), and complementation of the respiratory chain deficient phenotype of Pol γ disease mutations (13). The results presented here suggest that RNR overexpression has partially opposite effects in mammals, which illustrates the marked differences in dNTP pool maintenance between organisms. However, we cannot exclude the possibility that increased RNR activity or dNTP availability *in vivo* could be beneficial in cases with increased mtDNA turnover or mutagenesis. The increased carcinogenesis in RNR^{Tg} mice (3) illustrates the hazards of altering dNTP pool maintenance and further reduces the potential of RNR as a therapeutic tool.

The mechanisms governing mtDNA copy number in tissues are starting to come into focus. In mice, overexpression of the histone-like packaging protein TFAM or of the mtDNA helicase Twinkle increase mtDNA copy number two to three-fold (14, 15). The mRNA level of Twinkle and the protein level of TFAM correlate linearly with mtDNA content, suggesting that these may be limiting

factors in determining the amount of mtDNA. Defects in mitochondrial dNTP pool maintenance proteins cause loss of mtDNA, indicating that these factors are essential for mtDNA maintenance (7, 33-36). However, their contribution to the physiological control of mtDNA copy number is not well characterized. Heart-specific overexpression of the salvage pathway enzyme thymidine kinase 2 (TK2) in mice resulted in a 300-fold increase in enzyme activity and produced a ~30% increase in mtDNA copy number (37). Therefore, a very large increase in TK2 activity modestly influences mtDNA levels, potentially through increases in deoxycytidine and thymidine nucleotide pools. Our results show that although RNR is involved in the synthesis of all four dNTPs, very high levels of the enzyme do not increase mtDNA copy number and instead perturb mtDNA homeostasis. This finding is in line with Twinkle and TFAM being the main regulators of mtDNA level under normal circumstances.

A possible mechanism for nuclear control over mtDNA copy number would be to alter the transcription of mtDNA maintenance genes. In yeast, the first established signalling pathway that regulated mtDNA copy number is activated by the Mec1p/Rad53p kinases and leads to induction of RNR expression (12). The related ATM (ataxia-telangiectasia mutated) kinase in humans was also found to influence RNR expression and mtDNA homeostasis (38). We found the transcription of *Rrm1* and *Rrm2b* to be downregulated in two independent mouse models with increased mtDNA copy number, suggesting an intimate

feedback mechanism between transcriptional regulation of RNR subunits and mtDNA levels. RNR could thus contribute to a regulatory mechanism for nuclear control of mtDNA copy number *in vivo*. Such a signalling pathway could involve p53, a tumour suppressor and ATM target, which influences the expression level of p53R2 and is known to localize in small amounts to mitochondria (39).

RNR is rate-limiting for *de novo* dNTP synthesis, so any alteration to RNR activity is expected to induce changes in dNTP pools. These changes are transmitted into mitochondria, since the mitochondrial and cytosolic dNTP pools are in rapid communication (40). Direct measurement of dNTP pools from animal tissues is complicated by dNTP dephosphorylation caused by the anaerobiosis that immediately follows the death of the animal (30). Our extraction method was optimized to minimize nucleotide degradation during extraction, and the ATP, ADP and AMP levels were used as internal controls to ensure comparability across samples. We documented clear and reproducible differences in total dNTP pools between RNR overexpressors and wild-type mice.

Firstly, there were significant increases in the levels of dATP and dCTP both in the $Rrm2^{Tg}$ and $p53R2^{Tg}$ mice. Rrm2 induced higher dNTP increases than p53R2, which is consistent with Rrm2 being more active than p53R2 *in vitro* (41). Rrm1 overexpression alone was able to induce a detectable, albeit not

statistically significant, increase in dATP and dCTP levels, and overexpression of Rrm1 together with either small subunit led to a clear trend towards higher levels of dATP and dCTP. This apparent synergy suggested that co-overexpression of both subunits led to an increase in the abundance of the tetramer, with subsequent effects on nucleotide pools.

The allosteric regulation of RNR promotes a balanced production of all four dNTPs and therefore manipulation of RNR expression might be expected to influence the levels of all four dNTPs equally (1). However, we found remarkable dNTP pool imbalances in the RNR^{Tg} mice. The dGTP pools were unchanged whereas dTTP pools were actually decreased in $p53R2^{Tg}$ as well as $Rrm1^{Tg}$+$p53R2^{Tg}$ mice. This finding illustrates the need for tight control of the relative activities of the large number of anabolic and catabolic enzymes that determine the final dNTP composition *in vivo* (42). For instance, the synthesis of thymidine phosphates requires – as an additional step – reductive methylation of RNR-generated deoxyuridine monophosphate, which is catalyzed by thymidylate synthase. Hence, induction of RNR could cause a substrate overload for the endogenous thymidylate synthase, which in turn could explain why increased RNR does not increase the dTTP level. Furthermore, the specificity of RNR for GDP reduction is induced by the binding of dTTP to the specificity site of Rrm1 (1). Thus, a relative lack of dTTP could explain why the dGTP pools did not increase in our mice. The

dNTP imbalance was not due to depletion of any of the substrates of RNR, since the levels of ADP, CDP, UDP and GDP were similar in all genotypes.

Unbalanced dNTP pools are known to cause mutagenesis in both nuclear (43) and mitochondrial (28) genomes. Given the presence of altered dNTP pools in RNR^{Tg} mice, the likely mechanism of progressive mtDNA depletion in bitransgenic mice is inefficient mtDNA replication caused by perturbed dNTP balance. Initiation of nuclear DNA replication is influenced by the dNTP pool (44, 45), and an imbalanced pool could lead to reduced frequency of mtDNA replication initiation. mtDNA depletion was specifically restricted to bitransgenic mice, which was consistent with them displaying the largest dNTP alterations. The fact that *Rrm2*^{Tg} and *p53R2*^{Tg} mice also had altered dNTP pools but no mtDNA depletion, suggests a threshold effect for the relative dNTP levels above which mtDNA replication becomes inefficient. Nevertheless, we cannot exclude that co-overexpression of Rrm1 and the small subunit gave rise to additional, unidentified effects, which did not occur upon overexpression of one subunit. Moreover, mtDNA depletion was observed only in the skeletal muscle, although the transgenes were overexpressed in both the skeletal and cardiac muscles, suggesting tissue specific mechanisms in the regulation of nucleotide pools and/or mtDNA maintenance.

Altered dNTP pool balance is a hallmark of MNGIE disease, where deficiency of the catabolic enzyme thymidine phosphorylase (TP) leads to elevated dTTP pools, which cause mtDNA depletion, deletions and point mutations in humans (28). Contrary to MNGIE, however, we found no increase in mtDNA point mutations or deletions in the RNR^{Tg} mice. There are at least two possible explanations for the absence of mtDNA instability, other than depletion, in our mice. Firstly, the dNTP changes were almost opposite to those in MNGIE, i.e. the relative dTTP level decreased instead of increasing. Further studies are needed to elucidate the exact effect of changes in the relative levels of each of the four dNTPs on mtDNA replication frequency and fidelity. Secondly, the life-span of a mouse may be too short to develop significant amounts of mtDNA deletions or point mutations in the setting of dNTP imbalance. In support of this, the MNGIE mouse model lacking TP and the related uridine phosphorylase (UP) displayed increased dTTP in brain, and, similar to RNR^{Tg} mice, developed progressive mtDNA depletion, but no deletions or point mutations (27). The authors argued that this was at least partly due to the short life-span of mice, emphasizing the differences in dNTP maintenance and disorders between species.

In conclusion, we have established that expression of recombinant RNR in mice leads to dNTP pool imbalance and progressive depletion of mtDNA. This is in contrast to previous findings in yeast, in which RNR is a positive regulator

of mtDNA abundance. Furthermore, endogenous RNR expression is responsive to increased mtDNA copy number and a potential modifier of mtDNA homeostasis. The dNTP pool imbalance and mtDNA decrease caused by excess RNR suggests that balanced amounts of RNR are essential for mtDNA maintenance *in vivo*, and that RNR is unlikely to be an optimal target for therapeutic engineering of mtDNA levels in mammals.

FUNDING AND ACKNOWLEDGEMENTS

This work was supported by Academy of Finland to [H.T. and A.S.]; University of Helsinki [to A.S.]; Sigrid Juselius Foundation [to A.S.]; Jane and Aatos Erkko Foundation [to A.S.]; Helsinki Biomedical Graduate School [to E.Y.]; the Cornell University Center for Vertebrate Genomics [to J.P. and X.X.]; and National Institutes of Health training grant number T32GM07617 [to J.P.].

The authors thank Prof. Gerald S. Shadel for reagents, Dr Patrick Stover for use of UHPLC system and Prof. Vera Bianchi for expert advice.

References

1. Nordlund P & Reichard P (2006) Ribonucleotide reductases.

2. Fan H, Villegas C, & Wright JA (1996) Ribonucleotide reductase R2 component is a novel malignancy determinant that cooperates with activated oncogenes to determine transformation and malignant potential. *Proc Natl Acad Sci U S A* 93(24):14036-14040.

3. Xu X*, et al.* (2008) Broad overexpression of ribonucleotide reductase genes in mice specifically induces lung neoplasms. *Cancer Res* 68(8):2652-2660.

4. Pontarin G*, et al.* (2007) p53R2-dependent ribonucleotide reduction provides deoxyribonucleotides in quiescent human fibroblasts in the absence of induced DNA damage. *J Biol Chem* 282(23):16820-16828.

5. Nakano K, Balint E, Ashcroft M, & Vousden KH (2000) A ribonucleotide reductase gene is a transcriptional target of p53 and p73. *Oncogene* 19(37):4283-4289.

6. Tanaka H*, et al.* (2000) A ribonucleotide reductase gene involved in a p53-dependent cell-cycle checkpoint for DNA damage. *Nature* 404(6773):42-49.

7. Bourdon A*, et al.* (2007) Mutation of RRM2B, encoding p53-controlled ribonucleotide reductase (p53R2), causes severe mitochondrial DNA depletion. *Nat Genet* 39(6):776-780.

8. Kimura T*, et al.* (2003) Impaired function of p53R2 in Rrm2b-null mice causes severe renal failure through attenuation of dNTP pools. *Nat Genet* 34(4):440-445.

9. Tyynismaa H*, et al.* (2009) A heterozygous truncating mutation in RRM2B causes autosomal-dominant progressive external ophthalmoplegia with multiple mtDNA deletions. *Am J Hum Genet* 85(2):290-295.

10. Shaibani A*, et al.* (2009) Mitochondrial neurogastrointestinal encephalopathy due to mutations in RRM2B. *Arch Neurol* 66(8):1028-1032.

11. Boulet L, Karpati G, & Shoubridge EA (1992) Distribution and threshold expression of the tRNA(Lys) mutation in skeletal muscle of patients with myoclonic epilepsy and ragged-red fibers (MERRF). *Am J Hum Genet* 51(6):1187-1200.

12. Taylor SD*, et al.* (2005) The conserved Mec1/Rad53 nuclear checkpoint pathway regulates mitochondrial DNA copy number in Saccharomyces cerevisiae. *Mol Biol Cell* 16(6):3010-3018.

13. Baruffini E*, et al.* (2006) Genetic and chemical rescue of the Saccharomyces cerevisiae phenotype induced by mitochondrial DNA polymerase mutations associated with progressive external ophthalmoplegia in humans. *Hum Mol Genet* 15(19):2846-2855.

14. Ekstrand MI*, et al.* (2004) Mitochondrial transcription factor A regulates mtDNA copy number in mammals. *Hum Mol Genet* 13(9):935-944.

15. Tyynismaa H*, et al.* (2004) Twinkle helicase is essential for mtDNA maintenance and regulates mtDNA copy number. *Hum Mol Genet* 13(24):3219-3227.

16. Alam TI*, et al.* (2003) Human mitochondrial DNA is packaged with TFAM. *Nucleic Acids Res* 31(6):1640-1645.

17. Kaufman BA*, et al.* (2007) The mitochondrial transcription factor TFAM coordinates the assembly of multiple DNA molecules into nucleoid-like structures. *Mol Biol Cell* 18(9):3225-3236.

18. Parisi MA & Clayton DA (1991) Similarity of human mitochondrial transcription factor 1 to high mobility group proteins. *Science* 252(5008):965-969.

19. Ylikallio E, Tyynismaa H, Tsutsui H, Ide T, & Suomalainen A (2010) High mitochondrial DNA copy number has detrimental effects in mice. *Hum Mol Genet* 19(13):2695-2705.

20. Ikeuchi M*, et al.* (2005) Overexpression of mitochondrial transcription factor a ameliorates mitochondrial deficiencies and cardiac failure after myocardial infarction. *Circulation* 112(5):683-690.

21. Tyynismaa H*, et al.* (2005) Mutant mitochondrial helicase Twinkle causes multiple mtDNA deletions and a late-onset mitochondrial disease in mice. *Proc Natl Acad Sci U S A* 102(49):17687-17692.

22. Hakansson P, Hofer A, & Thelander L (2006) Regulation of mammalian ribonucleotide reduction and dNTP pools after DNA damage and in resting cells. *J Biol Chem* 281(12):7834-7841.

23. Sherman PA & Fyfe JA (1989) Enzymatic assay for deoxyribonucleoside triphosphates using synthetic oligonucleotides as template primers. *Anal Biochem* 180(2):222-226.

24. Ferraro P, Franzolin E, Pontarin G, Reichard P, & Bianchi V (2010) Quantitation of cellular deoxynucleoside triphosphates. *Nucleic Acids Res* 38(6):e85.

25. Kochanowski N*, et al.* (2006) Intracellular nucleotide and nucleotide sugar contents of cultured CHO cells determined by a fast, sensitive, and high-resolution ion-pair RP-HPLC. *Anal Biochem* 348(2):243-251.

26. Ashley N*, et al.* (2007) Defects in maintenance of mitochondrial DNA are associated with intramitochondrial nucleotide imbalances. *Hum Mol Genet* 16(12):1400-1411.

27. Lopez LC*, et al.* (2009) Unbalanced deoxynucleotide pools cause mitochondrial DNA instability in thymidine phosphorylase-deficient mice. *Hum Mol Genet* 18(4):714-722.

28. Nishino I, Spinazzola A, & Hirano M (1999) Thymidine phosphorylase gene mutations in MNGIE, a human mitochondrial disorder. *Science* 283(5402):689-692.

29. Faupel RP, Seitz HJ, Tarnowski W, Thiemann V, & Weiss C (1972) The problem of tissue sampling from experimental animals with respect to freezing technique, anoxia, stress and narcosis. A new method for sampling rat liver tissue and the physiological values of glycolytic intermediates and related compounds. *Arch Biochem Biophys* 148(2):509-522.

30. Ferraro P, Nicolosi L, Bernardi P, Reichard P, & Bianchi V (2006) Mitochondrial deoxynucleotide pool sizes in mouse liver and evidence for a transport mechanism for thymidine monophosphate. *Proc Natl Acad Sci U S A* 103(49):18586-18591.

31. Schwenke WD, Soboll S, Seitz HJ, & Sies H (1981) Mitochondrial and cytosolic ATP/ADP ratios in rat liver in vivo. *Biochem J* 200(2):405-408.

32. Bulst S*, et al.* (2009) In vitro supplementation with dAMP/dGMP leads to partial restoration of mtDNA levels in mitochondrial depletion syndromes. *Hum Mol Genet* 18(9):1590-1599.

33. Akman HO*, et al.* (2008) Thymidine kinase 2 (H126N) knockin mice show the essential role of balanced deoxynucleotide pools for mitochondrial DNA maintenance. *Hum Mol Genet* 17(16):2433-2440.

34. Mandel H*, et al.* (2001) The deoxyguanosine kinase gene is mutated in individuals with depleted hepatocerebral mitochondrial DNA. *Nat Genet* 29(3):337-341.

35. Saada A*, et al.* (2001) Mutant mitochondrial thymidine kinase in mitochondrial DNA depletion myopathy. *Nat Genet* 29(3):342-344.

36. Zhou X*, et al.* (2008) Progressive loss of mitochondrial DNA in thymidine kinase 2-deficient mice. *Hum Mol Genet* 17(15):2329-2335.

37. Hosseini SH*, et al.* (2007) Targeted transgenic overexpression of mitochondrial thymidine kinase (TK2) alters mitochondrial DNA (mtDNA) and mitochondrial polypeptide abundance: transgenic TK2, mtDNA, and antiretrovirals. *Am J Pathol* 170(3):865-874.

38. Eaton JS, Lin ZP, Sartorelli AC, Bonawitz ND, & Shadel GS (2007) Ataxia-telangiectasia mutated kinase regulates ribonucleotide reductase and mitochondrial homeostasis. *J Clin Invest* 117(9):2723-2734.

39. Mihara M*, et al.* (2003) p53 has a direct apoptogenic role at the mitochondria. *Mol Cell* 11(3):577-590.

40. Pontarin G, Gallinaro L, Ferraro P, Reichard P, & Bianchi V (2003) Origins of mitochondrial thymidine triphosphate: dynamic relations to cytosolic pools. *Proc Natl Acad Sci U S A* 100(21):12159-12164.

41. Guittet O*, et al.* (2001) Mammalian p53R2 protein forms an active ribonucleotide reductase in vitro with the R1 protein, which is expressed both in resting cells in response to DNA damage and in proliferating cells. *J Biol Chem* 276(44):40647-40651.

42. Rampazzo C*, et al.* (2010) Regulation by degradation, a cellular defense against deoxyribonucleotide pool imbalances. *Mutat Res*.

43. Reichard P (1988) Interactions between deoxyribonucleotide and DNA synthesis. *Annu Rev Biochem* 57:349-374.

44. Anglana M, Apiou F, Bensimon A, & Debatisse M (2003) Dynamics of DNA replication in mammalian somatic cells: nucleotide pool modulates origin choice and interorigin spacing. *Cell* 114(3):385-394.

45. Chabes A & Stillman B (2007) Constitutively high dNTP concentration inhibits cell cycle progression and the DNA damage checkpoint in yeast Saccharomyces cerevisiae. *Proc Natl Acad Sci U S A* 104(4):1183-1188.

Chapter 3: Lethal Deregulation of Ribonucleotide Reductase in Transgenic Mice[1]

ABSTRACT

Mammalian genome stability is dependent in part on the availability of nucleotides for nuclear and mitochondrial DNA replication and repair. Elevated dNTP levels promote survival following DNA damage but also decrease replication fidelity and are mutagenic, necessitating tight control of nucleotide metabolism. The cytosolic enzyme ribonucleotide reductase (RNR) catalyzes the rate-limiting step in *de novo* dNTP biosynthesis. The enzyme consists of two nonidentical homodimeric subunits, a large R1 subunit (encoded by the *Rrm1* gene) and a small R2 subunit (encoded by *Rrm2* or *p53R2*). Regulation of RNR is accomplished through multiple mechanisms including control of R2 subunit protein levels and negative feedback regulation through the activity site within the R1 subunit. In order to study the effect of loss of allosteric feedback control, we created a mouse model featuring a hyperactive mutant form of the enzyme. The D57N mutation within the activity site disables feedback inhibition and results in a mutator phenotype in cultured cells. Two independent transgenic lines that broadly overexpressed the *Rrm1*^{D57N} mutant to different extents displayed no overt phenotypes. I therefore tested the

[1] Jennifer L. Page, Emil Ylikallio, Xia Xu, Joshua Levy, Joshua Darfler, Rachel Peters, Teresa Southard, Henna Tynnismaa, Anu Suomalainen, and Robert S. Weiss. Manuscript in preparation.
Author contributions are indicated within figure legends by author's initials.

hypothesis that more severe phenotypes would arise upon simultaneous overexpression of *Rrm1*^{D57N} and either small subunit. For this purpose, I crossed mice from each *Rrm1-D57N*^{Tg} strain to *Rrm2*- or *p53R2*-overexpressing mice. Interestingly, combining overexpression of *Rrm1*^{D57N} and either small subunit caused synthetic lethality. By contrast, bitransgenic mice overexpressing wild type *Rrm1* and either small RNR subunit were born at expected frequencies and appeared grossly normal. The extent of *Rrm1*^{D57N} overexpression affected the timing of lethality in bitransgenic animals; higher levels of *Rrm1*^{D57N} overexpression were associated with embryonic lethality while more modest *Rrm1*^{D57N} overexpression caused postnatal death. Rare surviving adult *Rrm1*^{D57N} + *Rrm2* bitransgenic mice exhibited severe muscle degeneration and characteristics of premature aging. I hypothesize that simultaneously overriding two primary RNR regulatory mechanisms results in greatly elevated RNR activity, producing abnormal dNTP pools that interfere with genome maintenance and function. These and further experiments will provide insights into how the control of nucleotide levels through regulation of RNR catalytic activity impacts genomic stability and mammalian development.

INTRODUCTION

Mammalian cells contain two separate and functional genomes, the proper maintenance of which is critical for survival. In addition to the nuclear genome, comprised of approximately 3.4 gigabases of DNA and encoding roughly 28,000 genes in mice (Ensembl assembly m37), eukaryotic cells

maintain a mitochondrial genome, which is multicopy, comprised of approximately 16 kilobases of DNA and only encodes 39 genes. One of the key determinants in genome maintenance is the availability of dNTPs for DNA synthesis. Efficient and faithful replication by the 3 main replicative polymerases, DNA Pol δ, Pol ε, and the mitochondrial DNA Pol γ, relies on adequate and balanced nucleotide pools. All three polymerases contain exonucleolytic proofreading domains that function to prevent DNA mismatches in the presence of balanced nucleotide pools, but all three are also subject to increases in replication errors when the nucleotide pools are perturbed(2-5). Elevated nucleotide pools increase the error rate of all three polymerases and result in increased mutation rates(6). Conversely, elevated nucleotide pools have also been shown to improve cell survival following DNA damage, by promoting lesion bypass(7). This has the added effect of suppressing potentially deleterious repair mechanisms such as sister chromatid exchange and hyperrecombination, thus stabilizing the genome(8).

Unbalanced nucleotide pools are highly mutagenic(9, 10). During DNA synthesis, excessive amounts of an incorrect nucleotide at the site of elongation can dramatically increase mismatches(2), and also can promote frameshift errors by yeast Pol α and in HeLa cell extracts(11). The stimulation of the mismatch-repair system by these replication errors and subsequent repair creates transient DNA damage that can also stimulate S-phase checkpoint activation(12). At the most extreme, severely unbalanced dNTP

pools, particularly those that deplete one or more specific nucleotides, can trigger activation of the S-phase checkpoint(10) or stimulate deletions within the mitochondrial DNA(13).

Another significant effect of unbalanced nucleotide pools is depletion of mitochondrial DNA(14). Mitochondrial DNA depletion syndromes are a set of heterologous disorders characterized by a mitochondrial DNA copy number that is typically less than 30% of the wild type level. The mtDNA depletion can cause phenotypes in a range of tissues that have high energy needs, such as brain(15), liver(16), and skeletal muscle . Mutations causing mtDNA depletion are found mostly in genes responsible for nucleotide metabolism, such as *de novo* synthesis (by the small ribonucleotide reductase subunit)(17-19), nucleotide salvage pathways (by thymidine kinase and deoxyguanosine kinase)(16, 20-22), and nucleotide degradation (by thymidine phosphorylase and uridine phosphorylase)(15, 23, 24).

Control over nucleotide abundance and pool balance is accomplished in part through the cytosolic enzyme ribonucleotide reductase (RNR)(25). RNR catalyzes the rate-limiting step in *de novo* dNTP biosynthesis(26), the removal of the 2'-hydroxyl from the nucleoside diphosphate to produce the deoxynucleoside diphosphate. The mammalian enzyme is composed of two subunits, a large R1 subunit encoded by a single gene, *Rrm1*, and a small R2 subunit, encoded by either *Rrm2* or *Rrm2b* (a.k.a. *p53R2*)(27). All three RNR proteins are localized to the cytoplasm for activity(28), even after DNA

damage(25). dNTPs are produced in the cytosol and move into either the nucleus or the mitochondria in order to take part in DNA replication or DNA repair(25).

Control of RNR activity in mammals is primarily accomplished through two main partially redundant mechanisms. The first mechanism limits the availability of the R2 subunit to specific stages of the cell cycle. The S-phase R2 gene, *Rrm2*, is not expressed in mammalian cells during quiescent stages of the cell cycle(29), but is strongly induced in S-phase to complex with *Rrm1* and synthesize dNTPs for DNA synthesis(30). The Rrm2 protein is targeted for proteolytic degradation at the G2/M transition by the APC^{Cdh1} complex(31), limiting the bulk of RNR activity to S-phase. The p53R2 protein is expressed at low levels throughout the cell cycle and a complex of Rrm1 and p53R2 is continually active(29).

We have previously reported that transgenic mice that overexpress either small RNR subunit, *Rrm2* or *p53R2*, develop spontaneous lung tumors at a high frequency(1). We found that this lung tumorigenesis proceeds through a mutagenic mechanism. While we found that reactive oxygen species were increased in cells overexpressing either small subunit, potentially providing a mechanism for the increased mutation rate, we were unable to exclude elevated RNR activity and increased nucleotide pools as a cause of mutagenesis. In that study we were unable to detect changes in dNTP pools in the lungs when individual RNR subunits were overexpressed(1), but we were

later able to observe dNTP pool alterations in the skeletal muscle (Chapter 2), suggesting increased RNR activity due to loss of one regulatory mechanism. We have also generated mice that feature simultaneous overexpression of *Rrm1* and either small RNR subunit. In these mice the overexpressed small subunits were able to form more active complexes with overexpressed Rrm1, elevating RNR activity. This had the effect of altering nucleotide pools and causing age-dependent mtDNA depletion(32).

A second regulatory mechanism governing RNR activity is allosteric feedback control. The R1 subunit contains two allosteric regulatory sites. A specificity site monitors the ratio of the four dNTPs in order to keep the ratios balanced. Mutation of residues within this site in yeast lead to severely unbalanced and mutagenic dNTP pools(10). The activity site controls enzyme activity by monitoring the ratio of ATP to dATP, functioning as the second main RNR regulatory mechanism (26). The specificity site binds dATP with much higher affinity than does the activity site, so that the level of dATP must be relatively high before further activity is inhibited(33). The proposed mechanism by which dATP binding can inhibit enzyme activity is by blocking the radical transfer pathway, preventing the radical from reaching the catalytic site and being used to reduce the substrate(33). Binding of the stimulant ATP allows for an additional hydrogen bond that moves key residues out of the transfer path; when dATP is bound, the residues block the radical transfer pathway(34). Mutation of residues within this site abolish dATP recognition by

the enzyme and allow for further enzyme activity(33). In yeast and mammals, the critical residue in dATP recognition is Asp 57(7, 35). When mutated to an asparagine (D57N), the enzyme becomes constitutively active and elevates dNTP pools(7). The *Rrm1*^{D57N} mutation was shown in both yeast and in mammalian cell culture models to be mutagenic(7, 35). Further experiments in yeast involved overexpression of the *rnr1-D57N* mutant(36). In yeast, the large subunit is limiting for activity while the small subunits are in excess; therefore by overexpressing the feedback-resistant form, the authors were able to simultaneously disrupt both main regulatory mechanisms controlling RNR activity. This more thorough deregulation resulted in constitutively elevated dNTP pools that were able to inhibit origin firing in S-phase and cause a slow-growth phenotype. To date, no studies have been performed to test the physiological effect of the *Rrm1*^{D57N} mutation in an *in vivo* animal model. We therefore generated transgenic mice that broadly overexpress the *Rrm1*^{D57N} mutant to a high degree.

Here we report on the first mouse model of loss of allosteric feedback control of RNR in mice, as well as the effect of simultaneous disruption of multiple regulatory modes of RNR. I found that mice that overexpress Rrm1-D57N alone are grossly normal. However, when I combined overexpression of Rrm1-D57N with overexpression of either small subunit, I found that the combination causes synthetic lethality in mice. The timing of the lethality depends on which small subunit is overexpressed, as well as the

overexpression level of the large subunit. These manipulations will allow us to study the effects of various degrees of RNR deregulation in mice, and more completely understand the complex regulation of this critical enzyme.

MATERIALS AND METHODS

Plasmids. An expression plasmid encoding mouse *Rrm1* was constructed in the pCaggs expression vector as described previously(1). In order to improve expression in mice, UTR sequences were removed. The *Rrm1* ORF was amplified from pCaggs-Rrm1 with primers F: 5'-CTCGTCGACATGCATGTGATCAAGCGAGATGGC-3' and R: 5'-TCAGGATCCACACATCAGGCACTC-3'. The PCR product was cloned into pCR2.1 with the Topo-TA cloning kit (Strategene). Following sequencing analysis of the insertion fragment ends to confirm no PCR-induced mutations, the PCR-amplified Rrm1 cDNA was digested out with StuI and replaced by the non-amplified StuI fragment from pCaggs-Rrm1. Fragment orientation was confirmed by SphI and EcoRI digestion. The *Rrm1* ORF was then excised from pCR2.1 with SalI/XhoI digest and ligated into XhoI-linearized pCaggs. Fragment orientation was confirmed by BamHI and SalI/XhoI digests. The Rrm1-D57N mutation was inserted by site-directed mutagenesis. Briefly, primers D57N (5'-CCACAGTGGAACTGAACACCCTGGCTGCT-3') and D57N-AS (5'-AGCAGCCAGGGTCAGTTCCACTGTGG-3') were used to amplify the entire pCaggs-Rrm1-ORF-new plasmid. Following DpnI digestion, products were transformed into DH5α and cultured on NZY^{+} medium. The presence of

the mutation was confirmed by XcmI digest, as the D57N mutation destroys an XcmI site. The pCaggs-Rrm1-D57N clone was confirmed to be free of other mutations by sequencing.

Transgenic mice. Transgenic mice were generated by microinjection of linear plasmid DNA into the male pronucleus of FVB/N zygotes. The pCaggs-Rrm1-D57N plasmid was linearized by SalI digestion. Transgenic founder mice were identified by Southern blot analysis. Transgenic mice were maintained as hemizygotes on the FVB/N inbred background strain. Genotyping of mice expected to carry a single RNR transgene was performed as previously described(1). In crosses between *Rrm1*^{Tg} or *Rrm1-D57N*^{Tg} and *Rrm2*^{Tg} or *p53R2*^{Tg}, mice were genotyped by Southern blot as described below.

Big Blue mutation rate assay

Rrm1-D57N^{Tg} or *Rrm1-D57N*^{Tg} *Msh6*$^{+/-}$ (37) mice were crossed to Big Blue^{Tg} mice(38-40) or Big Blue^{Tg} *Msh6*$^{+/-}$ mice, respectively. All mice were aged to 90 days in order to allow mutations to accumulate. Tissues were harvested and snap-frozen in liquid nitrogen immediately following euthanasia by CO_2 asphyxiation.

Frozen tissue was homogenized in a Dounce homogenizer (Wheaton) using the loose pestle by 15 strokes in the presence of: 3.3 g/L $Na_2HPO_4 \cdot 7H_2O$, 8 g/L NaCl, 0.2 g/L KCl, 0.2 g/L KH_2PO_4, and 0.05M EDTA, pH 8.0, supplemented with RNaseA at 200 μg/mL. Following homogenization, the samples were transferred to a 50-mL conical tube containing 3 mL of the

digestion solution (34 mg Proteinase K, 6.8 mL dH_2O, 3.4 mL 10% SDS, 6.8 mL 0.25M EDTA, pH 7.5). Samples were allowed to digest at 50ºC for 4 hours (lung), 2 hours (spleen), or 3 hours (thymus) with gentle inversion of the tubes every 60 minutes. DNA was then isolated via sequential phenol-chloroform extractions and precipitated with the stepwise addition of 100% ethanol. The DNA was allowed to dry only briefly at RT before 1mL sterile H_2O was added. DNA was allowed to dissolve for up to 4 days at 4ºC. Approximately 8μL of DNA was added to 1 red tube of Transpack λ phage recovery packaging extract (Stratagene) and incubated at 30ºC for 90 minutes. 12μL Transpack packaging extract from the blue tube was added to each λ recovery sample and mixed by pipetting. The samples were further incubated at 30ºC for 90 minutes. Following packaging, the phage were used to infect G1250 *E. coli* for 15 minutes and then were plated on TB1 agar plates. Total plaque-forming units (PFU) were estimated by averaging the total number of plaques on triplicate plates incubated at 37ºC for 24 hours. Total mutant plaques were estimated by counting the total number of plaques on 10 replicate plates incubated at 24ºC for 48 hours. All potential mutant plaques were picked and dissolved in SM buffer overnight. Confirmation of potential plaques was performed by infecting fresh G1250 cells at 24ºC for 48 hours. DNA from confirmed mutant plaques was amplified by PCR with primers “cII-For2” (5’-CCGCTCTTACACATTCCAGC-3’) and “*cII*-Rev1” (5’-CCTCTGCCGAAGTTGAGTAT-3’) and sequenced with primer “*cII*-For1” (5’-

CCACACCTATGGTGTATG-3') to obtain the specific mutation. Final mutation rate and spectra were determined by the total number of unique mutations compared to the total PFU.

Southern blot analysis. DNA extracted from tails of adult mice or yolk sacs of embryos was subjected overnight to transgene-specific restriction digest and separated on 0.8% agarose gel. The *Rrm1* and *Rrm1-D57N* transgenes were detected by digestion with BamHI (Fermentas) and the *p53R2* transgene was detected by digestion with EcoRV (Fermentas). Following alkaline transfer to a nylon membrane (GeneScreen Plus, Perkin Elmer), the presence of transgene DNA was detected with a transgene-specific radiolabeled probe.

Northern blot analysis. Total RNA was extracted from mouse cells with RNAStat-60 (TelTech, Inc) and separated on agarose/formaldehyde gel. RNA is transferred to a nylon membrane (GeneScreen, Perkin Elmer) and detected with Rrm1-specific radiolabeled probe.

Immunoblot analysis. Tissue extracts were prepared by lysis in RIPA buffer (150mM NaCl, 50 mM NaF, 1% NP-40, 0.8% DOC, 0.1% SDS, 50 mM Tris pH 8.0, and 5 mM EDTA) supplemented with protease inhibitors (apropinin, 2μg/mL; leupeptin, 2μg/mL; and PMSF, 20μg/mL) and sodium orthovanadate (400 μM) as a phosphatase inhibitor. Extracts were separated on 10% polyacrylamide gel and transferred to PVDF membrane (Perkin Elmer). R1 protein was detected by AD203, mouse monoclonal anti-R1 (InRo Biomedtek),

and loading was assessed by detecton of α-tubulin with mouse monoclonal anti-α-tubulin (Sigma).

Histology. Adult mice were euthanized by overdose with carbon dioxide. Neonates (mice ages P10 and younger) were euthanized by decapitation. Tissues for histological analysis were excised and fixed overnight at room temperature in 10% buffered formalin. Tissues were sectioned at 5mm thickness prior to staining with hematoxylin and eosin (H&E) or Masson's trichrome, or Periodic Acid Schiff's stain. Sample dehydration, embedding, sectioning, and staining were conducted by the Core Histology Lab in the College of Veterinary Medicine at Cornell University.

Southern blotting for mtDNA copy number determination.

Total DNA was isolated from tissues by proteinase K digestion and standard phenol-chloroform extraction. Southern blotting was performed essentially as described (41). Briefly, three micrograms total DNA was digested with SacI overnight at 37°C, samples were then separated by electrophoresis in an agarose gel and blotted by alkaline transfer onto a Hybond N+ membrane (Amersham Biosciences). The membrane was hybridized overnight at 68°C in a roller hybridizer using 5 μCi/ml ^{32}P-dCTP labeled (PCR-generated) mouse mtDNA probe, and 18S rDNA probe in pBR322 plasmid. Phosphoimager analysis was done with Typhoon 9400 (Amersham Biosciences) and mtDNA was quantified against the 18S rDNA signal using ImageQuant v5.0 software (Amersham Biosciences).

Real time PCR.

For mtDNA quantification, the quantitative real-time (Q)PCR reactions were done with 25 ng total DNA used as template and normalizing the *mt-Cytb* gene amplification level (primer sequences: 5'-GCTTTCCACTTCATCTTACCATTTA-3' and 5'-TGTTGGGTTGTTTGATCCTG-3') against the nuclear beta actin gene (primer sequences: 5'-GGAAAAGAGCCTCAGGGCAT-3' and 5'-GAAGAGCTATGAGCTGCCTGA-3'). Samples were run on an Abi Prism SDS 7000 machine (Applied Biosystem). Amplification conditions were: 95°C for 7 minutes followed by 35 cycles of 95°C for 10 seconds and 60°C for 30 seconds. Dissociation curves were checked to ensure the existence of a single PCR product. Each sample was run in duplicate, and samples with significant variation between duplicates were excluded. QPCR data were analyzed using 7000 System Sequence Detection Software version 1.2.3 (Applied Biosystems).

Long PCR.

Long PCR to amplify the entire mitochondrial genome or selectively deleted mtDNA molecules was done using the Expand Long Template PCR System (Roche) with primers 5'- GAG GTG ATG TTT TTG GTA AAC AGG CGG GGT -3' and 5'- GGT TCG TTT GTT CAA CGA TTA AAG TCC TAC GTG -3'. 50 ng total DNA was used as template. Cycling conditions were: 92°C for 2 minutes followed by 30 cycles of 92°C for 10 seconds and 68°C for 12 minutes. PCR

products were separated by electrophoresis on 1% agarose gels and visualized with a Typhoon 9400 scanner (Amersham Biosciences). Primers hybridized to the control region of mtDNA located at nucleotide positions 1953-1924 and 2473-2505.

RESULTS

Generation of Rrm1-D57N transgenic mice and expression analyses

To generate transgenic mice overexpressing *Rrm1*^{D57N}, the G to A transition within codon 57 was introduced by site-directed mutagenic PCR. Two independent transgenic founder animals were obtained (Figure 3.1A, lanes 6 and 12). The founder animal in lane 12 shows a more intense band than the founder in lane 6; leading us to hypothesize that the founder in lane 12 would show more robust overexpression than the founder in lane 6. Therefore, the resulting strains are referred to hereafter as *Rrm1-D57N(low)*^{Tg} (lane 6) and *Rrm1-D57N(high)*^{Tg} (lane 12). The strains were maintained on a pure FVB/N background.

Endogenous and transgenic expression was assessed in a variety of tissues in *Rrm1-D57N(high)*^{Tg} and wild-type FVB mice by Northern blot analysis (Figure 3.1B). In wild type FVB mice, *Rrm1* was detected most strongly in the most proliferative tissues, the testis and thymus (Figure 3.1B, left). Northern blot analysis of *Rrm1-D57N(high)*^{Tg} mice revealed two bands corresponding to *Rrm1* transcript; the upper band is from the endogenous locus while the lower band, corresponding to the transcript from the transgene,

runs at a lower molecular weight due to the removal of 5'-UTR sequence. The upper band is the predominant band in the spleen and thymus, while the lower band from the transgene predominates in lung, liver, kidney, and skeletal muscle.

The expression results obtained by Northern blot analysis were confirmed by immunoblot (Figure 3.1C). I assessed total R1 protein levels in tissues obtained from wild type FVB mice (wt), *Rrm1-D57N(low)*^{Tg} mice (L), and *Rrm1-D57N(high)*^{Tg} (H) mice. In agreement with the Southern blot in Fig 3.1A, *Rrm1-D57N(high)*^{Tg} mice showed higher R1 protein levels than *Rrm1-D57N(low)*^{Tg} mice, which were intermediate between wild type and *Rrm1-D57N(high)*^{Tg} levels. To obtain a more precise value for *Rrm1-D57N* overexpression in tissues from transgenic mice, I utilized the serial dilution method described in Chapter 2. Because pCaggs drives the greatest expression in skeletal and cardiac muscle, I assessed the level of D57N overexpression in these two tissues (Figure 3.2). I found that the *D57N(low)*^{Tg} is expressed roughly 94-fold (93.99x) in the skeletal muscle while the *D57N(high)*^{Tg} is expressed over 600-fold (608.41x).

Limited phenotypes in *Rrm1-D57N*^{Tg} mice

I generated a cohort of mice expressing *Rrm1-D57N(low)*^{Tg} or *Rrm1-D57N(high)*^{Tg} with control littermates. Mice were maintained to a maximum of 18 months of age and monitored. Because mice overexpressing *Rrm2*^{Tg} or *p53R2*^{Tg} displayed an increase in spontaneous lung tumorigenesis, I primarily

monitored mice for the development of lung cancer. Of 44 total wild type mice, 12 had developed lung adenomas or adenocarcinomas by 18 months of age, roughly 26% of the total (Table 3.1). This number is consistent with the reported background lung tumor incidence in wild type FVB/N mice of approximately 31%(42). Mice expressing the *Rrm1-D57N(low)* transgene showed a 36.73% incidence of cancer, and mice with the *Rrm1-D57N(high)* transgene showed a 34.62% incidence, for a combined 36% of *Rrm1-D57N* mice with lung tumors. By chi-squared analysis, this increase in lung tumorigenesis is significant (p=0.013). While the total lung tumor incidence is increased, the mean size of tumors in *Rrm1-D57N*^{Tg} mice was not increased with respect to the mean tumor size of wild type mice. Tumor-bearing wild type mice had an average lung tumor diameter of 2.72 ± 4.4 mm while tumor-bearing Rrm1-D57N^{Tg} mice had an average lung tumor diameter of 2.51 ± 3.2mm. Pathological grade was not affected by Rrm1-D57N overexpression, as 2 of 44 transgene-negative control mice developed adenocarcinomas (4.5%) while 3 of 67 Rrm1-D57N transgenic mice developed adenocarcinomas (4.4%). Overall, overexpression of Rrm1-D57N was able to increase the incidence of lung tumors in FVB mice, but did not drive lung tumorigenesis, in contrast to overexpression of *Rrm2* or *p53R2*.

Overexpression of *Rrm1-D57N* did not increase mutation rate as measured by the Big Blue mutation detection system

Multiple studies have reported that the *Rrm1-D57N* mutation is mutagenic(7, 35). In order to determine if *Rrm1-D57N* transgenic mice suffered a higher mutation rate than transgene-negative control mice, I crossed each D57N transgenic mouse strain independently to Big Blue mice. Big Blue mice carry multiple copies of the λ phage genome as a transgene. From the phage genome, the *cII* gene functions to control expression of the temperature-sensitive *cI* gene. The *cI* gene product represses the transcription of genes that control lysis, committing the phage for lysogeny. When incubated at 24°C, only phage with a mutant *cII* gene will be able to form plaques, while all phage can form plaques at 37°C, allowing for standardization of packaging efficiency. Therefore, the *cII* gene serves as a mutational reporter(43).

Due to the presence of lung tumors in small-subunit-overexpressing mice, I analyzed the mutation rate in lung tissues from *Rrm1-D57N(low)*^{Tg} and *Rrm1-D57N(high)*^{Tg} mice with transgene-negative FVB mice serving as a control (Figure 3.3). I found no changes in mutant frequency between the three genotypes, and there was high variability between the samples, as was also found in other studies using Big Blue mice(44). The wild type mice had a mean mutant frequency of 3.61 x 10^{-6}, *Rrm1-D57N(low)*^{Tg} mice had 3.59 x 10^{-6} mutants, and *Rrm1-D57N(high)*^{Tg} mice displayed a mutant frequency of 4.09 x

10^{-6}. I next wanted to ask if the mutational spectrum was changed upon Rrm1-D57N overexpression. To answer this, we sequenced the *cII* genes isolated from individual plaques (Table 3.2). I found that transitions were more likely than transversions or deletions in all genotypes, and overexpression of either D57N transgene increased the proportion of mutations that were transitions. In other studies, base substitutions comprised about 85% of all detected mutations at the *cII* locus(43). Our results were fairly consistent with that number, having roughly 60-70% base substitutions. Roughly one-third of all mutations found in wild type mice are transitions (~38%), another one-third are transversions (~34), and the rest are insertions/deletions and non-*cII* mutations (~21% and 7%, respectively). In *Rrm1-D57N(low)*^{Tg} mice, 50% of all mutations are transitions, while 28% were transversions, 17% were insertions/deletions, and non-*cII* mutations made up the last 5%. The overall mutation spectrum was not significantly different from that of wild type mice (p=0.102, χ^2). In *Rrm1-D57N(high)*^{Tg} mice, two-thirds (67%) of the mutations are transitions, while less than one-third (21%) are transversions, and insertions/deletions and non-*cII* mutations, comprise 7% and 5%, respectively. This was significantly different from the mutation spectrum of wild type mice ($p = 6.07 \times 10^{-8}$, χ^2).

Overexpression of Rrm1-D57N on a mismatch-repair-deficient background does not affect lymphomagenesis.

The apparent contradiction between our data, which suggested that overexpression of *Rrm1-D57N* is not mutagenic, and the several published reports that indicate that it increases mutation frequency in multiple models could be explained by multiple hypotheses. Several factors could contribute to an apparent lack of mutagenesis: 1) functional mismatch-repair pathways may correct most, if not all, errors induced by elevated dNTP levels; 2) disabling a single mechanism controlling RNR activity may have limited effects on dNTP levels and mutation frequency; or 3) the Big Blue assay is not sensitive enough to detect modest changes in mutation rate. Even in wild-type mice, presence of a phage genome in mammalian cells may lead to increased efforts for transcriptional silencing. Methylation of cytidines at CpG sites is an epigenetic marker associated with transcriptional silencing. The methylated cytosine is subject to deamination into uridine(45) which will base-pair with adenine during the next round of DNA replication, leading to a G-C to A-T transition at CpG sites. This occurrence has been documented in the literature, with as many as 78% of the observed mutations at the *LacI* locus of the Big Blue transgene being transitions at CpG sites(38). Consistent with this is our .finding that most mutations observed in Big Blue mice, both with and without the Rrm1-D57N transgenes, are transitions at CpG sites, suggesting that the

Figure 3.1. **Generation of Rrm1-D57N overexpressing mice.** *A.* Southern blot analysis of DNA from potential Rrm1-D57N^{Tg} founder animals. Tail DNA from potential founder animals subjected to hybridization with Rrm1-specific radiolabeled probe. Arrows indicate bands corresponding to endogenous Rrm1 gene and Rrm1-D57N transgene. Asterisks denote founder DNA showing presence of Rrm1-D57N transgene. Note that the founder in lane 12 [referred to as Rrm1-D57N(high)] shows greater signal intensity and an additional transgene band, indicating integration of a greater amount of the transgene DNA than the founder in lane 6 [Rrm1-D57N(low)]. (X.X.) *B.* Northern blot analysis of Rrm1 expression in wild type and Rrm1-D57N(high) mice. Total RNA was extracted from the indicated tissues of wild type FVB (left panel(1)) and Rrm1-D57N(high) transgenic mice (right panel) and subjected to Northern blot analysis with a radiolabeled Rrm1-specific probe. Positions of endogenous- and Rrm1-D57N-derived transcripts are indicated. Total ethidium bromide-stained RNA is shown as a loading control. Note that skeletal muscle lane in right panel was intentionally underloaded. (X.X. and J.P.) *C.* Immunoblot analysis of Rrm1 protein expression in the indicated tissues of wild type (wt), Rrm1-D57N(low)^{Tg} (L), and Rrm1-D57N(high)^{Tg} (H) transgenic mice. Total protein from the indicated tissues was detected with R1-specific antibody. The same membrane was probed with antibody specific to α-tubulin as a loading control. (X.X.)

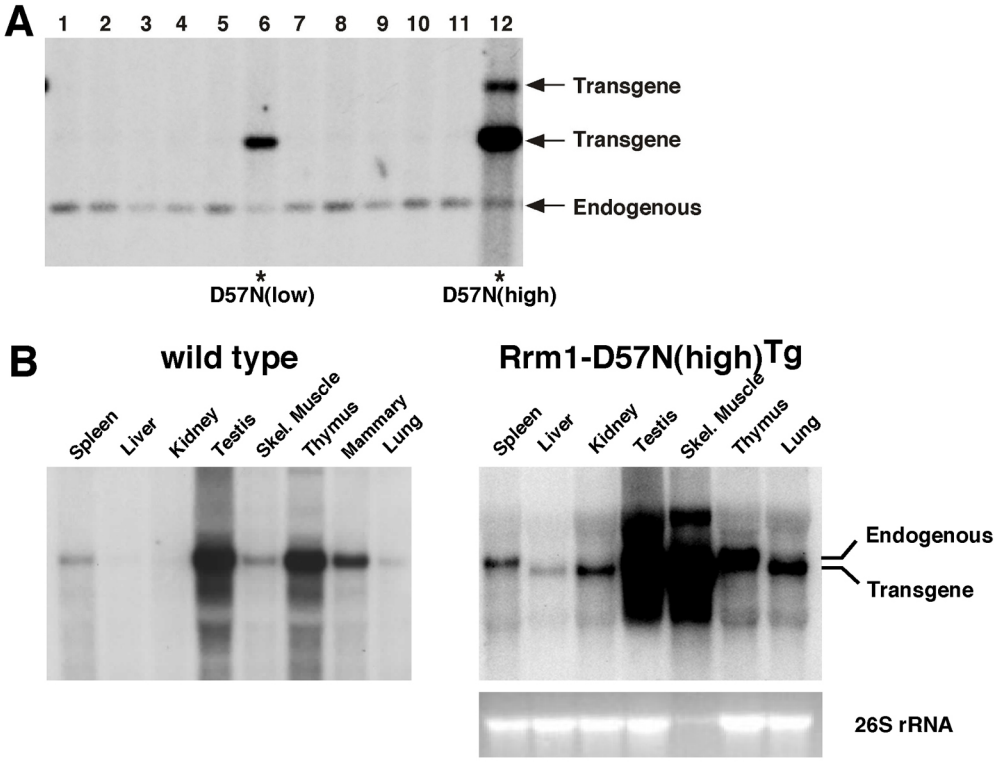
A
1 2 3 4 5 6 7 8 9 10 11 12
Transgene
Transgene
Endogenous
D57N(low)
D57N(high)
B
wild type
Rrm1-D57N(high)Tg
Spleen Liver Kidney Testis Skel. Muscle Thymus Mammary Lung
Spleen Liver Kidney Testis Skel. Muscle Thymus Lung
Endogenous
Transgene
26S rRNA
C
Liver Kidney Skel. Muscle Lung
wt L H wt L H wt L H wt L H
Rrm1
α-tubulin

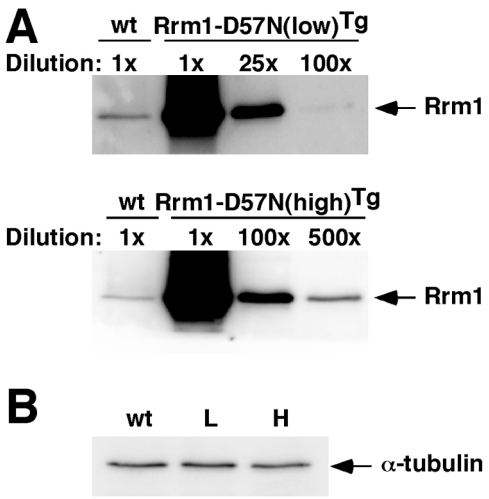

Figure 3.2. Quantification of transgenic overexpression by western blot. *A.* Serial dilutions quantifying Rrm1 expression in the skeletal muscle of Rrm1-D57N(low) and Rrm1-D57N(high) transgenic mice. Lysates from transgenic mice were serially diluted in RIPA buffer, and were compared to undiluted wild type sample. *B.* α-tubulin serves as a loading control. (J.P.)

Table 3.1. Analysis of lung neoplasms in Rrm1-D57N transgenic mice.[a]

Genotype	# animals	# with adenoma or adenocarcinoma	lung tumor %	% of animals with multiple tumors	average tumor diameter ± std (mm)
wild type FVB	44	12	27.27%	4.55%	2.72 ± 4.4
Rrm1-D57N(low)^{Tg}	49	18	36.73%	10.20%	2.65 ± 3.2
Rrm1-D57N(high)^{Tg}	26	9	34.62%	8.00%	2.16 ± 3.16

[a]Mice of the indicated genotypes were monitored until moribund or to a maximum age of 18 months, at which time they were necropsied and the overall phenotype recorded. The predominant phenotype was lung tumorigenesis, due in large part to the fact that the FVB inbred strain is prone to lung tumor development(42). Other criteria for tumorigenicity was not met in these mice, indicating that overexpression of Rrm1-D57N does not drive lung tumorigenesis. (J.P.)

mutations are due to methylation of cytidines to suppress expression of the viral genes and not the overexpressed RNR subunits. Because of the reduced sensitivity in detecting mutations because of CpG methylation, I sought to assess the mutagenicity of Rrm1-D57N overexpression by determining how overexpression interacts with a mismatch repair deficiency.

The mammalian mismatch repair system has two main mismatch-sensing complexes: MutSα, consisting of *Msh2* and *Msh6*, and MutSβ, consisting of *Msh2* and *Msh3*. MutSα recognizes mispairs and small insertions/deletions while MutSβ recognizes larger insertions and deletions. In mice, knockout of *Msh6* results in an increased incidence of lymphomas and other tumors to a smaller extent(37). I hypothesized that overexpression of *Rrm1-D57N* on an already sensitized background would synergize with *Msh6* deficiency to increase tumor incidence and shorten the tumor latency. To test this, I first crossed mice harboring a heterozygous mutation of *Msh6* to mice carrying either the *Rrm1-D57N(low)* or *Rrm1-D57N(high)* transgene. Mice heterozygous for *Msh6* and carrying the *Rrm1-D57N* transgene were interbred to littermates that were heterozygous for *Msh6* alone, generating mice carrying 6 possible genotypes. I first generated a cohort of these mice and monitored them for tumor formation. Mice were euthanized when moribund or when they reached 500 days of age. The median age of death for $Msh6^{-/-}$ mice was around 439 days, while the median age for $Rrm1\text{-}D57N^{Tg}$ $Msh6^{-/-}$ mice was

shortened to 292; however this difference was not significant by log rank test (Figure 3.4). Only 2 *Msh6*$^{+/-}$ mice died before the 500-day cutoff compared to 7 *Rrm1-D57N*^{Tg} *Msh6*$^{+/-}$ mice, this difference is also not significant. Mice were analyzed for the formation of lung tumors, lymphoma, and other tumors (Table 3.3). .None of the 13 *Msh6*$^{-/-}$ mice developed lung tumors compared to 14% (3 of 21) of *Rrm1-D57N*^{Tg} *Msh6*$^{-/-}$ mice; however due to small sample size this is not significant. The incidence of lymphomas was not changed in *Msh6*$^{-/-}$ mice when *Rrm1-D57N*^{Tg} was overexpressed. 84% of *Msh6*$^{-/-}$ mice developed lymphoma, while only 71% of *Rrm1-D57N*^{Tg} *Msh6*$^{-/-}$ mice developed lymphoma. Other tumors, such as skin papillomas, were observed at a higher frequency in *Rrm1-D57N*^{Tg} *Msh6*$^{-/-}$ mice than in *Msh6*$^{-/-}$ mice, but again, due to small sample size this is not significant. In the *Msh6*$^{+/-}$ mice, lung tumorigenesis was increased roughly 3-fold and lymphomagenesis was increased roughly 5-fold when Rrm1-D57N was overexpressed ($p=4.48 \times 10^{-7}$ and $p=4.44 \times 10^{-20}$, respectively, χ^2).

To further confirm that overexpression of Rrm1-D57N does not synergize with mismatch repair deficiency, I assayed the mutation rate using the Big Blue system. Loss of *Msh6* in mice was able to significantly elevate the mutant frequency compared to mice wild type or heterozygous for *Msh6*; however addition of either Rrm1-D57N transgene failed to further elevate mutant frequency (Figure 3.5).

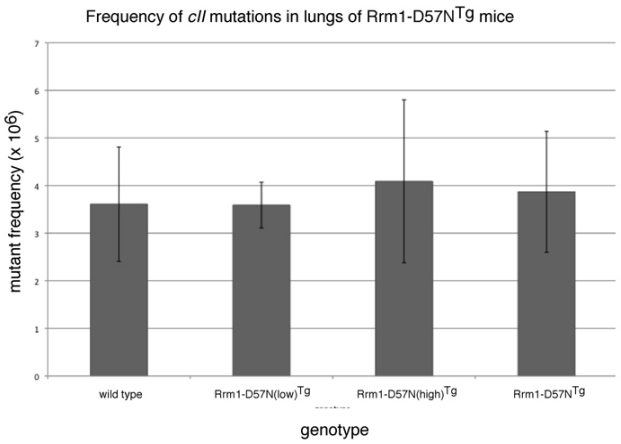

Figure 3.3. Mutant frequency in lung tissue from Rrm1-D57N transgenic mice as measured by the Big Blue assay. Data are represented as mean for each genotype. Wild type (n=3), *Rrm1-D57N(low)^{Tg}* (n=3) and *Rrm1-D57N(high)^{Tg}* (n=4) all displayed low mutant frequencies. Error bars, standard deviation. (J.P.)

Table 3.2. Spectrum of *cII* mutations observed in *Rrm1-D57N* transgenic mice[a].

Type of Mutation	wild type FVB		*Rrm1-D57N(low)*^{Tg}		*Rrm1-D57N(high)*^{Tg}		*Rrm1-D57N*^{Tg}	
	Number	Percent	Number	Percent	Number	Percent	Number	Percent
Transition	**11**	**37.93%**	**18**	**50.00%**	**38**	**66.67%**	**56**	**60.22%**
G:C--> A:T	10	34.48%	16	44.44%	37	64.91%	53	56.99%
A:T-->G:C	1	3.45%	2	5.56%	1	1.75%	3	3.23%
Transversion	**10**	**34.48%**	**10**	**27.78%**	**12**	**21.05%**	**22**	**23.66%**
G:C --> T:A	5	17.24%	5	13.89%	8	14.04%	13	13.98%
T:A--> G:C	0	0.00%	1	2.78%	1	1.75%	2	2.15%
T:A --> A:T	4	13.79%	1	2.78%	2	3.51%	3	3.23%
G:C --> C:G	1	3.45%	3	8.33%	1	1.75%	4	4.30%
Insertion/Deletion	**6**	**20.69%**	**6**	**16.67%**	**4**	**7.02%**	**10**	**10.75%**
1 bp insertion	2	6.90%	2	5.56%	2	3.51%	4	4.30%
2 or more insertions	0	0.00%	1	2.78%	0	0.00%	1	1.08%
1 bp deletion	2	6.90%	3	8.33%	2	3.51%	5	5.38%
2 or more deletions	2	6.90%	0	0.00%	0	0.00%	0	0.00%
Non-*cII* mutation	**2**	**6.90%**	**2**	**5.56%**	**3**	**5.26%**	**5**	**5.38%**
total	**29**	**100.00%**	**36**	**100.00%**	**57**	**100.00%**	**93**	**100.00%**

[a]Total genomic DNA was harvested from the lungs of wild type, *Rrm1-D57N(low)*^{Tg}, or *Rrm1-D57N(high)*^{Tg} mice and packaged into viable phage. The *cII* gene of confirmed plaques was amplified and sequenced. Duplicate mutations are assumed to arise from a clonal event and are omitted. (J.P. and J.D.)

The mutation spectra were quite variable (Table 3.4). In mice harboring wild type *Msh6*, the mutation spectra observed in the mice with the Rrm1-D57N transgene were significantly different from the spectra in the transgene-negative mice ($p = 2.39 \times 10^{-5}$, χ^2). Also in the *Msh6*$^{+/-}$ mice, the mutation spectra observed in the mice with the Rrm1-D57N transgene were significantly different from the spectra in the transgene-negative mice ($p = 3.58 \times 10^{-8}$, χ^2). Only in the *Msh6*$^{-/-}$ mice was there no difference in mutation spectra with or without the transgene ($p = 0.268$, χ^2).

Mismatch-repair deficiency primarily causes gastrointestinal tumors as addition to B-and T-cell lymphomas(37, 46), suggesting that analysis of proliferative tissues such as thymus and spleen may reveal increases in mutant frequency that analysis of lung tissue, being quiescent, cannot uncover. I therefore performed the analysis in spleen and thymus from one *Rrm1-D57N*^{Tg} *Msh6*$^{-/-}$ mouse and one *Msh6*$^{-/-}$ control. I again found no difference in mutant frequency between *Rrm1-D57N*^{Tg} *Msh6*$^{-/-}$ and transgene-negative *Msh6*$^{-/-}$ mice; the mutant frequencies in the thymus were 3.25×10^{-4} in the transgenic and 3.92×10^{-4} in the control and in the spleen, 3.73×10^{-4} in the transgenic and 3.63×10^{-4} in the control.

Overall, these data suggest that overexpression of Rrm1-D57N alone is not mutagenic. Furthermore, D57N overexpression was unable to synergize with dysfunction of the mismatch repair system to enhance mutagenesis,

further suggesting that loss of a single regulatory mechanism of RNR is not mutagenic.

Simultaneous overexpression of *Rrm1-D57N* and either small RNR subunit causes synthetic lethality

We previously reported that mice overexpressing *Rrm2* or *p53R2* develop lung tumors but are otherwise grossly normal. However, those mice only exhibited disruption of one RNR regulatory mechanism, control of RNR activity through limitation of small subunit protein levels. As previously stated, mice overexpressing *Rrm1-D57N* alone were also obtained at expected frequencies and were grossly normal. In order to assess the effect of simultaneous disruption of multiple RNR regulatory modes, I crossed mice overexpressing either small RNR subunit with mice overexpressing *Rrm1-D57N*. I used each Rrm1-D57N strain individually in these crosses, resulting in four possible overexpression combinations. Remarkably, I found that mice with either level of *Rrm1-D57N* overexpression and either small RNR subunit were inviable (Table 3.5). Specifically, of an expected 30 *Rrm1-D57N(high)*^{Tg} + *p53R2*^{Tg} bitransgenic mice, 0 were obtained. Likewise, 51.25 *Rrm1-D57N(low)*^{Tg} + *p53R2*^{Tg} bitransgenic mice were expected and 0 were observed, and 26.5 *Rrm1-D57N(high)*^{Tg} + Rrm2^{Tg} bitransgenic mice were expected and 0 were obtained. Of 69.75 expected *Rrm1-D57N(low)*^{Tg} + *Rrm2*^{Tg} bitransgenic mice expected, 5 were obtained that survived to adulthood. Of the five surviving bitransgenic adults, two survived only 21 days.

Table 3.3. Phenotypes observed in mice harboring *Rrm1-D57N*^{Tg} and *Msh6* deficiency.[a]

Mouse genotype		n. of animals	mean survival (days)	n. with lung tumor	%	n. with lymphoma	%	n. with other tumor	%
	Msh6$^{+/+}$	4	494.75	0	0.00%	1	25.00%	0	0.00%
	Msh6$^{+/-}$	20	494.45	1	5.00%	1	5.00%	1	5.00%
	Msh6$^{-/-}$	13	401.92	0	0.00%	11	84.62%	1	7.69%
	Msh6$^{+/+}$	2	500	2	100.00%	0	0.00%	0	0.00%
Rrm1-D57N^{Tg}	*Msh6*$^{+/-}$	24	461.21	4	16.67%	6	25.00%	2	8.33%
	Msh6$^{-/-}$	21	291.8	3	14.29%	15	71.43%	6	28.57%

[a]Mice were monitored until visibly ill and moribund or to a maximum age of 500 days, at which time they were taken for necropsy. (J.P.)

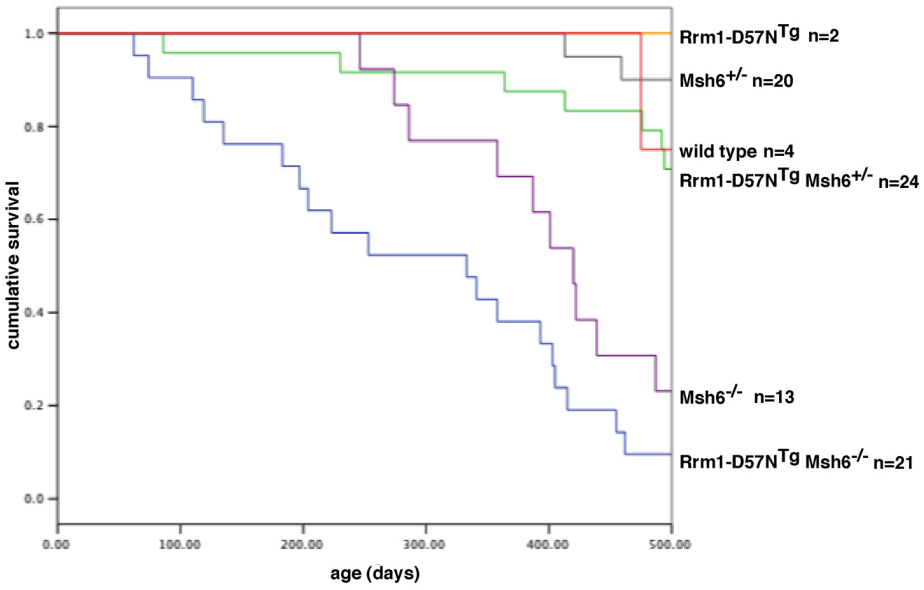

Figure 3.4. Survival of mice carrying the Rrm1-D57N transgene, mutation of Msh6, or both. Mice of the indicated genotypes were housed with littermates and monitored every three days to a maximum age of 500 days or until moribund. Survival in days was compared between genotypes. Analysis was performed with SPSS software.(J.P.)

One survived 25 days, and the last two mice were littermates, one female surviving 90 days and one male surviving 102 days. These results suggest that simultaneous disruption of multiple regulatory mechanisms of RNR is incompatible with survival.

Lethality manifests at different stages depending on cross

While rare surviving adult *Rrm1-D57N(low)*^{Tg} + *Rrm2*^{Tg} mice could be observed, no other cross exhibited any survivors. To determine the exact stage of lethality, I dissected embryos from *Rrm1-D57N(high)*^{Tg} x *p53R2*^{Tg} mice (Figure 3.6). Through embryonic day 11.5 (e11.5), bitransgenic embryos were observed at the expected frequencies, and most were grossly normal. At e12.5 and later, only dead *Rrm1-D57N(high)*^{Tg} + *p53R2*^{Tg} bitransgenic embryos were observed, and were still underrepresented (Figure 3.6A and Table 3.6). The frequency of resorbed embryos increased over the time frame analyzed, with few resorptions being observed before e10.5, but 5 or 6 resorptions at e11.5 and e12.5, respectively.

Bitransgenic embryos derived from crosses between *Rrm1-D57N(high)*^{Tg} and *Rrm2*^{Tg} mice displayed great variability in lifespan. At e13.5, the expected number of bitransgenic embryos was observed and bitransgenic embryos were grossly normal (Figure 3.6B and Table 3.6). However, embryo dissections at e15.5 revealed a sharp increase in abnormal or dead bitransgenic embryos. Of nine total embryos observed at e15.5, 6 were bitransgenic. Of these 6, one was normal while the other 5 appeared to have

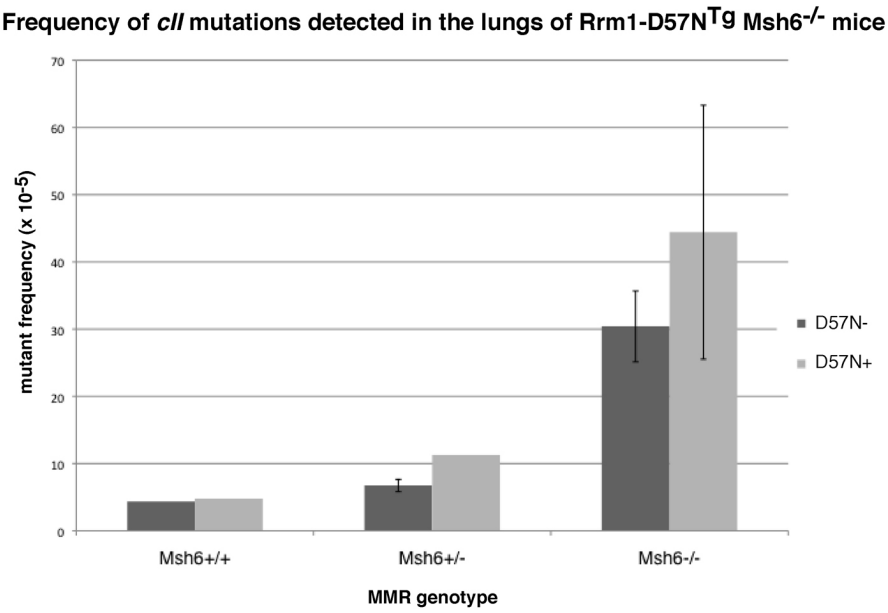

Figure 3.5. Frequency of *cII* mutations measured in the lungs of *Msh6*$^{+/+}$, *Msh6*$^{+/-}$, or *Msh6*$^{-/-}$ mice with or without the D57N transgene. Mice harboring the indicated genotypes and the Big Blue transgene were analyzed at 3 months of age. Data are represented as mean for each genotype. Error bars, standard deviation. Sample sizes: 2, *Msh6*$^{+/-}$; 3, *Msh6*$^{-/-}$; 3, *Rrm1-D57N*^{Tg} *Msh6*$^{-/-}$. For all others, n=1. (J.P.)

died by e14.5. Two of the dead bitransgenic embryos displayed neural defects (Figure 3.6B). A normal bitransgenic embryo was observed at e16.5, while no live or dead bitransgenic embryos were observed at e17.5 or e19.5, of approximately 3 expected at each time point. Surprisingly, one live bitransgenic neonate was observed at P0, while 2 more were found dead at P0.

The lifespan of *Rrm1-D57N(low)*^{Tg} + *p53R2*^{Tg} bitransgenic mice was intermediate between that of *Rrm1-D57N(high)*^{Tg} + *Rrm2*^{Tg} mice and *Rrm1-D57N(low)*^{Tg} + *Rrm2*^{Tg} mice (Figure 3.8A, B). *Rrm1-D57N(low)*^{Tg} + *p53R2*^{Tg} bitransgenic mice survived birth. They appeared normal for the first 1-2 days of life, after which time runting became apparent (Figure 3.8A). Bitransgenic mice developed large, protruding eyes after P3-P4. However, survival of these bitransgenics decreased rapidly at P5, with all bitransgenics observed dying at either P5 or P6. In order to determine the morphological defects causing lethality in these bitransgenics, a broad range of tissues were harvested and examined histologically; however, I was unable to detect any defects that could account for the postnatal lethality.

The *Rrm1-D57N(low)*^{Tg} + *Rrm2*^{Tg} bitransgenic mice (Figure 3.8C, D) also survived gestation to be born at expected frequencies. From there, the majority were able to survive 7 days; following that time there was a rapid decline in viability such that few were able to survive 14 days or longer.

Table 3. 4. Spectra of *cII* mutations observed in *Rrm1-D57N^{Tg} Msh6* mutant mice.[a]

Type of Mutation	wild type		*Rrm1-D57N^{Tg}*		*Msh6$^{+/-}$*		*Rrm1-D57N^{Tg}* + *Msh6$^{+/-}$*		*Msh6$^{-/-}$*		*Rrm1-D57N^{Tg}* + *Msh6$^{-/-}$*	
	Number	Percent	Number	Percent	Number	Percent	Number	Percent	Number	Percent	Number	Percent
Transition	**13**	**81.25%**	**12**	**60.00%**	**20**	**58.82%**	**11**	**55.00%**	**38**	**62.30%**	**44**	**69.84%**
G:C--> A:T	13	81.25%	11	55.00%	20	58.82%	10	50.00%	21	34.43%	39	61.90%
A:T-->G:C	0	0.00%	1	5.00%	0	0.00%	1	5.00%	17	27.87%	5	7.94%
Transversion	**2**	**12.50%**	**5**	**25.00%**	**8**	**23.53%**	**3**	**15.00%**	**8**	**13.11%**	**6**	**9.52%**
G:C --> T:A	2	12.50%	2	10.00%	3	8.82%	2	10.00%	3	4.92%	4	6.35%
T:A--> G:C	0	0.00%	0	0.00%	2	5.88%	0	0.00%	1	1.64%	2	3.17%
T:A --> A:T	0	0.00%	2	10.00%	1	2.94%	0	0.00%	3	4.92%	0	0.00%
G:C --> C:G	0	0.00%	1	5.00%	2	5.88%	1	5.00%	1	1.64%	0	0.00%
Insertion/Deletion	**1**	**6.25%**	**1**	**5.00%**	**4**	**11.76%**	**6**	**30.00%**	**13**	**21.31%**	**10**	**15.87%**
1 bp insertion	0	0.00%	0	0.00%	2	5.88%	4	20.00%	0	0.00%	4	6.35%
2 or more insertions	0	0.00%	0	0.00%	0	0.00%	0	0.00%	0	0.00%	0	0.00%
1 bp deletion	0	0.00%	1	5.00%	2	5.88%	2	10.00%	13	21.31%	6	9.52%
2 or more deletions	1	6.25%	0	0.00%	0	0.00%	0	0.00%	0	0.00%	0	0.00%
Non-cII mutation	**0**	**0.00%**	**2**	**10.00%**	**2**	**5.88%**	**0**	**0.00%**	**2**	**3.28%**	**3**	**4.76%**
total	**16**	**100.00%**	**20**	**100.00%**	**34**	**100.00%**	**20**	**100.00%**	**61**	**100.00%**	**63**	**100.00%**

[a]Total genomic DNA was harvested from the lungs of wild type, *Rrm1-D57N^{Tg},* and/or *Msh6* mutant mice and packaged into viable phage. The *cII* gene of confirmed plaques was amplified and sequenced. Duplicate mutations are assumed to arise from a clonal event and are omitted. (J.P.)

During the second week of life most remaining bitransgenics experienced a rapid weight loss and became moribund. They also began to display exterior phenotypes, such as runting, thin hair, poor posture, and large protruding eyes (Figure 3.8C). Rare surviving mice were obtained that could survive 19, 25, 90, or 102 days. These mice will be discussed further. All *Rrm1-D57N(low)*^{Tg} + *Rrm2*^{Tg} bitransgenic mice expired within 3 months of age, in contrast to mice harboring a single RNR transgene or *Rrm1*^{Tg} + *Rrm2*^{Tg} or *Rrm1*^{Tg} + *p53R2*^{Tg} bitransgenic mice, all of which appeared healthy and were able to survive beyond 12 months.

Pleural effusion characterizes *Rrm1-D57N(low)*^{Tg} + *Rrm2*^{Tg} bitransgenic animals

Despite the finding that rare surviving *Rrm1-D57N(low)*^{Tg} + *Rrm2*^{Tg} bitransgenic mice displayed premature aging phenotypes and severe skeletal and cardiac muscle degeneration, these defects are likely not to be the primary causes of the synthetic lethality observed. Skeletal and cardiac muscle degeneration were only observed in mice that survived at least 19 days of age or longer; the majority of bitransgenic mice died within the second week of life. I therefore sought to determine the defects that arise in the more severely affected mice via histological staining of a wide range of tissues at earlier time points. Mice were monitored and weighed daily from birth in order

to be able to predict when the bitransgenics might expire; at that time the entire litter was culled for histological analysis.

Brain, heart, lungs, liver, kidney, skeletal muscle, spleen, bone marrow, and GI tract were all examined by H&E staining for changes in morphology. I first noticed upon necropsy that bitransgenic mice, but not control mice, showed pleural effusion. Fluid accumulation affected the entire pleural cavity, and in mice surviving 8 days or later, also observed within the abdomen. In order to determine the type of the pleural effusion, I collected the fluid and analyzed the constituents. The data are summarized in Table 3.7. Pleural effusion was observed in neonates as early as P4. Later than P5, all bitransgenic neonates displayed the fluid accumulation. However, effusion was not observed in the mice surviving 19 days or longer.

Histological analysis of neonates aged at least 9 days old revealed small kidneys with a loss of medullary tubules, interstitial fibrosis and edema, along with multifocal dilated tubules in the cortex (Figure 3.8A). This was observed in two bitransgenics, aged 9 and 11 days.

Additionally, in neonates aged 6 days or more, the liver showed multifocal areas of hepatocellular swelling consistent with increased glycogen accumulation (Figure 3.8B). Hepatocellular swelling is caused by excessive accumulation of either glycogen or lipid. In order to distinguish between the two possibilities, we performed Periodic Acid Schiff's (PAS) staining on the

liver samples. PAS stains glycogen fuschia while lipid remains colorless. I found evidence of accumulation of both glycogen and lipid (Figure 3.8C). Kidney pathology was also found in the kidneys of aged mice overexpressing either *Rrm2* or *p53R2* (Figure 3.9). H&E staining reveals extensive protein accumulation in the collecting ducts of the medulla. The phenotype was more severe in mice harboring the $Rrm2^{Tg}$ than in mice overexpressing *p53R2*. Additional expression of $Rrm1^{Tg}$ did not increase the incidence or severity of the proteinuria.

Severe muscle degeneration in $Rrm1\text{-}D57N(low)^{Tg}$ + $Rrm2^{Tg}$ bitransgenic mice

Of approximately 70 $Rrm1\text{-}D57N(low)^{Tg}$ + $Rrm2^{Tg}$ bitransgenic adults expected, only 5 were observed. Rare surviving $Rrm1\text{-}D57N(low)^{Tg}$ + $Rrm2^{Tg}$ bitransgenic mice were runted compared to littermates. Throughout life, $Rrm1\text{-}D57N(low)^{Tg}$ + $Rrm2^{Tg}$ bitransgenic mice were hunched, inactive, and displayed small muscles and alopecia. A rare mouse surviving 19 days exhibited general wasting (Figure 3.10A) and inactivity. All $Rrm1\text{-}D57N(low)^{Tg}$ + $Rrm2^{Tg}$ bitransgenic mice showed a significant loss of body weight prior to death. Upon necropsy, we found that $Rrm1\text{-}D57N(low)^{Tg}$ + $Rrm2^{Tg}$ bitransgenic mice which survived 90 days or longer exhibited severe skeletal and cardiac muscle degeneration.

Table 3.5. Genotypes of offspring observed from crosses between mice overexpressing *Rrm1*^{Tg}, *Rrm1-D57N(low)*^{Tg}, or *Rrm1-D57N(high)*^{Tg} and mice overexpressing *Rrm2*^{Tg} or *p53R2*^{Tg}.[a]

cross	genotype	*Rrm1*^{Tg} (wt)	*Rrm1-D57N(low)*^{Tg}	*Rrm1-D57N(high)*^{Tg}
R1^{Tg} x *Rrm2*^{Tg}	wild type	57 (48.75)	96 (69.75)	33 (26.5)
	R1^{Tg}	54 (48.75)	93 (69.75)	35 (26.5)
	Rrm2^{Tg}	38 (48.75)	85 (69.75)	38 (26.5)
	R1^{Tg} + *Rrm2*^{Tg}	46 (48.75)	5 (69.75)[b]	0 (26.5)[b]
R1^{Tg} x *p53R2*^{Tg}	wild type	29 (37.25)	77 (51.25)	51 (30)
	R1^{Tg}	52 (37.25)	68 (51.25)	40 (30)
	p53R2^{Tg}	35 (37.25)	60 (51.25)	29 (30)
	R1^{Tg} + *p53R2*^{Tg}	33 (37.25)	0 (51.25)[b]	0 (30)[b]

[a]Mice harboring *Rrm1*^{Tg}, *Rrm1-D57N(low)*^{Tg}, or *Rrm1-D57N(high)*^{Tg} were crossed to mice carrying either the *Rrm2* or *p53R2* transgene. Progeny were genotyped at weaning by Southern blot. Observed numbers of animals of each genotype are indicated with expected number in parentheses.

[b] $p<0.05$, $\chi 2$ test. (J.P. and X.X.)

Hematoxylin and eosin staining of *Rrm1-D57N(low)*^{Tg} + *Rrm2*^{Tg} bitransgenic and control skeletal muscle samples reveals disorganized fibers, large, open nuclei, and decreased stainability in the bitransgenic (Figure 3.10Aiv). To further investigate the degree of muscle degeneration, I performed Masson's trichrome staining of duplicate sections of the same samples. Staining with Masson's trichrome stain also revealed severe degeneration in the bitransgenic, as demonstrated by vacuoles appearing within the skeletal muscle fibers and extensive fibrosis developing between muscle fibers (Figure 3.10Aviii). Histological analysis of cardiac muscle tissue also revealed severe degeneration (Figure 3.10B). Analysis of a wider range of tissues did not reveal degeneration, suggesting that degeneration was limited to skeletal and cardiac muscle tissues.

By contrast, mice overexpressing *Rrm1*^{Tg} + *Rrm2*^{Tg} or *Rrm1*^{Tg} + *p53R2*^{Tg} displayed only mild degeneration in the skeletal muscle (Figure 3.11) and histologically normal cardiac muscle (Figure 3.12).

Figure 3.6. Gross morphology of *Rrm1-D57N(high)^{Tg}* + *Rrm2^{Tg}* or *p53R2^{Tg}* bitransgenic embryos. *A. Rrm1-D57N(high)^{Tg}* + *p53R2^{Tg}* bitransgenic embryos. Bitransgenics are grossly normal through 10.5 dpc. At 11.5 dpc, dead bitransgenic embryos begin to be observed. *B. Rrm1-D57N(high)^{Tg}* + *Rrm2^{Tg}* bitransgenic embryos and controls. Bitransgenics are found dead as early as 13.5 dpc. However, some normal embryos are observed as late as e15.5. Arrow and arrowhead indicate head and spinal abnormalities. (J.P.)

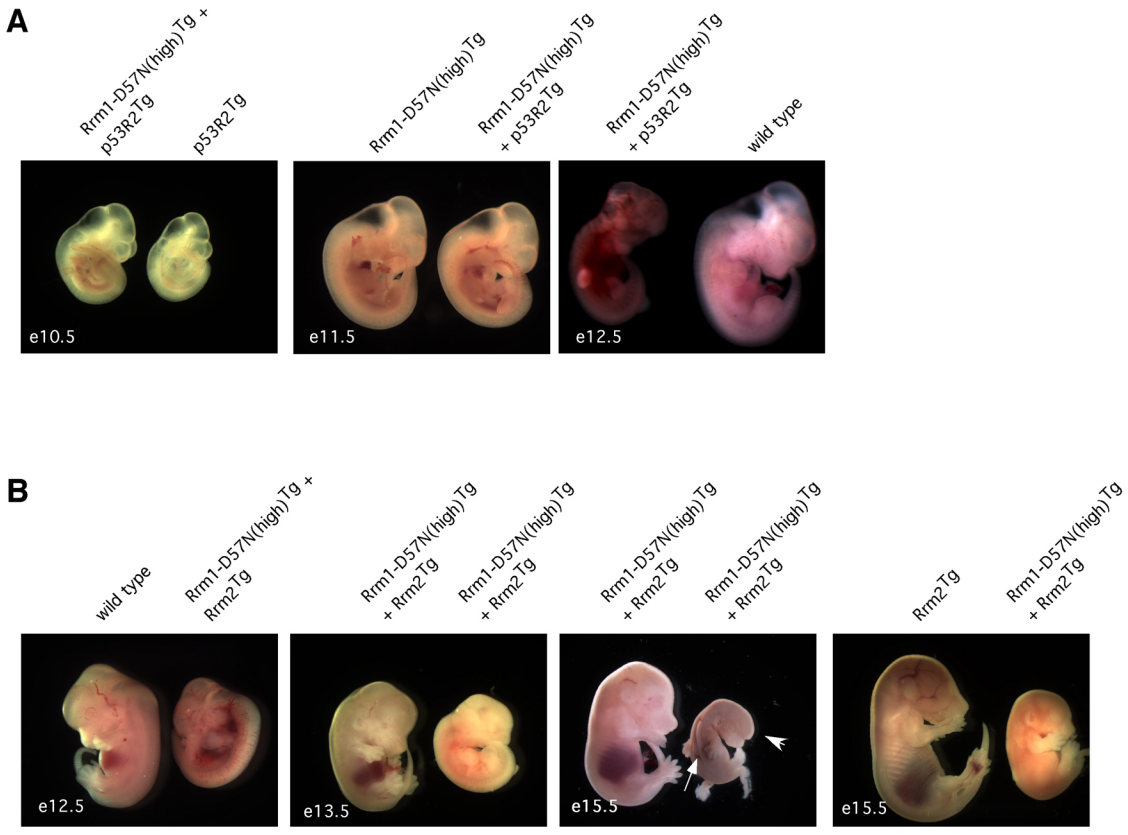
A
Rrm1-D57N(high)Tg +
p53R2Tg
p53R2Tg
Rrm1-D57N(high)Tg
Rrm1-D57N(high)Tg
+ p53R2Tg
Rrm1-D57N(high)Tg
+ p53R2Tg
wild type
e10.5
e11.5
e12.5
B
wild type
Rrm1-D57N(high)Tg +
Rrm2Tg
Rrm1-D57N(high)Tg
+ Rrm2Tg
Rrm1-D57N(high)Tg
+ Rrm2Tg
Rrm1-D57N(high)Tg
+ Rrm2Tg
Rrm1-D57N(high)Tg
+ Rrm2Tg
Rrm2Tg
Rrm1-D57N(high)Tg
+ Rrm2Tg
e12.5
e13.5
e15.5
e15.5

Table 3.6. Summary of embryos observed from *Rrm1-D57N(high)^{Tg}* x *Rrm2^{Tg}* or *p53R2^{Tg}* crosses[a].

	Rrm1-D57N(high)^{Tg} x *Rrm2^{Tg}*							
	wild type		*Rrm1-D57N^{Tg}*		*Rrm2^{Tg}*		bitransgenic	
stage	# obs	(#exp)	# obs	(#exp)	# obs	(#exp)	# obs	(#exp)
9.5	1	(1.75)	3	(1.75)	2	(1.75)	1	(1.75)
10.5	0	(0.75)	2	(0.75)	1	(0.75)	0	(0.75)
11.5								
12.5	3	(4)	3	(4)	6	(4)	4: 1[b]	(4)
13.5	2	(3.25)	2	(3.25)	5	(3.25)	4: 1[b]	(3.25)
14.5	2	(2.25)	1	(2.25)	4	(2.25)	2[b]	(2.25)
15.5	4	(5.5)	2	(5.5)	7: 1[b]	(5.5)	9: 6[b]	(5.5)
16.5	0	(0.75)	0	(0.75)	2	(0.75)	1	(0.75)
17.5	5	(6)	6	(6)	9: 1[b]	(6)	4: 3[b]	(6)
18.5								
19.5	4	(2.75)	4: 1[b]	(2.75)	3	(2.75)	0	(2.75)
P0	1	(0.75)	1	(0.75)	0	(0.75)	1	(0.75)

	Rrm1-D57N(high)^{Tg} x *p53R2^{Tg}*							
	wild type		*Rrm1-D57N^{Tg}*		*p53R2^{Tg}*		bitransgenic	
stage	# obs	(#exp)	# obs	(#exp)	# obs	(#exp)	# obs	(#exp)
9.5	5	(4.5)	6	(4.5)	3	(4.5)	4: 1[b]	(4.5)
10.5	4: 3[b]	(4.25)	2	(4.25)	6	(4.25)	5: 1[b]	(4.25)
11.5	11	(10)	10	(10)	12	(10)	7: 2[c]	(10)
12.5	10	(6)	5	(5)	4	(5)	2[c]	(5)
13.5	11	(7.75)	12: 2[b]	(7.75)	6: 1[b]	(7.75)	2[c]	(7.75)
14.5								
15.5								
16.5								
17.5								
18.5								
19.5								
P0								

[a]Embryos were analyzed at the indicated time points. The total number of embryos of each genotype observed were listed with the number of abnormal embryos indicated. Expected numbers of embryos were listed in parantheses.

[b]abnormal embryo, [c]dead embryo. (J.P.)

Figure 3.7. Reduced survival of bitransgenic mice. *A*. Gross morphology of *Rrm1-D57N(low)*^{Tg} + *p53R2*^{Tg} bitransgenic mice at P8. *B*. Reduced survival of bitransgenic mice derived from *Rrm1-D57N(low)*^{Tg} x *p53R2*^{Tg} cross. Pups were counted on P0 (day of birth) and monitored daily. Pups were genotyped by Southern blot analysis of tail DNA at 21 days of age or when found dead. Bitransgenic mice (purple line) have a 50% survival rate of 5 days. *C*. Gross morphology of *Rrm1-D57N(low)*^{Tg} + *Rrm2*^{Tg} bitransgenic mice at P15. Bitransgenic mice are runted and show alopecia and decreased activity. A bitransgenic mouse (right) is pictured at P15 with a wild type littermate (left). *D*. Survival of *Rrm1-D57N(low)*^{Tg} + *Rrm2*^{Tg} bitransgenic mice. Pups were genotyped by Southern blot analysis of tail DNA at 21 days of age or when found dead. Bitransgenics surviving past 21 days of age were housed with sex-matched littermates and monitored frequently, and euthanized when moribund. (J.P)

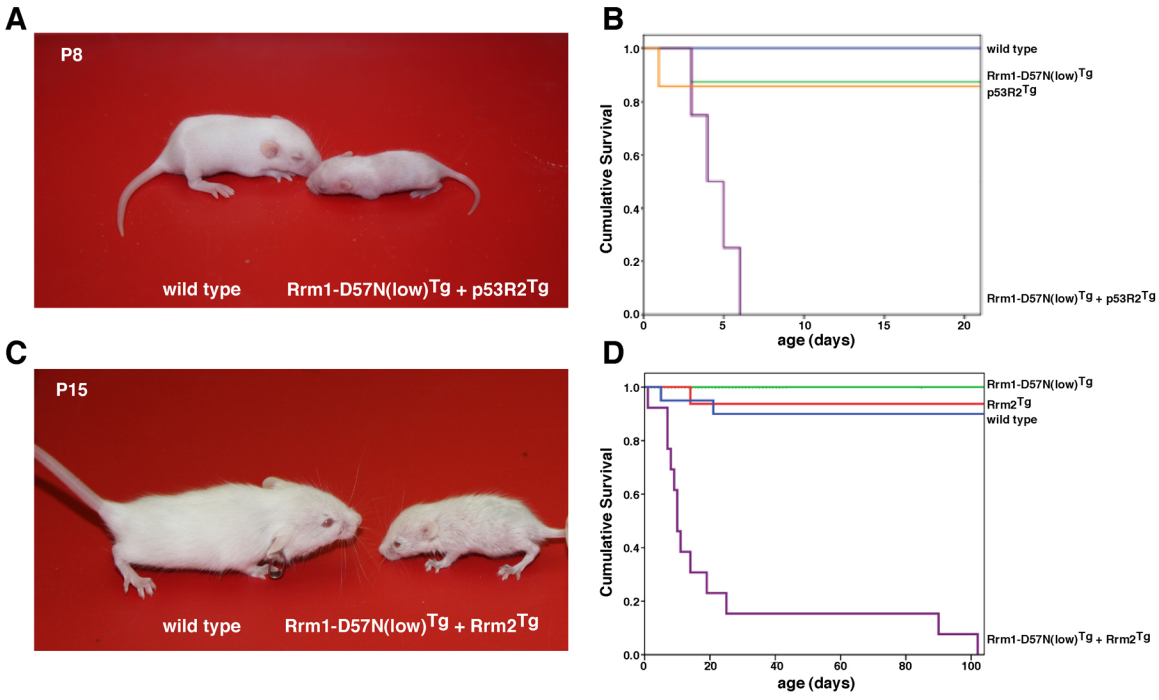
A
P8
wild type
Rrm1-D57N(low)Tg + p53R2Tg
B
Cumulative Survival
1.0
0.8
0.6
0.4
0.2
0.0
0
5
10
15
20
age (days)
wild type
Rrm1-D57N(low)Tg
p53R2Tg
Rrm1-D57N(low)Tg + p53R2Tg
C
P15
wild type
Rrm1-D57N(low)Tg + Rrm2Tg
D
Cumulative Survival
1.0
0.8
0.6
0.4
0.2
0.0
0
20
40
60
80
100
age (days)
Rrm1-D57N(low)Tg
Rrm2Tg
wild type
Rrm1-D57N(low)Tg + Rrm2Tg

Table 3.7. Analysis of fluid collected from *Rrm1-D57N(low)*^{Tg} + *Rrm2*^{Tg} bitransgenic mice.

Neonate	age (days)	mass of pup (g)	fluid recovered (mL)	total protein (g/dL)	albumin (g/dL)
1	6	ND	80	1.4	1.0
2	12	ND	ND	1.8	ND
3	12	ND	ND	1.8	ND
4	7	ND	ND	ND	1.1
5	8	2.5	135	ND	1.0
mean ± st dev	N/A	N/A	N/A	1.67 ± 0.23	1.03 ± 0.05

[a]Neonates were monitored and weighed daily until visibly ill and/or failed to thrive (failed to gain weight or lost weight). Mice were euthanized and pleural fluid collected. Total protein content or albumin content was measured by the Clinical Pathology Lab, College of Veterinary Medicine, Cornell University. ND, not determined. (J.P and T.S.)

Mitochondrial genome instability does not cause synthetic lethality in the bitransgenics

We previously reported that mice simultaneously overexpressing *Rrm1*^{Tg} and either *Rrm2*^{Tg} or *p53R2*^{Tg} displayed age-dependent mitochondrial DNA depletion in the skeletal muscle as a result of dNTP pool imbalance(32). Our finding of severe skeletal muscle degeneration in surviving *Rrm1-D57N(low)*^{Tg} + *Rrm2*^{Tg} bitransgenic mice led us to hypothesize that the degeneration was caused by an instability of the mitochondrial genome, leading to dysfunctional mitochondria. The degeneration was also observed in the cardiac muscle, and if due to mtDNA depletion, this could link the RNR regulation to a concrete phenotype causing lethality. In order to test this hypothesis, we measured mtDNA copy number in MEFs overexpressing both *Rrm1-D57N(low)*^{Tg} and *p53R2*^{Tg} or *Rrm1-D57N(high)*^{Tg} and *Rrm2*^{Tg}(Figure 3.13A). To mimic the quiescent state of skeletal muscle, we serum-starved the MEFs, trapping the majority of cells in G1. We found no depletion of mitochondrial DNA in either the *Rrm1-D57N(low)*^{Tg} + *p53R2*^{Tg} or the *Rrm1-D57N(high)*^{Tg} + *Rrm2*^{Tg} bitransgenic cell lines or any of the controls. Because the mtDNA depletion in the other mouse model was age-dependent, we asked if *Rrm1-D57N*^{Tg} + *Rrm2*^{Tg} or *p53R2*^{Tg} bitransgenic mice would display mtDNA depletion as they aged. The early lethality of the *Rrm1- D57N(low)*^{Tg} + *p53R2*^{Tg} bitransgenic

Figure 3.8. Spectrum of phenotypes in *Rrm1-D57N^{Tg}* + *Rrm2^{Tg}* bitransgenic neonates. *A.* H&E analysis of P11 kidney in wild type (left panel) and *Rrm1-D57N(low)^{Tg}* + *Rrm2^{Tg}* bitransgenic animals (right panel). The bitransgenic shows degeneration of cortical tubules (arrows), dilated tubules in the medulla (arrowheads), and fibrosis (thick arrows). Scale bars, 100mm. *B.* H&E analysis of liver from wild type (left) and bitransgenic littermate (right). Arrow indicates focus of hepatocytes with abnormal accumulations of lipid or glycogen, leading to swollen appearance. Scale bars, 20mm. *C.* Periodic acid Schiff's stain of neonate livers at P6. Yellow arrows indicate hepatocytes with glycogen accumulation (fuschia), while blue arrowheads indicate hepatocytes with lipid accumulation. Glycogen is abundant in the wild type liver but does not accumulate within hepatocytes. Scale bars, 25mm. (J.P., R.P., and T.S.)

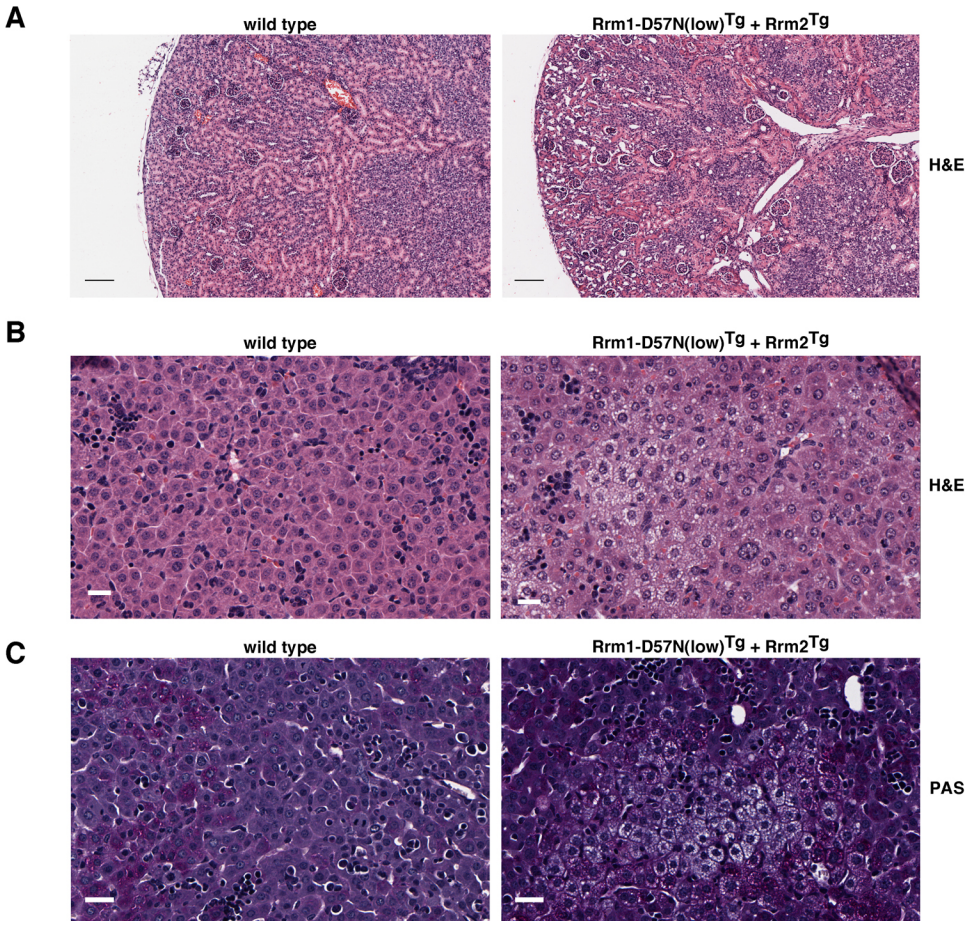
A
wild type
Rrm1-D57N(low)Tg + Rrm2Tg
H&E
B
wild type
Rrm1-D57N(low)Tg + Rrm2Tg
H&E
C
wild type
Rrm1-D57N(low)Tg + Rrm2Tg
PAS

Figure 3.9. Proteinuria in kidneys of mice overexpressing either small RNR subunit. Tissues were stained with H&E following overnight fixation. Collecting ducts of kidneys with excessive protein accumulation stain bright pink with eosin. Images are representative of their genotype. Numbers indicate total number of mice resembling image over total number of mice of that genotype. (T.S. and J.P.)

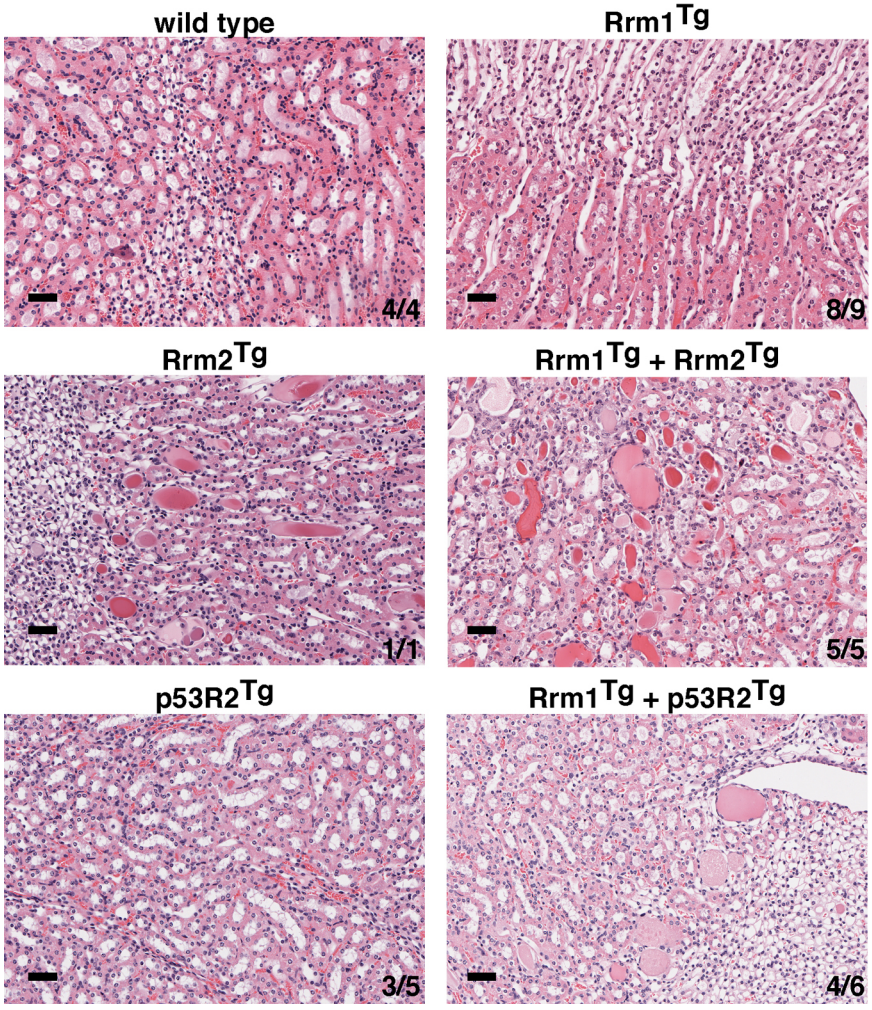
wild type
4/4
Rrm1Tg
8/9
Rrm2Tg
1/1
Rrm1Tg + Rrm2Tg
5/5
p53R2Tg
3/5
Rrm1Tg + p53R2Tg
4/6

neonates and the embryonic demise of bitransgenics harboring *Rrm1-D57N(high)^{Tg}* necessitated mtDNA measurements in *Rrm1-D57N(low)^{Tg}* + *Rrm2^{Tg}* bitransgenics. We were able to measure mtDNA copy number in bitransgenic mice at P4, P8, P19, P25, and P90 or P102 mice (Figure 3.13B). We found the mtDNA copy number in skeletal muscle of control mice increased with age, while mtDNA copy number in the skeletal muscle of bitransgenic mice failed to expand to the same level throughout development. In juvenile mice, mtDNA copy number was equal to controls, but by P19 was only ~50% of the wild type level.

It is a possibility that skeletal muscle degeneration in the *Rrm1-D57N(low)^{Tg}* + *Rrm2^{Tg}* bitransgenic mice was giving the appearance of depleted mtDNA when the mitochondria are actually unaffected. To attempt to control for this, we also measured mtDNA content in the heart, kidney, and liver of juvenile and young adult mice (Figure 3.13B). In a previous study (Chapter 2), we were unable to detect mtDNA depletion in these tissues in aged *Rrm1^{Tg}* + *Rrm2^{Tg}* or *Rrm1^{Tg}* + *p53R2^{Tg}* adult bitransgenic mice. However, these tissues also show degenerative phenotypes in *Rrm1-D57N(low)^{Tg}* + *Rrm2^{Tg}* bitransgenic mice. Therefore, if the observed mtDNA depletion is solely due to tissue degeneration and not to defects in mtDNA maintenance, then we would see depletion in the heart, kidney, and liver as well as in the skeletal muscle.

Figure 3.10 Muscle degeneration in *Rrm1-D57N(low)^{Tg}* + *Rrm2^{Tg}* bitransgenic adult mice. Degeneration of skeletal (*A*) and cardiac (*B*) muscle in *Rrm1-D57N(low)^{Tg}* + *Rrm2^{Tg}* bitransgenic adults. Tissues from 90-day old mice were fixed overnight in formalin at room temperature prior to embedding and sectioning. Tissues were stained with H&E (i-iv) or Masson's trichrome (v-viii). Both skeletal and cardiac muscle from bitransgenic mice (*A*: iv, viii, *B*: iv, viii) display irregular fiber size, decreased stainability, loss of striation (black arrows), large internal nuclei (white arrows), interstitial replacement fibrosis (white arrowheads), and vacuoles within muscle fibers (black arrowheads). (J.P. and R.P.)

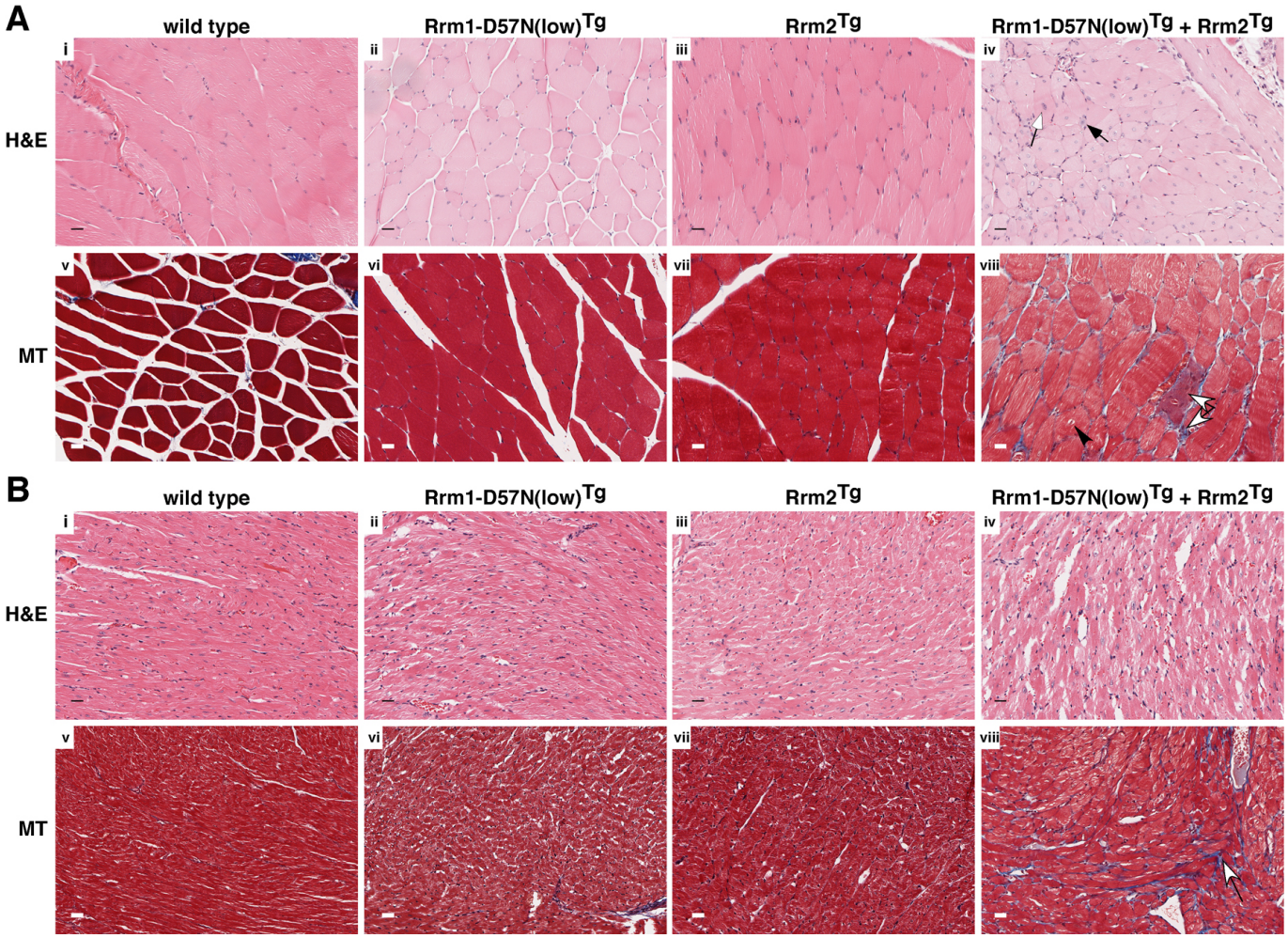
A
wild type
Rrm1-D57N(low)Tg
Rrm2Tg
Rrm1-D57N(low)Tg + Rrm2Tg
H&E
MT
i
ii
iii
iv
v
vi
vii
viii
B
wild type
Rrm1-D57N(low)Tg
Rrm2Tg
Rrm1-D57N(low)Tg + Rrm2Tg
H&E
MT
i
ii
iii
iv
v
vi
vii
viii

Figure 3.11. Analysis of skeletal muscle from wild type, *Rrm1*^{Tg} + *Rrm2*^{Tg}, and *Rrm1*^{Tg} + *p53R2*^{Tg} adult mice. *A*. Skeletal muscle from young (3 months; top) or aged (12 months; bottom) mice was stained with H&E. Bitransgenics show more variable fiber size, increased number of nuclei, and internal nuclei. *B*. Masson's trichrome stain was performed on aged wild type and bitransgenic mice. Scale bars represent 25mm. Scale bars represent 50mm.(J.P. and T.S.)

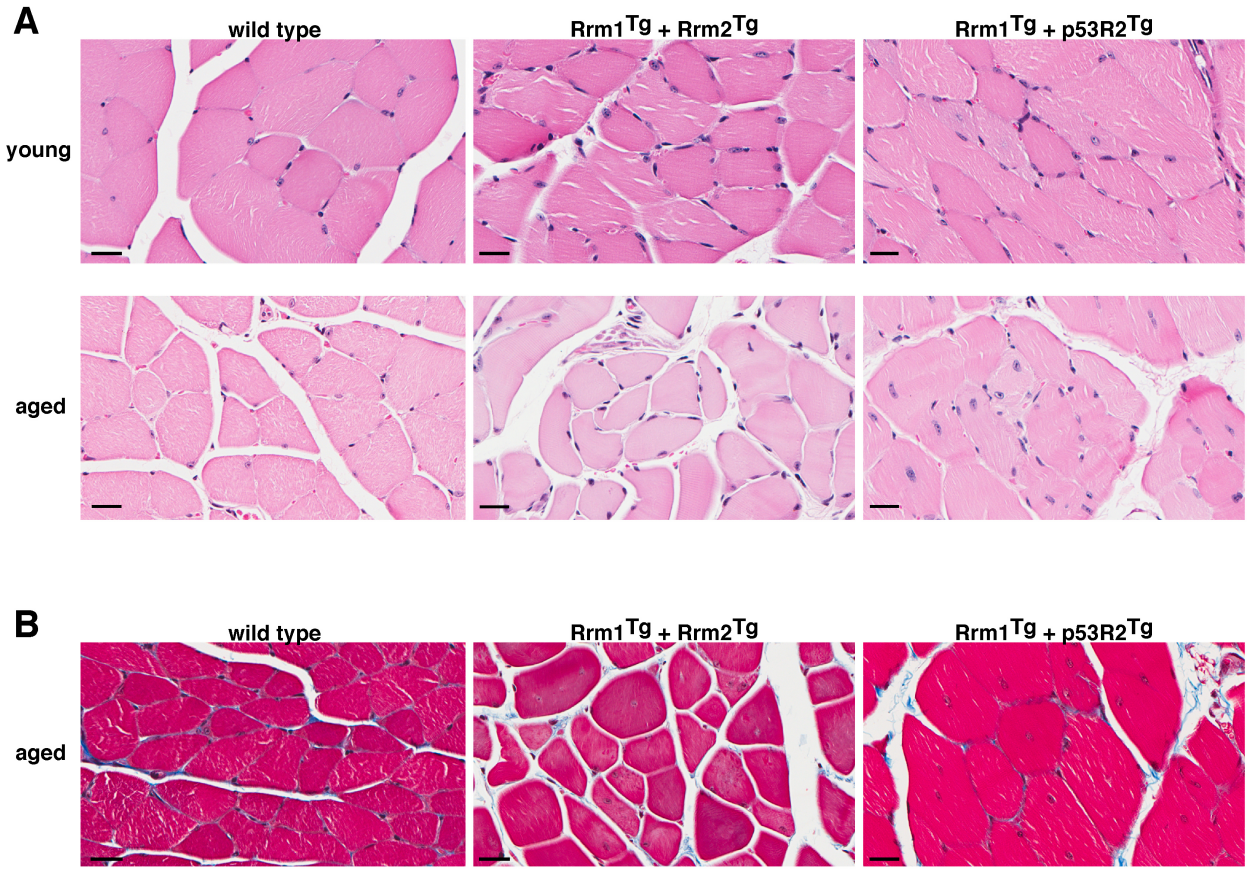
A
wild type
Rrm1Tg + Rrm2Tg
Rrm1Tg + p53R2Tg
young
aged
B
wild type
Rrm1Tg + Rrm2Tg
Rrm1Tg + p53R2Tg
aged

Figure 3.12. Analysis of cardiac muscle from wild type, *Rrm1*^{Tg} + *Rrm2*^{Tg}, and *Rrm1*^{Tg} + *p53R2*^{Tg} adult mice. *A*. Cardiac muscle from young (3 months; top) or aged (12 months; bottom) mice was stained with H&E. Bitransgenics are normal relative to control mice. *B*. Masson's trichrome stain was performed on aged wild type and bitransgenic mice. Scale bars repesent 50mm. (J.P. and T.S.)

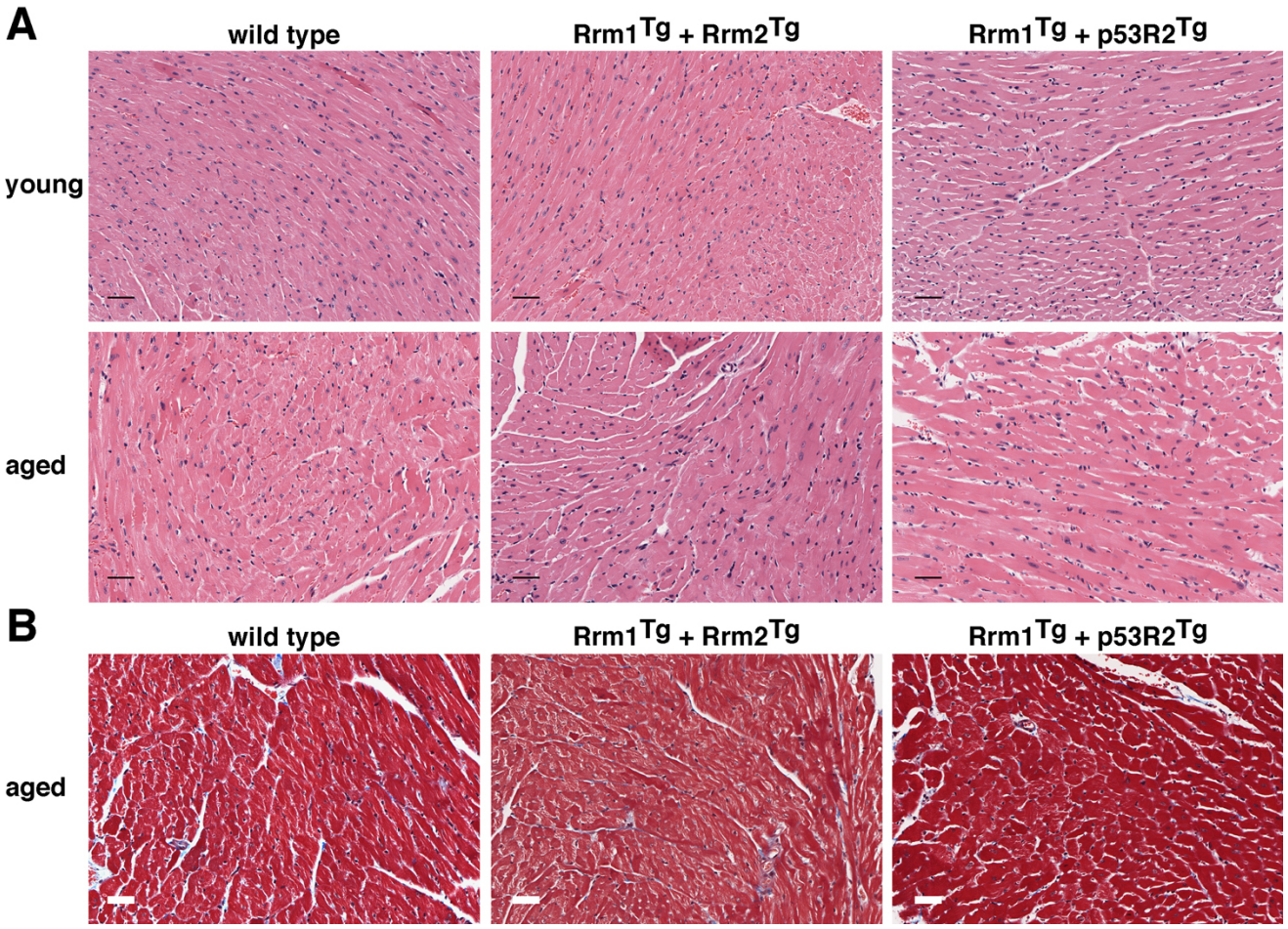
A
wild type
Rrm1Tg + Rrm2Tg
Rrm1Tg + p53R2Tg
young
aged
B
wild type
Rrm1Tg + Rrm2Tg
Rrm1Tg + p53R2Tg
aged

If, however, degeneration is not causing the observed depletion, then mtDNA content in these tissues would remain at wild type levels in the *Rrm1-D57N(low)^{Tg} + Rrm2^{Tg}* bitransgenic mice.

The results were largely inconclusive. *Rrm1-D57N(low)^{Tg} + Rrm2^{Tg}* bitransgenic mice did not show mtDNA depletion in the cardiac muscle as they aged (p=0.104, Student's t-test), suggesting either no defect in maintaining mtDNA in *Rrm1-D57N(low)^{Tg} + Rrm2^{Tg}* bitransgenic mice, or that an mtDNA maintenance defect is restricted to the skeletal muscle, as previously observed (Chapter 2). However, to a small extent kidney and liver both showed mtDNA depletion with age, but neither of these is statistically significant (kidney, p=0.18, Student's t-test; too few samples to analyze liver).

Mitochondrial genome instability can also manifest as increased point mutations(47) within critical OX-PHOS genes, or large deletions within the genome. We sequenced mtDNA in several regions but found no increase in mtDNA point mutations (data not shown). It has been further reported that dNTP pool imbalances can stimulate long deletions within mitochondrial DNA(13). We therefore performed long PCR to assess the total size of the mtDNA in bitransgenic mice (Figure 3.13C). In both wild type and *Rrm1-D57N(low)^{Tg} + Rrm2^{Tg}* bitransgenic mice, we were able to detect only full-length mtDNA (16kb).

To connect mtDNA depletion to the skeletal muscle degeneration, it

was necessary to determine if mitochondrially-encoded complexes were functional. In order to test this, we performed COX activity stain on frozen skeletal muscle from the P25 bitransgenic, which displayed ~50% mtDNA, and a wild type littermate. As a control for mitochondrial presence, we also stained for the activity of the nuclear-encoded SDH complex (Figure 3.13D). We found normal COX activity in the muscle of the bitransgenic mouse, and no increase in SDH signal.

We hypothesized that the lack of mitochondrial dysfunction at P25 could be due to the young age of the bitransgenic. We were able to detect mtDNA depletion in mice as young as 19 days; however, it may take more time for dysfunctional mitochondria to appear and cause phenotypic effects. We therefore tested the expression of SDH from the skeletal muscle of a bitransgenic at P90. We hypothesized that if the mitochondrial DNA was causing dysfunction throughout life, then at P90 we would be able to see SDH upregulation as a compensatory strategy for mitochondrial dysfunction. The results are presented in Figure 3.13E. We found increased staining for SDH in the skeletal muscle of the bitransgenic relative to the control. We also found subsarcolemmal accumulations of mitochondria (arrows), which is a second compensation mechanism for sub-functional mitochondria. These data suggest that simultaneous overexpression of Rrm1-D57N and either small RNR subunit does not cause mitochondrial genome instability early in life, but only as bitransgenic mice age, and therefore does not cause the observed

synthetic lethality.

Rrm1-D57N^{Tg} + *Rrm2*^{Tg} or *p53R2*^{Tg} bitransgenic MEFs proliferate normally

To investigate possible causes for embryonic lethality, I wanted to determine if simultaneous disruption of multiple regulatory modes of RNR could affect cell cycle progression. A model of *rnr1-D57N* overexpression in yeast had previously reported that increases in dNTP pools caused a delay in origin firing in S-phase(36). The similarities between their model and ours prompted us to assess the ability of cells overexpressing either *Rrm1-D57N*^{Tg} in combination with either small RNR subunit to proliferate (Figure 3.6). I isolated mouse embryonic fibroblasts (MEFs) from embryos derived from each of the four combinations. The cells were assessed for proliferative ability by culturing on a 3T3 protocol with counting at every passage; population doublings were calculated and compared to wild type or single transgenic controls. I found no proliferation defects in any combination of bitransgenics (Figure 3.14). Bitransgenic cell lines from each combination doubled their populations at the same rate as control cell lines and did not senesce prematurely. I therefore conclude that simultaneous overexpression of Rrm1-D57N and either small RNR subunit does not cause proliferation defects in MEFs.

DISCUSSION

The mechanisms governing regulation of ribonucleotide reductase are

well known. RNR activity is known to be controlled in eukaryotes through small inhibitory proteins such as *SML1*(48) (in yeast), differential subcellular localization (in yeast), limitation of protein levels of a single subunit (the small subunits in mammals and the large subunit in yeast)(30, 49), and allosteric feedback control(50). We previously reported that overexpression of either small RNR subunit in mice causes lung cancer via a mutagenic mechanism(1). Noting that one mechanism of RNR regulation had been disabled, leading to the phenotype, we sought to deregulate RNR by an independent mechanism. Our initial hypothesis was that overexpression of either small subunit would disable a single regulatory mechanism of RNR, limitation of small subunit protein levels, and therefore increase active RNR complex and elevate dNTP pools. Increased dNTP pools have been reported to be mutagenic in multiple studies(5, 7, 9, 35, 36, 51). I hypothesized that mutating the allosteric activity site would disrupt the other main regulatory mechanism in mammals but also cause an increase in dNTPs; therefore the activity site mutant would also be tumorigenic. To test this prediction, we generated transgenic mice that overexpressed the mutant form of the large subunit. We obtained two independent transgenic lines that both show significant overexpression in a multitude of tissues. Despite the very high-level overexpression of *Rrm1* in the *Rrm1-D57N* transgenic lines, the mice were born at expected frequencies and were grossly normal.

Overexpression of either small RNR subunit, Rrm2 or p53R2, caused

lung tumorigenesis at a high frequency. Overexpression of the small subunits removes one regulatory mechanism of RNR, and I hypothesized that removing the other RNR regulatory mechanism would have a similar effect. I first analyzed the lung tumor phenotype in Rrm1-D57N(low)^{Tg} and Rrm1-D57N(high)^{Tg} mice. I found that the incidence of lung tumors was moderately increased in Rrm1-D57N^{Tg} mice, but neither the average tumor size, malignancy, nor tumor latency was affected. This was in contrast to the lung tumors observed in Rrm2^{Tg} and p53R2^{Tg} mice(1).

This supports our previous hypothesis that overexpression of the radical-producing subunits of RNR increases reactive oxygen species, thus increasing the mutation rate, and is therefore tumorigenic in the lungs of transgenic mice. In contrast, overexpression of Rrm1-D57N does not drive lung tumorigenesis, and if anything, facilitates lung tumor formation in strains that are predisposed to carcinogenesis. Because deregulating RNR by disabling allosteric feedback control had limited phenotypes, I sought to further deregulate the enzyme by simultaneously disrupting both main regulatory modes. In yeast, simultaneous disruption of the two main regulatory mechanisms caused constitutively elevated dNTP pools, which resulted in proliferation defects(36). In order to determine if mice would have a similar phenotype, I crossed mice overexpressing either Rrm1-

Figure 3.13. mtDNA integrity in bitransgenic mice. *A.* mtDNA copy number in bitransgenic MEFs from the Rrm1-D57N(low)^{Tg} x p53R2^{Tg} cross. MEFs at passage 2 were cultured in 2% serum for 8 days prior to extraction of total DNA. mtDNA was quantified by qPCR and normalized to the nuclear 18S rRNA. *B.* mtDNA copy number in tissues from bitransgenic mice from the Rrm1-D57N(low)^{Tg} x Rrm2^{Tg} cross. Total DNA was extracted from skeletal muscle, heart, kidney, or liver of bitransgenic and control mice at different stages of development: juvenile=P4, P8; young adult= P19, P25; aged adult=P90, P102. mtDNA was quantified as in part A. *C.* Long PCR on mtDNA from skeletal muscle of Rrm1-D57N(low)^{Tg} + Rrm2^{Tg} bitransgenic and wild type littermate at P25. Only the full 16 kb mtDNA is detected. *D.* Activity of respiratory chain complexes in skeletal muscle of Rrm1-D57N(low)^{Tg} + Rrm2^{Tg} bitransgenic and wild type littermate at P25. Tissues are stained for activity of the mtDNA-encoded complex IV (COX, brown), the nDNA-encoded complex II (SDH, blue), or both, *E.* Abundance of total SDH protein (brown) in skeletal muscle of Rrm1-D57N(low)^{Tg} + Rrm2^{Tg} bitransgenic and wild type littermate at P102. Arrows indicate subsarcolemmal accumulations of mitochondria. Nuclei are counterstained blue with hematoxylin. (E.Y.)

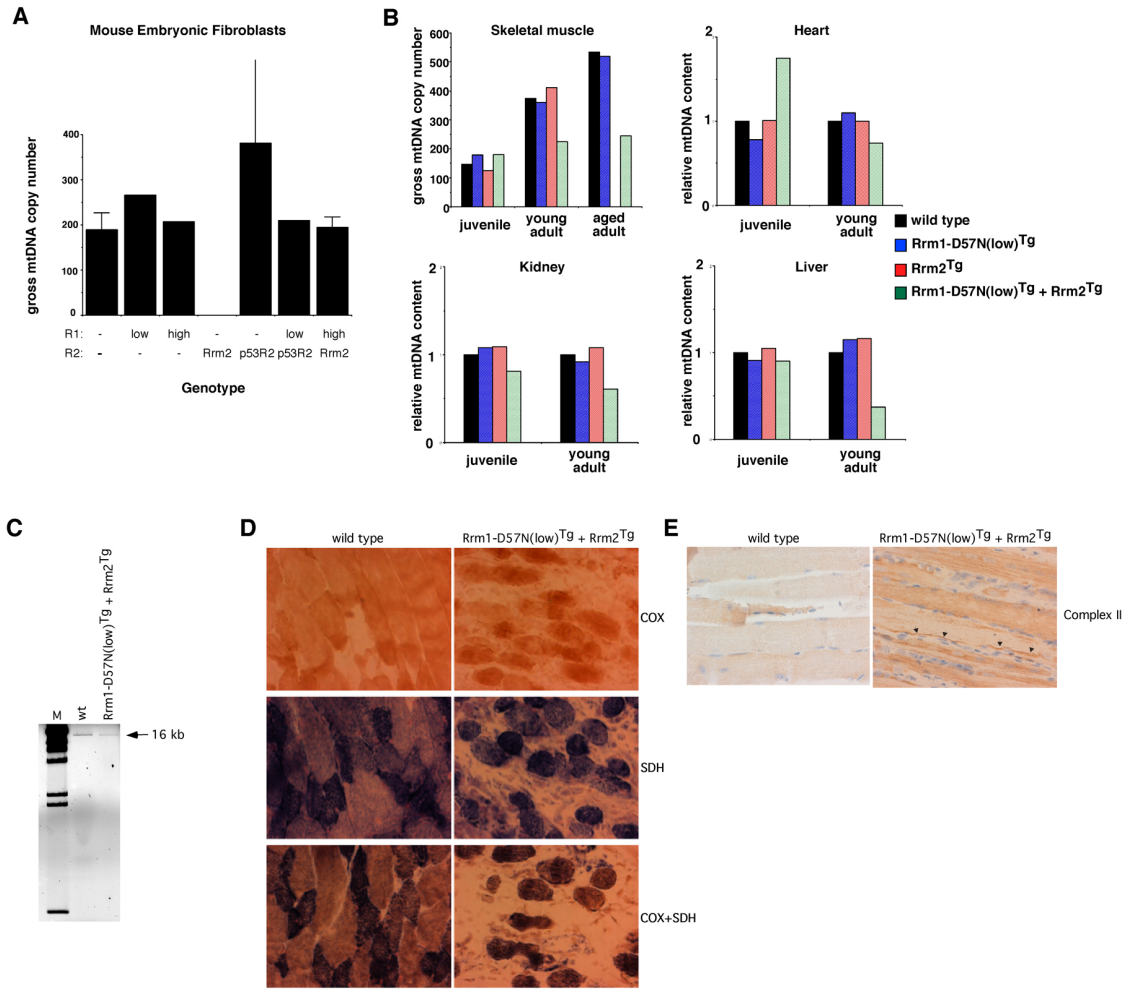
A
Mouse Embryonic Fibroblasts
gross mtDNA copy number
400
300
200
100
0
R1: - low high - - low high
R2: - - - Rrm2 p53R2 p53R2 Rrm2
Genotype
B
Skeletal muscle
gross mtDNA copy number
600
500
400
300
200
100
0
juvenile
young adult
aged adult
Heart
relative mtDNA content
2
1
0
juvenile
young adult
wild type
Rrm1-D57N(low)Tg
Rrm2Tg
Rrm1-D57N(low)Tg + Rrm2Tg
Kidney
relative mtDNA content
2
1
0
juvenile
young adult
Liver
relative mtDNA content
2
1
0
juvenile
young adult
C
Rrm1-D57N(low)Tg + Rrm2Tg
M
wt
16 kb
D
wild type
Rrm1-D57N(low)Tg + Rrm2Tg
COX
SDH
COX+SDH
E
wild type
Rrm1-D57N(low)Tg + Rrm2Tg
Complex II

D57N transgene to mice overexpressing either small RNR subunit. In mice, cell proliferation defects would be expected to lead to embryonic lethality, as cell division is required for embryogenesis. Our first observation was that the combination of Rrm1-D57N and either small RNR subunit caused synthetic lethality in mice, which would be predicted by the previous model. I next found that the timing of the lethality was determined by which specific transgenic combination was expressed. Combination of *Rrm1-D57N(high)*^{Tg} with either small subunit caused embryonic lethality, with *p53R2*^{Tg} being more severe than *Rrm2*^{Tg}. Having less mutant *Rrm1* allows the *Rrm1-D57N(low)*^{Tg} strain to survive longer, through gestation, when paired with *Rrm2*^{Tg} or *p53R2*^{Tg}, but the lifespan is still significantly shortened and lasts a matter of days. Again, having *p53R2*^{Tg} made the phenotype more severe than having *Rrm2*^{Tg}. This may be due to the differential patterns of expression of *Rrm2* and *p53R2*. *p53R2* is expressed at very low levels throughout the cell cycle, while during S-phase, *Rrm2* is expressed very highly. High-level overexpression of *p53R2* would then be expected to cause a more significant deregulation of RNR than overexpression of *Rrm2*.

That some bitransgenic mice are able to survive through gestation was surprising, given that the effects of similar RNR deregulation in yeast caused proliferation defects and would be expected to cause only embryonic lethality

Figure 3.14. Proliferation of cells overexpressing either Rrm1-D57N transgene and either small RNR subunit. Cells were maintained in media with 10% serum and passed every 3 days with counting. Cumulative population doublings were calculated and plotted vs. time. (J.P.)

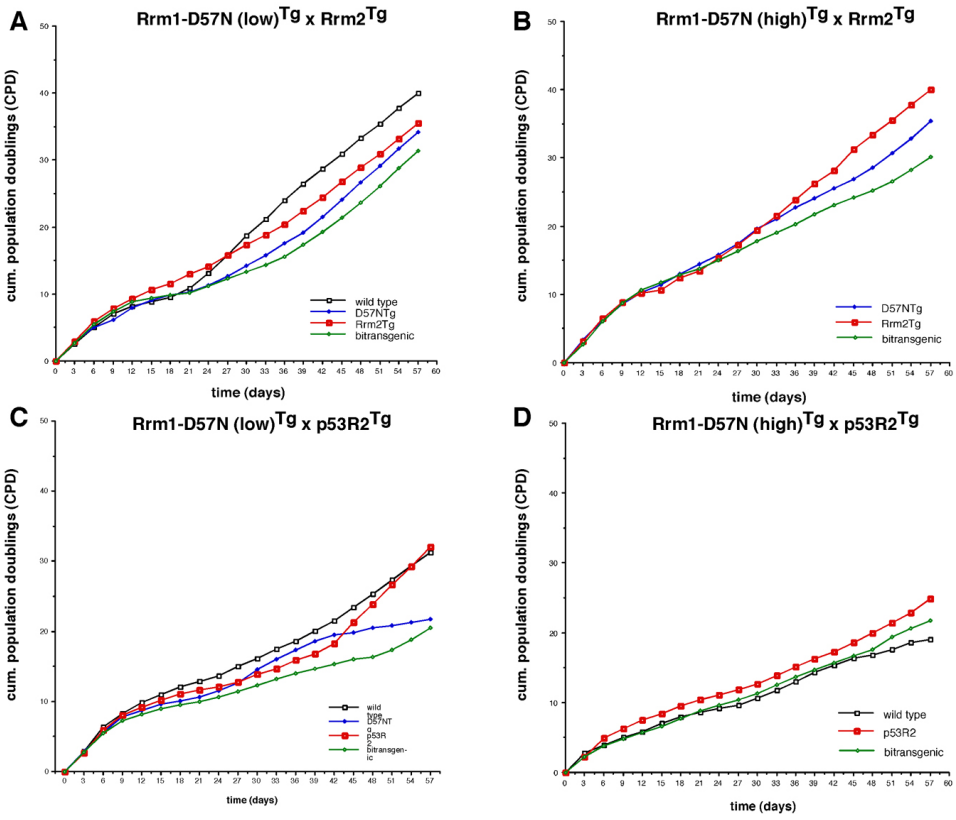
A
Rrm1-D57N (low)Tg x Rrm2Tg
cum. population doublings (CPD)
time (days)
wild type
D57NTg
Rrm2Tg
bitransgenic
B
Rrm1-D57N (high)Tg x Rrm2Tg
cum. population doublings (CPD)
time (days)
D57NTg
Rrm2Tg
bitransgenic
C
Rrm1-D57N (low)Tg x p53R2Tg
cum. population doublings (CPD)
time (days)
wild type
D57NTg
p53R2
bitransgenic
D
Rrm1-D57N (high)Tg x p53R2Tg
cum. population doublings (CPD)
time (days)
wild type
p53R2
bitransgenic

in mice. Also inconsistent with the yeast model was the finding that MEFs expressing all four combinations of *Rrm1-D57N* and either small subunit proliferated normally relative to controls. These findings indicate that while RNR is deregulated to a lethal extent in these mice, it is not sufficiently altered to cause cellular defects.

Rrm1-D57N(low)^{Tg} + *Rrm2*^{Tg} bitransgenic mice, the least severe combination, were severely underrepresented in adulthood, most having succumbed to illness within the first 2 weeks of life. Rare surviving bitransgenic adults displayed severe skeletal and cardiac muscle degeneration. In addition to muscle degeneration, they also displayed a general wasting phenotype, kyphosis, and alopecia. Taken together, these phenotypes are consistent with premature aging. Mice harboring a proofreading-deficient DNA Pol γ also display these phenotypes(47), suggesting that destabilization of the mitochondrial genome may play a role in this synthetic lethality. We also noted that mice that overexpress *Rrm1*^{Tg} and *Rrm2*^{Tg} or *p53R2*^{Tg} displayed severe age-dependent mtDNA depletion (Chapter 2). This strengthens the link between RNR deregulation and mitochondrial genome instability. All together, these results suggested that synthetic lethality in *Rrm1-D57N(low)*^{Tg} + *Rrm2*^{Tg} bitransgenic mice may be mediated through mitochondrial genome instability. However, analysis of mtDNA content at various ages as well as assays for the function of mtDNA-encoded complexes did not support this notion. Young *Rrm1-D57N(low)*^{Tg} +

Rrm2^{Tg} bitransgenic mice did not show mtDNA depletion. The rare *Rrm1-D57N(low)*^{Tg} + *Rrm2*^{Tg} bitransgenic mice that survived to adulthood did show a reduction in mtDNA content, but we must conclude that mtDNA depletion does not cause lethality in these bitransgenic mice, as most *Rrm1-D57N(low)*^{Tg} + *Rrm2*^{Tg} bitransgenic mice die during the second week of life, when no mtDNA depletion was observed, and only rarely survive long enough to display such phenotypes. Nevertheless, given the mtDNA depletion observed in the *Rrm1*^{Tg} + *Rrm2*^{Tg} and *Rrm1*^{Tg} + *p53R2*^{Tg} bitransgenic mice and that in our model RNR is expected to be further deregulated, we do expect that if given enough time, the combination of *Rrm1-D57N(low)*^{Tg} + *Rrm2*^{Tg} would cause mtDNA depletion. We hypothesize that we were unable to observe such depletion because of the short lifespan of *Rrm1-D57N(low)*^{Tg} + *Rrm2*^{Tg} bitransgenic mice. Therefore, the mtDNA depletion is secondary to the lethal defect in *Rrm1-D57N(low)*^{Tg} + *Rrm2*^{Tg} bitransgenic mice, and the actual cause of the lethality is yet to be determined.

A third hypothesis to explain the particular phenotypes observed in the *Rrm1-D57N(low)*^{Tg} + *Rrm2*^{Tg} bitransgenic mice links cellular control of nucleotide levels and hypertension. Elevated and/or unbalanced nucleotide pools are known to be mutagenic, and can have such severe consequences as mtDNA depletion (Chapter 2) and genomic instability(2, 13). A defense against unbalanced nucleotide pools is through nucleotide degradation, in which dNTPs are cleaved by deaminases and nucleoside phosphorylases and

either returned to the substrate cycles or excreted(52). For purines especially, elevated degradation products in the bloodstream of mice or humans can have adverse effects. The products of purine nucleotide degradation, xanthine, hypoxanthine, and uric acid, are elevated in the blood of hypertensive patients(53) and elevating uric acid causes hypertension in rats(54). Among other phenotypes, hypertension causes pleural effusion(55) and glaucoma(56), which are either observed in our mice or are similar to phenotypes observed in our mice. Therefore, I hypothesize that simultaneous disruption of both main RNR regulatory pathways in *Rrm1-D57N(low)*^{Tg} + *Rrm2*^{Tg} bitransgenic mice elevates nucleotide pools, which are quickly degraded in an attempt to keep levels balanced. The increase in xanthine, hypoxanthine, and especially uric acid in the blood triggers hypertension, which results in pleural effusion and eventually suffocates the bitransgenic mice at a young age.

A second, but not exclusive, pathway to arrive at hypertension is through kidney disease. Defects in protein uptake within the proximal renal tubules can cause hypertension, leading to pleural effusion and ultimately, death(57). Kidney degeneration, characterized by loss of both cortical and medullary renal tubules, fibrosis, and dilation of medullary tubules, was found in juvenile bitransgenics (P9 and P11). Similar phenotypes were observed in mice lacking Myosin-VI(57), which functions in endocytosis. Interestingly, mutation of *Myo6* in mice led to elevated blood pressure and decreased body

weight in adults. Pleural effusion was also observed in *Rrm1-D57N(low)*^{Tg} + *Rrm2*^{Tg} bitransgenic mice, and subsequent analysis of the fluid revealed it to be transudative in nature, as opposed to exudative. Transudative pleural effusions are caused by defects such as hypertension, kidney failure, and heart failure and are characterized by low protein and albumin content(55). Exudative pleural effusions are characterized by high protein and albumin content, and are caused by local lesions such as lung tumors(55).

Another link between RNR and kidney defects was found in the kidneys of aged *Rrm2*^{Tg} and *p53R2*^{Tg} mice, as well as bitransgenics harboring *Rrm1*^{Tg} and either small subunit. I observed proteinuria upon histological staining of kidneys from mice overexpressing either small RNR subunit. The *Myo6* mutant mice also showed significant albuminuria, suggested to begin during kidney development and affect phenotypes throughout the life of the animal(57). This possibly supports a link between impaired protein uptake by the kidneys during development and hypertension, which could later lead to pleural effusion in our bitransgenic neonates.

This hypothesis may help explain the lethality in the *Rrm1-D57N(low)*^{Tg} + *Rrm2*^{Tg} bitransgenic mice, but they survive significantly longer than bitransgenics from the other crosses, most notably the crosses involving *Rrm1-D57N(high)*^{Tg}. Bitransgenic embryos harboring the *Rrm1-D57N(high)* transgene and either small subunit showed defects in the vasculature. *Rrm1-D57N(high)*^{Tg} + *p53R2*^{Tg} and *Rrm1-D57N(high)*^{Tg} + *Rrm2*^{Tg} embryos showed

vascular defects in the yolk sac and hemorrhages in the near the dorsal aorta. While links between this and nucleotide metabolism are unclear, the development of pleural effusion in neonates and hemorrhages in embryos may suggest a more general vascular defect as the cause of all of the observed synthetic lethality.

Nucleotides also play significant roles in many other processes and as signaling molecules. While ATP stimulates muscle contraction, dATP stimulates even stronger contractions. An increase in dATP could possibly induce stronger contractions within the cardiac muscle, leading to increased blood pressure and the downstream phenotypes associated with it. Other possible effects of elevated RNR activity include depletion of nucleotide precursors, which could limit the nucleotides available for RNA synthesis and signaling. Further work is needed in order to determine the full extent of perturbations to nucleotide pools caused by RNR deregulation.

Deregulation of RNR in mice by small subunit overexpression causes lung tumorigenesis and moderately elevated dNTP pools, while overexpression of the feedback-resistant mutant *Rrm1-D57N* had limited phenotypes. Only when these two regulatory modes were simultaneously disabled were phenotypes observed, suggesting that these two mechanisms are partially redundant. The timing of the lethality is dependent on the degree of RNR deregulation, with higher-level overexpression of *Rrm1-D57N*^{Tg} or either small subunit resulting in more severe defects and earlier lethality. In

yeast, simultaneous loss of both regulatory modes caused proliferation defects, while the cells were able to survive. All together, I conclude that severe deregulation if RNR in multicellular organisms has hazardous consequences, and further work will allow us to explore the ability of cells to maintain their genomes in the presence of deregulated RNR.

ACKNOWLEDGMENTS

I would like to thank Dr. Patrick Stover for allowing use of the UPLC and for technical advice. I would also like to thank Christina Cota for valuable suggestions regarding embryonic phenotypes.

REFERENCES

1. Xu X, Page JL, Surtees JA, Liu H, Lagedrost S, Lu Y, et al. Broad overexpression of ribonucleotide reductase genes in mice specifically induces lung neoplasms. Cancer Res. 2008;68(8):2652-60. PMCID: 2459241.

2. Kunkel T. DNA replication fidelity. Journal of Biological Chemistry. 2004;279(17):16895.

3. Kunkel T, Mosbaugh D. Exonucleolytic proofreading by a mammalian DNA polymerase. gamma. Biochemistry. 1989;28(3):988-95.

4. Song S, Pursell Z, Copeland W, Longley M, Kunkel T, Mathews C. DNA precursor asymmetries in mammalian tissue mitochondria and possible contribution to mutagenesis through reduced replication fidelity. Proceedings of the National Academy of Sciences of the United States of America. 2005;102(14):4990.

5. Byrnes JJ, Downey KM, Black VL, So AG. A new mammalian DNA polymerase with 3' to 5' exonuclease activity: DNA polymerase delta. Biochemistry. 1976;15(13):2817-23.

6. Meuth M. The molecular basis of mutations induced by deoxyribonucleoside triphosphate pool imbalances in mammalian cells. Experimental cell research. 1989;181(2):305-16.

7. Chabes A, Georgieva B, Domkin V, Zhao X, Rothstein R, Thelander L. Survival of DNA damage in yeast directly depends on increased dNTP levels allowed by relaxed feedback inhibition of ribonucleotide reductase. Cell. 2003;112(3):391-401.

8. Fasullo M, Tsaponina O, Sun M, Chabes A. Elevated dNTP levels suppress hyper-recombination in Saccharomyces cerevisiae S-phase checkpoint mutants. Nucleic Acids Res. 2010;38(4):1195-203. PMCID: 2831302.

9. Kunz B, Kohalmi S. Modulation of mutagenesis by deoxyribonucleotide levels. Annual review of genetics. 1991;25(1):339-59.

10. Kumar D, Viberg J, Nilsson AK, Chabes A. Highly mutagenic and severely imbalanced dNTP pools can escape detection by the S-phase checkpoint. Nucleic Acids Res. 2010.

11. Bebenek K, Roberts J, Kunkel T. The effects of dNTP pool imbalances on frameshift fidelity during DNA replication. Journal of Biological Chemistry. 1992;267(6):3589.

12. Hastak K, Paul RK, Agarwal MK, Thakur VS, Amin AR, Agrawal S, et al. DNA synthesis from unbalanced nucleotide pools causes limited DNA damage that triggers ATR-CHK1-dependent p53 activation. Proc Natl Acad Sci U S A. 2008;105(17):6314-9. PMCID: 2359797.

13. Song S, Wheeler LJ, Mathews CK. Deoxyribonucleotide pool imbalance stimulates deletions in HeLa cell mitochondrial DNA. J Biol Chem. 2003;278(45):43893-6.

14. Suomalainen A, Isohanni P. Mitochondrial DNA depletion syndromes - Many genes, common mechanisms. Neuromuscul Disord. 2010.

15. Lopez LC, Akman HO, Garcia-Cazorla A, Dorado B, Marti R, Nishino I, et al. Unbalanced deoxynucleotide pools cause mitochondrial DNA instability in thymidine phosphorylase-deficient mice. Hum Mol Genet. 2009;18(4):714-22. PMCID: 2638828.

16. Lee W, Sokol R, editors. Liver disease in mitochondrial disorders2007: New York: Thieme-Stratton, c1981-.

17. Bourdon A, Minai L, Serre V, Jais JP, Sarzi E, Aubert S, et al. Mutation of RRM2B, encoding p53-controlled ribonucleotide reductase (p53R2), causes severe mitochondrial DNA depletion. Nat Genet. 2007;39(6):776-80.

18. Kollberg G, Darin N, Benan K, Moslemi AR, Lindal S, Tulinius M, et al. A novel homozygous RRM2B missense mutation in association with severe mtDNA depletion. Neuromuscul Disord. 2009;19(2):147-50.

19. Kimura T, Takeda S, Sagiya Y, Gotoh M, Nakamura Y, Arakawa H. Impaired function of p53R2 in Rrm2b-null mice causes severe renal failure through attenuation of dNTP pools. Nat Genet. 2003;34(4):440-5.

20. Akman HO, Dorado B, Lopez LC, Garcia-Cazorla A, Vila MR, Tanabe LM, et al. Thymidine kinase 2 (H126N) knockin mice show the essential role of balanced deoxynucleotide pools for mitochondrial DNA maintenance. Hum Mol Genet. 2008;17(16):2433-40.

21. Gotz A, Isohanni P, Pihko H, Paetau A, Herva R, Saarenpaa-Heikkila O, et al. Thymidine kinase 2 defects can cause multi-tissue mtDNA depletion syndrome. Brain. 2008;131(Pt 11):2841-50.

22. Mandel H, Szargel R, Labay V, Elpeleg O, Saada A, Shalata A, et al. The deoxyguanosine kinase gene is mutated in individuals with depleted hepatocerebral mitochondrial DNA. Nat Genet. 2001;29(3):337-41.

23. Nishino I, Spinazzola A, Hirano M. Thymidine phosphorylase gene mutations in MNGIE, a human mitochondrial disorder. Science. 1999;283(5402):689-92.

24. Pugmire M, Ealick S. Structural analyses reveal two distinct families of nucleoside phosphorylases. Biochemical Journal. 2002;361(Pt 1):1.

25. Pontarin G, Fijolek A, Pizzo P, Ferraro P, Rampazzo C, Pozzan T, et al. Ribonucleotide reduction is a cytosolic process in mammalian cells independently of DNA damage. Proc Natl Acad Sci U S A. 2008;105(46):17801-6. PMCID: 2584719.

26. Kolberg M, Strand KR, Graff P, Andersson KK. Structure, function, and mechanism of ribonucleotide reductases. Biochim Biophys Acta. 2004;1699(1-2):1-34.

27. Tanaka H, Arakawa H, Yamaguchi T, Shiraishi K, Fukuda S, Matsui K, et al. A ribonucleotide reductase gene involved in a p53-dependent cell-cycle checkpoint for DNA damage. Nature. 2000;404(6773):42-9.

28. Engstrom Y, Rozell B, Hansson HA, Stemme S, Thelander L. Localization of ribonucleotide reductase in mammalian cells. EMBO J. 1984;3(4):863-7. PMCID: 557439.

29. Hakansson P, Hofer A, Thelander L. Regulation of mammalian ribonucleotide reduction and dNTP pools after DNA damage and in resting cells. J Biol Chem. 2006;281(12):7834-41.

30. Chabes AL, Bjorklund S, Thelander L. S Phase-specific transcription of the mouse ribonucleotide reductase R2 gene requires both a proximal repressive E2F-binding site and an upstream promoter activating region. J Biol Chem. 2004;279(11):10796-807.

31. Chabes AL, Pfleger CM, Kirschner MW, Thelander L. Mouse ribonucleotide reductase R2 protein: a new target for anaphase-promoting complex-Cdh1-mediated proteolysis. Proc Natl Acad Sci U S A. 2003;100(7):3925-9. PMCID: 153024.

32. Ylikallio E, Page JL, Xu X, Lampinen M, Bepler G, Ide T, et al. Ribonucleotide reductase is not limiting for mitochondrial DNA copy number in mice. Nucleic Acids Res. 2010;38(22):8208-18. PMCID: 3001089.

33. Ingemarson R, Thelander L. A Kinetic Study on the Influence of Nucleoside Triphosphate Effectors on Subunit Interaction in Mouse Ribonucleotide ReductaseÜ. Biochemistry. 1996;35(26):8603-9.

34. Uppsten M, Farnegardh M, Domkin V, Uhlin U. The first holocomplex structure of ribonucleotide reductase gives new insight into its mechanism of action. Journal of molecular biology. 2006;359(2):365-77.

35. Caras IW, Martin DW, Jr. Molecular cloning of the cDNA for a mutant mouse ribonucleotide reductase M1 that produces a dominant mutator phenotype in mammalian cells. Mol Cell Biol. 1988;8(7):2698-704. PMCID: 363480.

36. Chabes A, Stillman B. Constitutively high dNTP concentration inhibits cell cycle progression and the DNA damage checkpoint in yeast Saccharomyces cerevisiae. Proc Natl Acad Sci U S A. 2007;104(4):1183-8. PMCID: 1783093.

37. Edelmann W, Yang K, Umar A, Heyer J, Lau K, Fan K, et al. Mutation in the mismatch repair gene Msh6 causes cancer susceptibility. Cell. 1997;91(4):467-77.

38. You Y, Halangoda A, Buettner V, Hill K, Sommer S, Pfeifer G. Methylation of CpG dinucleotides in the lacI gene of the Big BlueÆ transgenic mouse. Mutation Research/Genetic Toxicology and Environmental Mutagenesis. 1998;420(1-3):55-65.

39. Hill KA, Halangoda A, Heinmoeller PW, Gonzalez K, Chitaphan C, Longmate J, et al. Tissue-specific time courses of spontaneous mutation frequency and deviations in mutation pattern are observed in middle to late adulthood in Big Blue mice. Environ Mol Mutagen. 2005;45(5):442-54.

40. Stiegler GL, Stillwell LC. Big Blue transgenic mouse lacI mutation analysis. Environ Mol Mutagen. 1993;22(3):127-9.

41. Tyynismaa H, Mjosund KP, Wanrooij S, Lappalainen I, Ylikallio E, Jalanko A, et al. Mutant mitochondrial helicase Twinkle causes multiple mtDNA deletions and a late-onset mitochondrial disease in mice. Proc Natl Acad Sci U S A. 2005;102(49):17687-92.

42. Mahler JF, Stokes W, Mann PC, Takaoka M, Maronpot RR. Spontaneous lesions in aging FVB/N mice. Toxicol Pathol. 1996;24(6):710-6.

43. Harbach P, Zimmer D, Filipunas A, Mattes W, Aaron C. Spontaneous mutation spectrum at the lambda cII locus in liver, lung, and spleen tissue of Big BlueÆ transgenic mice. Environmental and molecular mutagenesis. 1999;33(2):132-43.

44. Sato H, Sone H, Sagai M, Suzuki K, Aoki Y. Increase in mutation frequency in lung of Big BlueÆ rat by exposure to diesel exhaust. Carcinogenesis. 2000;21(4):653.

45. Bianchi V. Regulation of deoxynucleotide pools by substrate cycles. Adv Exp Med Biol. 1998;431:501-6.

46. Jiricny J. The multifaceted mismatch-repair system. Nature Reviews Molecular Cell Biology. 2006;7(5):335-46.

47. Trifunovic A, Wredenberg A, Falkenberg M, Spelbrink J, Rovio A, Bruder C, et al. Premature ageing in mice expressing defective mitochondrial DNA polymerase. Nature. 2004;429(6990):417-23.

48. Chabes A, Domkin V, Thelander L. Yeast Sml1, a protein inhibitor of ribonucleotide reductase. J Biol Chem. 1999;274(51):36679-83.

49. Chabes A, Thelander L. Controlled protein degradation regulates ribonucleotide reductase activity in proliferating mammalian cells during the normal cell cycle and in response to DNA damage and replication blocks. J Biol Chem. 2000;275(23):17747-53.

50. Elledge SJ, Zhou Z, Allen JB. Ribonucleotide reductase: regulation, regulation, regulation. Trends Biochem Sci. 1992;17(3):119-23.

51. Goodman M, Creighton S, Bloom L, Petruska J, Kunkel T. Biochemical basis of DNA replication fidelity. Critical reviews in biochemistry and molecular biology. 1993;28(2):83-126.

52. Rampazzo C, Miazzi C, Franzolin E, Pontarin G, Ferraro P, Frangini M, et al. Regulation by degradation, a cellular defense against deoxyribonucleotide pool imbalances. Mutat Res. 2010;703(1):2-10.

53. Nagaya N, Uematsu M, Satoh T, Kyotani S, Sakamaki F, Nakanishi N, et al. Serum uric acid levels correlate with the severity and the mortality of primary pulmonary hypertension. American journal of respiratory and critical care medicine. 1999;160(2):487.

54. Mazzali M, Hughes J, Kim YG, Jefferson JA, Kang DH, Gordon KL, et al. Elevated uric acid increases blood pressure in the rat by a novel crystal-independent mechanism. Hypertension. 2001;38(5):1101-6.

55. Zocchi L. Physiology and pathophysiology of pleural fluid turnover. Eur Respir J. 2002;20(6):1545-58.

56. Langman MJ, Lancashire RJ, Cheng KK, Stewart PM. Systemic hypertension and glaucoma: mechanisms in common and co-occurrence. Br J Ophthalmol. 2005;89(8):960-3. PMCID: 1772770.

57. Gotoh N, Yan Q, Du Z, Biemesderfer D, Kashgarian M, Mooseker MS, et al. Altered renal proximal tubular endocytosis and histology in mice lacking myosin-VI. Cytoskeleton (Hoboken). 2010;67(3):178-92.

Chapter 4: Allosteric feedback regulation of Ribonucleotide Reductase is crucial for survival in mice[1]

Abstract

Ribonucletotide reductase (RNR) catalyzes the rate-limiting step in *de novo* dNTP biosynthesis and so is a key regulator of nucleotide pools, controlling the availability of dNTPs for DNA replication and DNA repair. In order to tightly regulate nucleotide availability, the activity of RNR must be carefully controlled. The mechanisms involved in regulating the activity of RNR have been well established in recent years. In mammals, the two main regulatory mechanisms include transcriptional control of RNR genes and allosteric feedback control. Consequences of deregulating RNR by way of disabling the activity site are well characterized in yeast. Importantly, Chabes and Stillman found that yeast that overexpressed *rnr1-D57N* exhibited reduced replication origin firing and slow growth. However, transgenic animal models featuring overexpression of the *Rrm1*^{D57N} mutant are grossly normal, indicating that the presence of the wild type allele at the endogenous locus allows for adequate feedback control. We hypothesized that targeting the *Rrm1*^{D57N} mutation directly to the endogenous Rrm1 locus would remove all allosteric feedback inhibition and RNR would be constitutively active. We therefore generated mice with *Rrm1*^{D57N} targeted to the endogenous locus and obtained germline transmission in two independent mouse strains. We found that homozygosity of *Rrm1*^{D57N} causes embryonic lethality in mice, slow growth of cultured MEFs, and p21 upregulation. Heterozygous mice are born at expected frequencies and are grossly normal, which is inconsistent with

[1] Jennifer L. Page, Sarah Lagedrost, Lee Gerwitz, Teresa Southard, and Robert S. Weiss. Unpublished results.

reports that *Rrm1*^{D57N} is a dominant mutation. We hypothesize that, as in the Chabes-Stillman model, persistent elevated dNTP concentrations may act to inhibit firing of replication origins and slow growth, which is lethal in a developing embryo. This work underscores the importance of tightly controlled RNR activity in mammals.

Introduction

Accurate genome replication requires an adequate and balanced supply of dNTPs, the precursors for DNA synthesis. Insufficient levels of one or more dNTPs leads to replication stress and activation of the S-phase checkpoint(1), and depletion of mitochondrial DNA[(2)]. However, increased nucleotide pools are mutagenic in yeast[(3)] and mammalian cells[(4)]. Severely unbalanced nucleotide pools have been proposed to be a signal for apoptosis(5). The rate-limiting step in dNTP biosynthesis, the removal of the 2'-OH from the ribonucleoside diphosphate to produce the deoxyribonucleoside diphosphate, is catalyzed by the cytosolic enzyme ribonucleotide reductase (RNR)(6). RNR is comprised of two subunits. The large subunit is a homodimer encoded by a single gene, Rrm1, while the small subunit is either a homodimer of the Rrm2 gene product or the p53R2 gene product. Regulation of RNR activity is a principal mechanism by which cells can ensure an optimal nucleotide pool. Mammalian cells are known to utilize two main mechanisms to control RNR activity, limitation of small subunit protein levels and allosteric feedback inhibition.

The small subunit Rrm2 is induced as the cell enters S-phase so that it can complex with Rrm1 to provide dNTPs for DNA replication. Following S-phase, Rrm2 is specifically degraded by the APC^{Cdh1} complex in order to limit the bulk of RNR activity to S-phase(7). The small subunit p53R2 is expressed

at low and constant levels throughout the cell cycle, where it can form a complex with Rrm1 to provide dNTPs for basal DNA repair and mitochondrial DNA synthesis(8). Following DNA damage, p53R2 is induced by p53 in order to rapidly provide dNTPs for repair of the damage(9). We previously reported that mice that overexpress either small RNR subunit Rrm2 or p53R2 developed lung tumors at a high frequency(10), suggesting that tight control of the small subunit protein levels is critical.

Regulation of RNR activity in the yeast *Saccharomyces cerevisiae* follows a different pattern. Yeast *RNR1* is tightly linked to the cell cycle and during S-phase, mRNA levels show a 10-fold increase compared to resting phases(11). In contrast, *RNR*2 mRNA was abundant throughout the cell cycle and levels showed at most a 2-fold increase as cells reached S-phase(12). A second mechanism for inhibition of RNR activity in yeast relies on binding of small protein inhibitors to the R1 subunit. The small protein SML1 (suppressor of *mec1* lethality) binds the R1 subunit in G1 phase and prevents activity. Due to sequence homology between the C-termini of SML1, RNR2, and RNR4, it was hypothesized that binding of SML1 to RNR1 would involve the same interaction domain as RNR1-RNR2 binding and inhibition would be competitive; however, inhibition appeared noncompetitive(13). No mammalian homologs of SML1p have been identified yet. A fourth regulatory mechanism controlling RNR activity in yeast is differential subcellular localization. During quiescent phases of the cell cycle, Rnr2p and Rnr4p are anchored in the nucleus by Wtm2(14). Following DNA damage or during S-phase, Rnr2p and Rnr4p are released and translocate into the cytosol and complex with Rnr1p(14).

Control of RNR activity through allosteric feedback inhibition involves two separate effector binding sites. A specificity site binds dNTPs in a feedback loop in order to determine substrate choice. Mutation of residues within this site lead to unbalanced nucleotide pools(1). In cultured mammalian cells, an isolated mutation was able to confer resistance to excessive levels of dGTP, although the specific mutation was never reported(15). In yeast, a series of mutations within Loop 2, proposed to be the functional part of the allosteric specificity site, create unbalanced nucleotide pools(1). Despite causing extreme variations in the concentration of each dNTP relative to one another, most mutations did not trigger activation of the intra-S-phase checkpoint. Only mutations which specifically caused depletion of at least one dNTP activated the S-phase checkpoint, suggesting that while mutagenic, unbalanced nucleotide pools can be tolerated(1).

A second binding site, the activity site, monitors the ratio of ATP vs. dATP, so that ATP stimulates enzyme activity while dATP inhibits further production of dNTPs. Mutation of a critical and conserved residue within the activity site, aspartic acid 57 to asparagine, destroys the ability of the activity site to respond to dATP binding and allowed mammalian cells to survive in the presence of excessive dATP(16). Work by Reichard *et al.* shows that the Rrm1-D57N mutant binds dATP with wild type affinity, but that dATP stimulates rather than inhibits enzyme activity(17). In yeast, when expressed under the endogenous promoter, the *rnr1-D57N* mutant elevated dNTP pools by approximately 3-fold and conferred a mutator phenotype(3). The Rrm1-D57N mutant is also mutagenic in mammalian cells(16). As a result of dNTP pool expansion, cells showed improved survival following DNA damage. Yeast which overexpressed *rnr1-D57N* under a gal-inducible promoter showed an

approximately 35-fold increase in [dNTP], resulting in slow growth(18). Activation of the intra-S-phase checkpoint was not observed. The slow growth phenotype was characterized by reduced loading of the S-phase initiator protein Cdc45p. This data indicated that cells which overexpress *rnr1-D57N* were inhibited in activating origins to enter S-phase. Further reduction of the available pre-RCs by disabling function of the origin recognition complex (ORC) would then be expected to worsen the phenotype observed in rnr1-D57N overexpressing cells. Simultaneous expression of *orc2-1* or *orc5-1* mutants caused synthetic sickness in the cells with overexpressed *rnr1-D57N*, suggesting that inhibition of origin firing in *rnr1-D57N*-overexpressing cells is the cause of the slow growth. Cells that overexpressed *rnr1-D57N* accumulated in G1 phase of the cell cycle, while cells that overexpressed RNR1 in the same manner did not(18). Together these results suggest that excessively elevated dNTPs may act as a signal for inhibiting DNA replication in cells.

Inhibition of pre-RC activation is one of the functions accomplished by the p53-dependent checkpoint protein p21(19). p21 is a member of the CIP/KIP family of CDK inhibitors (CKIs), along with p27 and p57(20). p21 was shown to interact with both Cdk2 and Cdk3 by a yeast two-hybrid screen, and to negatively regulate the cyclin A-Cdk2 complex in cultured human fibroblasts(21). p21 is able to effectively block phosphorylation of Rb by both A-type and E-type cyclin/Cdk complexes(21), leading to G1 arrest(22). p21 can also directly bind PCNA in order to block binding sites for DNA polymerase d(19).

Previous work by us indicates that overexpression of Rrm1-D57N in mice is not sufficient to cause overt phenotypes (Chapter 3). Rrm1-D57N-

overexpression was not tumorigenic and was not mutagenic, either alone or in combination with mismatch-repair deficiency. Only when overexpression of Rrm1-D57N was combined with overexpression of either small RNR subunit, relieving RNR of both main regulatory mechanisms, was a phenotype observed, in the form of synthetic lethality. Even then, primary MEFs cultured from bitransgenic embryos proliferated normally, suggesting no prolonged G1 phase as in Chabes and Stillman(18). We hypothesized that the limited phenotypes observed may be due to variable expression levels of the Rrm1-D57N transgene in different tissues, minimizing the observable effects of Rrm1-D57N overexpression. We reasoned that in order to observe the full effects of loss of dATP inhibition, the Rrm1-D57N mutation must be targeted to the endogenous locus, thereby standardizing expression and effects as well as removing all activity site function. Here we report that loss of allosteric feedback control in mice causes embryonic lethality, and preliminary work suggests that cells fail to progress beyond G1 phase normally, indicating that in mammals, as in yeast, dNTP pools may be a signal determining whether it is appropriate to fire origins.

Materials and Methods

Generation of *Rrm1*^{D57N} targeting construct.

The Rrm1 genomic locus was modified using recombineering(23, 24). A BAC clone (411e05) derived from 129/svev mice was electroporated into SW106 cells(25). Oligos used to generate various constructs are listed in Table 4.1. The D57N point mutation was introduced using the GalK replacement system, in which the wild-type guanidine base was replaced by homologous recombination with the bacterial GalK gene (generating the JePa1 plasmid).

Recombined clones were screened on MacConkey's agar plates, in which cells able to use galactose are red. The GalK gene was then replaced with the mutant adenine by homolgous recombination, and cells were analyzed for loss of the ability to utilize galactose by growth on 2'-deoxygalactose plates. Positive clones were then confirmed by sequencing of the mutated exon (the JePa2 plasmid). A 12-kb region containing approximately half of the Rrm1 locus was subcloned into the PL253 plasmid, introducing a bacterial TK element outside the region of homology (JePa3). A floxed Neo cassette was introduced into the second intron approximately 500bp from the mutated base pair by homologous recombination (JePa4), generating the *Rrm1*$^{D57N\text{-}Neo}$ (hereafter referred to as *Rrm1*^{Neo}) allele. The final construct was confirmed by sequencing of cloning junctions and restriction digests.

Table 4.1. Primers used to generate *Rrm1*$^{D57N\text{-}Neo}$ mice.

Primer	Sequence	Description	Purpose
JLP1	5'-CTC TGC GGC CGC CAA GGC AGC CCA GTA GCG GG-3'	Gap repair proximal forward	generate homologous arms for gap repair
JLP2	5'-ATA AGC CAA TAT AGA GA-3'	Gap repair proximal reverse	
JLP3	5'-CTC AAG CTT CGC CTC TGA CCA GGC ATG CA-3'	Gap repair distal forward	
JLP4	5'-CTC ACT AGT AGA ATC AGG GTC TTC CTA TA-3'	Gap repair distal reverse	
JLP5	5'-CTC GTC GAC CCA CTT ACC AGT GAG TAG AT-3'	Neo insert upstream forward	generate homologous arms for Neo cassette insertion
JLP6	5'-CTC GAA TTC CAT CTC CCA CTA TAC AC-3'	Neo insert upstream reverse	
JLP7	5'-CTC GGA TCC CCT CCG TGG GGA GTG CTT GT-3'	Neo insert downstream forward	
JLP8	5'-CTC GCG GCC GCT CCC AAG AGT TAC TGT GTC ACT-3'	Neo insert downstream reverse	
JLP9	5'-CAT GAA AGT AAT CCA AGG CCT ATA TAG TGG GGT CAC CAC AGT GGA ACT GCC TGT TGA CAA TTA ATC ATC GGC A-3'	GalK forward	amplify GalK cassette to replace wild type 'G'
JLP10	5'-TCA GGG TGC TTC GTG GTC AAG GTC GCG GCT GTC TCA GCA GCC AGG GTG TTC AGC ACT GTC CTG CTC CTT-3'	GalK reverse	
JLP11	5'-CAT GAA AGT AAT CCA AGG CCT ATA TAG TGG GGT CAC CAC AGT GGA ACT GAA CAC CCT GGC TGC TGA GAC AGC CGC GAC CTT GAC CAC GAA GCA CCC TGA-3'	GalK oligo coding	replace GalK with mutant 'A'
JLP12	5'-TCA GGG TGC TTC GTG GTC AAG GTC GCG GCT GTC TCA GCA GCC AGG GTG TTC AGC TCC AGT TCC ACT GTG GTG ACC CCA CTA TAT AGG CCT TGG ATT ACT TTC ATG-3'	GalK oligo complement	
JLP13	5'-CTC AGA TCA CCA TGA AGG TAA TCC-3'	GalK sequencing forward	confirm mutation insertion
JLP14	5'-GGA TGG CAT AGT CAG GGT GCT TCG T-3'	GalK sequencing reverse	
JLP15	5'-TGT TCC TCCG GGAAAG CTC-3'	Exon 3 forward	confirm GalK insertion or loss by size
JLP16	5'-AGT TCC CAT GCT GCC AC-3'	Exon 3 reverse	
JLP17	5'-CTC GAA TTC CCC TCT CCT CTC AGC CAC GT-3'	D57N proximal external probe forward	confirm correct targeting in ES cells
JLP18	5'-CTC GAA TTC GTT TCT CTC CAG GCA GTC CC-3'	D57N proximal external probe reverse	
JLP19	5'-CTC GAA TTC AGG GGC CTT GAG TTT GAT TC-3'	D57N distal external probe forward	
JLP20	5'-CTC GAA TTC CTA GCA TTA GTC TAC CAG GG-3'	D57N distal external probe reverse	

Embryonic stem cell culture and selection.

TC-1 embryonic stem cells(26) were cultured on feeders in DMEM supplemented with 15% fetal bovine serum, and in the presence of leukemia inhibitory factor (LIF). 2 x 10^7 cells were electroporated with 40mg of the SalI-linearized JePa4 DNA and seeded approximately 5 x 10^6 cells/plate. Cells were grown for 7 days in the presence of G418 and FIAU. Surviving clones were isolated and expanded prior to screening by Southern blot.

Southern blot analysis.

Total genomic DNA isolated from ESC clones was digested overnight with BclI and separated on 0.8% agarose gel. DNA fragments were immobilized on a nylon membrane (GeneScreen Plus, Perkin Elmer) and detected by hybridization with a DNA probe homologous to a region immediately 3' to the targeted sequence (Probe C, Figure 4.1A). Probe C was generated using primers JLP 19 and JLP20. The Neo element introduces a novel BclI site that cuts the approximately 15 kb wild type band to 12 kb. To confirm the presence of a single targeting construct, total DNA was digested with EcoRV and detected with a Neo element-specific probe (Probe B, Figure 4.1A).

To simultaneously detect all three alleles at the *Rrm1* locus, DNA was digested overnight with BamHI. DNA fragments were separated on 0.8% gel as previously described and subjected to a unique probe that hybridized 5' of the Neo insertion (Probe A, Figure 4.1A). Probe A was generated using primers JLP5 and JLP6. HR insertion of the floxed Neo cassette left a residual BamHI site 3' of the Neo element which is maintained following Cre excision, allowing the wild type *Rrm1* allele to be detected as a long 12kb band (with no

novel BamHI), the *Rrm1*^{Neo} allele as a 10-kb band (Figure 4.1D), and the *Rrm1*^{D57N} (Cre excised) allele as a short 400bp band.

PCR genotyping of *Rrm1*^{D57N} knock-in mice

Primers were designed to the targeted locus to uniquely recognize specific elements within each allele. “D57N KI For3” (Primer 1 in Figure 4.1) (5’-TGGTAGTGGGAGATGCCTCC-3’) detected the unmodified wild type allele at the location that would be disrupted by Neo insertion. “Neo 3’-YAZ” (5’-GGTATCGCCGCTCCCGATTCGCAG-3’) hybridizes within the inserted Neo cassette (Primer 4 in Figure 4.1). “D57N KI For2” (5’-GAATTCCTGCAGCCCAATTCC-3’) hybridizes to a region 5’ of the distal LoxP site that is residual PL453 sequence and is retained in the second intron following Cre excision of the Neo element (Primer 3, Figure 4.1). Each individual forward primer was paired 1:1 with “D57N KI Rev” (5’-ACTTTCATGGTGATCTGAGC-3’), which hybridizes to the 5’ end of exon 3 (Primer 2, Figure 4.1). PCR to detect the wild type and the Cre-excised allele were hybridized at 65°C. PCR to detect the longer Neo product was hybridized at 60°C. All PCRs were run 35 cycles. Product sizes were wild type *Rrm1*, 400bp; *Rrm1*^{D57N}, 450bp; *Rrm1*^{Neo}, 800bp.

Immunoblotting

Total protein extracts were prepared from e10.5 embryos by lysis in 40-50 mL RIPA buffer supplemented with protease inhibitors and sodium orthovanadate as a phosphatase inhibitor as described in Chapter 3. Extracts were separated on 10% polyacrylamide gel and transferred to PVDF membrane (Perkin Elmer). R1 protein was detected by AD203, mouse monoclonal anti-R1, and

loading was assessed by detection of a-tubulin with mouse monoclonal anti-a-tubulin.

Northern blot analysis.

Total RNA was extracted from mouse cells with RNAStat-60 (TelTech, Inc) and separated on agarose/formaldehyde gel. RNA was transferred to a nylon membrane (GeneScreen, Perkin Elmer) and detected with Rrm1-specific radiolabeled probe as previously reported(10).

Culture of mouse embryonic fibroblasts (MEFs)

MEFs were isolated from e10.5 embryos derived from *Rrm1*$^{+/D57N}$ heterozygous or *Rrm1*$^{+/Neo}$ heterozygous intercrosses. Following dissection from the yolk sac and decidua, whole embryos were placed into one well of a 96-well plate and incubated for 1 minute in 100mL trypsin. 200mL media was added and the embryo was disaggregated by pipetting. The cells were cultured in DMEM supplemented with 10% fetal bovine serum (FBS), 1% nonessential amino acids, 1% L-glutamine, and 1% penicillin-streptomycin (Mediatech) in 12-well plates until confluent. A subset of the cells were later cultured on plates coated with 0.1% gelatin in PBS. The same set of cells was further cultured in DMEM supplemented with 20% FBS. Cells were seeded in 10^6 cells/plate in triplicate plates. Every 3 days, the cells were counted and split to fresh 10-cm plates or fed 10 mL fresh media if not confluent. Data for the triplicate plates were averaged and population doublings calculated.

cDNA synthesis and sequencing

1μg of total RNR from mouse embryonic fibroblasts was reversed-transcribed using the Superscript II system (Invitrogen). cDNAs were synthesized using random hexamers according to the manufacturer's instructions. The Rrm1 cDNA was amplified using primers "D57N 5'-UTR" (5'-CCCTCCACATCTGACAGTCGTCTC-3') and "mRNR1-Rev" (5'-GCTGTGGTCTTTCAGCCACTTTAC-3'). The reaction was carried out according to manufacturer's directions. Purified cDNAs were sequenced from both directions using "mRNR1-For" (5'-AGTCATGTGATCAAGCGAGATGGC=3') AND "mRNR1-Rev". All sequencing was carried out by the Core Sequencing Facility of the Biotechnology Resource Center, Cornell University, Ithaca, NY.

Results

Generation of *Rrm1*^{D57N} knock-in mice.

We previously reported (Chapter 3) that mice that overexpress the Rrm1-D57N mutant are grossly normal. We hypothesized that due to variable expression patterns and levels in these transgenic mice, that we were only able to observe limited phenotypes. We therefore sought to disbable allosteric feedback control by targeting the point mutation to the endogenous locus, to deregulate RNR without the need for overexpression. The *Rrm1*^{D57N} point mutation was introduced into the endogenous *Rrm1* locus in mouse by homologous recombination in mouse embryonic stem (ES) cells (Figure 4.1A). A guanine-to-adenine transition was introduced into the third exon of mouse Rrm1, converting a conserved aspartic acid to asparagine within the activity site. The construct was electroporated into TC-1 ES cells from the 129/svev

strain, and of 80 G418- and FIAU-resistant clones screened by Southern blot analysis, 2 were found to have integrated the construct into the correct locus (Figure 4.1B). The clones were further confirmed to have received only one copy of the construct by Southern blot analysis using a probe specific to the introduced *Neo* cassette (Figure 4.1C). Further Southern blot analysis using multiple probes directed to unique regions of the construct confirmed that the integrity of the construct was maintained during targeting and selection (Figure 4.1D). Sequencing of the targeted exon from genomic DNA isolated from both positive clones confirmed the presence of the point mutation (Figure 4.1E). Both clones were independently microinjected into C57Bl/6 blastocysts. One clone, designated ESC 15, gave rise to 3 chimeric mice, 2 males and one female. Both males transmitted the mutant allele to the next generation, while the female did not, resulting in the "D57N knock-in-15" (DKI-15) mouse strain. The other clone, designated ESC 55, gave rise to 5 chimeras, 3 males and 2 females. One male transmitted the mutated allele to offspring, while the rest did not, resulting in the DKI-55 mouse strain.

Heterozygous $Rrm1^{+/D57N\text{-}Neo}$ offspring mice were crossed to *Meox2-Cre* knock-in mice to excise the "floxed" Neo allele. Meox2-Cre mice express Cre under the control of the endogenous Meox2 promoter. Cre activity is detected as early as e5 and is throughout the embryo proper and extra-embryonic mesoderm(27). Cre expression resulted in the mutated locus harboring the point mutation in exon 3 and a residual LoxP site. Cre excision was confirmed by PCR detection of the generated $Rrm1^{D57N}$ allele and excision efficiency was assessed by simultaneous detection by Southern blot of the Rrm1, $Rrm1^{Neo}$, and $Rrm1^{D57N}$ alleles. $Rrm1^{+/D57N\text{-}Neo}$ and $Rrm1^{+/D57N}$ heterozygous mice derived from each independently targeted clone were maintained and

characterized separately on a pure 129/svev background, but were found to be grossly normal and the two strains indistinguishable from one another. Because Neo elements have been shown in other mouse models to result in hypomorphic alleles of targeted genes, we maintained mice from both strains with the Neo cassette preserved (*Rrm1*^{Neo}). Both *Rrm1*$^{+/D57N}$ and *Rrm1*$^{+/Neo}$ heterozygous mice were able to survive 18 months of age. These results indicate that mice harboring the *Rrm1*^{D57N} allele are viable.

Rrm1$^{+/Neo}$ and _Rrm1_$^{+/D57N}$ heterozygous mice display increased lung tumorigenesis compared to wild type.

To determine the *in vivo* effects of heterozygosity of the *Rrm1*^{D57N} mutation, we maintained a cohort of wild type and heterozygous mice to the age of 18 months and monitored the mice for signs of disease. The majority of mice of all genotypes, wild type, *Rrm1*$^{+/D57N}$, and *Rrm1*$^{+/Neo}$, survived the full 18 months. The inbred 129 strains have multiple reported phenotypes, ranging from megaesophagus (33% in females and 27% in males), testicular degeneration, ovarian atrophy, nephropathy, cardiomyopathy, and lung cancer. Reported lung cancer incidences vary widely, from 4%-46%, although whether the reported incidences depend on specific substrains was not indicated. 4/62 (6%) *Rrm1*$^{+/+}$ developed lung adenomas within 18 months of age, compared to 9/61 (14%) of *Rrm1*$^{+/Neo}$ mice and 10/55 (18%) of *Rrm1*$^{+/D57N}$ mice (p=0.02 and 0.002, respectively, chi-square). Overall, lung tumors in *Rrm1*^{D57N} mice were not more malignant than those in wild type mice, as only

one *Rrm1*$^{+/D57N}$ mouse developed an adenocarcinoma, compared to 0 from the other genotypes. The incidence of megaesophagus was increased in *Rrm1*$^{+/Neo}$ mice relative to *Rrm1*$^{+/+}$ and *Rrm1*$^{+/D57N}$, with 9/61 (15%) *Rrm1*$^{+/Neo}$ mice displaying megaesophagus compared to 2/62 (3%) of wild type and 2/55 (3%) *Rrm1*$^{+/D57N}$ mice. 5 wild type females developed uterine hemorrhages or tumors, as did 5 *Rrm1*$^{+/D57N}$ females; however, 0 *Rrm1*$^{+/Neo}$ females developed any uterine pathology.

The *Rrm1*^{D57N} and *Rrm1*^{Neo} alleles are expressed and translated.

To assess expression of the modified alleles, we performed Northern blot analysis on total RNA extracted from e10.5 embryos. We found that overall levels of Rrm1 mRNA were unchanged in heterozygous mice for both *Rrm1*$^{+/Neo}$ and *Rrm1*$^{+/D57N}$ (Figure 4.2A). The *Rrm1*$^{Neo/Neo}$ lane showed wild type levels of expression, while the *Rrm1*$^{D57N/D57N}$ lane appeared lighter in intensity. However, a single band was observed for each genotype at the expected molecular weight, indicating that no aberrant transcripts were formed. This was further confirmed through amplification of the Rrm1 cDNAs. Immunoblot analysis on lysates isolated from embryos at the same stage revealed modest decreases in protein level, but could also be due to a technical issue with band smearing (Figure 4.2B). The heterozygotes expressed averaged 77% of the wild type level of Rrm1, while the homozygous mutants averaged 73%. Neither of these was statistically significant by Student's t-test ($p=0.1$ and $p=0.2$, respectively). Most importantly, only a single 90-kD band was detected in both the heterozygous and homozygous samples, indicating that the mutant protein was stable and

not truncated (Figure 4.2B). These results indicate that the mutant allele is expressed and generates a stable protein, of which only residue 57 is altered.

Homozygosity of *Rrm1*^{D57N} results in midgestational embryonic lethality in mice.

We interbred heterozygous mice both with and without the Neo cassette to obtain homozygous mutant mice (Table 4.1). Of 154 offspring genotyped from the *Rrm1*$^{+/D57N\text{-}Neo}$ x *Rrm1*$^{+/Neo}$ intercross, no *Rrm1*$^{Neo/Neo}$ homozygotes were observed. Similarly, of 140 offspring genotyped from the *Rrm1*$^{+/D57N}$ x *Rrm1*$^{+/D57N}$ intercross, no homozygotes were observed. Offspring were obtained in an approximately 1 wt: 2 heterozygote: 0 homozygote ratio, further suggesting that the *Rrm1*$^{Neo/Neo}$ and *Rrm1*$^{D57N/D57}$N genotypes are incompatible with survival, while heterozygotes are viable. We initiated timed mating experiments in order to characterize the apparent embryonic lethality in *Rrm1*^{D57N} homozygous embryos.

Preliminary work revealed that homozygous embryos were generally normal at e8.5. Homozygous embryos at e9.5 were smaller than littermates (Figure 4.2). We found abnormal homozygous embryos through 10.5 days post coitus (dpc), and 0 live homozygous embryos at 11.5dpc or later (Figure 4.2). Additionally, mouse embryonic fibroblasts (MEFs) cultured from embryos at 13.5 dpc failed to proliferate. Likewise, *Rrm1*$^{Neo/Neo}$ homozygous MEFs from 13.5 dpc embryos could not be cultured.

Cell proliferation defects in *Rrm1*^{D57N} homozygous MEFs.

To partially elucidate the cause of death in *Rrm1*^{D57N} homozygous embryos, we sought to assess their ability to proliferate under standard cell culture conditions. Because homozygous embryos are dead by e13.5, MEFs were cultured from e10.5 day embryos. Wild-type MEFs showed a

characteristic proliferation curve, with regular population doublings at low passages and entrance into a senescent state around passage 7 (Figure 4.3). However, both *Rrm1*$^{+/D57N}$ and *Rrm1*$^{D57N/D57N}$ MEFs showed defects in proliferation. Both genotypes of MEFs required additional time to reach confluency, necessitating more time between passages. Both genotypes also reached senescence prematurely, and were already senescing when the assay began, so that the cells were unable to be passed for two weeks. Morphologically, homozygous cells displayed a flattened phenotype and resembled cells undergoing serum starvation (data not shown), suggesting that *Rrm1*$^{D57N/D57N}$ homozygous MEFs may be trapped in a quiescent stage of the cell cycle.

p21 activation in *Rrm1*^{D57N} MEFs

To investigate the causes of the slow growth in the *Rrm1*^{D57N} MEFs, we tested for cell cycle checkpoint activity that may be retarding the growth of these cells in culture. To determine if there was indeed accumulation of cells in G1 phase, which was causing slow growth of *Rrm1*$^{D57N/D57N}$ MEFs, we assessed p21 induction via Northern blot analysis. While *Rrm1*$^{+/+}$ MEFs showed limited expression of p21, both *Rrm1*$^{+/D57N}$ and *Rrm1*$^{D57N/D57N}$ MEFs showed increased p21 expression (n=1). *Rrm1*$^{+/D57N}$ MEFs showed 1.77-fold expression relative to wild type, and *Rrm1*$^{D57N/D57N}$ MEFs showed a 2.54-fold increase (Figure 4.4).

This result was confirmed by qRT-PCR analysis. These data suggest that p21 might be functioning to prevent homozygous and heterozygous MEFs from entering S-phase of the cell cycle.

Figure 4.1 Generation of *Rrm1*^{D57N} knock-in mice. *A*. Targeting construct. The construct contains the modified exon harboring the point mutation, a floxed Neo cassette for positive selection in ES cells, and a TK element outside the region of homology for negative selection in ES cells. *B-D*. Southern blot analysis of correctly targeted clones. *B*. Insertion of Neo element introduces a novel BclI site, which cuts a 15kb band to approximately 12 kb when detected with probe C. *C*. Confirmation of a single construct element within the targeted locus, detected by probe B. *D*. Various digestions confirming retained integrity of the construct upon homologous recombination, each detected using probe A. *E*. Genomic sequence following homologous recombination. In each mutant clone, two peaks are observed within codon 57; the wild type G and the mutant A.

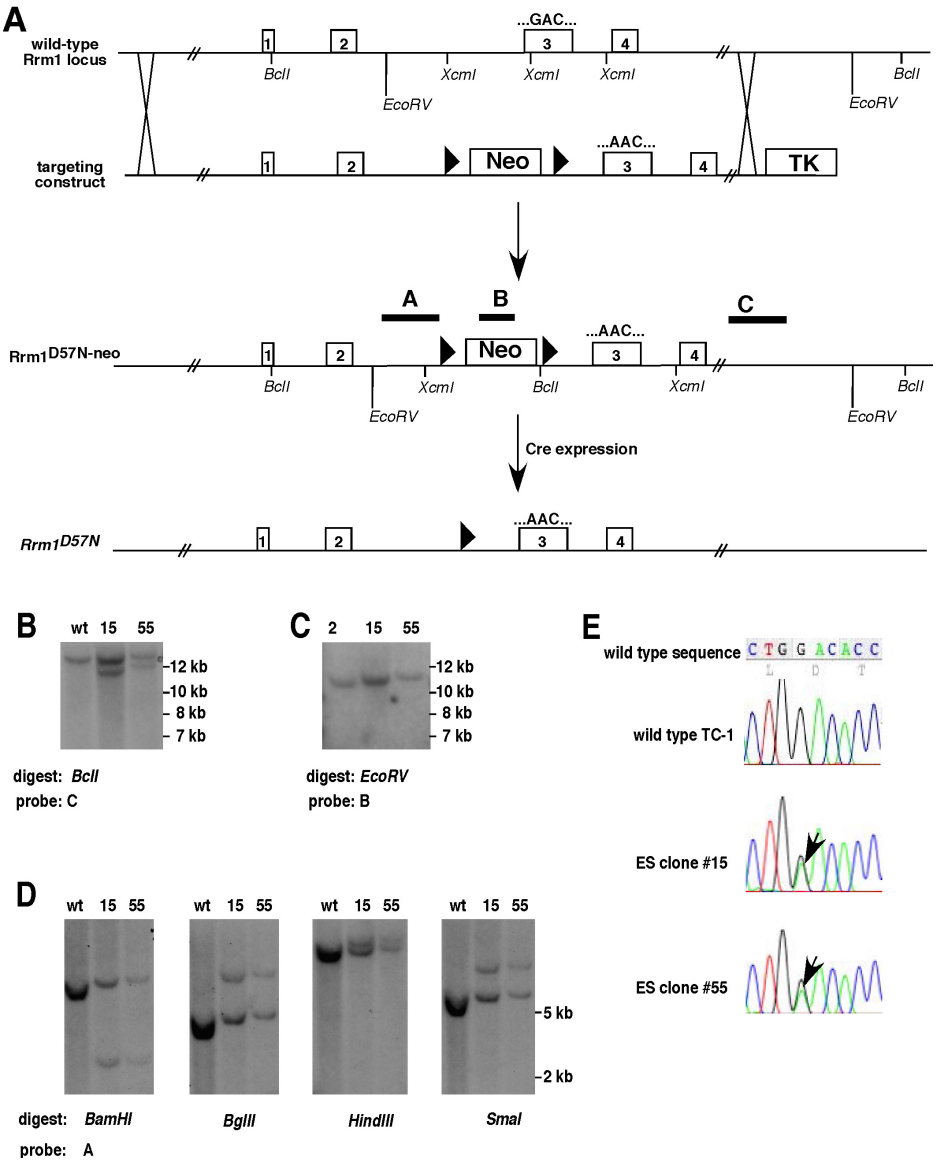
A
wild-type Rrm1 locus
...GAC...
BclI
EcoRV
XcmI
XcmI
XcmI
BclI
EcoRV
targeting construct
...AAC...
Neo
TK
A
B
C
Rrm1D57N-neo
...AAC...
Neo
Cre expression
Rrm1D57N
...AAC...
B
wt 15 55
12 kb
10 kb
8 kb
7 kb
digest: BclI
probe: C
C
2 15 55
12 kb
10 kb
8 kb
7 kb
digest: EcoRV
probe: B
D
wt 15 55
wt 15 55
wt 15 55
wt 15 55
5 kb
2 kb
digest: BamHI
BglII
HindIII
SmaI
probe: A
E
wild type sequence
C T G G A C A C C
wild type TC-1
ES clone #15
ES clone #55

Discussion

Several studies have underscored the necessity of RNR feedback control in maintaining genome stability(1, 3, 5, 16, 18, 28). In this study we presented evidence that allosteric feedback regulation is crucial to the survival of mice. We generated mice harboring a targeted mutation of Rrm1-D57N via homologous recombination in TC-1 mES cells (Figure 1). We obtained two independent correctly-targeted clones, referred to as ESC#15 and ESC#55. From microinjection of these cells in C57Bl/6-derived blastocycts, we obtained a total of 9 chimeric animals, 5 males and 4 females. Three of the 5 males transmitted, two from ESC 15 and one from ESC 55. Expression analyses on embryos obtained from $Rrm1^{+/Neo}$ or $Rrm1^{+/D57N}$ heterozygote intercrosses revealed that the Rrm1 mRNA was produced at wild type levels and was stable (Figure 4.2). This result indicates that the targeted allele is as expected, with no other changes or mutations introduced other than the intended D57N mutation. The result obtained from the $Rrm1^{Neo}$ allele further indicates that we did not generate a hypomorphic allele of Rrm1, as in previous models from our lab(29) . Mice harboring a single targeted $Rrm1^{D57N}$ allele were viable and obtained at expected frequencies. Despite reports that the $Rrm1^{D57N}$ mutation is dominant and causes a mutator phenotype, our $Rrm1^{+/Neo}$ and $Rrm1^{+/D57N}$ heterozygous mice showed no major tumor pathology or displayed a shorter lifespan, indicating that heterozygosity of Rrm^{D57N} is compatible with survival. lWe were surprised to observe that homozygosity of $Rrm1^{D57N}$ was lethal in mice (Table 4.1). Presence or absence of the Neo cassette within the targeted allele did not affect expression of the targeted allele (Figure 4.2).

Figure 4.2 Expression analysis of *Rrm1*$^{+/+}$, *Rrm1*$^{+/D57N}$, and *Rrm1*$^{D57N/D57N}$ embryos. *A*. Northern blot. Total RNA from embryos at e10.5 was detected by an Rrm1-specific radiolabeled probe. GAPDH is used as a loading control. *B*. Total protein was extracted from embryos at e10.5 and separated on a 10% SDS-PAGE gel. Rrm1 was detected by probing with AD203, mouse monoclonal anti-Rrm1 antibody. a-tubulin serves as a control for loading.

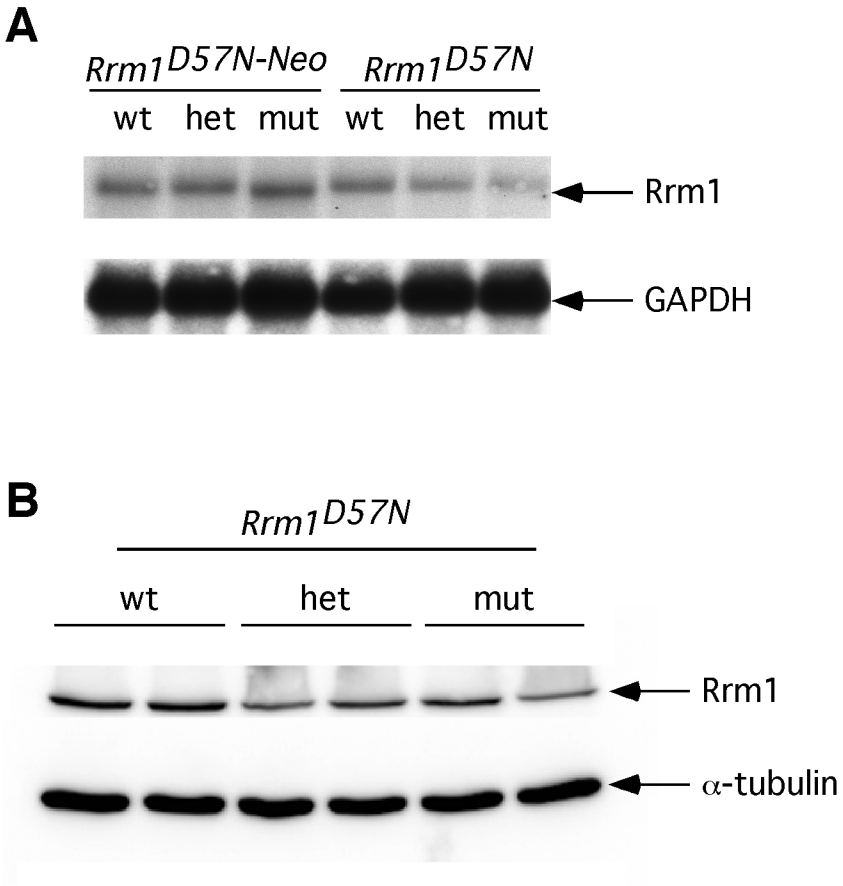
A
Rrm1D57N-Neo
Rrm1D57N
wt
het
mut
wt
het
mut
Rrm1
GAPDH
B
Rrm1D57N
wt
het
mut
Rrm1
α-tubulin

Table 4.2. Offspring obtained from *Rrm1*$^{+/D57N\text{-}Neo}$ and *Rrm1*$^{+/D57N}$ heterozygote intercrosses[a].

Genotype	# expected	# observed
Rrm1$^{+/+}$	38.5	59
Rrm1$^{+/Neo}$	77	95
Rrm1$^{Neo/Neo}$	38.5	0
total		154
	p<<0.01	

Genotype	# expected	# observed
Rrm1$^{+/+}$	35	44
Rrm1$^{+/D57N}$	70	96
Rrm1$^{D57N/D57N}$	35	0
total		140
	p<<0.01	

[a]Female mice heterozygous for *Rrm1*^{D57N} or *Rrm1*^{Neo} were crossed to males of the same genotype. Offspring were genotyped at weaning by PCR. The total numbers of mice of each genotype observed are listed to the right of the total number expected. [b]$p<0.01$, c^2.

A

	Rrm1$^{+/D57N}$ x *Rrm1*$^{+/D57N}$					
	Rrm1$^{+/+}$		*Rrm1*$^{+/D57N}$		*Rrm1*$^{D57N/D57N}$	
stage	# obs	(#exp)	# obs	(#exp)	# obs	(#exp)
8.5	5:3[b]	(4)	9: 1[b]	(8)	2: 1[b]	(4)
9.5	3	(2.5)	5: 2[b]	(5)	2	(2.5)
10.5	4	(3.25)	4: 3[b]	(6.5)	5: 5[b]	(3.25)
11.5	1	(2.5)	5: 3[b]	(5)	4: 4[b]	(2.5)
12.5	2:1[b]	(3.75)	13: 3[b]	(7.5)	0	(3.75)

[a]Rrm1$^{+/D57N}$ females were mated to males of the same genotype. At the indicated time points, embryos were dissected and analyzed for gross morphology. The observed number of embryos of each genotype is shown with the number of abnormal embryos (superscript b) indicated. Expected numbers of embryos are shown in parentheses.

B

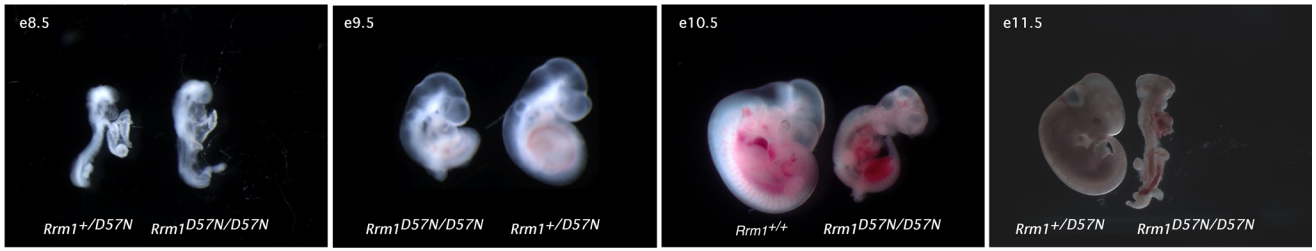

Figure 4.3 Lifespan of *Rrm1*$^{D57N/D57N}$ homozygous embryos. *A*. Embryos obtained from crosses between *Rrm1*$^{+/D57N}$ x *Rrm1*$^{+/D57N}$ mice. Timed mating experiments were initiated and embryos analyzed at the indicated timepoints. The total number of embryos of each genotype observed were listed with number of abnormal embryos indicated. Expected numbers of embryos are listed in parentheses. [b]abnormal embryo. *B*. Representative images of homozygous embryos with control littermates. Homozygous embryos appear grossly normal at e8.5, but are small as soon as e9.5. All homozygous embryos observed at e10.5 or later were dead.

Similar to the Rrm1-D57N transgenic mice, Rrm1+/Neo and Rrm1+/D57N heterozygous mice showed an increase in the incidence of lung tumors, but did not develop larger or more malignant tumors. We hypothesize that heterozygosity of *Rrm1*^{D57N} or overexpression of Rrm1-D57N moderately elevates dNTP pools, which facilitates lung tumorigenesis in strains predisposed to lung cancer. Elevated dNTPs would be expected to benefit proliferative cells, but not necessarily transform them.

The lethality caused by homozygosity of the *Rrm1*^{D57N} allele initially led us to hypothesize that hyperactive RNR in this model was elevating dNTP pools and disrupting mitochondrial DNA maintenance as in our previous studies (Chapters 2 and 3). However, inconsistent with this hypothesis was the observation that MEFs cultured from homozygous embryos showed dramatic proliferation defects (Figure 4.3). Previous work on MEFs with defects in oxidative phosphorylation often show wild type proliferation in standard media containing glucose, due to an ability to produce energy via glycolysis. Culturing these cells in media containing galactose as the only carbon source leads to inviability(30, 31) . Consistent with these reports, we previously showed that Rrm1-D57N(low)^{Tg} + p53R2^{Tg} bitransgenic MEFs showed mtDNA depletion but no proliferation defect in standard media (Chapter 3). These data suggest that lethality in *Rrm1*^{D57N} homozygotes is caused by an event that is independent from mitochondrial genome instability, as mtDNA depletion does not affect fibroblast proliferation in our models.

The second main finding contradictory to mitochondrial genome instability as the cause of the lethality was that p21 is upregulated in homozygous MEFs. p21 functions at multiple steps throughout the cell cycle,

the most relevant being inhibition of origin firing to initiate S-phase. When DNA damage is present, p21 inhibits the cyclin D2/Cdk2 complex to prevent replication origin firing in order to avoid replication of damaged DNA.

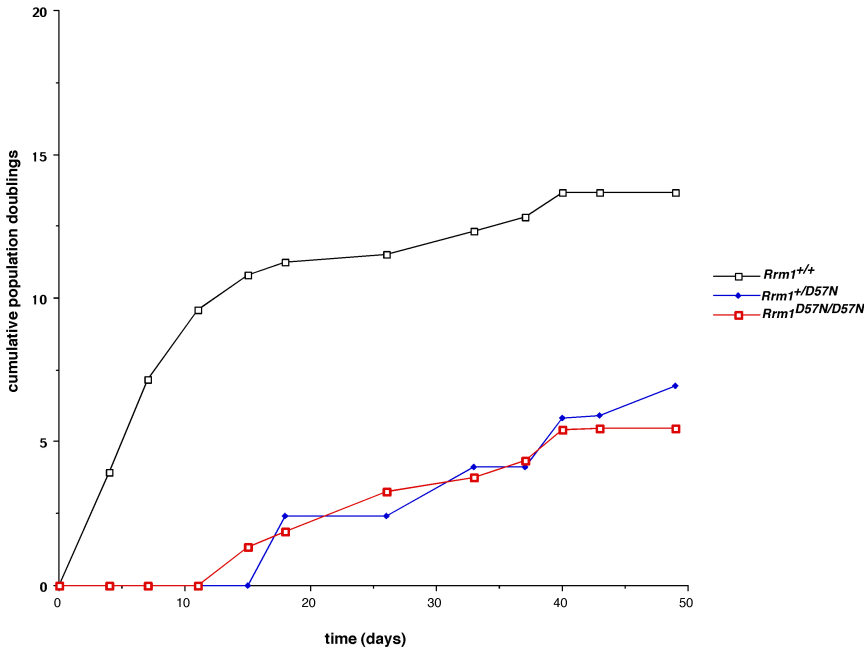

Figure 4.4. Proliferation of MEFs isolated from *Rrm1*$^{D57N/D57N}$ homozygous embryos. Fibroblasts were cultured from knock-in embryos at e10.5. Cells were seeded 10^6 per plate every 3 days, Data is represented as cumulative population doublings vs. time.

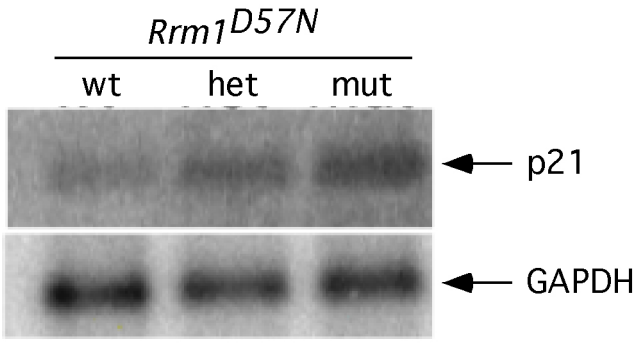

Figure 4.5. p21 expression is induced in *Rrm1*$^{D57N/D57N}$ homozygous MEFs. Total RNA was isolated from wild type, heterozygous, or homozygous MEFs and separated on a 0.8% agarose gel. Following immobilization on a nylon membrane, gene expression was detected by hybridization to specific radiolabeled probes. GAPDH serves as a loading control.

The model proposed by Chabes and Stillman is largely consistent with what we observed in the *Rrm1*^{D57N} knock-in mice. When yeast cells are induced to overexpress the *rnr1-D57N* mutant, they proliferate poorly due to a failure to fire replication origins. Similarly, when mouse embryonic fibroblasts are homozygous for the *Rrm1*^{D57N} mutant, they also proliferate poorly and show an upregulation of p21, which inhibits the G1- to S-phase transition. Chabes and Stillman suggest that in yeast, persistent elevated dNTP levels mimic a DNA damage-response state, in which dNTPs are rapidly elevated following DNA damage in order to allow for repair. In the absence of DNA damage, constitutively elevated dNTP levels may "trick" the cell into behaving as though DNA damage is present and that attempting replication would be hazardous, leading to inhibition of replication origin firing. We propose that a similar mechanism exists in mammalian cells, where in the absence of DNA damage but in the presence of elevated dNTPs, p21 may be signaled to inhibit the Cyclin D/Cdk2 complex to prevent S-phase entry(19).

While our preliminary results somewhat agree with the findings of Chabes and Stillman and seem to support their proposed model, the differences between the two systems cannot be overlooked. Notably, by overexpressing the *rnr1-D57N* mutant, they were able to simultaneously disrupt what are thought of as the two main regulatory mechanisms controlling RNR activity: limitation of protein levels of one of the two subunits (in this case the large subunit), and allosteric feedback control. Our bitransgenic mouse model would be expected to be more similar to their yeast model than our *Rrm1*^{D57N} knock-in mouse model. Most importantly, while it is clear that proper allosteric feedback regulation is necessary for survival of mice, only one

regulatory mechanism is disabled in the knock-in mouse model. Although proteins levels of the small subunits were not tested in *Rrm1*^{D57N} embryos or MEFs, it is expected that the small subunits are expressed normally, still limiting the availability of nucleotides outside S-phase.

To account for the observed cell proliferation defects, we might speculate that the low levels of p53R2 protein that are continuously present during quiescent phases are able to complex with *Rrm1*^{D57N} and generate enough dNTPs to block entry into S-phase. In this way, RNR is truly constitutively active through all cell cycle phases. Further work will be necessary to establish whether p53R2 interacts with *Rrm1*^{D57N} to elevate dNTP pools, and whether cells are blocked in G1 phase as a result.

Alternatively, the lethality may be caused by nuclear genome instability (GIN). The Rrm1-D57N mutation has been shown to be mutagenic (3, 16). More serious GIN might be observed in the form of chromosome breaks or loss, and can easily activate checkpoints and cause slow cell proliferation or apoptosis, both of which are fatal to a developing embryo. We could detect these by analyzing metaphases of heterozygous and homozygous MEFs. When metaphase chromosomes are spread out on slides and stained with Giemsa, breaks are readily apparent. Sections of homozygous embryos from e9.5 and e10.5 may show increased instability when stained for g-H2AX, confirming nuclear GIN.

References

1. Kumar D, Viberg J, Nilsson AK, Chabes A. Highly mutagenic and severely imbalanced dNTP pools can escape detection by the S-phase checkpoint. Nucleic Acids Res. 2010;38(12):3975-83. PMCID: 2896522.

2. Gotz A, Isohanni P, Pihko H, Paetau A, Herva R, Saarenpaa-Heikkila O, et al. Thymidine kinase 2 defects can cause multi-tissue mtDNA depletion syndrome. Brain. 2008;131(Pt 11):2841-50.

3. Chabes A, Georgieva B, Domkin V, Zhao X, Rothstein R, Thelander L. Survival of DNA damage in yeast directly depends on increased dNTP levels allowed by relaxed feedback inhibition of ribonucleotide reductase. Cell. 2003;112(3):391-401.

4. Weinberg G, Ullman B, Martin DW, Jr. Mutator phenotypes in mammalian cell mutants with distinct biochemical defects and abnormal deoxyribonucleoside triphosphate pools. Proc Natl Acad Sci U S A. 1981;78(4):2447-51. PMCID: 319363.

5. Oliver F, Collins M, Lopez-Rivas A. dNTP pools imbalance as a signal to initiate apoptosis. Cellular and Molecular Life Sciences. 1996;52(10):995-1000.

6. Kolberg M, Strand KR, Graff P, Andersson KK. Structure, function, and mechanism of ribonucleotide reductases. Biochim Biophys Acta. 2004;1699(1-2):1-34.

7. Chabes AL, Pfleger CM, Kirschner MW, Thelander L. Mouse ribonucleotide reductase R2 protein: a new target for anaphase-promoting complex-Cdh1-mediated proteolysis. Proc Natl Acad Sci U S A. 2003;100(7):3925-9. PMCID: 153024.

8. Hakansson P, Hofer A, Thelander L. Regulation of mammalian ribonucleotide reduction and dNTP pools after DNA damage and in resting cells. J Biol Chem. 2006;281(12):7834-41.

9. Tanaka H, Arakawa H, Yamaguchi T, Shiraishi K, Fukuda S, Matsui K, et al. A ribonucleotide reductase gene involved in a p53-dependent cell-cycle checkpoint for DNA damage. Nature. 2000;404(6773):42-9.

10. Xu X, Page JL, Surtees JA, Liu H, Lagedrost S, Lu Y, et al. Broad overexpression of ribonucleotide reductase genes in mice specifically induces lung neoplasms. Cancer Res. 2008;68(8):2652-60. PMCID: 2459241.

11. Elledge SJ, Zhou Z, Allen JB. Ribonucleotide reductase: regulation, regulation, regulation. Trends Biochem Sci. 1992;17(3):119-23.

12. Elledge SJ, Davis RW. Two genes differentially regulated in the cell cycle and by DNA-damaging agents encode alternative regulatory subunits of ribonucleotide reductase. Genes Dev. 1990;4(5):740-51.

13. Chabes A, Domkin V, Thelander L. Yeast Sml1, a protein inhibitor of ribonucleotide reductase. J Biol Chem. 1999;274(51):36679-83.

14. Lee YD, Elledge SJ. Control of ribonucleotide reductase localization through an anchoring mechanism involving Wtm1. Genes Dev. 2006;20(3):334-44. PMCID: 1361704.

15. Eriksson S, Gudas LJ, Clift SM, Caras IW, Ullman B, Martin DW, Jr. Evidence for genetically independent allosteric regulatory domains of the protein M1 subunit of mouse ribonucleotide reductase. J Biol Chem. 1981;256(19):10193-7.

16. Caras IW, Martin DW, Jr. Molecular cloning of the cDNA for a mutant mouse ribonucleotide reductase M1 that produces a dominant mutator phenotype in mammalian cells. Mol Cell Biol. 1988;8(7):2698-704. PMCID: 363480.

17. Reichard P, Eliasson R, Ingemarson R, Thelander L. Cross-talk between the allosteric effector-binding sites in mouse ribonucleotide reductase. J Biol Chem. 2000;275(42):33021-6.

18. Chabes A, Stillman B. Constitutively high dNTP concentration inhibits cell cycle progression and the DNA damage checkpoint in yeast Saccharomyces cerevisiae. Proc Natl Acad Sci U S A. 2007;104(4):1183-8. PMCID: 1783093.

19. Abbas T, Dutta A. p21 in cancer: intricate networks and multiple activities. Nat Rev Cancer. 2009;9(6):400-14. PMCID: 2722839.

20. Ekholm SV, Reed SI. Regulation of G(1) cyclin-dependent kinases in the mammalian cell cycle. Curr Opin Cell Biol. 2000;12(6):676-84.

21. Harper JW, Adami GR, Wei N, Keyomarsi K, Elledge SJ. The p21 Cdk-interacting protein Cip1 is a potent inhibitor of G1 cyclin-dependent kinases. Cell. 1993;75(4):805-16.

22. Jung YS, Qian Y, Chen X. Examination of the expanding pathways for the regulation of p21 expression and activity. Cell Signal. 2010;22(7):1003-12. PMCID: 2860671.

23. Lee EC, Yu D, Martinez de Velasco J, Tessarollo L, Swing DA, Court DL, et al. A highly efficient Escherichia coli-based chromosome engineering system adapted for recombinogenic targeting and subcloning of BAC DNA. Genomics. 2001;73(1):56-65.

24. Liu P, Jenkins NA, Copeland NG. A highly efficient recombineering-based method for generating conditional knockout mutations. Genome Res. 2003;13(3):476-84. PMCID: 430283.

25. Warming S, Costantino N, Court DL, Jenkins NA, Copeland NG. Simple and highly efficient BAC recombineering using galK selection. Nucleic Acids Res. 2005;33(4):e36. PMCID: 549575.

26. Deng C, Wynshaw-Boris A, Zhou F, Kuo A, Leder P. Fibroblast growth factor receptor 3 is a negative regulator of bone growth. Cell. 1996;84(6):911-21.

27. Tallquist M, Soriano P. Epiblast-restricted Cre expression in MORE mice: a tool to distinguish embryonic vs. extra-embryonic gene function. genesis. 2000;26(2):113-5.

28. Kumar D, Viberg J, Nilsson AK, Chabes A. Highly mutagenic and severely imbalanced dNTP pools can escape detection by the S-phase checkpoint. Nucleic Acids Res. 2010.

29. Levitt PS, Zhu M, Cassano A, Yazinski SA, Liu H, Darfler J, et al. Genome maintenance defects in cultured cells and mice following partial inactivation of the essential cell cycle checkpoint gene Hus1. Mol Cell Biol. 2007;27(6):2189-201. PMCID: 1820507.

30. Hayashi J, Ohta S, Kikuchi A, Takemitsu M, Goto Y, Nonaka I. Introduction of disease-related mitochondrial DNA deletions into HeLa cells lacking mitochondrial DNA results in mitochondrial dysfunction. Proc Natl Acad Sci U S A. 1991;88(23):10614-8. PMCID: 52980.

31. Hofhaus G, Johns DR, Hurko O, Attardi G, Chomyn A. Respiration and growth defects in transmitochondrial cell lines carrying the 11778 mutation associated with Leber's hereditary optic neuropathy. J Biol Chem. 1996;271(22):13155-61.

Chapter 5: Summary and Future Directions

5.1 Models for RNR regulation and consequences of deregulation

Our lab has developed several mouse models in which RNR is deregulated, in order to understand why the enzyme is so tightly controlled and the consequences of deregulating the enzyme.

5.1A Deregulation by small subunit overexpression

We first disabled the enzyme by overexpressing the small subunits. We hypothesized that this would have the effect of making the enzyme constitutively active, as normally the small subunit is limiting. Rrm2, one small subunit gene, is only expressed during S-phase in order to provide dNTPs for DNA synthesis, while p53R2, the other small subunit gene, is expressed constantly but at low levels. Therefore, increasing the amounts of either of these two genes would allow the cells to have functional RNR throughout the entire cell cycle, thus increasing the enzyme activity. When these genes were individually overexpressed in mice, they primarily caused lung tumor formation. We hypothesize that this is due to increased oxidative stress as the result of overproducing radical-generating proteins. Supporting this is the tissue specificity. The lungs are already a high-oxygen environment and the DNA is under constant attack of reactive oxygen species (ROS). We hypothesize that increasing the levels of a protein that produces a radical further increases ROS, and overwhelms DNA repair machinery that was already saturated, therefore becoming mutagenic and causing lung tumors. It

was found that a precipitating event in lung tumor formation was mutation of K-ras, and oncogene that is mutated in many cases of human lung cancer and causes lung cancer in mice when mutated.

While the mechanism of lung tumor induction is likely unlinked to RNR activity, we do have indications that RNR activity is elevated in the tissues of mice overexpressing either small subunit. In a later study (Chapter 2), we found in skeletal muscle, a tissue that overexpresses all of the RNR transgenes highly, that dNTP pools are elevated. Both *Rrm2*^{Tg} and *p53R2*^{Tg} were able to generate altered nucleotide pools. The nucleotide pools alterations may also play a role in the lung tumorigenesis, by enhancing the mutation rate or by providing additional dNTPs that cancer cells need in order to proliferate.

A third phenotype observed in *Rrm2*^{Tg} and *p53R2*^{Tg} mice was the development of proteinuria within the kidneys as the mice aged. This phenotype could have a number of possible causes. This phenotype was not observed in *Rrm1*^{Tg} mice, and like the lung cancer phenotype, may be linked to the small subunits' ability to generate a radical. The kidney contains many ROS-generating oxidases, and like the lungs, kidney DNA and cells are under constant attack by ROS(1). Increased damage in the kidney by ROS can lead to proteinuria, renal damage, and hypertension(1). Alternatively, the reason for the lack of the kidney phenotype in the *Rrm1*^{Tg} mice could be due to limited overexpression of this transgene in most tissues. Current data in our lab supports the ROS mechanism for inducing proteinuria, as in cultured cells

Rrm2 and p53R2 overexpression are known to elevate ROS. A model summarizing the findings is shown in Figure 5.1.

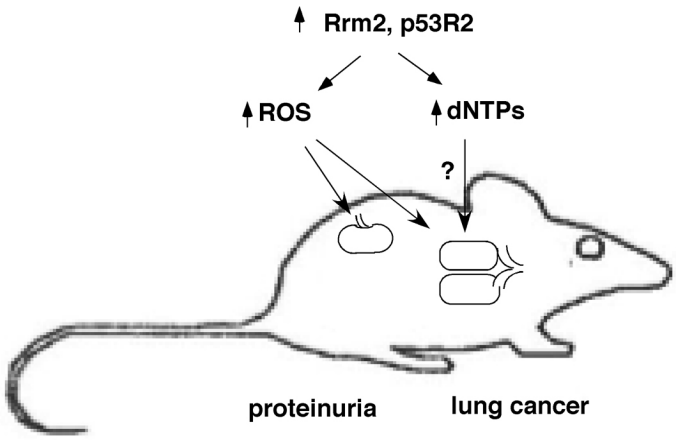

Figure 5.1. Possible mechanism explaining formation of phenotypes in *Rrm2Tg* and *p53R2Tg* mice. Overexpression of radical-producing subunits elevates ROS, which leads to lung cancer and kidney defects, especially proteinuria. Increased small subunit expression may also increase dNTP pools, facilitating lung tumorigenesis.

5.1B Overexpression of multiple wild type RNR subunits

Since these mouse models deregulated RNR by only a single mechanism, further deregulation of RNR was sought. In order to do this, we crossed mice overexpressing Rrm1 with mice overexpressing either Rrm2 or p53R2. We found that simultaneous overexpression of *Rrm1*^{Tg} and *Rrm2*^{Tg} or *p53R2*^{Tg} led to severely unbalanced nucleotide pools in the skeletal muscle. Simultaneous overexpression of *Rrm1*^{Tg} with *Rrm2*^{Tg} showed a synergistic increase in dNTP pools over that of *Rrm1*^{Tg} or *Rrm2*^{Tg} alone, suggesting that the two overexpressed subunits were combining to form more active complex than is formed when either is expressed alone, and this was elevating RNR activity. The same synergistic effect was seen in the muscle of mice overexpressing *Rrm1*^{Tg} and *p53R2*^{Tg} (Chapter 2). Of the tissues overexpressing these transgenes, the muscle shows the highest level of expression. In skeletal muscle, but not in other muscle, we found that the mitochondrial DNA was depleted, and that this progressed with age. We hypothesize that the tissue specificity is due to the very high levels of overexpression of each subunit. That RNR deregulation causes mtDNA depletion was not entirely unexpected, however, all previous models of RNR deregulation and mtDNA depletion focused on non-functional RNR. In many mouse models and in human cases, dysfunction of RNR genes, most notably *p53R2*, resulted in mtDNA depletion(2-4). In yeast, overexpression of RNR

genes results in increases in mtDNA(5); therefore we hypothesized that overexpression of RNR would result in mtDNA expansion. However, these models from which we based our predictions did not show unbalanced nucleotide pools; instead, nucleotide pools were uniformly increased while remaining balanced. In our models, nucleotide pools were significantly unbalanced. It is well known that unbalanced nucleotide pools cause mtDNA depletion(6-8), providing a clear mechanism by which RNR overexpression in mice causes mtDNA depletion.

In these bitransgenic mice, we also observed lung cancer phenotypes similar to those observed in mice overexpressing *Rrm2*^{Tg} or *p53R2*^{Tg} alone. This further supports a role for ROS in lung tumorigenesis, as overexpressing *Rrm1*^{Tg} on top of either small subunit should no further increase ROS, while it would be expected to elevate RNR activity, as we observed in the skeletal muscle. Therefore, increased RNR activity plays only a limited role in lung tumor formation. Similarly, we also found proteinuria in the bitransgenics at the same rate as in the small subunit overexpressors, also supporting a role for increased ROS but not increased activity, for the same reasons outlined above. A model summarizing the possible mechanisms giving rise to these phenotypes is shown in Figure 5.2.

5.1C Deregulation of RNR by loss of allosteric feedback control

We also wanted to understand the effect of deregulating RNR by an independent mechanism. Both models described previously feature loss of the

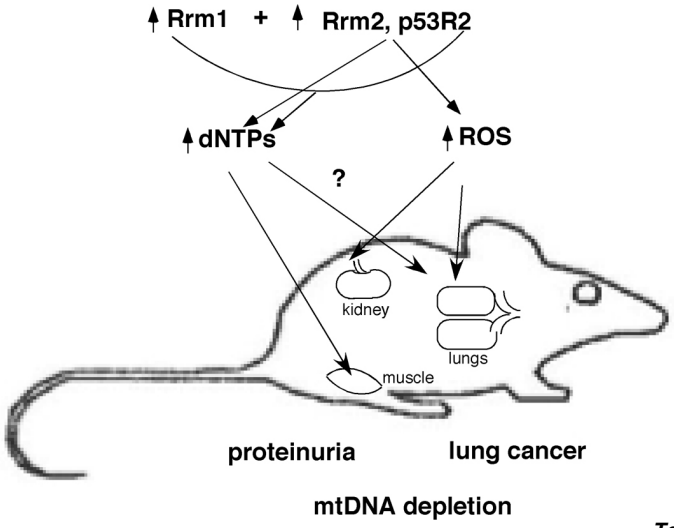

Figure 5.2. Model for development of phenotypes in *Rrm1*^{Tg} + *Rrm2*^{Tg} and *Rrm1*^{Tg} + *p53R2*^{Tg} bitransgenic mice. As before, small subunit overexpression generates ROS, which causes lung cancer and proteinuria. Interaction of Rrm1 and either small subunit increases RNR activity, elevating and unbalancing dNTP pools and causing mtDNA depletion in the muscle.

same regulatory mechanism, which is limitation of small subunit availability. The second main regulatory mechanism in mammals of allosteric feedback control. To disable this, we generated transgenic mice that broadly overexpress the Rrm1-D57N point mutation in most tissues. Of two independent transgenic lines obtained, both were grossly normal throughout adulthood. Both lines displayed a moderate increase in lung tumor incidence compared to control mice, but did not display other features of a tumorigenic phenotype. While dNTP pools were not measured in the lungs of D57N transgenic mice, we hypothesize that deregulation of this regulatory mechanism moderately elevates dNTP pools which, in strains predisposed to lung cancer, facilitates tumorigenesis by allowing for increased cell proliferation. The fact that Rrm1-D57N mice do not show other characteristics consistent with a tumorigenic phenotype, such as increased malignancy, size or decreased latency, also lends support to the ROS model for small subunit overexpression-induced carcinogenesis. We also failed to observe proteinuria in the kidneys of adult D57N transgenic mice despite significant overexpression of the transgene within this tissue, also suggesting increased ROS as the mechanism for proteinuria.

5.1D Simultaneous disruption of multiple RNR regulatory modes

Because each model featuring loss of one regulatory mechanism showed somewhat limited phenotypes with regards to RNR activity, we sought

to simultaneously disable both regulatory mechanisms. In yeast, similar RNR perturbations had the effect of causing cell proliferation defects and sick cells(9). We therefore crossed mice from each *Rrm1-D57N* transgenic line to mice overexpressing either small subunit. We found that all four possible combinations caused synthetic lethality. The crosses that utilized *Rrm1-D57N(high)*^{Tg} showed embryonic lethality while the crosses with *Rrm1-D57N(low)*^{Tg} allowed mice to survive gestation.

When *Rrm1-D57N(high)*^{Tg} was combined with either small subunit, bitransgenic embryos showed embryonic lethality beginning as early as e11.5-e12.5. While overall numbers are small, bitransgenic embryos from both showed vascular defects, in the form of aortal hemorrhages and yolk sac vascular defects. These particular phenotypes were unexpected, as RNR perturbation has not previously been linked to vascular defects. However, the signaling networks governing development of the vasculature utilize cAMP, potentially linking nucleotide metabolism with vasculature defects. In *Rrm1-D57N(high)*^{Tg} + *Rrm2*^{Tg} bitransgenic embryos, neural defects were also observed, which may be secondary to the yolk sac defects. Potentially, failure to remove toxic metabolites from the amnion may perturb neural development, leading to the head and spine defects we observed.

The *Rrm1-D57N(low)*^{Tg} x *Rrm2*^{Tg} cross yielded a small number of bitransgenic mice that were able to survive to adulthood. In these mice, we found characteristics of premature aging. These mice phenocopied Polγ

mutator mice, leading us to hypothesize that the synthetic lethality was mediated through mtDNA instability. Given that we previously observed mtDNA depletion in *Rrm1*^{Tg} + *Rrm2*^{Tg} and *Rrm1*^{Tg} + *p53R2*^{Tg} bitransgenic mice, we naturally assessed mitochondrial genome stability in these mice. We were surprised to find that only mice that survive 3 months displayed any mtDNA instability. Some mtDNA depletion was observed in bitransgenic mice at P19 and 25, but this is 1) possibly an artifact due to the skeletal muscle degeneration, and 2) not the cause of the lethality as most bitransgenics died before this time.

We were then left to find a new hypothesis to explain the synthetic lethality in these bitransgenic mice. Histological analysis of neonates turned up new phenotypes that were previously not seen in *Rrm1*^{Tg} + *Rrm2*^{Tg} bitransgenic mice. These phenotypes include kidney degeneration, hepatocellular swelling in the liver, glaucoma, and pleural effusion. The common thread connecting these phenotypes may be hypertension, which also has links to nucleotide metabolism. We therefore hypothesize that simultaneous overexpression of *Rrm1-D57N(low)*^{Tg} and *Rrm2*^{Tg} leads to significantly elevated RNR activity. Preliminary data suggests that dNTP pools are severely perturbed in tissues from these mice, supporting our hypothesis. Increased dNTPs are subject to degradation in order to keep pools balanced(10), and the degradation products are deposited in the bloodstream. Degradation products such as uric acid have been shown to cause

hypertension in rats(11). Hypertension causes pleural effusion, which could ultimately be fatal to mice. Unfortunately, it is impossible to directly test bitransgenic neonates for hypertension, so we must take indirect approaches and look for changes upstream of hypertension, such as uric acid levels, and changes downstream, such as pleural effusion and glaucoma.

There are some caveats to this model. Firstly, it does not explain the kidney degeneration or the hepatocellular swelling in the bitransgenic mice. A second, related hypothesis can be made from this, in which kidney degeneration(12), possibly mediated through increased uric acid, causes hypertension, which leads to pleural effusion and death. The first model is favored because through analysis of the neonates, it was found that pleural effusion precedes kidney degeneration. We found pleural effusion in neonates as young as P4, while no kidney phenotypes were found until P9, when most bitransgenics are already dead. However, this does not necessarily indicate that this model is false. Kidneys and hypertension are linked through defective protein uptake in the kidney during development, which can cause hypertension but may not cause visible morphological changes. The finding of proteinuria in the kidneys of aged *Rrm2*^{Tg} mice also potentially supports decreased protein uptake by kidneys overexpressing *Rrm2*^{Tg}, and further deregulation of RNR may enhance this phenotype. Kidney degeneration may not be mediated through increased uric acid. As stated before, kidneys are susceptible to defects in mtDNA maintenance, and may therefore be affected

in bitransgenic mice. We found mild age-related mtDNA depletion in the kidneys of bitransgenic mice, indicating a possible interaction.

A second issue with the preferred hypothesis is that preliminary studies in serum uric acid levels in bitransgenic neonates failed to reveal increases. This does not necessarily indicate that increased nucleotide degradation is not occuring, or that uric acid levels are not increased enough to cause hypertension. It is still possible that hypertension mechanisms are highly sensitive to uric acid increases, while our assay is not; therefore we may not be able to detect potentially pathological changes. Most likely, the mechanism causing lethality in *Rrm1-D57N*^{Tg} + *Rrm2*^{Tg} bitransgenic mice is due to a combination of factors, possibly the ones listed above. Further work is needed to dissect out the causes and the phenotypes and determine what is pathologically relevant. A model summarizing the potential contributions of each of these pathways is shown in Figure 5.3.

5.1E *Rrm1*^{D57N} knock-in mice

In order to observe the effects of the *Rrm1*^{D57N} mutation without possible artifacts of overexpression, we generated mice with the *Rrm1*^{D57N} mutation targeted to the germline. We obtained 2 independent strains of mice that were phenotypically identical. Heterozygous mice were viable and expressed the mutant protein at close to normal levels. They were grossly normal, having a moderate increase in lung tumor incidence relative to wild type. Similar to the Rrm1-D57N^{Tg} mice, the tumor malignancy, size, or

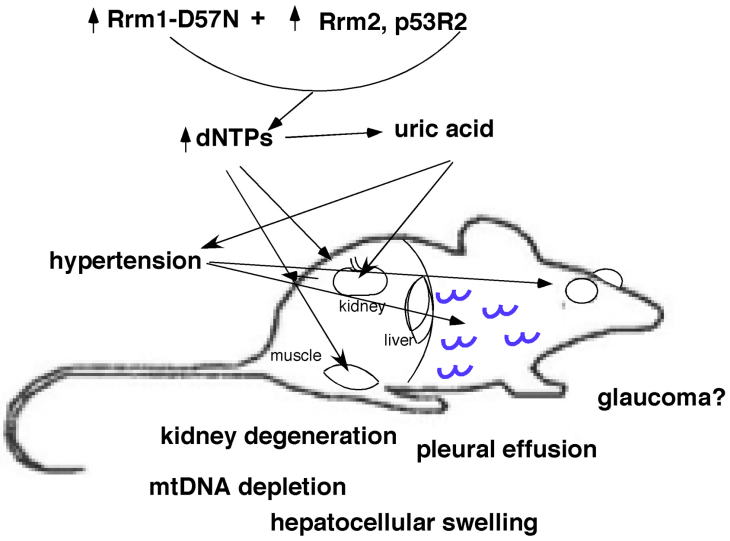

Figure 5.3. Development of phenotypes in *Rrm1-D57N(low)^{Tg}* + *Rrm2^{Tg}* bitransgenic mice. Deregulation of RNR results in elevated or unbalanced dNTP pools, which are degraded to uric acid or negatively affect mtDNA stability. Uric acid causes hypertension, which leads to pleural effusion and glaucoma (protruding eyes). Conversely, kidney dysfunction leads to hypertension and so on.

latency was unaltered, suggesting that the *Rrm1*^{D57N} mutation does not drive lung tumorigenesis. Instead, we hypothesize that moderately elevated dNTP pools facilitate lung tumor formation by transformed cells.

Homozygosity of *Rrm1*^{D57N} resulted in embryonic lethality. The embryos became small around e9.5, and were mostly dead by e10.5. This was surprising, as only one regulatory mechanism of RNR was perturbed. We were also surprised to find that homozygous and heterozygous MEFs showed proliferation defects. We must be cautious in interpreting that data, as the experiment was only conducted once. However, this finding did not fit with our previous results from bitransgenic MEFs, which all proliferated normally. Even the *Rrm1-D57N(high)*^{Tg} + *p53R2*^{Tg} bitransgenic MEFs, which were isolated at the same time point as *Rrm1*^{D57N} knock-in MEFs, showed no defects in cell proliferation. Therefore this lethality is mediated by a distinct mechanism than that which causes the synthetic lethality. Again, in yeast a slow growth phenotype was induced by overexpressing the *rnr1-D57N* mutant(9), in a model that shares some similarities with ours. We therefore looked for evidence of cell cycle delays in the homozygous MEFs, and found that p21 was upregulated. This could possibly function to prevent entry into S-phase, as was found in the yeast system.

This is very different from the *Rrm1-D57N*^{Tg} and synthetic lethal phenotypes. *The Rrm1-D57N*^{Tg} mice were viable and showed normal cell proliferation. While the bitransgenic mice are not viable, cells isolated from

bitransgenic embryos showed normal proliferation. We therefore conclude that the defects causing lethality in *Rrm1*^{D57N} homozygous mice are more severe than the synthetic lethal defects. We hypothesize that elevated dNTP pools in the homozygous cells are mimicking a state of DNA damage, in which dNTPs are elevated, and this prevents entry into S-phase, similar to as was seen in yeast. Further experiments, outlined below, are necessary to further characterize this lethality.

Overall, we believe our RNR mouse models provide useful tools by which to understand the regulation of dNTP pools and the effects of dNTP perturbation. A final model relating RNR manipulation, dNTP pool alterations, and phenotypes is shown in Figure 5.4.

5.2 Future Directions

5.2A. Identify and characterize a dNTP threshold effect.

Evidence from our various studies suggests that different phenotypes will be observed in the presence of altered dNTPs, depending on the severity of the dNTP alteration. In *Rrm1*^{Tg} + *Rrm2*^{Tg} and *Rrm1*^{Tg} + *p53R2*^{Tg} bitransgenic mice, we found unbalanced nucleotide pools that led to age-dependent mtDNA depletion. Preliminary work in *Rrm1-D57N(low)*^{Tg} + *Rrm2*^{Tg} bitransgenic neonates has suggested more dramatic dNTP pool alterations which may cause the observed synthetic lethality. We hypothesize that more moderate dNTP pool increases allowed for increased tumor formation in

Figure 5.4. Relationship between RNR manipulation, dNTP pool alterations, and phenotype. dNTP pool effects include both elevated pools, represented by height of the total bar, and pool imbalances, represented by the pie chart at the top of the bar. Blue, dATP; red, dGTP; green, dTTP; purple, dCTP. Overexpression of *Rrm2*^{Tg} or *p53R2*^{Tg} generates elevated and unbalanced dNTP pools, while simultaneous overexpression of both *Rrm1*^{Tg} and either small subunit generates further unbalanced pools and a greater increase in totoal dNTPs. Overexpression of Rrm1-D57N is hypothesized to result in moderately increased dNTP pools due to loss of a single RNR regulatory mechanism, and pools are balanced due to continued function of the specificity site. Overexpression of Rrm1-D57N and either small RNR subunit is hypothesized to generate significantly elevated nucleotide pools, which are also unbalanced. An *Rrm1*^{D57N} knock-in homozygote is expected to display increased but balanced dNTP pool alterations, leading to the observed cell proliferation defects. Phenotypes observed in mice of the indicated RNR manipulations are listed.

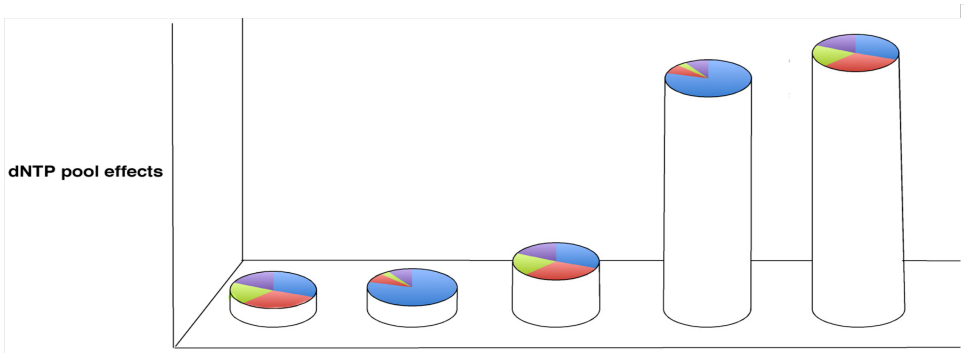
dNTP pool effects
RNR manipulation
Small subunit normal unlimited normal unlimited normal
Activity site normal normal mutant^Tg mutant mutant^KI
Phenotypes
Wild type limited limited Synthetic lethal Embryonic lethality
dATP
dGTP
dTTP
dCTP

Rrm1-D57N transgenic and knock-in heterozygous mice. Overexpression of Rrm1-D57N^{Tg} or heterozygosity of *Rrm1*^{D57N} elevated lung tumorigenesis to statistically significant levels. This observation assumes that dNTPs are elevated in the lungs of these mice, however we have not measured nucleotide pools. These observations together allow us to hypothesize that a dNTP threshold exists and that our various mouse models represent different dNTP levels across the continuum. This would suggest that dNTP measurements in the lungs of Rrm1-D57N^{Tg} and *Rrm1*$^{+/D57N}$ or *Rrm1*$^{+/Neo}$ mice would reveal moderate changes to dNTP pools; dNTP measurements in the skeletal muscle of Rrm1-D57N(low)^{Tg} + *Rrm2*^{Tg} bitransgenic neonates would reveal more dramatic dNTP pool alterations; in Rrm1-D57N(high)^{Tg} + *p53R2*^{Tg} embryos, the dNTP pool changes would be more dramatic still; and dNTP pools in *Rrm1*$^{D57N/D57N}$ or *Rrm1*$^{Neo/Neo}$ embryos would be most perturbed. In other words, dNTP pool changes would correlate closely with the phenotypes observed in the mice. In order to support this model, we would measure dNTP pools in the lungs of Rrm1-D57NTg and Rrm1+/D57N mice; in the skeletal muscle of Rrm1-D57N(low)^{Tg} + *Rrm2*^{Tg} bitransgenic neonates and Rrm1-D57N(high)^{Tg} + ***p53R2Tg*** bitransgenic embryos; and in *Rrm1*$^{D57N/D57N}$ and *Rrm1*$^{Neo/Neo}$ embryos.

5.2B. Does expression of Rrm1-D57N^{Tg} or *Rrm1$^{+/D57N}$* facilitate tumorigenesis in cancer-prone models?

Both mouse models of Rrm1-D57N revealed an increased incidence of lung tumorigenesis compared to wild type littermates. Based on our work investigating the ***Rrm2Tg*** and ***p53R2Tg*** lung tumor models(13), we expected that an increase in lung tumor incidence would be accompanied by an increase in tumor severity and a decrease in latency, but this was not the case for either model. We were surprised to find that only lung tumor incidence was increased, and this change was statistically significant in both models. We hypothesized that the D57N mutation acts to make RNR hyperactive, which elevates dNTP pools. Elevated dNTP pools are beneficial to dividing cells, so that they then facilitate tumor formation in cells that already contain the mutations necessary for transformation. Lungs are for the most part a quiescent tissue and cells are not constantly dividing. Therefore, additional replication help in the form of elevated dNTPs may be the final circumstance required to turn a mutant cell into a tumor cell. We can test this model by crossing mice overexpressing Rrm1-D57N^{Tg} or mice that are heterozygous for *Rrm1^{D57N}* or *Rrm1^{Neo}* to mice that harbor known tumorigenic mutations. This was already done with mice null for the mismatch repair factor Msh6. The Rrm1-D57N^{Tg} Msh6$^{-/-}$ mice had a mean lifespan that was nearly 100 days shorter than control Msh6$^{-/-}$ mice; however this was not statistically significant by log-rank test. When Msh6$^{+/-}$ mice were considered, the addition of Rrm1-

D57N^{Tg} again decreased the average lifespan. One factor in this lack of significance can be relatively small sample size. Perhaps addition of a greater number of mice to the analysis would provide a more definite understanding of the relationship between overexpression of Rrm1-D57N^{Tg} and loss of Msh6. Additionally, Rrm1-D57N could be overexpressed in the presence of mutated *K-ras* to further promote lung tumors, MMTV-Neu to promote mammary tumors, or in the *Mcm4^{Chaos3}* breast cancer model. Rrm1-D57N overexpression or heterozygosity of *Rrm1^{D57N}* may also be able to promote skin cancers in the two-step DMBA/TPA carcinogenesis model.

5.2C Characterize cell cycle defects in *Rrm1$^{D57N/D57N}$* MEFs

Preliminary work on homozygous *Rrm1$^{Neo/Neo}$* and *Rrm1$^{D57N/D57N}$* MEFs has suggested a defect in cell proliferation. Homozygous MEFs had poor population doublings and senesced prematurely. We were also able to detect upregulation of p21 in homozygous MEFs, suggesting a cell cycle delay. Chabes *et al*. showed that yeast that overexpressed *rnr1-D57N* were inhibited in entering into S-phase by the excessively high dNTP concentrations(9). These data together suggest that *Rrm1$^{D57N/D57N}$* and *Rrm1$^{Neo/Neo}$* MEFs also have defects in initiating S-phase. In order to assess whether *Rrm1$^{D57N/D57N}$* MEFs are stuck in G1 phase, we propose to perform flow cytometry to characterize the cell cycle profiles of homozygous MEFs and controls. We

predict that homozygous mutant cells will display a G1 delay and a reduced proportion of cells in S- or G2 phases.

5.2D Genotoxin resistance in *Rrm1*$^{+/D57N}$ mice

Chabes *et al*. reported that yeast cells harboring the *rnr1-D57N* mutation were more resistant to genotoxic stress than wild type yeast(14). Mutant yeast showed increased survival compared to wild type cells in the presence of 4-NQO, a UV mimetic. In this instance, *rnr1-D57N* mutant yeast were able to elevate dNTP levels to roughly 3-fold greater than wild type, allowing for DNA repair to occur more efficiently. Elevated dNTP pools can also promote lesion bypass(15) and suppress potentially deleterious repair methods such as sister chromatid exchange(16). We hypothesize that mice which harbor the *Rrm1*^{D57N} or *Rrm1*^{Neo} alleles would similarly be able to elevate dNTP pools and survive following genotoxic stress longer than wild type control mice. Experiments such as these are typically performed initially using cell culture models in order to assess such effects without distress to animals. However, in our system both homozygous and heterozygous cells proliferated poorly even in the absence of stress; it is therefore necessary to use surviving heterozygous mice, which are grossly normal. The poor cell proliferation could be an artifact of culturing conditions. Perhaps after the experiment is repeated under ideal conditions we may see normal proliferation in the heterozygotes which would justify the use of cells. We would assess the

survival of *Rrm1*$^{+/D57N}$ mice following treatment with several known genotoxins, in order to assess the ability to resist different types of DNA damage. Proposed treatments include ionizing radiation, which induces DNA double-strand breaks; mitomycin C (MMC), which affixes bulky adducts to DNA blocking accurate replication and transcription; and 4-NQO, the aforementioned UV mimetic. We predict that heterozygous mice will show a greater resistance to DNA-damaging agents than wild type mice.

In summary, perturbation of RNR activity and expression in mammals can have disastrous consequences. Much of our understanding of RNR regulation and the consequences of disrupting that regulation come from yeast. While yeast is a good cellular model for basic effects of RNR deregulation, it cannot provide the whole story. The effects of deregulating RNR in mammals are of particular interest to us as humans, for understanding our own biology of how dNTPs are produced and maintained, and providing insights into mechanisms of mutagenesis and cancer. We have established multiple models of RNR deregulation in mice, and using these models we have discovered the consequences of RNR deregulation in mammals. These and future experiments will allow us to better understand the importance of RNR regulation in mammals.

REFERENCES

1. Wilcox C. Reactive oxygen species: roles in blood pressure and kidney function. Current hypertension reports. 2002;4(2):160-6.

2. Bourdon A, Minai L, Serre V, Jais JP, Sarzi E, Aubert S, et al. Mutation of RRM2B, encoding p53-controlled ribonucleotide reductase (p53R2), causes severe mitochondrial DNA depletion. Nat Genet. 2007;39(6):776-80.

3. Kimura T, Takeda S, Sagiya Y, Gotoh M, Nakamura Y, Arakawa H. Impaired function of p53R2 in Rrm2b-null mice causes severe renal failure through attenuation of dNTP pools. Nat Genet. 2003;34(4):440-5.

4. Tyynismaa H, Ylikallio E, Patel M, Molnar MJ, Haller RG, Suomalainen A. A heterozygous truncating mutation in RRM2B causes autosomal-dominant progressive external ophthalmoplegia with multiple mtDNA deletions. Am J Hum Genet. 2009;85(2):290-5. PMCID: 2725268.

5. Lebedeva MA, Shadel GS. Cell cycle- and ribonucleotide reductase-driven changes in mtDNA copy number influence mtDNA Inheritance without compromising mitochondrial gene expression. Cell Cycle. 2007;6(16):2048-57. PMCID: 2606055.

6. Bulst S, Abicht A, Holinski-Feder E, Muller-Ziermann S, Koehler U, Thirion C, et al. In vitro supplementation with dAMP/dGMP leads to partial restoration of mtDNA levels in mitochondrial depletion syndromes. Hum Mol Genet. 2009;18(9):1590-9.

7. Lopez LC, Akman HO, Garcia-Cazorla A, Dorado B, Marti R, Nishino I, et al. Unbalanced deoxynucleotide pools cause mitochondrial DNA instability in thymidine phosphorylase-deficient mice. Hum Mol Genet. 2009;18(4):714-22. PMCID: 2638828.

8. Saada A. Deoxyribonucleotides and disorders of mitochondrial DNA integrity. DNA Cell Biol. 2004;23(12):797-806.

9. Chabes A, Stillman B. Constitutively high dNTP concentration inhibits cell cycle progression and the DNA damage checkpoint in yeast

Saccharomyces cerevisiae. Proc Natl Acad Sci U S A. 2007;104(4):1183-8. PMCID: 1783093.

10. Rampazzo C, Miazzi C, Franzolin E, Pontarin G, Ferraro P, Frangini M, et al. Regulation by degradation, a cellular defense against deoxyribonucleotide pool imbalances. Mutat Res. 2010.

11. Mazzali M, Hughes J, Kim YG, Jefferson JA, Kang DH, Gordon KL, et al. Elevated uric acid increases blood pressure in the rat by a novel crystal-independent mechanism. Hypertension. 2001;38(5):1101-6.

12. Feig DI, Nakagawa T, Karumanchi SA, Oliver WJ, Kang DH, Finch J, et al. Hypothesis: Uric acid, nephron number, and the pathogenesis of essential hypertension. Kidney Int. 2004;66(1):281-7.

13. Xu X, Page JL, Surtees JA, Liu H, Lagedrost S, Lu Y, et al. Broad overexpression of ribonucleotide reductase genes in mice specifically induces lung neoplasms. Cancer Res. 2008;68(8):2652-60. PMCID: 2459241.

14. Chabes A, Georgieva B, Domkin V, Zhao X, Rothstein R, Thelander L. Survival of DNA damage in yeast directly depends on increased dNTP levels allowed by relaxed feedback inhibition of ribonucleotide reductase. Cell. 2003;112(3):391-401.

15. Sabouri N, Viberg J, Goyal DK, Johansson E, Chabes A. Evidence for lesion bypass by yeast replicative DNA polymerases during DNA damage. Nucleic Acids Res. 2008;36(17):5660-7. PMCID: 2553575.

16. Fasullo M, Tsaponina O, Sun M, Chabes A. Elevated dNTP levels suppress hyper-recombination in Saccharomyces cerevisiae S-phase checkpoint mutants. Nucleic Acids Res. 2010;38(4):1195-203. PMCID: 2831302.

APPENDIX

Broad overexpression of ribonucleotide reductase genes in mice specifically induces lung neoplasms.

Xu X., J.L.Page, J.A. Surtees, H. Liu, S. Lagesdrost, Y. Lu, R. Bronson, E. Alani, A.Y. Nikitin, and R.S. Weiss. Cancer Research 2008 Apr 15;68(8) 2652-60.

DOI:10.1158/0008-5472.CAN-07-5873

Cancer Research

Broad Overexpression of Ribonucleotide Reductase Genes in Mice Specifically Induces Lung Neoplasms

Xia Xu, Jennifer L. Page, Jennifer A. Surtees, et al.

Cancer Res 2008;68:2652-2660. Published online April 15, 2008.

DOI:10.1158/0008-5472.CAN-07-5873

Research Article

Broad Overexpression of Ribonucleotide Reductase Genes in Mice Specifically Induces Lung Neoplasms

Xia Xu,[1] Jennifer L. Page,[1] Jennifer A. Surtees,[2] Houchun Liu,[1] Sarah Lagedrost,[1] Young Lu,[1] Roderick Bronson,[3] Eric Alani,[2] Alexander Yu. Nikitin,[1] and Robert S. Weiss[1]

Departments of [1]Biomedical Sciences and [2]Molecular Biology and Genetics, Cornell University, Ithaca, New York and [3]Rodent Histopathology Core, Harvard Medical School, Boston, Massachusetts

Abstract

Ribonucleotide reductase (RNR) catalyzes the rate-limiting step in nucleotide biosynthesis and plays a central role in genome maintenance. Although a number of regulatory mechanisms govern RNR activity, the physiologic effect of RNR deregulation had not previously been examined in an animal model. We show here that overexpression of the small RNR subunit potently and selectively induces lung neoplasms in transgenic mice and is mutagenic in cultured cells. Combining RNR deregulation with defects in DNA mismatch repair, the cellular mutation correction system, synergistically increased RNR-induced mutagenesis and carcinogenesis. Moreover, the proto-oncogene *K-ras* was identified as a frequent mutational target in RNR-induced lung neoplasms. Together, these results show that RNR deregulation promotes lung carcinogenesis through a mutagenic mechanism and establish a new oncogenic activity for a key regulator of nucleotide metabolism. Importantly, RNR-induced lung neoplasms histopathologically resemble human papillary adenocarcinomas and arise stochastically via a mutagenic mechanism, making RNR transgenic mice a valuable model for lung cancer. [Cancer Res 2008;68(8):2652–60]

Introduction

An adequate and balanced supply of deoxyribonucleotide triphosphates (dNTP) is essential for accurate DNA replication and repair. The rate limiting step in *de novo* dNTP biosynthesis is catalyzed by the enzyme ribonucleotide reductase (RNR). RNR reduces ribonucleoside diphosphate (NDP) to deoxyribonucleoside diphosphate, phosphorylation of which yields dNTP. RNR is composed of two nonidentical homodimeric subunits (1). The large R1 subunit harbors the catalytic site and is encoded by the *Rrm1* gene in mammals. The small R2 subunit contains an oxygen-bridged dinuclear iron center that generates a tyrosyl-free radical that is transferred to the R1 subunit for enzyme activity. Mammalian genomes contain two independent genes, *Rrm2* and *Rrm2b* (*p53R2*), that encode closely related R2 proteins. A complex of Rrm2 and Rrm1 accounts for most RNR activity during S phase. *p53R2* was originally identified as a target gene for the p53 tumor suppressor protein and is transcriptionally induced after DNA damage (2, 3). In addition to its role in stress responses, p53R2 is expressed at low levels throughout the cell cycle and complexes with Rrm1 to produce dNTPs for mitochondrial DNA replication (4).

Because intracellular nucleotide concentrations have a major effect on DNA replication fidelity (5), RNR enzyme activity is tightly controlled by several regulatory mechanisms. During an unperturbed cell cycle, the transcription of *Rrm1* and *Rrm2* is undetectable in G_0-G_1 phase and reaches maximal levels in S-phase cells (6–8). However, owing to its long half-life, Rrm1 protein levels are nearly constant throughout the cell cycle and in excess relative to the R2 subunit. RNR enzyme activity is therefore determined in part by R2 protein levels. Rrm2 protein is absent during G_0-G_1 phase, peaks in S phase, and then falls in mitosis after ubiquitination by the anaphase promoting complex (8–10). Consistent with a need for nucleotides during DNA repair, DNA damage and replication stress induce RNR expression in both yeast and mammalian cells in a manner dependent on DNA damage checkpoint pathways (11, 12). Whereas mammalian Rrm1 and Rrm2 proteins are cytoplasmic (13), p53R2 localizes to the nucleus in genotoxin-treated cells (2, 3), which may facilitate the localized production of nucleotides at DNA damage sites.

RNR enzyme activity is also controlled by two allosteric sites in the R1 subunit. A specificity site regulates the relative cellular concentration of each of the four dNTPs by influencing substrate choice, whereas an activity site regulates the total dNTP pool size by monitoring the ATP/dATP ratio. Analysis of the mutant Rrm1-D57N, which is insensitive to feedback inhibition by dATP due to a mutation in the activity site, indicates that loss of RNR allosteric control results in a mutator phenotype in both yeast and mammalian cells (14–16).

Although RNR is a major determinant of genomic integrity, the consequences of RNR deregulation in animals are unknown. We generated transgenic mice that overexpress *Rrm1, Rrm2,* or *p53R2* and found that overexpression of either small RNR subunit induced spontaneous lung neoplasms and was mutagenic in cultured cells. Defects in DNA mismatch repair (MMR) synergistically increased RNR-induced mutagenesis and carcinogenesis, and activating mutations in the proto-oncogene *K-ras* were identified in lung neoplasms from *Rrm2* and *p53R2* transgenic mice. These results identify mutagenic and carcinogenic effects of RNR deregulation *in vivo*.

Materials and Methods

Plasmids. Expression plasmids encoding mouse *Rrm1, Rrm2*, or *p53R2* were constructed in the pCaggs expression vector as described in Supplementary Materials and Methods.

Transgenic mice. Transgenic mice were generated in the *FVB/N* strain background, as described in Supplementary Materials and Methods. For analysis of tumor development, cohorts of mice were aged until moribund

Note: Supplementary data for this article are available at Cancer Research Online (http://cancerres.aacrjournals.org/).

Current address for J.A. Surtees: Department of Biochemistry, School of Medicine and Biomedical Sciences, State University of New York at Buffalo, Buffalo, NY.

Requests for reprints: Robert S. Weiss, Department of Biomedical Sciences, Cornell University, T2006C Veterinary Research Tower, Ithaca, NY 14853. Phone: 607-253-4443; Fax: 607-253-4212; E-mail: rsw26@cornell.edu.

doi:10.1158/0008-5472.CAN-07-5873

DOI:10.1158/0008-5472.CAN-07-5873

for 15 to 21 mo. *Msh6*-null mice (17) were obtained from the Mouse Models of Human Cancers Consortium, bred with $Rrm2^{Tg}$ or $p53R2^{Tg}$ mice, and aged until moribund for 6 or 17 mo. All mice were maintained identically, following guidelines approved by the Cornell University Institutional Laboratory Animal Use and Care Committee. Pathologic assessments were performed as described in Supplementary Materials and Methods.

Northern blot analysis. Total RNA was isolated from mouse cells and tissues using RNA STAT-60 (Tel-Test, Inc.), resolved on an agarose/formaldehyde gel, and hybridized with probes specific to mouse *Rrm1, Rrm2, p53R2*, or *Gapdh*.

Western blot analysis. Cell or tissue protein extracts were prepared as described in Supplementary Materials and Methods. The antibodies used were mouse anti-R1 (Bio Med Tek), goat anti-R2 (Santa Cruz Biotechnology), rabbit anti-p53R2 (ProSci-inc), and β-actin (Sigma).

Immunohistochemistry. Immunohistochemical detection of pro-SP-C and CC10 was performed on 5 μm paraffin sections using the Vectastain ABC kit (Vector Laboratories) as described in Supplementary Materials and Methods.

Generation of RNR overexpressing 3T3 cell pools. Pools of mouse NIH/3T3 fibroblasts that overexpress individual RNR genes were generated as described in Supplementary Materials and Methods.

Determination of mutation rates in mammalian and yeast cells. Mutation frequencies were determined in 3T3 cell pools and yeast strains by *Hprt* mutation and canavanine resistance assays, respectively, as described in Supplementary Materials and Methods.

Big Blue mutation rate assay. Big Blue *C57Bl/6* mice, hemizygous for the λ shuttle vector, were obtained from Stratagene and bred with $Rrm1^{Tg}$, $Rrm2^{Tg}$, $p53R2^{Tg}$, or $Msh6^{-/-}RNR^{Tg}$ mice. Mutation frequency in the resulting animals was determined as described in Supplementary Materials and Methods.

Sequencing of *K-ras* exons 1 and 2. DNA was prepared from tumor specimens isolated by laser microdissection, and *K*-ras exons 1 and 2 were PCR amplified and sequenced as described in Supplementary Materials and Methods.

Results

Generation of RNR transgenic mice and analysis of transgene expression. Deregulation of RNR is mutagenic in yeast and cultured mammalian cells (14, 16). To test the consequences of RNR deregulation in an animal model, we set out to generate transgenic mice featuring broad, high-level expression of the individual mouse RNR genes *Rrm1, Rrm2*, and *p53R2*, using pCaggs expression constructs that place the RNR genes under the control of chicken β-actin promoter and cytomegalovirus enhancer regulatory sequences. Six *Rrm1*, two *Rrm2*, and four *p53R2* transgene-positive founders were generated and subsequently maintained on a pure *FVB/N* strain background. RNR transgenic mice seemed grossly normal and were fertile. When bred with wild-type (WT) mice, *p53R2* hemizygotes produced fewer than the expected number of transgene positive offspring (205 *p53R2* transgene-positive and 349 transgene-negative mice were identified among 554 mice genotyped at weaning).

Endogenous and transgenic *Rrm1, Rrm2*, and *p53R2* mRNA expression was tested in a variety of organs by Northern blot analysis. The endogenous *Rrm1* and *Rrm2* genes were coordinately expressed, with highest expression in proliferative tissues, such as testis and thymus (Fig. 1*A, left*). Expression of the endogenous *p53R2* gene was undetectable in all tested WT *FVB* tissues. Importantly, $Rrm2^{Tg}$ and $p53R2^{Tg}$ mice showed high-level transgene expression in all tissues, with overexpression being highest in muscle (Fig. 1*A, right*). *Rrm1* overexpression was only observed in muscle and testis of $Rrm1^{Tg}$ mice. For technical reasons, the *Rrm1* transgene included additional noncoding cDNA sequences and was microinjected as a linearized construct without removal of plasmid backbone sequences, which may contribute to the relatively poor transgene expression.

Consistent with results from the Northern blot analyses, immunoblotting revealed that the Rrm2 and p53R2 proteins were highly overexpressed in all tested tissues from $Rrm2^{Tg}$ and $p53R2^{Tg}$ mice (Fig. 1*B*). Although Northern blotting failed to identify *p53R2* expression in WT tissues (Fig. 1*A*), low levels of p53R2 protein were apparent in most WT *FVB* tissues. Rrm1 protein overexpression was limited to muscle and to a lesser extent lung in $Rrm1^{Tg}$ mice compared with WT littermates. Together, these results establish the restricted overexpression of the large RNR subunit Rrm1 and the widespread, high-level overexpression of the small RNR subunits Rrm2 and p53R2 in transgenic mice.

Overexpression of the small RNR subunit promotes lung carcinogenesis. To identify spontaneous neoplasms and other abnormalities in RNR transgenic mice, we established a cohort consisting of 52 $Rrm1^{Tg}$, 75 $Rrm2^{Tg}$, and 81 $p53R2^{Tg}$ mice, as well as 49 transgene-negative control mice and aged them until they exhibited clinical illness. Notably, a significantly increased frequency of lung neoplasms was observed in $Rrm2^{Tg}$ and $p53R2^{Tg}$ mice (Table 1). Seventy-two percent of $Rrm2^{Tg}$ and 74% of $p53R2^{Tg}$ animals developed spontaneous lung neoplasms. By contrast, 31% of transgene-negative controls developed lung neoplasms, a frequency consistent with the reported incidence for aged WT *FVB* mice (18). The lung neoplasm incidence in $Rrm1^{Tg}$ mice was 31%, identical to that of the control animals and significantly less than that of $Rrm2^{Tg}$ or $p53R2^{Tg}$ mice (χ^2 analysis, $P < 0.05$). Lung neoplasms were observed in multiple independent $Rrm2^{Tg}$ and $p53R2^{Tg}$ lines, indicating that transgene integration site effects did not account for the neoplastic phenotype. Signs of clinical illness arose after a latency of 16 to 18 months for all genotypes. No differences in lung neoplasm incidence between sexes were noted for any of the transgenic lines. The frequency of epithelial hyperplasia of alveoli also was increased in $p53R2^{Tg}$ and especially $Rrm2^{Tg}$ mice. Other neoplasms, including papilloma, histiocytic sarcoma, mammary carcinoma, and lymphoblastic lymphoma, were observed in 13% of $Rrm1^{Tg}$, 12% of $Rrm2^{Tg}$, and 12% of $p53R2^{Tg}$ mice, but only 2% of transgene-negative mice.

The lung neoplasms in $Rrm2^{Tg}$ and $p53R2^{Tg}$ mice displayed several features consistent with a substantial lung cancer predisposition. A significantly greater lung neoplasm multiplicity was observed for $Rrm2^{Tg}$ and $p53R2^{Tg}$ mice, and the lung neoplasms in $Rrm2^{Tg}$ mice were also considerably larger than those from control animals (Table 1). The lung neoplasms from $Rrm2^{Tg}$ and $p53R2^{Tg}$ mice ranged from adenoma to advanced adenocarcinoma (Fig. 2*A, I–VI*) and resembled human glandular pulmonary neoplasms, particularly adenocarcinomas. RNR-induced lung adenocarcinomas were primarily of the papillary subtype and exhibited pleural invasion, heterogeneous growth pattern, nuclear atypia, high mitotic index, and blood vessel invasion (Fig. 2*A, III–VI*). A greater frequency of adenocarcinoma was observed in $Rrm2^{Tg}$ and $p53R2^{Tg}$ mice compared with $Rrm1^{Tg}$ or transgene-negative mice (Table 1), with *Rrm2* overexpression, in particular, eliciting pathologically advanced neoplasms. Together, these data indicate that overexpression of either small RNR subunit in mice promotes lung neoplasm formation, with *Rrm2* being more potent than *p53R2* with respect to tumor size, multiplicity, and malignancy.

To investigate the possible cell type of origin for RNR-induced lung neoplasms, we performed immunohistochemistry using

DOI:10.1158/0008-5472.CAN-07-5873

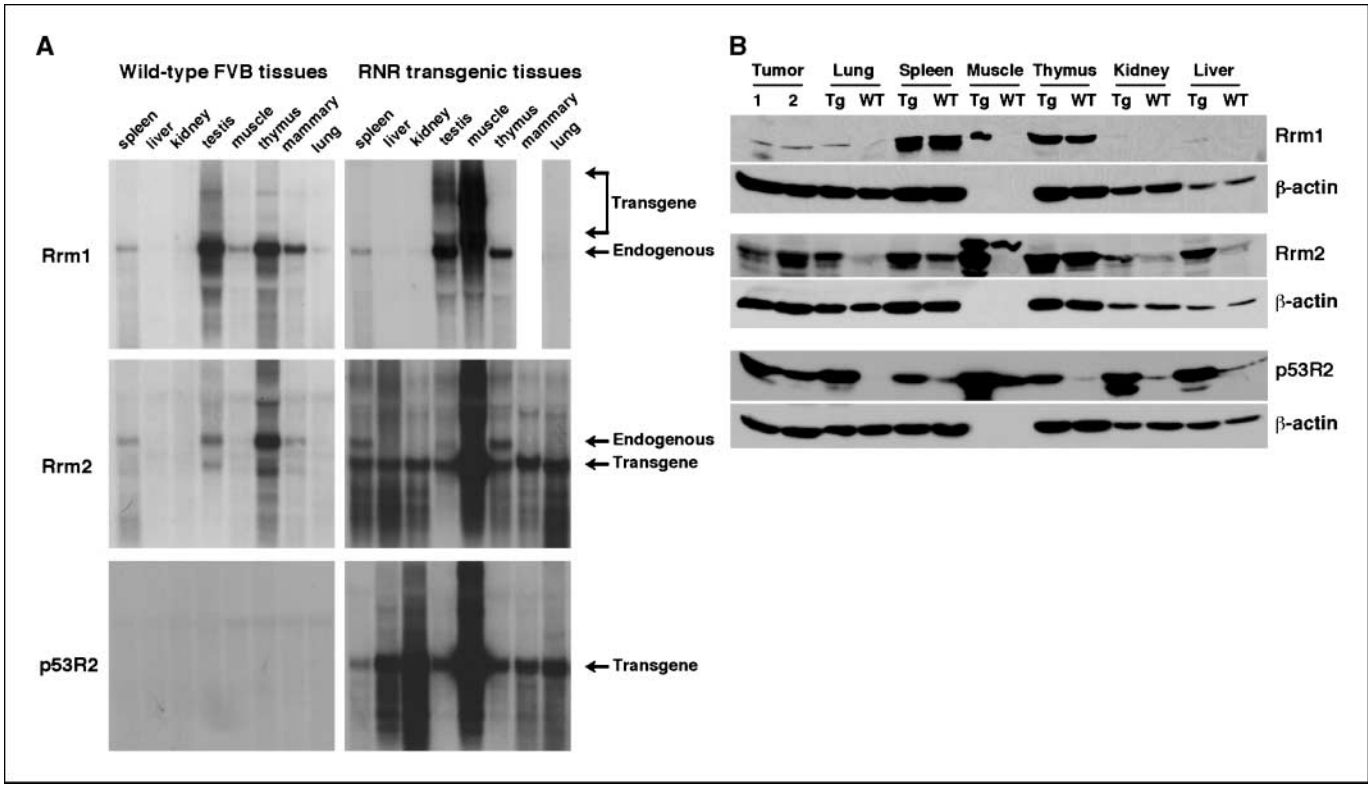

Figure 1. Widespread overexpression of RNR genes in transgenic mice. *A,* Northern blot analysis of RNR expression in WT and RNR transgenic mice. Total RNA was extracted from the indicated tissues from WT *FVB* mice (*left*) or RNR transgenic mice (*right*) and subjected to Northern blot hybridization with the indicated probes specific for *Rrm1, Rrm2*, or *p53R2*. Positions of endogenous and transgene-derived RNR transcripts are indicated. *B,* Western blot analysis of RNR protein expression in the indicated tissues from WT and RNR transgenic (*Tg*) mice, as well as lung neoplasms from the corresponding transgenic strains (*Tumor 1, Tumor 2*). Total protein from the indicated tissues was subjected to immunoblotting with antibodies specific to Rrm1, Rrm2, or p53R2. Duplicate membranes were immunoblotted for β-actin as a loading control.

antibodies against Clara cell antigen (CC10) and surfactant apoprotein-C (SP-C), markers that distinguish Clara and alveolar type II cells, respectively. Eight of eight lung neoplasms from $Rrm2^{Tg}$ and $p53R2^{Tg}$ mice were positive for SP-C (Fig. 2*A, VII*), whereas none was positive for CC10 (Fig. 2*A, VIII*). Adjacent bronchioles, on the other hand, were positive for CC10 and negative for SP-C, as expected. These results suggest that RNR-induced lung neoplasms arose from alveolar type II cells or their progenitors.

To confirm a causative role for RNR overexpression in lung carcinogenesis, we analyzed the expression of *Rrm1, Rrm2*, and *p53R2* in lung neoplasms by Northern (Fig. 2*B*) and Western (Fig. 1*B*) blotting. Lung neoplasms from $Rrm2^{Tg}$ and $p53R2^{Tg}$ animals showed prominent RNR overexpression, consistent with a

Table 1. Lung neoplasm characteristics in RNR overexpressing mice

Mouse genotype	No. animals	Percentage of mice with lung neoplasms	Percentage of mice with hyperplasia*	Average lung neoplasm size ± SD (mm)	Percentage of mice with multiple lung neoplasms	Percentage of mice with lung adenocarcinoma
WT FVB †	49	31%	12%	4.04 ± 3.98	8%	6%
$Rrm1^{Tg}$	52	31%	15%	3.96 ± 3.59	8%	10%
$Rrm2^{Tg}$	75	72% ‡	44% ‡	6.68 ± 4.22	53% ‡	40% ‡
$p53R2^{Tg}$	81	74% ‡	20%	4.26 ± 3.44	47% ‡	21%

NOTE: Mice were aged until moribund for up to 21 mo, euthanized by asphyxiation using carbon dioxide, and subjected to pathologic examination as described in Supplementary Materials and Methods.

*Includes mice that had both epithelial hyperplasia of alveoli and lung neoplasms.

†*WT FVB* refers to transgene-negative control mice.

‡Statistically significant difference ($P < 0.05$) relative to *WT FVB* mice. Incidences were compared by χ^2 analysis. Neoplasm sizes were compared by *t* test analysis.

DOI:10.1158/0008-5472.CAN-07-5873

causative role for RNR in the genesis of these lung lesions. By contrast, lung neoplasms from *Rrm1*^{Tg} mice did not display high-level transgene expression, providing further evidence that carcinogenesis in *Rrm2*^{Tg} and *p53R2*^{Tg} mice is highly specific. Overall, these data identify a novel oncogenic activity for the small RNR subunit.

Increased mutation frequency after RNR overexpression in cultured 3T3 cells. We hypothesized that RNR overexpression induced lung neoplasms through a mutagenic mechanism, because defects in RNR allosteric control result in increased mutation frequencies in yeast and mammalian cells (14, 16). To determine if RNR overexpression was similarly mutagenic, we generated *Rrm1, Rrm2*, or *p53R2* overexpressing NIH/3T3 cell pools using the same expression constructs as used to generate the transgenic mice. Overexpression of individual RNR genes in these cell pools was confirmed by Northern and Western blotting (Fig. 3*A* and *B*).

We then measured mutation frequency using the *Hprt* mutation detection assay, which identifies cells harboring *Hprt* mutations by virtue of their resistance to 6-thioguanine (19). In a representative experiment (Fig. 3*C*), a significantly increased mutation frequency was observed in a *Rrm2* overexpressing cell pool (9.0×10^{-6}) compared with *Rrm1* overexpressing or empty plasmid vector cell pools ($<0.7 \times 10^{-6}$ and $<0.8 \times 10^{-6}$, respectively). Three independent *Rrm2* overexpressing cell pools showed a consistently increased mutation frequency that was 9.9-fold to 16.0-fold greater than that observed for vector control cells. A *p53R2* overexpressing cell pool showed a more modestly, but nevertheless, significantly increased mutation frequency of 3.0×10^{-6} (Fig. 3*C*). However, mutation frequency in *p53R2* overexpressing cells varied, with three

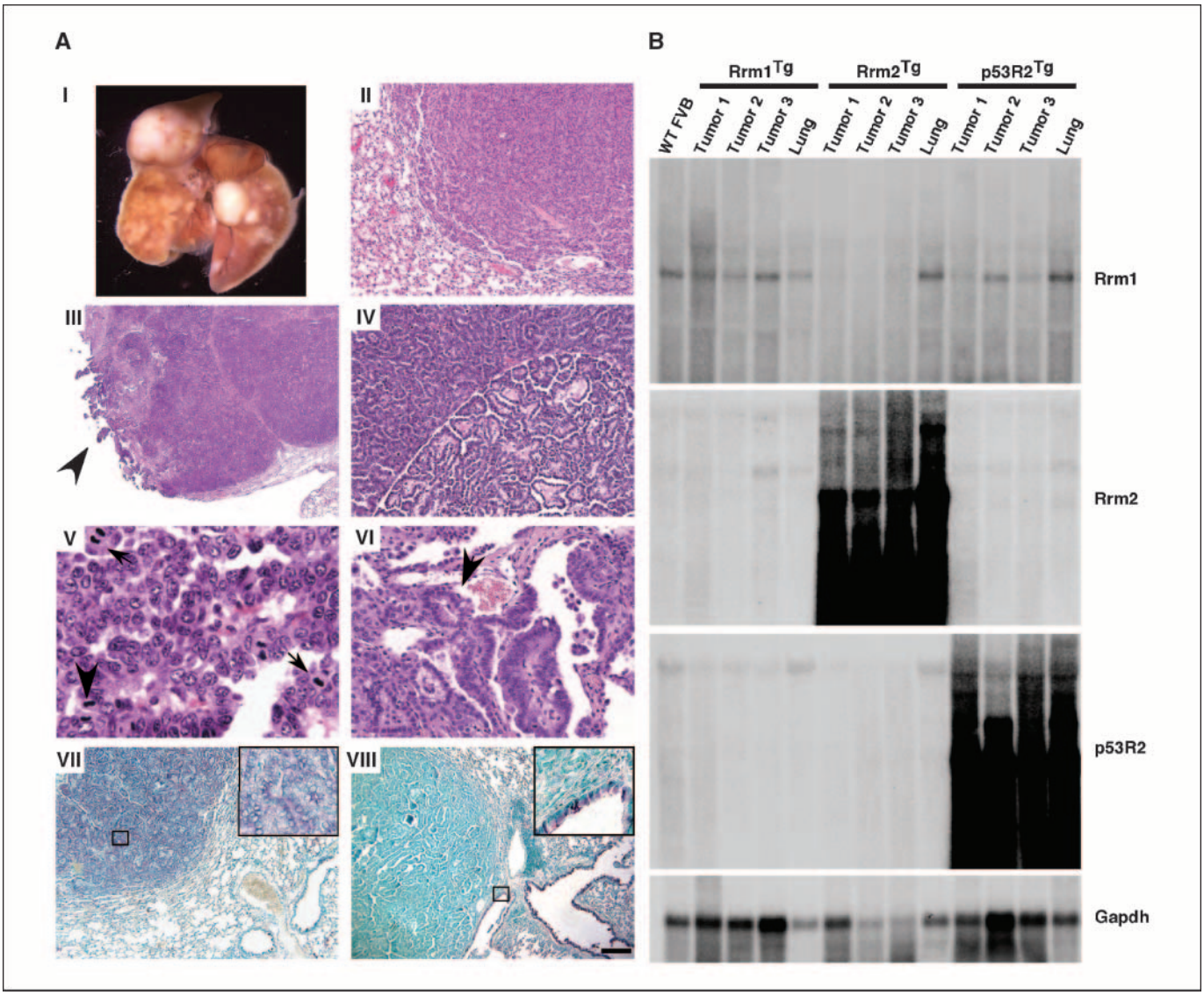

Figure 2. Histopathologic and molecular analysis of lung neoplasms from RNR transgenic mice. *A, I,* lungs from a *Rrm2*^{Tg} mouse with multiple independent neoplasms affecting several lobes. *II-VI,* H&E-stained sections of lung neoplasms. *II,* solid adenoma from a *p53R2*^{Tg} mouse. *III-VI,* papillary adenocarcinomas from *Rrm2*^{Tg} or *p53R2*^{Tg} mice showing pleural invasion (*arrow*; *III*), regional variation in growth pattern (*IV*), multiple mitotic figures (*arrows*; *V*), and blood vessel invasion (*arrow*; *VI*). *VII* and *VIII,* immunohistochemical staining of RNR-induced lung neoplasms for Pro-SP-C (*VII*) or CC10 (*VIII*) by the avidin-biotin complex method with methyl green counterstain. Inserts show higher magnification views of the boxed regions. *Calibration bar, II, IV,* 50 μm; *III,* 241 μm; *V,* 10 μm; *VI,* 25 μm; *VII, VIII,* 100 μm. *B,* Northern blot analysis of lung neoplasms from RNR transgenic mice. Total RNA was prepared from lung neoplasms (*Tumor 1, Tumor 2, Tumor 3*) or normal lung tissue (*Lung*) from RNR transgenic mice, as well as from WT *FVB* lung tissue. Northern blotting was performed with the indicated radiolabeled probes.

DOI:10.1158/0008-5472.CAN-07-5873

p53R2 overexpressing cell pools showing an elevated mutation frequency that was 4.2-fold to 11.2-fold greater than that for vector control cells, whereas two other *p53R2* overexpressing cell pools displayed no increase in mutation frequency. Whether this variability is due to differences in expression levels between individual cell pools, or to the fact that the mutation frequencies measured were near the lower end of sensitivity for this assay, has not been determined. However, three independent *Rrm1* overexpressing cell pools and another five empty plasmid vector cell pools showed no detectable increase in mutation frequency.

To determine the nature of the mutations conferring 6-thioguanine resistance, we sequenced the *Hprt* gene from individual colonies (20). Interestingly, four of seven *Hprt* mutations from the *Rrm2* overexpressing cell pool shown in Fig. 3*C* were G→T substitutions (Supplementary Table S1), which are relatively rare among reported spontaneous *Hprt* mutations (21). Similar results were obtained in a separate experiment with an independent *Rrm2* overexpressing cell pool (Supplementary Table S1). One of six mutations from the *p53R2* overexpressing cell pool shown in Fig. 3*C* also was a G→T mutation, but no G→T mutations were observed among six 6-thioguanine resistant clones from a second independent experiment (Supplementary Table S1). Collectively, the results indicate that overexpression of the small RNR subunit causes a mutator phenotype.

Combined defects in RNR regulation and MMR result in synergistic increases in mutagenesis and carcinogenesis. To further evaluate a role for mutagenesis in RNR-induced lung carcinogenesis, we investigated whether combining RNR deregulation with a defect in MMR, the repair system that suppresses mutation accumulation, would cause a synergistic increase in mutagenesis and carcinogenesis. In eukaryotic cells, a complex of Msh2-Msh6 is responsible for recognizing base-base mispairs and single-base insertion/deletions, whereas a Msh2-Msh3 complex detects larger insertion/deletion loops (22). We first tested this hypothesis in *Saccharomyces cerevisiae* by measuring the mutation rate by canavanine resistance assay in strains with deregulated RNR activity and mutations in MMR genes. To deregulate budding yeast RNR, we used the rnr1-D57N mutant, in which a single–amino acid change in the R1 activity site makes the enzyme insensitive to feedback inhibition by dATP (16). Consistent with published reports (14), *rnr1-D57N* yeast exhibited a 3.4-fold increase in mutation rate relative to the WT strain, which had a mutation rate of 1.5×10^{-7} (Fig. 4*A*). MMR-defective strains also displayed elevated mutation rates (*msh2Δ*: 28.4-fold; *msh3Δ*: 2.9-fold; *msh6Δ*: 9.8-fold), similar to previous reports (23). Notably, *rnr1-D57N msh2Δ* and *rnr1-D57N msh6Δ* double mutants displayed approximately multiplicative increases in mutation rate relative to the single mutants (61.4-fold and 23.8-fold, respectively). Multiplicative increases in mutagenesis are seen for mutations that affect factors acting in series in a common pathway (24), suggesting that the Msh2-Msh6 complex corrects DNA mismatches induced by RNR deregulation. By contrast, combining *rnr1-D57N* with *msh3Δ* resulted in only an additive increase in mutation rate (*rnr1-D57N msh3Δ:* 3.9-fold). The spectrum of mutations arising in WT

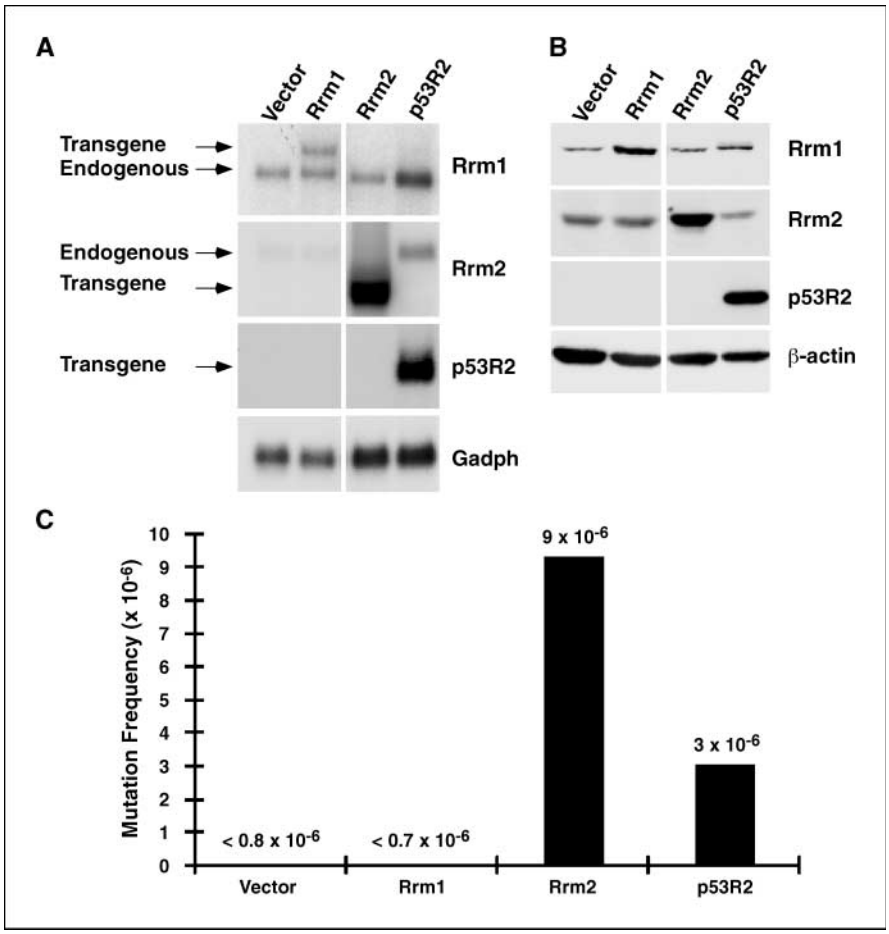

Figure 3. Increased mutation frequency in RNR overexpressing NIH/3T3 cell pools. *A,* Northern blot analysis of RNR expression in stable 3T3 cell pools transfected with either pCaggs empty vector or pCaggs RNR genes. Total RNA was extracted from the indicated cell lines and subjected to Northern blot hybridization with probes specific for *Rrm1, Rrm2, p53R2,* or *Gapdh. B,* Western blot analysis of RNR protein expression in RNR overexpressing 3T3 cells. Total protein was extracted from the indicated cell lines and subjected to immunoblotting with antibodies specific to Rrm1, Rrm2, or p53R2. Duplicate membranes were immunoblotted for β-actin as a loading control. Samples in *A* and *B* were run on single blots, which were then cropped to remove extraneous lanes. *C,* mutation frequency at the *Hprt* locus in *Rrm1, Rrm2*, and *p53R2* overexpressing 3T3 cells. Mutation frequency was determined by *Hprt* assay.

DOI:10.1158/0008-5472.CAN-07-5873

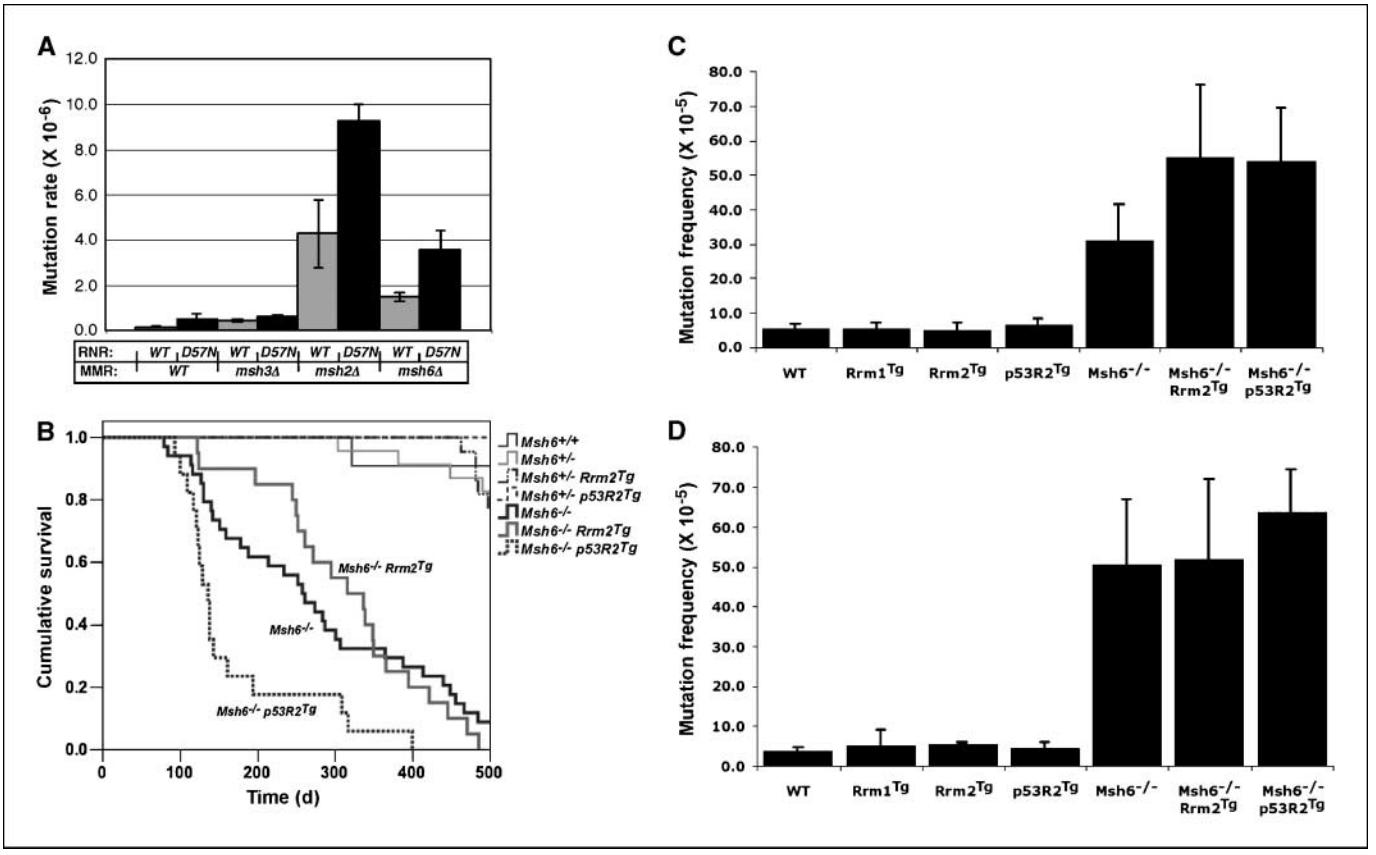

Figure 4. Genetic interactions between RNR and MMR. *A,* canavanine mutation rate assay for *RNR1(WT)* and *rnr1-D57N* strains on MMR-deficient backgrounds (*msh3Δ, msh2Δ, msh6Δ,* or *WT*) of *S. cerevisiae.* The forward mutation rate (per generation) to canavanine resistance was measured for the indicated single and double mutant combinations. Error bars show the 95% confidence interval. *B,* survival curves for $Msh6^{-/-}RNR^{Tg}$ ($Rrm2^{Tg}$ *or* $p53R2^{Tg}$) mice. Mice were aged until moribund for up to 17 mo. Survival curves were generated using SPSS software. The following number of animals was analyzed for each genotype: $Msh^{+/+}$ (11), $Msh6^{+/-}$ (23), $Msh6^{+/-}Rrm2^{Tg}$ (22), $Msh6^{+/-}p53R2^{Tg}$ (11), $Msh6^{-/-}$ (34), $Msh6^{-/-}Rrm2^{Tg}$ (20), $Msh6^{-/-}$ $p53R2^{Tg}$ (17). *C* and *D,* mutation frequency at the λ *cII* locus in lung (*C*) or spleen (*D*) tissues from RNR overexpressing and control mice. Genomic DNA was isolated from 3-mo-old mice of the indicated genotypes and packaged into infectious phage. Mutation frequency was determined based on the ratio of the number of mutant phage obtained to the total number of phage analyzed.

nr1-D57N, msh2Δ, and *msh6Δ* strains was consistent with previous publications (14, 23, 25) and included primarily base substitutions, as well as frameshift mutations for *msh2Δ* (Supplementary Table S2). The frequency of frameshift mutations involving single nucleotide insertions or deletions was substantially increased in *rnr1-D57N msh2Δ* and *rnr1-D57N msh6Δ* strains relative to the single mutants.

The synergistic effects of RNR deregulation and MMR deficiency on mutation rates in yeast prompted us to further test genetic interactions between RNR and MMR in mice by crossing RNR transgenic mice with *Msh6*-null mice (17). If RNR overexpression induces lung carcinogenesis through a mutagenic mechanism, *Msh6* deficiency would be predicted to accelerate lung carcinogenesis in RNR transgenic mice. A cohort of $Msh6^{-/-}$, $Msh6^{+/-}$, or $Msh6^{+/+}$ mice that also carried either the *Rrm2* or *p53R2* transgene was established and examined for survival and cancer susceptibility. Interestingly, the median life span for $Msh6^{-/-}p53R2^{Tg}$ mice (136 days) was significantly reduced compared with that of transgene-negative $Msh6^{-/-}$ mice (258 days; $P < 0.05$; log-rank test; Fig. 4*B*). The reduced survival of $Msh6^{-/-}p53R2^{Tg}$ mice was associated with early onset lymphomagenesis (Supplementary Table S3). Because these $Msh6^{-/-}p53R2^{Tg}$ mice died at a young age, we could not evaluate whether *Msh6* deficiency cooperated with *p53R2* overexpression in inducing lung neoplasms.

The survival rate for $Msh6^{-/-}Rrm2^{Tg}$ and transgene negative $Msh6^{-/-}$ mice was not significantly different ($P = 0.975$; log-rank test), suggesting that *Rrm2* overexpression, unlike *p53R2* overexpression, did not enhance lymphomagenesis (Fig. 4*B*). However, that 90% of $Msh6^{-/-}Rrm2^{Tg}$ mice had developed lung neoplasms despite their shortened life span of ~10 months was suggestive of a synergistic genetic interaction (Supplementary Table S3). To directly test whether lung carcinogenesis was accelerated in $Msh6^{-/-}Rrm2^{Tg}$ mice, we sacrificed a cohort of $Msh6^{-/-}Rrm2^{Tg}$ mice and littermate controls at 6 months of age. Three of 18 $Msh6^{+/+}Rrm2^{Tg}$ mice and 3 of 17 $Msh6^{+/-}Rrm2^{Tg}$ mice had developed lung neoplasms by 6 months, whereas no lung neoplasms were observed in transgene-negative $Msh6^{+/+}$ or $Msh6^{+/-}$ littermates (Table 2). Lung neoplasms were also observed in 2 of 13 $Msh6^{-/-}$ mice. *Msh6* deficiency strongly accelerated *Rrm2*-induced lung carcinogenesis, as 13 of 13 $Msh6^{-/-}Rrm2^{Tg}$ mice developed lung neoplasms by 6 months of age, with nine of these mice carrying multiple lung neoplasms.

To determine whether combining RNR overexpression with MMR deficiency would increase mutation frequency *in vivo*, we analyzed the mutation frequency at the λ phage *cII* locus in lung tissue from 3-month-old RNR^{Tg} mice, with or without *Msh6* deficiency, using the Big Blue transgene system (26). There was no difference in mutation frequency in RNR transgenic

DOI:10.1158/0008-5472.CAN-07-5873

mice compared with WT mice (Fig. 4*C* and Supplementary Table S4), possibly because the Big Blue system is relatively insensitive due to a high background mutation frequency. However, the mutation frequency in *Msh6*$^{-/-}$*Rrm2*^{Tg} ($55.2 \pm 20.9 \times 10^{-5}$) and *Msh6*$^{-/-}$*p53R2*^{Tg} ($54.0 \pm 15.4 \times 10^{-5}$) lung tissues was consistently higher than that in *Msh6*$^{-/-}$ lung tissue ($31.1 \pm 10.4 \times 10^{-5}$), although these differences were not statistically significant. By contrast, the mutation frequency was similar in spleen tissue from *Msh6*$^{-/-}$*Rrm2*^{Tg} ($52.0 \pm 20.1 \times 10^{-5}$) and *Msh6*$^{-/-}$ ($50.5 \pm 16.3 \times 10^{-5}$) mice, but slightly elevated in *Msh6*$^{-/-}$*p53R2*^{Tg} ($63.7 \pm 10.7 \times 10^{-5}$) animals (Fig. 4*D* and Supplementary Table S5). Together, these results indicate that MMR deficiency synergizes with RNR overexpression in a tissue-specific manner to increase mutagenesis and carcinogenesis.

RNR-induced lung neoplasms display a unique signature of *K-ras* activating mutations. A mutagenic mechanism implies that RNR overexpression triggers additional genetic alterations while promoting tumor development. Because mutations in codons 12 and 61 of the *K-ras* proto-oncogene are often observed in human and mouse lung cancers (27, 28), we examined the frequency of *K-ras* mutations in microdissected lung neoplasms from the RNR cohort. 100% of *Rrm2*-induced lung neoplasms and 79% of *p53R2*-induced lung neoplasms carried *K-ras* activating mutations (Supplementary Table S6), indicating that RNR-induced lung carcinogenesis frequently involves *K-ras* activating mutations. 56% and 100% of the rare lung neoplasms from transgene-negative control and *Rrm1*^{Tg} mice, respectively, also had *K-ras* mutations.

Sequence analysis revealed that the lung neoplasms from *Rrm2*^{Tg} and *p53R2*^{Tg} mice exhibited distinct mutation spectra relative to those from transgene-negative and *Rrm1*^{Tg} mice (Supplementary Table S7). In particular, 50% of the *K-ras* codon 12 mutations from *Rrm2*-induced lung neoplasms were G→T transversions (GGT→GTT, G12V), as were 30% of those from *p53R2*-induced lung neoplasms. By contrast, lung neoplasms from transgene-negative and *Rrm1*^{Tg} mice showed exclusively G→A transitions (GGT→GAT, G12D) in *K-ras* codon 12. We conclude that *K-ras* activating mutations, common events in lung carcinogenesis, are central to *Rrm2*-induced and *p53R2*-induced lung carcinogenesis and arise through a mechanism that seems distinct from that underlying spontaneous lung tumor development in WT animals.

Discussion

RNR enzyme activity has long been positively correlated with cancer cell division (29), and RNR inhibition is an effective strategy for suppressing tumor proliferation and survival (30). Yet, investigation of the effects of RNR deregulation in animal models has been incomplete. We report that overexpression of *Rrm2* or *p53R2* specifically induces lung but not other neoplasms at high frequency in transgenic mice. Previous studies indicated that human RRM2 has transforming activity in cultured cells (31), whereas p53R2 has been suggested to have tumor suppressor activity based on its regulation by p53 and its role in the DNA damage response (2). RNR may be an example of a growth regulator that has dual roles both as a tumor suppressor and oncogene. Whereas impaired RNR function can trigger genomic instability by limiting nucleotide availability for DNA replication and repair purposes, RNR hyperactivity may be equally detrimental due to its mutagenic effects. Interestingly, the genomic regions containing human *RRM2* (2p25-2p24) and *p53R2* (8q23.1) are commonly amplified in human lung cancers (32–35), raising the possibility that RNR deregulation might have a causative role in human lung carcinogenesis. Because RNR is a DNA damage-inducible enzyme, our results also suggest that increased RNR levels due to chronic DNA damage in the lungs of smokers may contribute to tumor development.

In contrast to *Rrm2*^{Tg} and *p53R2*^{Tg} mice, *Rrm1*^{Tg} mice did not show increased lung carcinogenesis. This might be due to the relatively limited overexpression of the *Rrm1* transgene or the fact that the R2 subunit is the limiting component of the enzyme (7, 36). However, Rrm1 shows tumor suppressor activity both in cultured cells and human lung cancer patients (37–39). Consistent with our findings, *Rrm1* overexpression in another mouse model also did not result in any overt spontaneous phenotypes and instead was reported to suppress chemical carcinogenesis in the lung (40). Thus, lung tumor induction

Table 2. Combining RNR overexpression with MMR deficiency results in a synergistic increase in lung carcinogenesis

Mouse genotype	No. animals	Percentage of mice with lung neoplasms	Percentage of mice with multiple lung neoplasms	No. lung neoplasms per mouse* ± SD	Average lung neoplasm size ± SD (mm)	Percentage of mice with lymphoma
Msh6$^{-/-}$*Rrm2*^{Tg}	13	100%†	69%†	2.9 ± 1.99	1.30 ± 0.54	31%
Msh6$^{-/-}$	13	15%	0%	1.0 ± 0	1.25 ± 1.06	8%
Msh6$^{+/-}$*Rrm2*^{Tg}	17	18%	0%	1.0 ± 0	0.73 ± 0.68	12%
Msh6$^{+/-}$	10	0%	0%	N/A	N/A	0%
Msh6$^{+/+}$*Rrm2*^{Tg}	18	17%	6%	1.33 ± 0.58	1.23 ± 0.25	0%
Msh6$^{+/+}$	14	0%	0%	N/A	N/A	0%

NOTE: Mice were aged for 6 mo, euthanized by asphyxiation using carbon dioxide, and subjected to pathologic examination as described in Supplementary Materials and Methods. Only mice that lived to 6 mo were included. Four *Msh6*$^{-/-}$*Rrm2*^{Tg} mice died before 6 mo due to lymphoma, one of which also had a lung neoplasm. Four *Msh6*$^{-/-}$ mice died before 6 mo due to lymphoma.

*Values refer to the average number of lung neoplasms per mouse among tumor-bearing animals only.

†Statistically significant difference ($P < 0.01$) relative to *Msh6*$^{-/-}$, *Msh6*$^{+/-}$*Rrm2*^{Tg}, or *Msh6*$^{+/+}$*Rrm2*^{Tg} mice as determined by Fisher's exact test.

DOI:10.1158/0008-5472.CAN-07-5873

might be specific to the small RNR subunit and independent of RNR enzyme activity.

We determined that RNR-induced lung tumorigenesis proceeded through a mutagenic mechanism. Overexpression of *Rrm2* or *p53R2*, but not *Rrm1*, in 3T3 cells resulted in a significant increase in mutation frequency. Additional experiments in budding yeast indicated that MMR normally corrects base mispairs that arise due to RNR deregulation, as multiplicative increases in mutation rate were observed when the allosteric site mutant *rnr1-D57N* was combined with MMR gene mutations. A similar genetic interaction between RNR and MMR was observed in mice. *Msh6*-null mice develop primarily lymphoma (17), and *p53R2* overexpression cooperated with *Msh6*-deficiency to cause an earlier onset of lymphomagenesis and shortened life span in $Msh6^{-/-}p53R2^{Tg}$ mice compared with $Msh6^{-/-}$ controls. We also observed that *Msh6* deficiency strongly accelerated *Rrm2*-induced lung carcinogenesis, with 100% of $Msh6^{-/-}Rrm2^{Tg}$ mice developing lung neoplasms by 6 months of age. The accelerated lung carcinogenesis in $Msh6^{-/-}Rrm2^{Tg}$ mice was associated with increased mutation frequency in lung tissue, whereas the accelerated lymphomagenesis in $Msh6^{-/-}p53R2^{Tg}$ mice correlated with a modestly elevated mutation frequency in spleen tissue. The synergy observed between these pathways raises the possibility that aberrant RNR expression may be selected for in MMR-deficient cancers.

A key question arising from this study is the molecular basis for mutagenesis and lung tumor induction by *Rrm2* and *p53R2* overexpression. One possibility is that increased RNR expression leads to dNTP level alterations that impair replication fidelity and trigger mutations in growth regulatory genes. Abnormal nucleotide levels result in increased base misinsertion during DNA replication, as well as decreased proof-reading due to enhanced polymerization rates (5). Consistent with the notion that regulators of nucleotide biosynthesis can influence cell transformation, overexpression of another enzyme involved in dNTP biosynthesis, thymidylate synthase, transforms cultured cells (41) and promotes tumor formation in transgenic mice (42).

Alternatively, carcinogenesis due to R2 subunit overexpression could be independent of nucleotide metabolism. One possibility is that free radical production by Rrm2 and p53R2 contributes to cell transformation. During each catalytic cycle the small RNR subunit generates a tyrosyl radical that normally is transferred to the active site in Rrm1 for use in NDP reduction (1). R2 protein overexpression might lead to increased radical generation and the formation of reactive oxygen species (ROS), which cause oxidative DNA damage and are mutagenic. ROS also have mitogenic effects and can play a direct role in neoplastic transformation (43). Notably, human RRM2 protein generates ROS *in vitro*, although recombinant p53R2 was reported in the same study to have antioxidant activity, despite the fact that both RRM2 and p53R2 generate tyrosyl-free radicals (44). G→T transversions, a signature of oxidative DNA damage, were detected at *K-Ras* codon 12 in lung neoplasms from $Rrm2^{Tg}$ and $p53R2^{Tg}$ mice, and also at the *Hprt* locus in *Rrm2* and *p53R2* overexpressing 3T3 cells. Because MMR corrects mismatches arising from both replication errors (22) and oxidative DNA damage (45), the multiplicative increases in mutagenesis and carcinogenesis observed when combining RNR overexpression with MMR deficiency are compatible with both dNTP level alterations and increased ROS production as possible mechanisms of action.

The possibility that R2 subunit overexpression induces mutagenesis and tumorigenesis through excessive free radical production may account for the observation that RNR transgenic mice, despite broad RNR overexpression, develop lung but not other neoplasms at high frequency. The lung is an oxygen-rich environment with a high basal level of ROS (46) and thus may be more susceptible to increased free radical production. Alternatively, it could be that the mutational targets of RNR dictate the tissue specificity. Indeed, activated *K-ras* preferentially induces lung neoplasms in mice (47). Other more trivial explanations for the lung-specific carcinogenesis, such as subtle transgene expression level differences or varying DNA repair efficiencies among tissues, also cannot be ruled out.

Although *Rrm2* and *p53R2* encode related R2 proteins, they did not give identical results in our experiments. Whereas overexpression of either was capable of inducing lung neoplasms, *Rrm2* overexpression elicited larger and more malignant tumors. *p53R2* overexpression, on the other hand, significantly accelerated lymphomagenesis in *Msh6*-null mice, suggesting a broad effect of *p53R2* overexpression. *Rrm2* also was more mutagenic than *p53R2* in cultured cells and induced a greater proportion of G→T transversions in both the *Hprt* and *K-ras* genes. One possible explanation for the partially distinct phenotypes associated with *Rrm2* and *p53R2* is that both dNTP alterations and ROS production can contribute to neoplastic transformation and that these activities differ between Rrm2 and p53R2. The distinct subcellular localizations of Rrm2 and p53R2 (2, 3, 13) could contribute to such differing effects on dNTP biosynthesis or ROS production.

Mouse models hold great promise for facilitating the development of diagnostic tools, prognostic markers, and therapeutics for lung cancer, the leading cause of cancer death world-wide. Like human lung adenocarcinomas (48), the RNR-induced lung neoplasms expressed SP-C, a marker of type II alveolar cells. Furthermore, RNR-induced lung neoplasms arose with moderate latency in a stochastic process associated with an elevated mutation rate, suggesting that this may be a particularly authentic model for lung cancer. A mutagenic mechanism for RNR-induced lung carcinogenesis implies that several genetic alterations are required for lung carcinogenesis. Consistent with this model, we observed activating *K-ras* mutations at very high frequency in RNR-induced lung neoplasms. *K-ras* has been reported to be mutated in 90% of mouse lung neoplasms and as many as 25% of human lung adenocarcinomas (27, 28). That G→T transversions in *K-ras* codon 12 were detected in RNR-induced lung neoplasms further validates this lung cancer model, as G→T transversions are the most common mutations at *K-ras* codon 12 in human lung cancers and correlate with a poorer prognosis (49, 50). Continued use of the RNR lung cancer model has great potential for revealing additional genetic alterations that contribute to lung tumor initiation and progression.

Acknowledgments

Received 10/15/2007; revised 1/14/2008; accepted 2/13/2008.

Grant support: NIH grants GM53085 (E. Alani), CA96823 (A.Y. Nikitin), and RR017595 (A.Y. Nikitin). X. Xu was supported by a Genomics Scholar Award from the Cornell University Center for Vertebrate Genomics, J.L. Page was supported by NIH training grant T32GM07617, and J.A. Surtees was a Research Fellow of the National Cancer Institute of Canada supported with funds from the Terry Fox Run.

The costs of publication of this article were defrayed in part by the payment of page charges. This article must therefore be hereby marked *advertisement* in accordance with 18 U.S.C. Section 1734 solely to indicate this fact.

DOI:10.1158/0008-5472.CAN-07-5873

We thank Dr. Phil Leder for his support of this project, Dr. Lars Thelander for *Rrm1* and *Rrm2* cDNA clones, Dr. Andrei Chabes for yeast strains 4069-4C and 4069-8C, Charlene Manning and Dr. Jianrong Lu for assistance with plasmid cloning, Nick Fuda for contributions to the yeast mutation rate analyses, Anne Harrington for performing transgene microinjections, and Dr. Ruth Collins and Dr. Sylvia Lee for helpful discussions.

References

1. Nordlund P, Reichard P. Ribonucleotide reductases. Annu Rev Biochem 2006;75:681–706.
2. Tanaka H, Arakawa H, Yamaguchi T, et al. A ribonucleotide reductase gene involved in a p53-dependent cell-cycle checkpoint for DNA damage. Nature 2000;404:42–9.
3. Nakano K, Balint E, Ashcroft M, Vousden KH. A ribonucleotide reductase gene is a transcriptional target of p53 and p73. Oncogene 2000;19:4283–9.
4. Thelander L. Ribonucleotide reductase and mitochondrial DNA synthesis. Nat Genet 2007;39:703–4.
5. Mathews CK. DNA precursor metabolism and genomic stability. FASEB J 2006;20:1300–14.
6. Bjorklund S, Skog S, Tribukait B, Thelander L. S-phase-specific expression of mammalian ribonucleotide reductase R1 and R2 subunit mRNAs. Biochemistry 1990;29:5452–8.
7. Mann GJ, Musgrove EA, Fox RM, Thelander L. Ribonucleotide reductase M1 subunit in cellular proliferation, quiescence, and differentiation. Cancer Res 1988;48:5151–6.
8. Eriksson S, Graslund A, Skog S, Thelander L, Tribukait B. Cell cycle-dependent regulation of mammalian ribonucleotide reductase. The S phase-correlated increase in subunit M2 is regulated by *de novo* protein synthesis. J Biol Chem 1984;259:11695–700.
9. Chabes AL, Pfleger CM, Kirschner MW, Thelander L. Mouse ribonucleotide reductase R2 protein: a new target for anaphase-promoting complex-Cdh1-mediated proteolysis. Proc Natl Acad Sci U S A 2003;100:3925–9.
10. Chabes A, Thelander L. Controlled protein degradation regulates ribonucleotide reductase activity in proliferating mammalian cells during the normal cell cycle and in response to DNA damage and replication blocks. J Biol Chem 2000;275:17747–53.
11. Elledge SJ, Zhou Z, Allen JB, Navas TA. DNA damage and cell cycle regulation of ribonucleotide reductase. Bioessays 1993;15:333–9.
12. Hakansson P, Hofer A, Thelander L. Regulation of mammalian ribonucleotide reduction and dNTP pools after DNA damage and in resting cells. J Biol Chem 2006;281:7834–41.
13. Engstrom Y, Rozell B. Immunocytochemical evidence for the cytoplasmic localization and differential expression during the cell cycle of the M1 and M2 subunits of mammalian ribonucleotide reductase. EMBO J 1988;7:1615–20.
14. Chabes A, Georgieva B, Domkin V, Zhao X, Rothstein R, Thelander L. Survival of DNA damage in yeast directly depends on increased dNTP levels allowed by relaxed feedback inhibition of ribonucleotide reductase. Cell 2003;112:391–401.
15. Reichard P, Eliasson R, Ingemarson R, Thelander L. Cross-talk between the allosteric effector-binding sites in mouse ribonucleotide reductase. J Biol Chem 2000;275:33021–6.
16. Caras IW, Martin DW, Jr. Molecular cloning of the cDNA for a mutant mouse ribonucleotide reductase M1 that produces a dominant mutator phenotype in mammalian cells. Mol Cell Biol 1988;8:2698–704.
17. Edelmann W, Yang K, Umar A, et al. Mutation in the mismatch repair gene Msh6 causes cancer susceptibility. Cell 1997;91:467–77.
18. Mahler JF, Stokes W, Mann PC, Takaoka M, Maronpot RR. Spontaneous lesions in aging FVB/N mice. Toxicol Pathol 1996;24:710–6.
19. Fenwick RG. The HGPRT system. In: Gottesman M, editor. Molecular Cell Genetics.1st ed. New York: Wiley; 1985. p. 333–73.
20. Wijnhoven SW, Kool HJ, van Oostrom CT, et al. The relationship between benzo(*a*)pyrene-induced mutagenesis and carcinogenesis in repair-deficient Cockayne syndrome group B mice. Cancer Res 2000;60:5681–7.
21. Zhang LH, Vrieling H, van Zeeland AA, Jenssen D. Spectrum of spontaneously occurring mutations in the hprt gene of V79 Chinese hamster cells. J Mol Biol 1992;223:627–35.
22. Modrich P. Mechanisms in eukaryotic mismatch repair. J Biol Chem 2006;281:30305–9.
23. Lau PJ, Flores-Rozas H, Kolodner RD. Isolation and characterization of new proliferating cell nuclear antigen (POL30) mutator mutants that are defective in DNA mismatch repair. Mol Cell Biol 2002;22:6669–80.
24. Morrison A, Johnson AL, Johnston LH, Sugino A. Pathway correcting DNA replication errors in *Saccharomyces cerevisiae*. EMBO J 1993;12:1467–73.
25. Marsischky GT, Filosi N, Kane MF, Kolodner R. Redundancy of *Saccharomyces cerevisiae* MSH3 and MSH6 in MSH2-dependent mismatch repair. Genes Dev 1996;10:407–20.
26. Jakubczak JL, Merlino G, French JE, et al. Analysis of genetic instability during mammary tumor progression using a novel selection-based assay for *in vivo* mutations in a bacteriophage λ transgene target. Proc Natl Acad Sci U S A 1996;93:9073–8.
27. You M, Candrian U, Maronpot RR, Stoner GD, Anderson MW. Activation of the Ki-ras protooncogene in spontaneously occurring and chemically induced lung tumors of the strain A mouse. Proc Natl Acad Sci U S A 1989;86:3070–4.
28. Mills NE, Fishman CL, Rom WN, Dubin N, Jacobson DR. Increased prevalence of K-ras oncogene mutations in lung adenocarcinoma. Cancer Res 1995;55:1444–7.
29. Elford HL, Freese M, Passamani E, Morris HP. Ribonucleotide reductase and cell proliferation. I. Variations of ribonucleotide reductase activity with tumor growth rate in a series of rat hepatomas. J Biol Chem 1970;245:5228–33.
30. Shao J, Zhou B, Chu B, Yen Y. Ribonucleotide reductase inhibitors and future drug design. Curr Cancer Drug Targets 2006;6:409–31.
31. Fan H, Villegas C, Wright JA. Ribonucleotide reductase R2 component is a novel malignancy determinant that cooperates with activated oncogenes to determine transformation and malignant potential. Proc Natl Acad Sci U S A 1996;93:14036–40.
32. Wong MP, Fung LF, Wang E, et al. Chromosomal aberrations of primary lung adenocarcinomas in nonsmokers. Cancer 2003;97:1263–70.
33. Goeze A, Schluns K, Wolf G, Thasler Z, Petersen S, Petersen I. Chromosomal imbalances of primary and metastatic lung adenocarcinomas. J Pathol 2002;196:8–16.
34. Pei J, Balsara BR, Li W, et al. Genomic imbalances in human lung adenocarcinomas and squamous cell carcinomas. Genes Chromosomes Cancer 2001;31:282–7.
35. Lui WO, Tanenbaum DM, Larsson C. High level amplification of 1p32–33 and 2p22–24 in small cell lung carcinomas. Int J Oncol 2001;19:451–7.
36. Engstrom Y, Eriksson S, Jildevik I, Skog S, Thelander L, Tribukait B. Cell cycle-dependent expression of mammalian ribonucleotide reductase. Differential regulation of the two subunits. J Biol Chem 1985;260:9114–6.
37. Gautam A, Li ZR, Bepler G. RRM1-induced metastasis suppression through PTEN-regulated pathways. Oncogene 2003;22:2135–42.
38. Fan H, Huang A, Villegas C, Wright JA. The R1 component of mammalian ribonucleotide reductase has malignancy-suppressing activity as demonstrated by gene transfer experiments. Proc Natl Acad Sci U S A 1997;94:13181–6.
39. Zheng Z, Chen T, Li X, Haura E, Sharma A, Bepler G. DNA synthesis and repair genes RRM1 and ERCC1 in lung cancer. N Engl J Med 2007;356:800–8.
40. Gautam A, Bepler G. Suppression of lung tumor formation by the regulatory subunit of ribonucleotide reductase. Cancer Res 2006;66:6497–502.
41. Rahman L, Voeller D, Rahman M, et al. Thymidylate synthase as an oncogene: a novel role for an essential DNA synthesis enzyme. Cancer Cell 2004;5:341–51.
42. Chen M, Rahman L, Voeller D, et al. Transgenic expression of human thymidylate synthase accelerates the development of hyperplasia and tumors in the endocrine pancreas. Oncogene 2007;26:4817–24.
43. Droge W. Free radicals in the physiological control of cell function. Physiol Rev 2002;82:47–95.
44. Xue L, Zhou B, Liu X, et al. Structurally dependent redox property of ribonucleotide reductase subunit p53R2. Cancer Res 2006;66:1900–5.
45. Slupphaug G, Kavli B, Krokan HE. The interacting pathways for prevention and repair of oxidative DNA damage. Mutat Res 2003;531:231–51.
46. Rahman I. Oxidative stress, chromatin remodeling and gene transcription in inflammation and chronic lung diseases. J Biochem Mol Biol 2003;36:95–109.
47. Johnson L, Mercer K, Greenbaum D, et al. Somatic activation of the K-ras oncogene causes early onset lung cancer in mice. Nature 2001;410:1111–6.
48. Linnoila RI, Mulshine JL, Steinberg SM, Gazdar AF. Expression of surfactant-associated protein in non-small-cell lung cancer: a discriminant between biologic subsets. J Natl Cancer Inst Monogr 1992:61–6.
49. Keohavong P, DeMichele MA, Melacrinos AC, Landreneau RJ, Weyant RJ, Siegfried JM. Detection of K-ras mutations in lung carcinomas: relationship to prognosis. Clin Cancer Res 1996;2:411–8.
50. Rodenhuis S, Slebos RJ, Boot AJ, et al. Incidence and possible clinical significance of K-ras oncogene activation in adenocarcinoma of the human lung. Cancer Res 1988;48:5738–41.